Activation of Dinitrogen By Polynuclear Metal Complexes

Devender Singh, **William R. Buratto**, **Juan F. Torres**, **Leslie J. Murray**[*]

Center for Catalysis, and Florida Center for Heterocyclic Compounds, Department of Chemistry, University of Florida, Gainesville, FL 32611-7200, USA

Abstract

Activation of dinitrogen plays an important role in daily anthropogenic life and the processes by which this fixation occurs has been a longstanding and significant research focus within the community. One of the major fields of dinitrogen activation research is the use of multimetallic compounds to reduce and/or activate N_2 into a more useful nitrogen-atom source, such as ammonia. Here we report a comprehensive review of multimetallic-dinitrogen complexes and their utility towards N_2 activation, beginning with the *d*-block metals from Group 4 to Group 11, then extending to Group 13 (which is exclusively populated by B complexes), and finally the rare-earth and actinide species. The review considers all polynuclear metal aggregates containing two or more metal centers in which dinitrogen is coordinated or activated (*i.e.*, partial or complete cleavage of the N_2 triple bond in the observed product). Our survey includes complexes in which mononuclear N_2 complexes are used as building blocks to generate homo- or hetero-multimetallic dinitrogen species, which allow one to evaluate the potential of heterometallic species for dinitrogen activation. We hightlight some of the common trends throughout the periodic table, such as the differences between coordination modes as it relates to N_2 activation and potential functionalization, the effect of polarizing the bridging N_2 ligand by employing different metal ions of differing Lewis acidities. By providing this comprehensive treatment of polynuclear metal dinitrogen species, this Review aims to outline the past and provide potential future directions for continued research in this area.
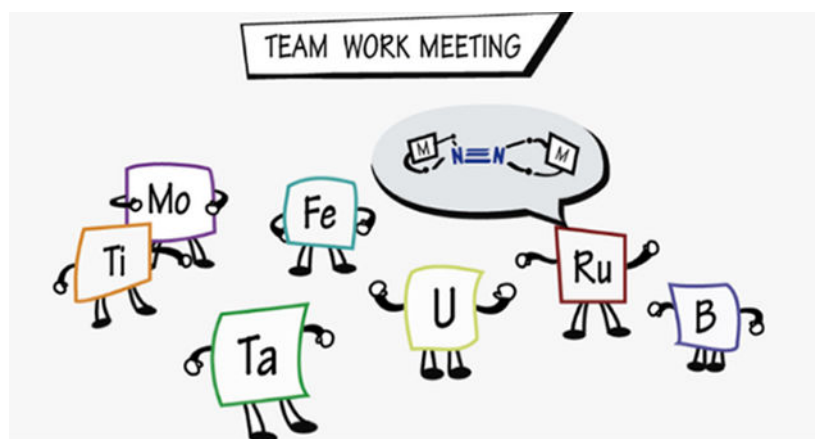
Graphical Abstract

[*]**Corresponding Author:** murray@chem.ufl.edu.

Author Contributions

The manuscript was written through contributions of all authors.

The authors declare no competing financial interests

Keywords

Dinitrogen activation; multimetallic dinitrogen; redox cooperativity; nitrogen fixation

1. Introduction

Dinitrogen activation has attracted substantial research interest for more than a half-century,[1,2] arising from both the societal import of N_2 fixation and the fundamental understanding of the design criteria needed to activate small-molecule substrates. As evidenced by its common use as an inert gas in chemistry, the N_2 molecule is challenging to activate and functionalize, which is attributed to the lack of a dipole moment in the diatomic and the strong π- and σ-bonding interactions prevalent for the second row p-block atoms.[3] Notably, the hydrogenation of dinitrogen is spontaneous under standard conditions with $\Delta G_f^o(\mathrm{NH_3}) = -16.48$ kJ/mol, and the six-electron, six-proton reduction of N_2 to ammonia is moderately endergonic (Scheme 1).[4] It is evident, therefore, that the challenge associated with dinitrogen activation is one of kinetics rather than spontaneity. To highlight this point, the bond dissociation free energy (BDFE) for carbon monoxide (*viz.* 1072 kJ/mol) exceeds that for N_2 (*viz.* 947 kJ/mol). However, CO functionalization has strong precedent (e.g., CO insertion, hydroformylation, Fischer-Tropsch reaction, Water-Gas shift reaction), whereas analogous reactions for dinitrogen remain rare. This difference can be attributed to the superior σ-donor and π-acceptor properties of CO versus N_2.

There are several factors that make N_2 reduction kinetically difficult, with the major hurdle being the large HOMO-LUMO gap of 10.82 eV.[5] Consequently, direct reduction of N_2 is energetically expensive—note the very unfavorable one-electron reduction of N_2 (Scheme 1). Additionally, the low proton affinity and high ionization potential of dinitrogen make direct protonation or oxidative activation of N_2 challenging under standard conditions.[6] The predominant approach for surmounting this kinetic challenge in activating N_2 is to coordinate dinitrogen to unsaturated centers—dinitrogen adducts are known for p-, d-, and f-block elements—followed by intramolecular charge transfer and downstream functionalization of the N_2 fragment. Within this coordination paradigm, however, the lack of a dipole moment and relatively high energy π^* orbitals result in N_2 being a poor σ-donor

and π-acceptor. Thus, the N$\equiv$N bond is not only strong and direct reduction kinetically difficult, but the interactions with a potential reactive atom (*e.g.*, transition metal ion) are also weak.

For mononuclear systems, circumventing these problems typically relies on employing reducing metal centers (*e.g.*, formal Fe^0 centers). An alternative strategy, however, is to coordinate N$_2$ to multiple metal ions to leverage the combined reducing power of the aggregate to activate the bound N$_2$ molecule. One can use this strategy to effect (*i*) N$\equiv$N bond scission to afford diazenido-, hydrazido-, or nitrido-metal species (Scheme 2) or (*ii*) sequential reduction and protonation or hydrogenation of a coordinated N$_2$ in a proton-coupled electron transfer, or PCET (Scheme 3). In the former case, the metal centers backbond into the N$_2$ fragment to generate a formally reduced N$_2$ derived ligand; in some cases, the systems are best described as charge transfer from the reduced metal centers to the N$_2$ ligand. The seminal example of multimetallic cleavage of N$_2$ to metal nitrides is from Cummins and coworkers in which two equivalents of a tris(amido)-molybdenum(III) complex react with one equivalent of N$_2$ to afford the corresponding Mo$^{VI}\equiv$N complex.[7–9] Coupling (*i*) to (*ii*) has also been effective; that is, partial activation of N$_2$ followed by reduction and functionalization to complete dinitrogen bond cleavage.[10]

The PCET approach can operate under two limiting scenarios: a distal or an alternating pathway. The former occurs with protonation of the distal N atom of the bound N$_2$ with reduction ultimately leading to the metal nitride and one equivalent of ammonia. The latter pathway involves alternating protonation of the distal and proximal N atoms to generate diazenide and hydrazide complexes with N–N cleavage resulting in ammonia and metal-amide or ammine products. Yandulov and Schrock reported the first catalytic N$_2$ to NH$_3$ conversion on a monometallic Mo complex by the distal pathway,[11–13] and later work by Peters and coworkers extended such catalysis to monometallic iron complexes.[10,14–22]

Our focus is on multimetallic dinitrogen activation by molecular systems, and specifically, we consider systems in which the dinitrogen-derived bridging ligand(s) coordinated to multiple redox-active centers has been validated experimentally (e.g., X-ray diffraction or absorption spectroscopic methods). Although a number of the compounds presented in this review have been covered by prior reviews by Hidai, Gambarotta, and Fryzuk, these reviews have limited scope (e.g., early transition metals) or have placed particular emphasis on functionalization of the coordinated N$_2$.[23–28] Contrastingly, our goal here is to be comprehensive with respect to known multimetallic-dinitrogen species, and to avoid—where reasonably possible—discussing the downstream reactivity of the coordinated N$_2$. Complementing our efforts here are the reviews by Schneider and Chirik, and their respective coworkers, which focus on metal nitrides and on N$_2$ functionalization and are a part of this special issue.[29,30] Our discussion will begin with the prevalent modes of dinitrogen coordination and highlight the electronic effects necessary to bind and activate the N$\equiv$N bond. Subsequently, we will summarize the reported compounds up to 2019 in order of the *d*-, *p*-, and then *f*- block compounds. In each grouping, we highlight compounds of novel structure types or strategies, such as seminal examples of specific coordination modes. For those examples in which vibrational data are the exclusive criterion for discussion (*i.e.*, structural novelty or proof of concept is not demonstrated), we consider the formally N$_2{}^{2-}$

oxidation level as our benchmark, while acknowledging that the extent of activation is a sliding scale and any potential limiting criteria can be viewed as arbitrary.[31] If vibrational data are lacking for a specific compound, we default to using the imperfect approach of comparing the N–N bond distances to gauge N_2 activation.

2. Dinitrogen Coordination to Multiple Metal Centers

The first example of dinitrogen coordination is the report of the family of $[Ru(N_2)(NH_3)_5]X_2$ complexes ($X = Br^-$, I^-, BF_4^-, and PF_6^-) in 1965 by Allen and Senoff.[32] The infrared spectrum of these complexes evidenced a N–N stretching vibration at ~200 cm^{-1} below that of free dinitrogen (i.e., 2170–2115 cm^{-1} for the complexes vs. 2359 cm^{-1} for N_2). Shortly thereafter, Taube reported that this ruthenium-dinitrogen adduct reacts with the aqua precursor $[Ru(NH_3)_5(OH_2)]^{2+}$ to afford a (μ–1,2-dinitrogen)diruthenium species, $[Ru(NH_3)_5]_2(\mu$–1,2-N_2), providing the first example of a dimetallic dinitrogen complex.[33] The N–N stretching mode was assigned to a weak absorption at ~2060 cm^{-1} for the tetrafluoroborate salt, lower than that for the monometallic complex. Indeed, this trend of greater extent of activation of the N_2 ligand based on vibrational spectroscopy is generally observed for multimetallic species. A similar trend is well documented for metal carbonyl complexes wherein bridging modes result in markedly lower C≡O vibrational frequencies, but do not correlate with substantially elongated C≡O bond lengths in solid state structures. Thus, the aggregate effects greater overall activation of N_2, although each metal-dinitrogen interaction in the multimetallic is on average weaker than many comparable monometallic species.

Since that initial report of the μ–1,2 mode for dinitrogen coordination, a number of compounds containing up to four metal centers have been isolated and characterized with the growing body of work suggesting preferred coordination modes of dinitrogen in multimetallic systems.[23,28] Coordination modes observed hitherto are depicted in Figure 1.

To simplify our analysis of coordination modes, we exclude *s*-block metals in our description of multimetallic coordination modes and consider only the connectivity of the redox active centers (e.g., *d*-block metal) and dinitrogen donor. Given the requirement for π-backbonding interactions to stabilize the metal-dinitrogen adduct, almost all reported examples employ low-valent metal centers and greater N_2 activation is typically observed for the more electropositive early transition metals as compared to the late transition metals.

Beginning with the simplest scenario, two commonly observed coordination modes for dinuclear-dinitrogen adducts are the μ–1,2 or μ-η^2:η^2 modes (Figure 2). The former, also known as an end-on/end-on bridging mode, results in near linear M–N–N–M units for the *d*-block elements as such an arrangement maximizes the π-backbonding interaction between the metal d_π and N_2 π^* orbitals. The second common dimetallic-dinitrogen coordination mode, *viz.* the μ-η^2:η^2 or side-on/side-on, has not been reported for molecular complexes comprising late transition metals, but rather is only observed for the early transition metals and for *f*-block compounds. Similar M–N_2 π-backbonding interactions as for the μ–1,2 mode are present here with the planar M–N_2–M favored as compared to the butterfly geometry (Figure 1). The primary difference that arise from the dinitrogen orbitals involved

in the M–N$_2$ σ interaction is that the highest energy filled σ_g^+ orbital of N$_2$ acts as the σ donor for the linear arrangement, whereas a π bonding orbital for the side-on/side-on mode. The preference for the μ–1,2 vs. μ-η^2:η^2 modes depends on steric effects enforced by the supporting ligand, metal-ion type, formal oxidation state, and coordination number; the latter three influence the energies of the metal orbitals needed to constitute the σ- and π-bonds for the M–N$_2$ unit.[34] Finally, the rarest dimetallic coordination mode for N$_2$ is the μ-η^1:η^2 mode, which has only been reported for Ti, Zr, and Ta. DFT calculations on Ta complexes of this type evidence π-backbonding interactions between the metal d_π orbitals and the N$_2$ π* and the σ-bonding from the $3\sigma_g$ orbital of N$_2$ and one Ta center (η^1) and the filled π-bond of the N$_2$ to the other Ta center (η^2).[35] As one might predict, this coordination mode polarizes the N$_2$ ligand, allowing for facile asymmetric functionalization by electrophiles.

Few examples of μ_3- and μ_4-dinitrogen complexes have been reported as compared to the dimetallic cases. One can consider these coordination modes as extensions of the dinuclear cases; indeed, in almost all cases related dinuclear fragments have been reported. Homonuclear trimetallic examples are only reported for Ta, Ti, and Cu as well as a handful of heterometallic M$_2$M′ compounds (M′ = Group 13 center) for which the formally redox-neutral Group 13 electrophile functionalizes a precursor μ-η^1:η^2 complex. The μ_3-η^2:η^2:η^2-dinitrogen is only known for Sm wherein the Sm$_3$N$_2$ core is pseudo-C_{2v} symmetric with a near planar Sm$_2$(μ-η^2:η^2-N$_2$) fragment. Lastly, the μ_4-η^1:η^2:η^2:η^1 mode is only reported thus far for two tetrasamarium complexes. A number of examples of this bridging mode are, however, known if one substitutes one of the redox active metal centers for an *s*-block metal ion. In this mode, the M$_4$N$_2$ core is approximately planar with a near linear M$_2$(μ–1,2-N$_2$) fragment as one might anticipate from our discussion of the μ-η^2:η^2 and the μ–1,2 coordination modes.

3.   Dinitrogen Activation by Multimetallic Complexes

As noted above, the report by Taube and coworkers of the μ–1,2-dinitrogen diruthenium complex was the first example of multimetallic dinitrogen activation. Our survey below begins with the *d*-block metals starting with Group 4 and ending with Group 11, followed by considering N$_2$ activation by boron compounds, which is the only representative from Group 13. Lastly, we review the literature on complexes of the rare earth elements and actinides. We consider cases in which the metal centers are redox-active and the N$_2$ fragment is derived from atmospheric dinitrogen; thus, complexes in which a monometallic-dinitrogen species is capped by a borane, alane, or other Lewis acid are omitted. One observes the following. First, greater activation of the N$_2$ unit for the second and third row transition metal complexes as compared to the analogous first row compounds in the early *d*-block with that trend eroding as one moves to the later transition metals. Second, greater activation of bound N$_2$ for the earlier more electropositive metals as compared to the late transition metals. This latter trend is consistent with the greater reducing strength and stability of higher oxidation states of early vs. late metals, leading to greater charge transfer to the dinitrogen ligand. The trend is consistent with the classical ligand field picture wherein the metal is considered as the Lewis acid and the ligand as Lewis base (i.e., metal orbitals are significantly higher in energy than the ligand orbitals); greater covalency is observed for the

late transition metals as a consequence of the closer energy match between the metal and ligand valence orbitals. Finally, access to the metal center as dictated by the ligand sterics tunes the complex nuclearity, allowing for isolation of discrete mono- and multi-metallic dinitrogen adducts, and also the extent of N_2 bond activation.

3.1. Group 4: Ti, Zr, Hf

In this section, we begin with dinitrogen adducts of bis(cyclopentadienyl)metal complexes as these complexes constitute the most well explored and largest family of metal-dinitrogen species in Group 4. That discussion is followed by the mono-cyclopentadienyl compounds, then the tetra- and tridentate PN ligand systems—many of which have both Ti and Zr complexes reported—and then complete our survey with the ligands for which only titanium examples have been reported.

3.1.1. Metallocene, *ansa*-metallocene, and related complexes.—In the 1960s, van Tamelen and coworkers first proposed that divalent titanium complexes were capable of binding dinitrogen reversibly and able to effect N_2 fixation to N_2H_4 and NH_3 and organic amines.[36] Shortly thereafter, Britzinger and coworkers proposed that a metastable [bis(η^5-cyclopentadienyl)titanium(II)] (μ-dinitrogen) or $(Cp_2Ti)_2(\mu-N_2)$ was accessible from the related monometallic hydride species;[37,38] however, sp^2 C–H activation by the low valent Ti center limits the stability of this species. Bercaw and coworkers substituted C–H for C–CH$_3$ on the Cp$^-$ ring, which limited degradation and sufficiently stabilized the dinitrogen adduct to allow for its characterization. Reaction of bis(η^5-pentamethylcyclopentadienyl)titanium(II) or decamethyltitanocene (Cp*$_2$Ti) with N_2 affords $(Cp*_2Ti)_2(\mu-1,2-N_2)$, **1-Cp***.[39] The solid state structure evidences a μ–1,2-dinitrogen ligand with a N–N bond length of 1.165 Å and Ti–N distance of 2.005–2.016 Å.[40] (Figure 3). The former metric is lengthened relative to free N_2 and comparable to that for N_2^{2-}, implying significant charge transfer and formal reduction of the dinitrogen ligand. In the years since this initial report for titanium, numerous other dinitrogen-metallocene compounds employing Group 4 metal ions have been reported with many notable examples reported by Chirik and coworkers. These complexes can be divided into three categories: the (μ–1,2-dinitrogen)bis(metallocene) species or type **A** (Figure 3), the (μ-(η^2:η^2)-dinitrogen)bis(metallocene) compounds or type **B** (Figure 5), and the (μ–1,2-dinitrogen)bis(metallocene) species supported by additional terminal, monodentate L- or X-type donors or type **C** (Figure 8, Figure 9). As one might predict, these categories are closely related with minor changes in ligand sterics resulting in a transition from **A** to **B**, or by addition of exogeneous ligands to **A-** or **B**-type compounds yielding the related type **C** complex. In addition, *ansa*-metallocene complexes related to **A-C** are also known.

Extending the work of Bercaw and Teuben and their respective coworkers, Hanna and Chirik reported a series of (μ–1,2-dinitrogen)bis(titanocene) adducts in which the sterics of the Cp$^-$ ring are systematically varied. Across the series, one notes comparable N–N bond distances for the μ–1,2-dinitrogen complexes supported by cyclopentadienyl donors, with values ranging from 1.157(1) in **1-Cp^{Me4,Xyl}** to 1.170(4) Å in **1-Cp′** (Figure 3).[41–44] Similar N–N bond distances are also observed for the (μ–1,2-dinitrogen)bis[(η^5-fulvene)(η^5-cyclopentadienyl)titanium) complexes **2-(*p*-tol)$_2$** and **2-Ad** (1.216(3) and 1.216(5) Å,

respectively) in which the substituent on the fulvene varies.[45,46] The comparable distances across the series reflect the constant formal oxidation states of the titanium centers as well as dinitrogen coordination mode. Reducing the sterics on the cyclopentadienyl ring results in a change to the μ-η^2:η^2 coordination mode for the dinitrogen ligand in the titanium complexes. For example, substituting one methyl group on each Cp^- ring in **1-Cp′** for an H atom yields the μ-η^2:η^2-dinitrogen complex in **1-Cp^{Me124}** (Figure 5).[42] A similar structure is observed for **1-Cp^{Me1iPr3}** and **1-Cp^{iPr13}**, and all three examples have comparable N–N bond lengths of ~1.21 Å.[47] Reducing the sterics from **1-Cp^{Me124}** by employing 1,3-dimethylcyclopentadienyl yields instead a trimetallic complex **1-Cp^{Me13}** in which C–H activation and C–C bond formation affords a dianionic fulvalenide ligand (Figure 4).[47] Notably, the three Ti centers in **1-Cp^{Me13}** result in one of the longest N–N bond distances for a titanocene type dinitrogen complex at 1.320(3) Å. Compound **1-Cp^{Me13}** bears similarity to the previously reported tetratitanium complex, **1-Cp**, from Pez and coworkers. Similar to **1-Cp^{Me13}**, C–H activation is observed during the reaction of (μ-η^1:η^5-cyclopentadienyl)(tris-η^5-cyclopentadienyl)dititanium with dinitrogen to afford [(η^5:η^5-$C_{10}H_8$)(η^5-Cp)$_2$Ti$_2$][μ-η^1:η^5-C_5H_4)(η^5-Cp)$_3$Ti$_2$]-(μ_3-η^1:η^2:η^1-N_2), **1-Cp**, from (Figure 4).[48] This reaction may proceed through the metastable blue (Cp_2Ti)$_2$(μ-N_2) species with C–H activation and H_2 elimination leading to C–C coupling to afford **1-Cp**, although detailed mechanistic studies have not been communicated.

Given the sensitivity of coordination mode on cyclopentadienyl substitution, the Zr and Hf congeners of the (μ–1,2-dinitrogen)bis(metallocenes) have not been observed; the larger ionic radii of Zr and Hf as compared to Ti counterpoise the steric constraints imposed by the cyclopentadienyl donors. The (Cp^R_2M)$_2$(μ-η^2:η^2-N_2) complexes (M = Zr or Hf) are exclusively observed for the mono-dinitrogen species. The Group 4 bis(metallocene)-dinitrogen adducts show increasing formal reduction of the N_2 ligand as one transitions from Ti to Zr and Hf. Magnetic susceptibilities of 2.7(2) μ_B and 2.2(2) μ_B in the solid phase and benzene solution for **1-Cp^{Me124}**, respectively, suggests two d^1 Ti(III) centers and consequently a formally diazenide ligand in line with the N–N bond distance (1.216(3) Å) and is further supported by the N–N stretching frequencies of 1742 and 1747 cm^{-1} for **1-Cp^{Me1iPr3}** and **1-Cp^{iPr13}**, respectively (N–N stretching frequency was not reported for **1-Cp^{Me124}**).[49,50] These data contrast the longer N–N bond distances (1.377(3) Å for **3-Cp′** and 1.423(11) Å for **4-Cp′**) for the Zr and Hf congeners and much lower ν_{N-N} of 922 cm^{-1} for **3-Cp′** pointing towards hydrazide level of reduction.[51–53] One notes that the Zr and Hf compounds have similar N–N bond distances that range from 1.377(3) Å for **3-Cp′** to 1.47(3) Å for **3-Cp^{TMS13}** and 1.423(11) Å for **4-Cp′** to 1.457(7) Å for **4-Cp^{Me124}** (Figure 5).[53–56] Unlike other bis(metallocene)-dinitrogen complexes prepared by chemical reduction of a metallocene halide precursor under an N_2 atmosphere, **3-Cp′** has also been synthesized by reductive elimination of the aryl groups in (η^5-Cp′)$_2$Zr(Ar)$_2$ (Ar = 4-Me-C_6H_4, C_6H_5, 4-Et-C_6H_4, 4-Ph-C_6H_4) under photochemical conditions.[57]

A comparison of the structures of the (μ-η^2:η^2-dinitrogen)bis(metallocene) for titanium, zirconium, and hafnium evidences two notable differences: First, the angle between the two centroid-metal-centroid planes of each metallocene unit (θ), or the angle between the wedges of each metallocene, is close to zero for the Ti compounds, but > 49° for the Zr and

Hf congeners except **3-Cp^{TMS13}**. Second, the dihedral angle between the M_2N_2 plane and the centroid-metal-centroid planes of each metallocene is nearly perpendicular for Ti, but more acute for the Zr and Hf analogs (Figure 5). DFT calculations reveal the consequence of the twists observed in the Zr and Hf congeners as compared to the Ti analogs (i.e., the two noted dihedral angles are non-zero): a π-bonding interaction between the out of phase linear combination of the frontier $1a_1$ orbitals on each metallocene fragment and the π^* orbital on N_2 leads to a metal-imide type bonding picture in Zr and Hf, whereas the coplanar wedges and the perpendicular relationship to the Ti_2N_2 plane lead to minimal—if any—multiple bonding character between the metal centers and the N_2 atoms.[58]

The *ansa*-metallocenes accentuate the mixing of the metallocene frontier orbitals to favor interactions with the non-cyclopentadienyl ligands. Consequently, one might anticipate that transitioning from the metallocene to the *ansa*-bridged congeners will favor π-backbonding into the N_2 bridge. Despite the expected electronic benefit, the greater steric constraints in the reported *ansa*-metallocene compounds prevents a faithful comparison. For example, only a minimal increase in the N–N distance is observed for the μ–1,2-dinitrogen dititanium complexes **5–1** and **5–2** (Figure 6) with values of 1.174(3) Å and 1.165(3) Å as compared to the non-*ansa* congeners **1-Cp^R**.[42] Similarly, the side-on/side-on dinitrogen-bridged bis(*ansa*-zirconocene) and bis(*ansa*-hafnocene) compounds demonstrate a comparable extent of N–N bond lengthening with values of 1.406(4) Å in **6–2** for Zr and 1.457(5) Å in **7** for Hf (Figure 7), which are within range for the non-*ansa*-metallocene compounds.[59,60] Of particular note is the more sterically-encumbered bis(*ansa*-zirconocene)-dinitrogen compound **6–1**, in which a short d(N–N) of 1.241(3) Å is observed for the N_2 ligand.[61]

Two general trends for Group 4 dinitrogen compounds are that (*i*) coordination of a terminal X or L type donor on each metal ion in the bis(metallocene)-dinitrogen adducts affords the μ–1,2-dinitrogen complexes, and (*ii*) increasing donor strength of the terminal X or L type ligand leads to greater activation of the μ–1,2-dinitrogen. The coordination isomerization and donor strength effect are most apparent from the following cases. First, similar d(N–N) values are observed for the formally Ti^{II} complexes **1-Cp^R** to the formally Ti^{III} complex **8-Cp,p-tolylide** (1.162 Å) and bond lengthening for **8-Cp,PMe$_3$** (1.191 Å) (Figure 9).[62,63] Second, the *ansa*-titanocene in **8-*ansa*** comprises has a slightly contracted bond distance as compared to the **5–1** and **5–2** as a consequence of the weak π-acidity of the terminal N_2 donors (Figure 10).[42] Third, the formally Zr^{II} complex **9-Cp*** and the formally Zr^{III} complex **9-Cp,X** and the mixed-valent congener **Na[9-Cp,X]** where X = bis(trimethylsilyl)methyl also have comparable bond lengths (Figure 8 and Figure 9).[64] Chirik and coworkers demonstrated through isotopic labeling studies that **3-Cp′** can coordinate additional dinitrogen donors to generate the **Cp′** congener for **9-Cp***, evidencing the sensitivity of the coordination mode to the presence of an ancillary donor.[55] One notes that the minimal change in bond length upon reduction of **9-Cp,X** to **Na[9-Cp,X]** suggests zirconium-centered reduction rather than dinitrogen-based.

Related to these Zr complexes is **10-A** (Scheme 4) in which the terminal chloride donors do not result in a change in coordination mode.[64] However, one-electron reduction of **10-A** results in a change in mode—which is reversible upon oxidation—to the μ–1,2 mode with close Cl···K$^+$ and N_2···K$^+$ contacts (**10-B**). A related di-hydride congener of **10-A** (^{t}Bu

instead of Ad) has also been reported and the N–N bond length of 1.243 Å is substantially shorter than that for **6–2**, highlighting both the oxidation state change as well as electronic structure changes resulting from having two ligands in the equatorial plane of the *ansa*-metallocene.

Fourth, the Hf analog **4-Cp′** undergoes coordination isomerization of the N_2 donor upon dimetallic oxidative addition. Reaction of **4-Cp′** with alkyl halides, R–X (X = Cl, Br, I), initially afford the corresponding μ–1,2-dinitrogen complexes **11-R/X** with the R and X coordinated to different Hf centers; disproportionation of these products yields **4-Cp′** and the monometallic Cp′$_2$Hf(R)(X) species.[65] The oxidative addition has radical character based on reaction with radical clock substrates wherein the ring opened or cyclized products are observed in **11-R/X** (Scheme 5). Oxidative addition of MeOTf is unique relative to the alkyl halides as ethane is produced and **11-OTf$_2$** is the major complex product.[66] The bond distances across the **11** series of complexes are comparable. Finally, the bis(hafnocene)-dinitrogen species **4-Cp^{Me124}** reacts with 4-(dimethylamino)pyridine (DMAP) to yield the mono(DMAP) adduct **12** (Figure 11). Isomerization is not observed and the N–N distance contracts substantially relative to **4-Cp^{Me124}**. The absence of isomerization and the N–N contraction are proposed to arise from the less steric encumbrance of the **Cp^{Me124}**, as compared to the other bis(hafnocene) compounds, and the lengthening of the Hf···Hf distance upon coordination of DMA from 3.8527(3) Å in **4-Cp^{Me124}** to 3.9406(13) Å in **12**, respectively.

The mixed indenyl-cyclopentadienyl zirconium complexes also allow access to dimetallic-dinitrogen species. In these complexes, the expanded donor properties of the 10 π-electron indenyl allow access to μ-indenyl species with closer metal-metal contacts. Two reduction outcomes were reported for the Cp*(η^5-Ind^{R1,R2})ZrCl$_2$ complexes (R^1/R^2 = Me/Me, iPr/Me, tBu/Me; Scheme 6).[67] Reduction under Ar occurs with chloride loss and generates the (η^9-Ind^{R1,R2})Cp*Zr^{II} complexes, **13-R^1/R^2**. Exposure of **13-R^1/R^2** to dinitrogen yields the *cis-μ*–1,2-dinitrogen complexes (η^5:η^2-Ind^{R1,R2})$_2$(Cp*Zr)$_2$(μ–1,2-N$_2$), **13N$_2$-R^1/R^2** with Zr–N–N bond angles of ~144° and a N–N bond distance of 1.197(3) Å ($\nu_{N–N}$ = 1563 cm^{-1}); this coordination mode is rare in dinitrogen coordination chemistry. The second outcome arises from reduction of the dichloride species in the presence of dinitrogen, which yields the chloride- and dinitrogen-bridged complexes [Cp*Zr]$_2$(η^4:η^5-Ind^{R1,R2})(μ-η^1:η^2-N$_2$)(μ-Cl), **14-R^1/R^2** (Scheme 6). The disposition of the indenyl substituents relative to the chloride and dinitrogen ligands affords two isomers, which evidence nominally different crystallographic parameters: the N–N distances are 1.196(4) Å and 1.220(10) Å for the *syn* and *anti* isomers of **14-iPr/Me**, respectively.

The bis(η^5-indenyl)zirconium complexes are also competent for N_2 activation. Addition of excess sodium-mercury amalgam (Na/Hg) to the dihalide complexes affords the dinitrogen-bridged dizirconium complexes **15-Na$_2$X$_2$** of which the chloride and the iodide congeners were structurally characterized (Scheme 7).[68] The N–N bond distances in **15-Na$_2$X$_2$** (1.352(5) Å and 1.316(5) Å for Cl and I, respectively) are comparable to that in the μ-η^2:η^2-dinitrogen complex **9-Cp′**, albeit with **15-Na$_2$X$_2$** being two electrons more reduced that **9-Cp′**. Compared to **13N$_2$-R^1/R^2** and **14-R^1/R^2**, the absence of π-backbonding from Zr to the

benzo unit of the indenyl donor in **15-Na$_2$X$_2$** affords more electron-rich metal centers, leading to greater activation of the μ–1,2-dinitrogen.

A few examples of Group 4 mono-cyclopentadienyl complexes supported by additional ancillary ligands have also been reported to coordinate dinitrogen. The chemistry of a family of *trans* bis(Cp*-amidinato/guadinato-metal)-dinitrogen complexes, **16** and **17**, has been advanced by Sita and coworkers (Figure 12 and Figure 13).[69,70] The bond metrics and angles for **16** bear a strong resemblance to the related β-diketiminate complex from Bai, *et al.* (**18**, Figure 14), as one might anticipate from a similar donor atom set.[71] An end-on/end-on mode is observed for **16** whereas a side-on/side-on mode are observed for the zirconium and hafnium analogs, **17**, consistent with the observations for the bis-metallocene compounds. The N–N bond distance increases from the lighter metal to the heavier counterparts with the hafnium congeners showing the longest N–N bond lengths reported of any Group 4 metal dinitrogen complex. In contrast to the bis-metallocene complexes, the M$_2$N$_2$ core is bent in a butterfly orientation rather than planar, with dihedral angles ranging from 20.0° in **17-C** to the two largest values of 31.3° and 33.3° in **17-E** and **17-D**, respectively. This bending is correlated with π-backdonation from each metal center to orthogonal π* orbitals on the N$_2$ fragment. These complexes boast the longest N–N distances in a dimetallic complex with values almost 0.2 Å greater than that in hydrazine.[49,51] Impressively, the N atoms in **17-D** and **17-E** can be alkylated with alkyl bromides—the first such example for any N$_2$ derived complex. A side-product containing a bromide bonded to each hafnium centers {Cp*Hf(Br)[N(Et)C(Me)N(Et)]}$_2$(μ-η^2:η^2-N$_2$) was observed for reaction of **17-E** with alkyl bromides.

In addition to the Sita and Stephan examples above, Nishibayashi and Hou have reported the remaining examples of mono-cyclopentadienyl complexes. Nishibayashi and coworkers accessed *cis*-μ–1,2-dinitrogen complexes of titanium and zirconium supported by a PNP pincer ligand and cyclopentadienyl (Figure 15).[72] Here, the PNP pincer ligand coordinates in a κ^2NP fashion in the case of Ti (**19-Ti**) affording a three-legged piano stool geometry with one dangling phosphine arm whereas the pincer coordinates κ^3PNP for the Zr congener (**19-Zr**) resulting in a four-legged-piano-stool geometry. The M$_2$N$_2$ core deviates significantly from linearity with Ti–N–N angles of 158.9° and 159.6° for **19-Ti** and 163.7° for **19-Zr**, and the N–N bond distances are comparable to previously discussed μ–1,2-dinitrogen compounds with values of 1.247(3) Å and 1.287(4) Å for **19-Ti** and **19-Zr**, respectively.

As noted above, one expects a linear M$_2$(μ–1,2-N$_2$) unit to maximize π-backbonding to the bound N$_2$ in these complexes. The deviations from linearity observed for a number of Group 4 complexes with elongated N–N bonds hint at charge transfer and decreased covalency for Ti, Zr, and Hf as compared to the late transition metals.

Notable among the previously discussed mono-cyclopentadienyl compounds is the example from Hou and coworkers, which is the first example of complete scission of N$_2$ by a titanium hydride complex.[73] Hydrogenolysis of (η^5-C$_5$Me$_4$SiMe$_3$)Ti(CH$_2$SiMe$_3$)$_3$ (**20-alk$_3$**) with H$_2$ affords heptahydride **20-H$_7$**, which readily cleaves N$_2$ to yield tri-titanium complexes with μ_3-nitride, μ-imide, and μ-hydride donors (Scheme 8). Cotreatment of **20-alk$_3$** with H$_2$ and N$_2$ instead generates a tetra-titanium complex with a cubane-like cluster containing two μ_3-

imides arising from N_2 bond scission. ^{15}N NMR kinetic studies at low temperature suggested a hydrazide intermediate; further characterization of this temperature-sensitive transient, however, has yet to be reported.

3.1.2. Tetra- and tridentate PN and related ligand complexes.—In addition to the Cp-ligated titanium centers, other supporting ligands have been utilized for coordination and activation of dinitrogen. A common aspect, however, remains the use of reducing titanium(II) or (III) species generated either *in situ* or first isolated.

Fryzuk and coworkers have utilized a tetranucleating $P^{Ph}{}_2N_2$ ligand to support dimetallic Ti and Zr dinitrogen complexes generated by reduction of the dichloride precursor with KC_8 (Figure 16)[74,75] In a theme repeated from the metallocene examples, the Ti_2 complex **21** is an end-on/end-on complex, whereas the Zr_2 analog is a μ-η^2:η^2- dinitrogen complex. In both complexes the N–N bond is quite elongated; the bond is of the order of hydrazide for **22-N₂** and the value in **21** is on par with those reported by Sita and coworkers (*viz.***16**). Compound **22-N₂** reacts with dihydrogen in toluene to afford **22-N₂H/H** in which N–H and Zr–H bonds are formed—the first example of Haber-Bosch-like reactivity in a molecular system (Scheme 9). The N–N bond contracts from **22-N₂** to **22-N₂H/H** (1.389 Å), suggesting oxidation of the N_2 ligand in **22-N₂** to facilitate Zr–H bond formation. A theoretical study on P_2N_2-Zr complexes shows a preference for folding the Zr_2N_2 core as the system becomes less sterically encumbered.[76] The electronic rationale for the bending in the absence of steric conflicts is that bending leads to more uniform distribution of electron density between the Zr centers and N_2 and enhance π bonding from the amide lone-pairs to Zr.[77]

Removal of a phosphine donor arm in **21** (*viz.* from $P^{Ph}{}_2N_2$ to $P^{Ph}N^{Ph}{}_2$) results in a dramatic change in the reduction outcome in the case of titanium: complete scission of the N–N bond and insertion of N atoms into the Ti–P bonds is observed.[75] The reaction is proposed to proceed with initial N_2 cleavage to the di(μ-nitride) followed by N-atom insertion to yield the observed product, **23** (Scheme 10). Contrastingly, the side-on/side-on bridged dizirconium complex **24** is isolable and is analogous to **22-N₂** if one accounts for substitution of a THF donor for the second phosphine arm (Figure 17). Although a titanium analog has not been reported, the $P^{tol}N^{Mes}{}_2$ ligand stabilizes a similar $Zr_2(\mu$-η^2:η^2-$N_2)$ species, **25–2THF**, in which THF coordinates to the metal center as in **24** (Figure 18). The solvent molecules in **25–2THF** can be readily substituted for pyridine or $PhPMe_2$ to afford the **25–2py** and **25-PR₃**, respectively, and with comparable N–N bond distances to that in **25–2THF**. In **25-PR₃**, only one $PhPMe_2$ is coordinated to the dimetallic, presumably because of steric crowding of the mesityl substituents. For **24** and the **25** series, the ZrN_2 plane contains the P-donor atom of the $P^RN^R{}_2$ ligand with the two zirconium-amide bonds lying perpendicular to that plane, likely arising from the favorable interactions from the π-donating amides. The similar N–N bond distances for **24** and the **25** series are noted despite the planar Zr_2N_2 unit in **24** vs. the slightly bent one in **25** (12.3°–15.4°). Similar H_2 activation is observed for **25-PR₃** as for **22-N₂** with formation of a Zr–H and N–H bonds.

Arnold and coworkers reported the di-titanium and dizirconium dinitrogen complexes bearing the tripodal $P_2^{Me2}N_2^{tBu}$ ligand (Figure 19).[78] In spite of the four pnictogen donor atoms afforded by the ligand, dinitrogen complexes **26-Ti/CH₂SiMe₃** and **26-Zr** retain only

κ^3NNP coordination to the metal centers with a halide or alkyl completing the metal coordination sphere. In the solid-state structure of these complexes, each metal center is penta-coordinate with one non-coordinated phosphine arm, likely due to steric congestion around the metal centers. The μ-η^2:η^2 mode is observed for **26-Zr** and the N–N distance is the longest reported for any dizirconium dinitrogen complex. The purported chloride analog **26-Ti/Cl** has an IR absorption at 1300 cm^{-1} attributed to the N–N stretching mode, comparable to that for **26-Ti/CH$_2$SiMe$_3$** (1270 cm^{-1}), implying that both complexes adopt a similar coordination mode.

Completing the combination of tridentate PN donor ligands are the PNP pincer type complexes reported by Hou (Ti, **27**) and Fryzuk (Zr, **28-X**) and their respective coworkers (Figure 20). The hydrogenation of a PNP-ligated organotitanium complex with H$_2$ yields the related titanium tetrahydride compound, which undergoes reductive elimination in the presence of N$_2$ to form $\{[(N^{PhPiPr}_2)Ti]_2(\mu\text{-}\eta^1:\eta^2\text{-}N_2)(\mu\text{-}H)_2\}$, **27**.[79] The N–N bond at 1.301(3) Å is one of the longest reported for any titanium complex, only exceeded by those distances in the titanotrane complexes (*vide infra*). As noted by van Tamelen,[36] a broad range of Ti complexes are competent for the partial or complete cleavage of N$_2$ to generate hydrogenated N$_2$ derived species and **27** is no exception; further reaction of **27** with H$_2$ effects N$_2$ cleavage and formation of a dititanium(IV) complex comprising N$_2$-derived μ-imide and μ-nitride ligands.

A related meridionally-coordinating ligand to that in **27** is the diarylether-dianilide pincer-type ligand that provides access to the μ–1,2-dinitrogen adduct, $[(^{iPr}NON)Ti(PMe_3)_2]_2(\mu$–1,2-N$_2)$ (**29**, Figure 21).[80] The synthesis proceeds through a proposed decomposition of $(^{iPr}NON)Ti(CH_2CHMe_2)_2$ in the presence of PMe$_3$ through β-hydride elimination, followed by H$_2$ reductive elimination, and then N$_2$ coordination. The N–N bond distance of 1.264(8) Å in **29** is expectedly shorter than that in **27** given the weaker donor strength of the ethereal oxygen atom.

Rettig, *et al.* reported the PNP pincer ligated Zr$_2$N$_2$ complex **28-Cl**,[81] which is conceptually related to **22-N$_2$** by removal of N donor; in fact, the N$_2$P ligands in **24** and **28-X** are conceptual deconstructions of the N$_2$P$_2$ macrocycle in **22-N$_2$**. The N–N bond length observed in the solid-state structure of **28-Cl** is 1.548(7) Å, which is one of the longest distances reported for any dinitrogen complex to date. Replacing the chloride with Cp$^-$ results in the formation of an end-on/end-on dinitrogen complex **28-Cp** as Cp$^-$ competes for metal π-backbonding interactions as well as introducing steric repulsions between Zr fragments.[34] To further highlight the electronic effects, the related aryloxide complexes **28-OAr** (ArO$^-$ instead of Cl$^-$) also afford the side-on/side-on complex $\{[(Pr^i_2PCH_2SiMe_2)_2N]Zr(OAr)\}\}_2(\mu\text{-}\eta^2:\eta^2\text{-}N_2)$ with a similar N–N bond length (1.528(7) Å) to the chloride congener.[82]

A few examples of ligands have been used in which only titanium-centered complexes are reported. Gambarotta and coworkers reported the first example of a titanium dinitrogen species without using cyclopentadienyl donors: $[Ti(TMEDA)(N(Me_3Si)_2)Cl]_2(\mu$–1,2-N$_2)$, **30** (Figure 22).[83] This complex was isolated from reaction of 1 equiv. LiHMDS with *trans*-Ti(TMEDA)$_2$Cl$_2$ and displayed an elongated N–N bond and short Ti–N(N$_2$) bonds with

distances of 1.289(9) and 1.762(5) Å, respectively, consistent with a diazenide (N_2^{2-}) complex. Contrastingly, upon addition of 2 equiv. LiHMDS to Ti(TMEDA)$_2$Cl$_2$, the formally dititanium(I/II) bis(μ-η^2:η^2-dinitrogen) complex, [Li(TMEDA)$_2$] [{(Me$_3$Si)$_2$N]$_2$Ti}$_2$(μ-η^2:η^2-N$_2$)$_2$], is isolated (**31**, Figure 22).[83] The N–N bond length (1.379(21) Å) is longer than the end-on/end-on complex as one might anticipate and suggests a formally $N_2^{3-/4-}$ ligand with Ti^{III} centers.

Despite extensive precedent for N$_2$ transformation to NH$_3$ and N$_2$H$_4$ by protonolysis or hydrogenation of dinitrogen adducts from late transition metals, examples of catalytic dinitrogen fixation employing titanium—or more broadly, any metal complex preceding Group 6—were unknown until recently. Doyle *et al.* provided the first such example based on titanatrane complex **32**, [(tren^{TMS})Ti]$_2$(μ–1,2-N$_2$) (tren^{TMS} = [N(CH$_2$CH$_2$NSiMe$_3$)$_3$]$^{3-}$) (Scheme 11).[84] The short N–N distance of 1.121(6) Å, observed X-band EPR signals, and solution magnetic susceptibility data agree with formally Ti^{III} centers in **32**. Data on the related two-electron reduced complexes K$_2${[(tren^{TMS})Ti]$_2$(μ–1,2-N$_2$)} or **32-red**, and [K(benzo-15-crown-5)]$_2${[(tren^{TMS})Ti]$_2$(μ–1,2-N$_2$)} or **32-crown** provide evidence for the significant N$_2$ π* character in the LUMO of **32**. Briefly, the ~0.2 Å increase in the N–N bond length, shorter Ti–N(N$_2$) distances, decreased N–N stretching frequency (1701 cm^{-1} vs. 1201/1246 cm^{-1} for **32** vs. **32-red/30-crown**), and calculated Mayer bond orders for the Ti–N(N$_2$) and N–N bonds are all consistent with reduction of **32** populating an orbital with significant N$_2$ π* character (Scheme 11). Notably, encapsulation of the K$^+$ ions in **32-red** to afford **32-crown** leads to an increase in the N–N stretching frequency, suggesting an electrostatic contribution from the close association of the K$^+$ cations with the N$_2$ ligand in **32-red**. Protonolysis of **32-red** affords predominantly N$_2$H$_4$ (0.88 equiv.) together with a smaller amount of NH$_3$ (0.13 equiv.). Complex **32-red** is competent for atmospheric N$_2$ fixation to ammonia, using [Cy$_3$PH][I] and KC$_8$ as the proton and electron source, respectively, with the optimized conditions afford 18 equiv. NH$_3$ per **32-red**.

A bis(titanatrane) dinitrogen complex **33**, [[K(THF)$_2$][K$_2$(μ-THF)]{[O$_3$C]Ti)$_2$(μ–1,2-N$_2$)}]$^-$, from Nakanishi *et al.* bears structural similarity to **32-red** ([O$_3$C]$^{4-}$ = [(3,5-^{t}Bu$_2$-2-O-C$_6$H$_2$)$_3$C]$^{4-}$, Figure 23).[85] The N–N bond length (1.320(5) Å), short Ti–N bond distances (1.797(4)–1.802(4) Å), and the N–N stretching frequency (1265 cm^{-1}) support Ti–N multiple bond character and a $N_2^{2-/4-}$ formalism and are comparable to those values reported for **32-red**. The reduced dinitrogen fragment in **33** reacts in a nucleophilic fashion with CO$_2$, tert-butylisocyanate, and phenylallene to generate the C–N bonded product.

One other complex has been reported in which approximate three-fold rotational symmetry about the Ti atoms is enforced. Reduction of the subsite-differentiated hetero-cubane cluster Cp*$_3$Mo$_3$(μ_3-S)$_4$TiCl$_2$ or (Mo$_3$TiS$_4$)Cl$_2$ with 4 equiv. KC$_8$ under a dinitrogen atmosphere yields an octanuclear complex in which dinitrogen bridges two cubanes, *viz.* [K(THF)]$_2$[(Mo$_3$TiS$_4$)$_2$(μ–1,2-N$_2$)], **34-K$_2$** (Figure 24).[86] As observed in the bis-titanatrane complexes **32-red** and **33**, K$^+$ cations are in close contact with the bridging N$_2$ ligand in **34-K$_2$**. The elongated N–N bond (1.294(7) Å) and low energy for the N–N stretching mode from resonance Raman spectra (1240 cm^{-1}) indicate a strong back bonding interaction from the Ti centers to the N$_2$ donor, with the latter formally between diazenide and hydrazide. Addition of 6–10 equiv. KC$_8$ to **34-K$_2$** affords trace amounts of [K$_3$(THF)$_5$][(Mo$_3$TiS$_4$)$_2$(μ

$-1,2$-N_2)] (**34-K$_3$**). X-ray diffraction analysis showed a similar N–N bond length and elongation of the Ti–Mo and Mo–Mo distances as compared to those in **34-K$_2$**, suggesting a metal-based reduction instead of the bridging N_2 unit.

Using amidinates and guanidinates, Arnold and coworkers accessed a series of μ–1,2-dinitrogen-dititanium compounds of the type [(XC(NR)$_2$)$_2$Ti]$_2$(μ–1,2-N$_2$), **35-X/R** (Figure 25).[87] The N–N and Ti–N(N$_2$) bond metrics across the series suggest double bond character in the Ti–N(N$_2$) bond. Coordination of pyridine to **35-Ph/SiMe$_3$** results in a shortening of the N–N bond and lengthening of the Ti–N(N$_2$) bonds; for **35-Ph/SiMe$_3$/py**, the N–N and Ti–N(N$_2$) bond length is 1.264(5) Å and ~1.800 Å, respectively.

Mindiola and coworkers reported a [(P$^{i\mathrm{Pr}}$N$^{\mathrm{tol}}$)$_2$Ti]$_2$(μ–1,2-N$_2$) (**36**, Figure 26) and investigated possible scission of dinitrogen to the terminal-nitride complex.[88] The crystallographically observed N–N bond length of 1.252(8) Å agrees well with other titanium complexes supported by ligands bearing pnictogen donor atoms (e.g., **21**–**32**, **35-X/R**). N–N cleavage was, however, not observed upon further reduction of **36**, which contrasts the result reported by Fryzuk for **23** and is attributed to the rigidity of the P$^{i\mathrm{Pr}}$N$^{\mathrm{tol}}$ ligand.

The final titanium example is that from Kawaguchi and coworkers who reported (μ–1,2-dinitrogen)dititanium complexes bearing bulky p-terphenoxide ligands (denoted OO^{2-}) (Figure 27). In the series of complexes [(OO)Ti(L)]$_2$(μ–1,2-N$_2$) (**37-L**), the large bite angle of OO^{2-} enforces a pseudo-square pyramidal coordination environment about the Ti centers with the bridging N_2 occupying the axial site.[89] The energy of the N–N stretching mode for **37-DME** and **37-Py** of 1394 and 1362 cm^{-1}, respectively, suggest substantial backbonding from titanium to N_2.

3.2 Group 5: V, Nb, and Ta

The reported dinitrogen complexes of the Group 5 metals are exclusively dimetallic with the μ–1,2 coordination mode predominating. Churchill and Schrock reported alkylidene complexes of the type [Ta(R)Cl(PMe$_3$)$_2$]$_2$(μ–1,2-N$_2$), **38–1** (R = neopentylidene or Np$^{\mathrm{ene}}$) and **38–2** (R = ethylene or Et$^{\mathrm{ene}}$), synthesized by reduction of TaCl$_3$(R)(PMe$_3$)$_2$ in the presence of excess PMe$_3$ under a dinitrogen atmosphere.[90] Substitution of the chloride ligand in **38–1** can be effected using neopentyllithium or methyllithium to generate [Ta(Np$^{\mathrm{ene}}$)(R$'$)(PMe$_3$)$_2$]$_2$(μ–1,2-N$_2$), R = Me **38–3** and R = Np **38–4** (Figure 28). Complex **38–3** was the first crystallographically characterized multimetallic dinitrogen species of Group 5 metal. The observed N–N and M–N(N$_2$) bond distances, ^{15}N-NMR chemical shifts, and $\nu_{\mathrm{N–N}}$ at 847 cm^{-1} strongly indicate metal-imide character and substantial charge transfer to the N_2 ligand. Such activation of the N_2 ligand is common for Group 5 metal complexes with a formal N_2^{4-} or a diimide ligand and metal ions in the +4 or +5 oxidation states typically invoked. Building from this seminal report, more than fifty-five Group 5 dimetallic-dinitrogen complexes have been reported with various supporting ligands, including cyclopentadienyl, chelating ligands with pnictogen or chalcogen donor atoms, and other organometallic ligands (*e.g.*, mesityl). Our survey begins with complexes that are part of isostructural series for different metal ion types (*e.g.*, isostructural V$_2$ and Ta$_2$

complexes), and then ends with compounds for which examples of only one metal ion type (*e.g.*, only V complex known). For both sections, we begin with aromatic or closely related ligands (*e.g.*, Cp) and subsequently consider other supporting ligands in decreasing ligand denticity.

3.2.1. Dinitrogen complexes of Group 5 metals using common supporting ligands.

—The cyclopentadienyl-amidinate/guanidinate supported dimetallic dinitrogen species **39-M/R** (**M** = V, Nb, Ta and **R** = Me, Ph, and NMe$_2$) constitute the only isostructural series with representatives from each of the Group 5 metals (Figure 29).[91,92] These complexes are typically synthesized by chemical reduction of the pentavalent precursors. For example, reduction of Cp*[N(^{i}Pr)C(Me)N(^{i}Pr)]TaCl$_3$ with 4 equiv. KC$_8$ yielded {Cp*Ta[N(^{i}Pr)C(Me)N(^{i}Pr)]}$_2$(μ–1,2-N$_2$) (**39-Ta/Me**). Across the **39** series, the dinitrogen ligand is coordinated in a μ–1,2 fashion even for the Nb and Ta congeners, contrasting the transition from the μ–1,2 in Ti to the μ-η^2:η^2 mode observed for the analogous Zr and Hf analogs. Consistently then, one notes that the N–N bond distances for **39** (Figure 29), with values from 1.225(2) Å for **39-V/Me** and ~1.31 Å for **39-Ta/Ph** and **39-Ta/NMe$_2$**, are comparable to **16** (1.270(2) Å), and decidedly shorter as compared to those of **17**, for which the values range from 1.518 Å for **17-Zr** to 1.635(5) Å for **17-E** (Figure 13). Isomerization of the μ–1,2 isomers of **39** to the side-on/side-on coordination mode is likely thermally accessible, making it a plausible transition state for the observed N–N bond homolysis for **39-Nb/R** and **39-Ta/R** complexes (Scheme 12).[93,94] Additional support for this isomerization is provided by the observed product (**40-R**) from the reaction of **39-Ta/R** with N$_2$O, in which a side-on/side-on hydrazide ligand is observed (Scheme 13). The ligand sterics strongly influence the stability of the N$_2$ complex primarily through changes in $S^{\ddagger}$ for conversion of the μ–1,2-dinitrogen species to the di(μ-nitride) isomer. Complex **39-Ta/Me** readily reacts with H$_2$, phenylsilane, and diphenylsulfide; for example, reaction with phenylsilane affords {Cp*Ta(R$'$)[N(^{i}Pr)C(Me)N(^{i}Pr)]}(μ–1,2-N$_2$){Cp*TaR[N(^{i}Pr)C(Me)N(^{i}Pr)]} (**41-R/R$'$**, R = SiH$_2$Ph, R$'$ = H; Figure 30).[95] These reactions result from a bimetallic oxidative addition with retention of the bridging N$_2$ ligand and minimal changes to the N–N bond distances. These products of oxidative addition are structurally related to the di-chloride complex *rac*-{Cp*Ta(Cl)[N(^{i}Pr)C(Me)N(^{i}Pr)]}$_2$(μ–1,2-N$_2$) or **41-Cl/Cl** (Figure 31), which is accessed by reduction of Cp*[N(^{i}Pr)C(Me)N(^{i}Pr)]TaCl$_3$ with 2.5 equiv. of KC$_8$. The N–N bond (1.29(1) Å) is elongated in this compound relative to free N$_2$, but the value is comparable to that of **39-Ta/Me**, suggesting a metal-centered reduction as one transitions from the formally more-oxidized Ta centers in the dichloride compared to those in **39-Ta/Me**. Although analogous complexes of V and Nb are not reported, we consider the tantalum amidate complexes **42-R/R$'$** (Figure 32) here insofar as the comparison to the amidinate complex **41** is worthwhile.[96] Of the two synthesized examples, the only solid state structure reported was that for **42-Xyl/^{t}Bu** in which a primary coordination sphere is strongly similar to that in **41** with the amidinate in **41** substituted to an amidate to afford **42-Xyl/^{t}Bu**. Consistently then, the N–N distance of 1.292(4) Å is determined for **42-Xyl/^{t}Bu**, which is within error of the value determined for **41.**

The remaining examples comprise complexes in which the same ligand has been used for only two of the possible three metals. Mindiola and coworkers reported the V and Nb complexes, **43-V/N** and **43-Nb**, of closely related PNP ligands derived from diphenylamine (Figure 33 and Figure 34).[97–100] The metal coordination sphere is completed by chloride (**43-Nb**) or an imide or alkylidene (**43-V/N** or /**Np**, respectively). The N–N bond distances nominally increase as one moves from imide to alkylidene and then from V to Nb with values ranging from 1.222(4) Å to 1.277(6) Å for **43-V/N** to **43-V/Nb**. The calculated Mayer bond orders for **43-V/Nb** are consistent with the bond metrics, with values of 1.3 and 1.5 for the $Nb–N(N_2)$ and N–N bonds, respectively.

In contrast to the monoanionic PNP ligand based on diphenylamine, the Fryzuk group developed a dianionic diamide-phosphine ligand, NPN^{Ph}, for which the Ph superscript refers to the substituent on the amide N atoms. Complexes of Nb and Ta are known for this ligand set; the chemistry of the Ta congener has been reported to a greater extent. The ligand does not adopt the meridional orientation of a typical pincer ligand, but rather coordinates in a facial geometry, as noted for the $Nb_2(\mu–1,2-N_2)$ complex **44-Nb** (Figure 35).[35] The extent of activation of the N_2 fragment in this complex (d(N–N) = 1.237(4) Å) is comparable to that of the example from Mindiola **43-Nb**, in agreement with analogous formally $[Nb_2(N_2)]^{6+}$ fragments and the $\mu–1,2$-dinitrogen coordination mode observed in both.

In contrast to **44-Nb** in which reduction of the metal halide precursor was used to access the N_2 adduct, the hydride route was used for the related Ta complex: the ditantalum tetra(μ-hydride) complex **44-Ta/4H** reacts readily with dinitrogen to generate $(NPN^{Ph}Ta)_2(\mu-H)_2(\mu-\eta^1:\eta^2-N_2)$, **44-Ta/2H,N$_2$** (Scheme 14).[101] As noted previously, the side-on/end-on coordination mode is uncommon in dinitrogen chemistry and, here, the steric constraints placed on the metal-metal distance as a consequence of the small bridging hydrides precludes access to the end-on/end-on bridging mode. Such a comparison is reminiscent of the short metal-metal separations enforced in the indenyl dizirconium complex **14-R^1/R^2** in which a similar $\mu-\eta^1:\eta^2$ interaction is observed. Indeed, insertion of propene into **44-Ta/2H,N$_2$** affords the terminal dipropyl complex $(NPN^{Ph}Ta(nPr))_2(\mu–1,2-N_2)$ relaxing the short metal-metal separation (albeit introducing new conflicts between the ligand and the propyl groups).

The last category of isostructural complexes comprises the monodentate amide and RO^- ligands. For the amides, examples in which the R substituents are identical have been reported. These compounds are the ($\mu–1,2$-dinitrogen)-bis[tris(dialkylamido)vanadium/niobium] complexes **45-M/R** in which M/R = V/iPr, V/Cy, and Nb/Cy (Figure 36).[97,102] Access to the tris(amide) and $\mu–1,2$-dinitrogen complexes for V and Nb contrasts the bis(amide) and side-on/side-on N_2 ligands in **31**, reflecting the greater extent of reduction of the metal centers and the sterics of the R group in **31** as compared to **45**. The reported values for d(N–N) of 1.27(1) Å and 1.34(1) for the V and Nb congeners of **45** agree with the observed trend of greater activation by the heavier d-block metal. By comparison, $^tBu_2MeCO^-$ and $^tBu_3SiO^-$ were employed for V (**46-V**) and Nb (**46-Nb**), respectively, to generate complexes with approximate D_{3d} symmetry for the $(RO)_6M_2(\mu–1,2-N_2)$ core (Figure 37).[103,104] Complex **46-V** is the only example of a vanadium dinitrogen complex supported by alkoxide donors. The N–N bond distances and V–N bond distances (longest

values of 1.232(3) Å and 1.773(2) Å, respectively) agree with the expected change in the donor properties from amide to alkoxide. Complex **46-Nb** has a singlet ground state, it is generated from the $S = 1$ Nb(OSi^{t}Bu$_3$)$_3$(PMe$_3$) complex with catalytic amounts of reductant under an N$_2$ atmosphere. This orbital symmetry forbidden reaction begins with initial formation of an $S = \frac{1}{2}$ [(^{t}Bu$_3$SiO)$_3$NbN$_2$]$^-$ transient, which subsequently displaces PMe$_3$ on an unreacted Nb(OSi^{t}Bu$_3$)$_3$(PMe$_3$) to afford the one-electron reduced form of **46-Nb**. Oxidation of this anionic species by an equivalent of Nb(OSi^{t}Bu$_3$)$_3$(PMe$_3$) restarts the substitution process to ultimately afford **46-Nb** as the observed major product. As for the **45-V/R** and **46-V**, the N–N bond distances for the siloxide complex **46-Nb** are slightly shorter than that of the **45-Nb** (1.310(4) Å vs. 1.34(1) Å).

3.2.2. Ligand systems unique to vanadium-dinitrogen complexes.—Only two examples of dinitrogen-bridged cyclopentadienyl-vanadium fragments have been reported thus far. The first is the amidinate complex **39-V/Me** from Sita and coworkers which was discussed above as part of the amidinate-cyclopentadienyl series.[91] The other example is **47**, which was reported by Liang and Liu (Figure 38).[105] Here, the short N–N bond distance of 1.212(8) Å is consistent with competing π-backbonding interactions between the V center and the cyclopentadienyl and alkyne, which deplete the electron density at the metal center available for π-bonding to N$_2$.

Transitioning to all N-atom donor ligands, the tetradentate tris(aminoethyl)amine derived (or tren^{3-}) ligands and the tridentate 1,1,1-tris(isopropylaminomethyl)ethane afford μ–1,2-dinitrogen divanadium complexes with comparable structures (Figure 39).[106,107] For example, tren^{3-} complexes **48-X** adopt approximate D_{3d} symmetry as does **49** and exhibit similar N–N and V–N(N$_2$) bond distances across the four compounds. The ν_{NN} energies for **48-X** range from 1399 to 1402 cm^{-1} and are in good agreement with the observed crystallographic N–N distances. The slight elongation of the N–N bond in **49** as compared to **48–1** or **–2** is consistent with the expected weaker V–N$_2$ σ interaction. Using a dianionic N$_3$ tripodal chelate related to the triamide in **49**, Clentsmith, *et al.* demonstrated complete cleavage of dinitrogen at vanadium centers—the first example of N$_2$ to two nitrides on V (Scheme 15).[108] One-electron reduction of the bis(amido)amine-ligated vanadium(III) chloride yields the di(μ-nitrido)divanadium(V) complex **50**, for which the crystallographic μ-Nμ-N distance of 2.50(2) Å far exceeds that for hydrazine (*cf.* 1.45 Å).[51,109] One electron reduction of **50** yields the anionic mixed-valent V$^{IV/V}$$_2$ complex, which is structurally unremarkable compared with **50** in the context of N$_2$ activation.

A few meridional, chelating ligands have been exploited in vanadium dinitrogen chemistry. Starting with all N chelates, Vidyaratne and Gambarotta (**51–1** and **–2**) and Milsmann and Chirik (**51–3**) reported the synthesis of divanadium-dinitrogen adducts supported by redox active pyridine diimine chelates (Figure 40).[110,111] The comparable ligand field for these complexes translates into analogous N–N and V–N(N$_2$) bond distances with values ranging from 1.232(3)–1.259(6) Å for the former and 1.777(2)–1.798(2) Å for the latter metrics. The M–N–N angles slightly deviate from linearity with values ranging from 162.4(2) to 167.2(1)°, and likely arise from the steric effects of the near interdigitated diisopropylphenyl

groups. The bond metrics for the pyridine diimine chelates in **51–1** and **–2** imply a reduced ligand.

Somewhat related to the N_3 *mer*-chelates in **51** is the (μ–1,2-dinitrogen)divanadium complex **52** from Vidyaratne, *et al.* wherein the metal coordinates to the central *N*-methylpyrrole ring in an η^5 manner.[112] The N–N and V–N(N_2) bond lengths (*viz.* 1.248(5) Å and 1.752(6) Å, respectively) compare favorably to those in **48**, **49** and **51**, suggesting a formal V oxidation state of +3 or greater in **52** and contradicting the solution magnetic moment of 3.52 μ_B/per V atom. Surprisingly, reduction of **52** affords the (μ-nitrido)divanadium(III/IV) complex (Scheme 16) as well as other unidentified by-products, implying the N–N bond cleavage with possible intermediacy of mononuclear vanadium nitride species.

Nishibayashi and coworkers used the diphosphinopyrrolide ligand in **19** to synthesize the related divanadium complex **53** (Figure 41) in which the π-donating phenoxide completes the coordination sphere. Complexes **43-V/R** have related ligand fields arising from a comparable PNP pincer ligand and ancillary π-donating ligands (*i.e.*, RHC^{2-}, RN^{2-}, and RO^-). From the analogous N–N and V–N(N_2) bond distances across the series, one infers similar formal charges of the N_2 ligand (*i.e.*, diazenide), suggesting V oxidation states of +4 in **43-V/R** and +3 in **53**.[113] Compound **53** is a competent catalyst for N_2 fixation to NH_3, albeit less effective based on turnovers than examples to be presented later, with highest reported turnovers of 12 equiv. NH_3 and 1.8 equiv. N_2H_4 per complex.

The final two examples of compounds with all pnictogen donor atoms are the amidinate (**54**) and the β-diketiminate (**55**) complexes. The bis[bis(amidinato)vanadium] μ–1,2-dinitrogen complexes [(RNC(R′)NR)$_2$V](μ–1,2-N_2), **54–1** or **–2** (R/R′ = $SiMe_3$/Ph for **54–1** and Cy/Me for **54–2**) (Figure 42), are accessed by reduction of the respective monometallic V^{III} chloride precursor using $NaHBEt_3$.[114] Only **54–2** was characterized by X-ray crystallography; the reported N–N and V–N(N_2) distance of 1.235(6) Å and 1.756(5) Å, respectively, are analogous to the examples mentioned above both in metrics and in the formal oxidation state assignments for the V_2N_2 fragment.

Complex **55** synthesized by exposure of ($^{Me}NacNac^{DIPP}$)V^{II}(OAr) was the first example of dinitrogen coordination by a three coordinate vanadium(II) species (Figure 43).[115] Although structural data are not available, the N_2 stretching mode observed at 1374 cm^{-1} by resonance Raman spectroscopy together with computational studies are consistent with antiferromagnetically-coupled formally V^{III} centers and a N_2^{2-} bridge. Completing the examples with bidentate ligand is complex **56**, which was reported by Gambarotta and coworkers and was the first structurally characterized example of a polynuclear vanadium dinitrogen complex (Figure 44).[116] The observed d(N–N) of 1.228(4) Å and a short V–N(N_2) distance of 1.833(3) Å suggest considerable reduction of the dinitrogen with substantial contribution from the diazenide (N_2^{2-}) resonance form.

Lastly, we consider the examples employing monodentate ligands. Previously, we considered the amido and alkoxide examples; here, we consider the alkyl and aryl complexes for which only V examples are known. Buijink and Teuben reported the (μ–1,2-dinitrogen)bis(tris(neopentyl)vanadium) **57**, synthesized by metathesis between

$LiCH_2(CH_3)_3$ and $VCl_3(THF)_3$ (Figure 45).[117] The N–N bond length of 1.250(3) Å is comparable somewhat unexpectedly to that of **46-V**, but may arise from the different steric demands of the ligand. Floriani's redox series of (μ–1,2-dinitrogen)bis[(trimesityl)vanadium] complexes **58** wherein the formal charge of the $[V_2N_2]^{n+}$ core varies (n = 4–6) evidence comparable metal–N_2 and N–N bond distances (Scheme 17).[118] Magnetic susceptibility data and theoretical methods suggest reduction of the N_2 ligand, however, which is consistent with protonation of **58-K** or **58-K$_2$** to yield N_2H_4 (20% and 38%, respectively) and NH_3 (7% and 21%, respectively). One may then conclude that d(N–N) is not a reliable reporter for N_2 activation in metal-dinitrogen complexes; although, the modest yield of hydrogenated-N_2 products could suggest more complex reaction pathways involving redistribution of reducing equivalents. Indeed, the long bond distance observed in **58-Na$_2$** vs. **58-K** and **58-K$_2$** highlights the strongly activating effect of the Lewis acidic center proximal to the N_2 ligand.[119]

3.2.3.   Ligand systems unique to niobium-dinitrogen complexes.—Only three niobium only examples have been reported to date: the $P^{Ph}_2N_2$ macrocyclic ligand from Fryzuk's group, the calix[4]arene complexes by Floriani and coworkers, and the (μ–1,2-dinitrogen)-bis[tris(dithiocarbonato)niobium] complexes from Henderson, *et al.*.

Fryzuk and coworkers used their $P^{Ph}_2N_2$ macrocyclic ligand (see prior Ti and Zr examples **21** and **22**) to synthesize the corresponding μ–1,2-dinitrogen adduct **59–1** (Figure 46). The bond metrics are comparable to those of the diniobium compounds discussed above, with N–N and Nb–N(N_2) distances of 1.272(5) Å and 1.869(5)–1.840(6) Å, respectively.[94] EPR spectroscopic data recorded at 300 K reveal a decet of triplets ($I = {}^9/_2$ ^{93}Nb and $I = ½$ ^{31}P nuclei) at $g = 1.975$ indicating local d^1 character at each Nb, and variable-temperature magnetic susceptibility measurements could be well modeled assuming two antiferromagnetically-coupled $S = ½$ centers mediated by the N–N bridge. Notably, the dinitrogen ligand in the zirconium analog **22** adopts a μ-η^2:η^2 coordination mode rather than the μ–1,2 mode observed in **59**. In the side-on/side-on mode, the two π^* orbitals of N_2 gives rise to SALCs of π-type and δ-type symmetry, whereas the end-on/end-on orientation affords two orbitals of M–N π-symmetry. The preference for the respective bridging mode then lies in the relative occupation of the respective orbitals, with the formally d^1 Nb^{IV} and the N_2^{4-} affording weaker δ-interactions destabilizing the δ-bond, whereas this metal-based δ-type orbital is unoccupied for Zr^{IV}. Related to **59–1** are **59–2** and **–3** for which the N–N bond lengths of 1.280(7) Å and 1.250(3) Å and Nb–N(N_2) bond lengths of 1.869(5)–1.840(6) Å for **59–2** and 1.868(2)–1.875(2) Å for **59–3** are within error of those for **59–1**.[120] The compensatory effect of the strongly donating alkyl ligand on the crystallographic measure of N_2 activation is reminiscent of the similarities between **1-Cp*** and **8-Cp,p-C$_6$H$_4$CH$_3$**.

Rizzoli and coworkers reported complex **60-N$_2$** in which a μ–1,2-dinitrogen links two monoanionic niobium-calixarene species (Scheme 18). The N–N (1.39(2) Å) and Nb–N (1.75(1) Å) bond distances are indicative of Nb–N multiple bond character and N–N single bond character; this formalism is consistent with the Wittig-like reactivity observed for **60-N$_2$** with benzaldehyde, which yields the azine (PhCH=N–N=CHPh) and the corresponding

niobium oxide species.[121] Two-electron reduction of **60-N$_2$** results in N–N bond cleavage affording the di(μ-nitrido)diniobium(V) complex **60–2N**.

The transition from the μ–1,2 mode for the N$_2$ fragment in **60-N$_2$** to the di(μ-nitride) in **60–2N** could suggest intermediacy of two terminal nitrides or isomerization from a μ–1,2 to a μ-η^2:η^2 (or μ-η^2:η^1) coordination mode. Reduction of the THF solvate **60-N$_2$′** in dimethoxyethane (DME) affords **61**, in which the N$_2$ ligand now adopts a μ-η^2:η^2 mode with contraction of the Nb–Nb distance (4.8847(18) in **60-N$_2$** vs. 2.635(1) Å in **61**) and minimal change to the N–N bond distance (Scheme 19). These structural changes suggest that reduction of **60-N$_2$′** is initially metal-based rather than N$_2$-based.[93] Thermolysis of the N–N and Nb–Nb bonds in **61** can be effected in pyridine to generate di(μ-nitride) complex **62**.

The final Nb example is that from Henderson *et al.* who reported the μ–1,2-dinitrogen diniobium complex [(NEt$_2$CS$_2$)$_3$Nb]$_2$(μ–1,2-N$_2$) (**63**, Figure 47).[122] The N–N bond lengths of 1.25(2) Å are contracted as compared to the many of the discussed Nb$_2$N$_2$ complexes, suggesting Nb(IV) centers in the Nb(S$_2$CNEt$_2$)$_3$ fragment. Here, the Nb–N–N bond angles of 166.8(9)° and 163.1(9)° reflect a slightly bent coordination mode in a nominal *cis* orientation.

3.2.4. Ligands systems unique to tantalum-dinitrogen complexes.—Starting with the cyclopentadienyl complexes, Bregel and Eisenberg reported (Cp*$_2$TaCl)$_2$(μ–1,2-N$_2$) (Figure 48), 64,[123] which bears structural homology to **8-Cp,*p*-CH$_3$C$_6$H$_4$** (Figure 9) albeit with a slightly longer N–N bond length of 1.24(1) Å as compared to the Zr congener.

Disproportionation of (C$_5$Me$_4$R)$_2$Ta(μ-Cl)$_4$ under a dinitrogen atmosphere affords [(C$_5$Me$_4$R)$_3$Ta$_3$(μ-Cl)$_6$][(C$_5$Me$_4$R)TaCl$_4$] as one product, and [(C$_5$Me$_4$R)TaCl$_2$]$_2$(μ–1,2-N$_2$) **65-R** where R = Me or Et (Figure 49).[124] Structural characterization by X-ray crystallography of **65-Et** evidences a zig-zag Ta$_2$N$_2$ core with a Ta–N–N angle of 166.3(4)°, a N–N distance of 1.280(6) Å, and a short Ta–N distance of 1.804(3) Å. Extending to pseudohalides, Takada and Kinoshita reported [Cp*Ta(SC$_6$H$_4$Me)$_2$](μ–1,2-N$_2$), **66**, which was synthesized in a one pot reaction containing Cp*TaCl$_4$, di-p-tolyl disulfide, and KC$_8$.[125] As expected given the similarities of the monodentate ligands in **65** and **66**, the bond metrics and the zig-zag conformation of the Ta$_2$N$_2$ core are comparable; for example, the N–N bond distance in **66** is 1.281(7) Å. To explore the effect of heterometals on the extent of N$_2$ activation, **66** was reacted with M(CO)$_6$ sources under UV irradiation to generate the tetrametallic complexes **66–2M** (M = Cr, Mo) and **66-M** (M = Cr, Mo) (Scheme 20). The thiolate donors bridge the Ta and Group 6 metal centers, with no direct interaction between the Cr or Mo and the N$_2$ ligand. DFT calculations and experimentally-determined bond distances evidence minimal change to the Ta–N$_2$ bonding interactions upon coordination of the Group 6 metal.

Related to these mono-cyclopentadienyl complexes is the borrolide species **67** report by Sperry and Bazan (Figure 50).[126] The mononuclear precursor is nominally Ta^{II}, assuming a borrolide oxidation state formalism, and expectedly affords a dinitrogen complex with strong Ta–N(N$_2$) π-backbonding interactions. The N–N and Ta–N bond lengths are 1.309(9)

Å and 1.838(7) Å, respectively, and well within the range of the monocyclopentadienyl compounds discussed above.

Schrock and coworkers reported a rare example of a dimetallic dinitrogen complex supported by thiolate ligands. Treating $[TaCl_3(THF)_2](\mu-1,2-N_2)$ with 6 equiv. LiDIPT (DIPT =S-2,6-C_6H_3-$^iPr_2$) affords $[Ta(DIPT)_3(THF)]_2(\mu-1,2-N_2)$, **68–1** (Figure 51).[127] Unfortunately, the solid state structure of **68–1** is of sufficient quality to only validate connectivity, which is as depicted in Figure 51. The phenoxide analog **68–2** reported by the same authors afforded crystals of sufficient quality to allow determination of the lengths of the N–N bond (1.32(1) Å) and Ta-N(N_2) bonds (1.796 (5) Å); these metrics are reminiscent of other Ta_2N_2 fragments discussed above, such as **41-Ta/R** and **44-Ta/2H,N$_2$**.

3.3 Group 6: Cr, Mo, and W

Molybdenum is one of the most studied metals with respect to dinitrogen activation stemming in part from the initial reports of the molybdenum-dependent nitrogenases from *Azotobacter*. Unsurprisingly then, the dinitrogen chemistry of Group 6 is dominated by molybdenum compounds.[128,129] Our survey begins with molybdenum dinitrogen complexes and includes closely related dinitrogen complexes of Cr and W where appropriate. Subsequently, we consider the singular examples for Cr and then those for W.

3.3.1. Molybdenum complexes and related Cr and W compounds.—The first example of a multinuclear molybdenum dinitrogen complex is [Mo(dmpe)(η^6-mesitylene)]$_2$($\mu-1,2-N_2$) **69** from Forder and Prout for which d(N–N) = 1.14 Å and d(Mo–N) = 2.04 Å (Figure 52).[130] Related to this arene complex is the dinuclear tungsten piano stool complex **70** in which each metal is ligated by a dmpe and Cp$^-$ with a $\mu-1,2$-dinitrogen completing the metal coordination spheres (Figure 53).[131] Despite the differences in the formal metal charges for **69** and **70**, the N–N bond distance increases from **69** to **70** (d(N–N) = 1.22(1) Å), reflecting the difference in metal-ligand bonding and the donor properties of the aromatic ligand.

Other dimolybdenum dinitrogen complexes bearing aromatic ligands include the η^6-arene complex from Agapie and coworkers (Figure 54) and the η^5-Cp complexes from the groups of Nishibayashi (Figure 55) and Sita (Figure 56 and Figure 57).[69,132,133] For the former, protonation of the tris(pentafluorophenyl)borane adduct of the complex (C_6H_4(C_6H_4-P$^iPr_2$)$_2$)Mo(CO)$_2$ with H(OEt$_2$)BAr$^F_4$ (BAr$^F_4$ = tetrakis[3,5-bis-(trifluoromethyl)phenyl]borate) in the presence of N_2 affords a mixture of products from which **71** is one of the major products. The structural parameters for **71** are expectedly comparable to those reported by Forder and Prout; for example, the N–N distance is 1.174 Å compared to 1.14 Å in **69**.

Using 1,1′-bis(diethylphosphino)ferrocene (depf), Nishibayashi and coworkers synthesized the redox series of [Cp*Mo(depf)]$_2$($\mu-1,2-N_2$) **72** wherein the overall charge ranges from 0 to +2.[133] The N–N bond lengthens from 1.182(5) Å in **72** to 1.256(9) Å in **72^{2+}** and an inverse trend is noted for the Mo–N bonds, indicating that the HOMO is N–N π-bonding rather than metal centered. Complex **72^{1+}** undergoes photoinduced N–N bond cleavage to

liberate the corresponding nitride (depf)Cp*Mo≡N; oxidation of this mononuclear nitride complex result in dimerization to 72^{2+}.

Similar to their efforts with Group 5 metals, Sita and coworkers reported the isostructural molybdenum and tungsten congeners of **39**, *viz.* {Cp*[N(R)C(X)N(^{i}Pr)]M}$_2$(μ–1,2-N$_2$), **73-M/N^{R},X** (Figure 56).[69] The observed N–N bond lengths are comparable independent of metal ion type, and substituent R and X; for example, the N–N bond length for **73-Mo/N^{iPr},NMe$_2$** of 1.267(2) Å and for **73-W/N^{iPr},Me** of 1.277(8) Å are within error. Complexes **73-M/N^{iPr},Me** are thermally robust, but convert to the di(μ-nitride) by photolysis (Scheme 21).[134] In contrast, **73-M/N^{Et},Ph** effect N–N cleavage above 25 °C.[135] These results correlate ligand sterics in these complexes with longer N–N bond lengths and the thermal stability of the dinitrogen adduct towards di(μ-nitride) formation. Related to **73-Mo/N^{iPr},Me** is the *meso*-{Cp*[N(^{i}Pr)C(Me)N(^{i}Pr)]Mo(H)}$_2$(μ–1,2-N$_2$), **74**, which is synthesized by reaction of (Cp*[N(^{i}Pr)C(Me)N(^{i}Pr)])MoCl$_2$ with 2 equiv. *n*-BuLi.[69] The longer Mo–N(N$_2$) and shorter N–N bond distances are consistent with a higher metal oxidation state in **74** as compared to **73-Mo**.

Related to **74** are the stereoisomers of {Cp*[N(^{i}Pr)C(Me)N(^{i}Pr)]W(Cl)}$_2$(μ–1,2-N$_2$), **75**, accessed either by reduction of Cp*[N(^{i}Pr)C(Me)N(^{i}Pr)]WCl$_3$ with 2.5 equiv. KC$_8$ or reaction of **73-W/N^{iPr},Me** with excess PbCl$_2$. The isomers have comparable solid state structural metrics with d(N–N) values of 1.206(9) Å and 1.192(3) Å for the *rac* and *meso* isomers, respectively; the N–N bond lengths in **75** are shorter than in **73-W/N^{iPr},Me** consistent with a decrease in electron density at the metal center.

A seminal contribution in dinitrogen activation independent of metal ion is the report by Laplaza, *et al.* on the scission of N$_2$ upon exposure of a tris(anilido)molybdenum(III) complex to a dinitrogen atmosphere (Scheme 22).[9] A transient purple (μ-dinitrogen)dimolybdenum species **76** prior to N$_2$ bond activation is supported by X-ray absorption data, resonance Raman spectra ($\nu_{(N-N)}$ = 1630 cm^{-1}), solid state magnetometry, and X-ray crystallography.[8] These data evidence an elongated N–N and contracted Mo–N(N$_2$) bonds with values of 1.212(2) Å and 1.868(1) Å, respectively. The linear μ–1,2-dinitrogen complex is proposed to isomerize to a zig-zag transition state prior to N$_2$ cleavage and formation of the molybdenum nitride products (Scheme 22).[8,136]

In the redox series generated by oxidation of **76** (i.e., [**76**]$^{n+}$ where n = 1 or 2), one observes that the N–N bond lengthens with oxidation from 1.212(2) Å in **76** to 1.265(5) Å in [**76**]$^{2+}$ together with a contraction of the Mo–N(N$_2$) bonds (1.868(1) Å in **76** to 1.798(2) Å in [**76**]$^{2+}$). These changes arise from the relative energy of the N–N π bonding orbitals as compared to the Mo–N(N$_2$) bonding molecular orbitals; the LUMO in [**76**]$^{2+}$ is N–N π bonding whereas the HOMO is metal(d_π)–N$_2$(π*) backbonding nature. This lowering of the energy of metal-based orbitals relative to the N$_2$ bonding orbitals is a direct consequence of the gradual transition from more electropositive early to more electronegative late transition metals.

A putative monometallic Mo–N$_2$ adduct or potential scrambling of metal ions within the dimetallic are possible mechanistic considerations for formation of **76**, which are evidenced

by access to a series of heterodimetallic complexes **76-M** (M = Ti, Nb, and U).[136–139] The **76-M** complexes are isostructural with **76** from the perspective of the tris(anilido)molybdenum-dinitrogen fragment and the linear μ–1,2 coordination of N_2. The N–N bond distances and energies of the ν_{N-N} stretching mode are similar over the series, with the N_2 fragment nominally more activated when the heterometal is more reducing than the Mo center (Figure 58). A related compound **76-V,** obtained as shown in Scheme 23, results in a lower activation of μ-N_2 as compared to the compounds in the **76-M** series, and is attributed to the less donating ligand environment around the V ion for the former.[140]

The (μ–1,2-dinitrogen)bis(tris(mesityl)molybdenum) **77-Mo** reported by Floriani and coworkers from the reaction of mesityl magnesium bromide with $MoCl_4$ is structurally analogous to the tris-anilide congener **76**.[141] The N–N bond is longer and Mo–N bonds shorter in **77-Mo** than those in **76**, consistent with the difference in donor properties of the supporting ligands. In comparison to **76** which readily converts to the mononuclear molybdenum nitride, **77-Mo** is stable in benzene at reflux with no conditions reported to afford the Mo≡N species. However, exposure of **77-Mo** dissolved in benzene to UV irradiation effects N_2 cleavage—a rare example of photolytic N_2 cleavage in a bimetallic system—to yield [Mo(Mes)$_3$]$_2$(μ-N) (Scheme 24). This reaction is proposed to initially form the monometallic nitride Mo(Mes)$_3$(N) followed by reaction with unreacted **77-Mo**. In addition to **77-Mo**, Floriani and coworkers also synthesized a related ditungsten species (μ–1,2-dinitrogen)bis[chlorotri(mesityl)tungsten], **77-WCl**.[142] Reduction of **77-WCl** with Mg metal does not result in the loss of chloride only, but reductive aggregation is observed to afford the tri- and tetra-tungsten chain-like complexes **77-W$_3$** and **77-W$_4$** (Scheme 25). Across this series of W complexes, the N–N bond is shortest for **77-WCl** (1.180(16) Å) and, on average, the longest of **77-W$_3$** (1.272 Å average).

The tren^{3-} presents a similar trigonal triamide coordination environment to that observed in **76**; inclusion of an amine as an axial donor can aid in destabilizing a potential metal-nitride bond to favor reduction and protonation to imide or amide species. Expectedly then, Mo_2N_2 and heterometallic complexes analogous to **76** and **76-M** are also accessible with this ligand platform with various substituents on the tren^{3-} secondary amine N-atoms.[143–145] In the three reported cases, dinitrogen bridges two formally Mo^{III} centers (considering N_2 as a neutral bridge for simplicity) in a linear fashion and with N–N and Mo–N bond distances comparable to **76** (Figure 59). For **78–3**, no further reduction chemistry was observed in contrast to the two-electron reduction of the [(4-^{t}BuC$_6$H$_4$-NCH$_2$CH$_2$)$_3$N]MoCl precursor, which yields the monomeric diazenide complex. Scheer, *et al.* also reported the dinitrogen complex **78–4** as a side product in the synthesis of [(NpNCH$_2$CH$_2$)$_3$N]WCl (Np = neopentyl).[146] The N–N bond length of 1.39(2) Å in **78–4** is remarkably long and is among the longest known for a μ–1,2-dinitrogen complex, being shorter than only the diniobium calixarene complexes **60-N$_2$**.

A series of heteronuclear metal complexes containing trenMoN$_2$ fragments, **79-M/Mo$_n$** (M = Zr, V, Fe and n = 1, 2, or 3), were reported by O'Donoghue, *et al.*.[147] Spectroscopic data indicate Mo^{IV} centers with the μ–1,2-dinitrogen ligands best described as diazenide donors. Although the N–N bond distances are comparable across the series, the energy of the N–N

stretching mode increases as complex nuclearity increases. For example, this mode is observed at 1515 cm^{-1} in **79-Zr/Mo$_1$**, 1556 cm^{-1} in **79-Zr/Mo$_2$** and 1576 cm^{-1} in **79-Zr/Mo$_3$** (Figure 60). For the vanadium analogs, an equilibrium between **79-V/Mo$_2$** and **79-V/Mo$_3$** is observed due to ligand exchange with THF (Scheme 26). The last example is **79-Fe/Mo$_3$** (Figure 61), which is the only example of an iron-molybdenum dinitrogen complex. The Fe centers in **79-Fe/Mo$_3$** adopts an unusual trigonal planar coordination environment surrounded by the three [((Me$_3$Si-NCH$_2$CH$_2$)$_3$N)Mo(N$_2$)]$^-$ units. The μ–1,2-dinitrogen bridges are approximately linear with one being slightly bent with an ∠Fe–N–N = 156(2)°. This bending is proposed to arise from steric interactions rather than electronic effects. The N–N bond distances are comparable (1.20–1.27 Å) to the other heterometallics, although IR spectra ($\nu_{N–N}$ = 1703 cm^{-1}) suggest a significantly less activated N$_2$.

Meridionally-coordinating tridentate chelates have also been utilized in molybdenum-dinitrogen chemistry. Starting with all N-donor chelates, Cr (**80**) (Scheme 27) and Mo (**81-N$_2$** and **81-diene**) (Figure 62) complexes of pyridine(diimine) ligand were reported by Gambarotta and Chirik and their coworkers, respectively.[148–150] The N–N bond distances with values of 1.241(6) Å for **80** and 1.246(4) Å for **81-N$_2$** are elongated compared to other Cr and Mo complexes, which, together with the M–N(N$_2$) distances of 1.781(3) Å for **80** and 1.819(3)-1.823(3) Å for **81-N$_2$**, suggests appreciable backbonding from the metal to the bound N$_2$. For complex **80-diene**, the π-acidity of the butadiene results in less activation of the N–N bond (1.145(4) Å) based on the solid state structure, reinforcing the need for weakly π acidic ligands to favor N$_2$ bond lengthening. Reaction of **80** with 2 equiv. NaH gives **80-Na$_2$** (Scheme 27), in which the one hydride deprotonates the bis(imino)pyridine and the second is accepted by the N$_2$ ligand. The N-atoms derived originally from N$_2$ are significantly pyramidalized in **80-Na$_2$**. Taken together, deprotonation of the bis(imino)pyridine to the more donating anionic ene-amide ligand and the proximal alkali cations leads to a charge redistribution with formal reduction of the N$_2$ ligand.

The other example utilizing an all N-donor meridional chelate is the phenyl-substituted terpyridine complex [**82**]$^{2+}$ (Figure 63), in which the coordination sphere of each Mo center is completed by a methyldiphenylphosphine ligand.[151] The values of d(N–N) and $\nu_{N–N}$ of 1.203(3) Å and 1563 cm^{-1} are consistent with the reduced nature of this complex, and DFT calculations indicate that the HOMO comprises a mixture of N–N π bonding and Mo–N$_2$ π*. Examining the five-electron redox series [**82**]$^{n+}$ (n = 0, 1, 2, 3, or 4) by Raman and EPR spectroscopy corroborate these computational findings: $\nu_{N–N}$ decreases from 1563 cm^{-1} to 1477 cm^{-1} with increasing values of n from 2 to 4, and EPR spectra of [**82**]$^{3+}$ indicate that the SOMO is comprised of metal d_π orbital.

For the mixed pnictogen pincer type complexes reported by Nishibayashi and coworkers, the Mo centers adopt pseudooctahedral geometries each comprising a meridionally-ligated pincer ligand, two terminal η^1-dinitrogen donors, and a μ–1,2-dinitrogen. With the exception of **83^{Cy}-H**, **83^{iPr}-H**, and bis-arsine **84** complexes, the common structure type is the *trans-trans* configuration of the μ–1,2-dinitrogen and the pyridyl N donor of the pincer ligands with a dihedral angle greater than 60° between each MoE$_3$ plane (E = donor atoms on pincer ligands) (Figure 64). For **83^{Cy}-H**, **83^{iPr}-H**, and **84**, dubbed as *trans-cis* isomers, the MoE$_3$ planes are orthogonal and only one of the terminal N$_2$ ligands is *trans* to the μ-dinitrogen

(Figure 65). The bridging and terminal N–N bond distances vary slightly as a function of substituents; however, a strong correlation is observed between the IR-active N–N stretching mode for the *terminal* N_2 and the reduction potential of the complex.[152] In the series **83^{tBu}-R′** where R′ is H, Ph, SiMe$_3$, ^tBu, Me, or OMe, the yield of ammonia produced under catalytic conditions using CoCp$_2$ and lutidinium triflate ([LutH]OTf) increases with greater electron donation from the substituent with 52 and 44 equiv. for R′ = OMe and H, respectively.[153] Computational studies suggest that the terminal N_2 ligands undergo reduction and protonation and that the bridging N_2 functions as an electron transfer pathway with one Mo center acting as an electron reservoir.[154] However, the *trans-cis* complexes exhibit minimal catalytic N_2 fixation, suggesting that a near equivalent electronic structure at each Mo center is important for N_2 fixation. In addition, steric effects of the phosphine substituents influence the number of turnovers with **83^{Ph}-H** (2 NH$_3$ equiv.) being a poor catalyst in comparison to **83^{Ad}-H** (14 NH$_3$ equiv.).[155] Related to **83^{tBu}-H** are **83^{tBu}-4Cl** and **83^{tBu}-4CO**, in which the two terminal N_2 ligands on each Mo center are replaced by chloride or CO. The former has been structurally characterized and the observed N–N bond length (1.169(3) Å) is comparable to that of the *trans-trans* complexes.[156] In contrast, **83^{tBu}-4CO** was characterized only by vibrational spectroscopy, which evidenced a N–N stretching mode of similar energy (1893 cm^{-1}) to that of **83^{tBu}-H** (1890 cm^{-1}).

Substituting the pyridyl donor for imidazolyl in the pincer architectures yields the related *trans-trans* PCP-ligated Mo$_2$(μ–1,2-N$_2$) complexes **85** (Figure 66).[157] The N–N bonds in these complexes are on par with those for the PNP pincer compounds, such as **83^{tBu}-H**, with the stronger donating imidazolyl in **85–3** correlated with the longer N–N bond distance. These complexes are some of the most effective molecular catalysts for dinitrogen fixation to ammonia with **85–1** affording up to 230 equiv. NH$_3$ using CrCp*$_2$ and [LutH]OTf.[157] Recently, Ashida *et al.*, utilized a combination of SmI$_2$ and alcohols or water as a proton-coupled electron transfer reagent and recorded yields of 4350 equiv. NH$_3$ using the precursor {(^{tBu}P$_2$C)MoCl$_3$} of **85–1** as the catalyst.[158] The turnover frequency (117.0 min^{-1}) rivals that of the molybdenum-dependent nitrogenase (40–120 min^{-1}),[159] albeit with the more reducing SmI$_2$(OH$_2$) instead of NADH.

The bis(phosphinoethyl)amine and the bis(phosphinoethyl)phenylphosphine ligands provide a more flexible tri-pnictogen chelate as compared to the ligands in **80–85**. In the PNP system, coordinated amide is susceptible to protonation, providing a route to manage protons during chemical transformations. Silantyev *et al.*, reported the dinitrogen dimolybdenum complex [N(CH$_2$CH$_2$P^{t}Bu$_2$)$_2$ClMo]$_2$(μ–1,2-N$_2$), **86**, displaying a long N–N bond at 1.258(9) Å and low ν_{NN} stretching frequency of 1343 cm^{-1}.[160] Indeed, protonation of two amide donors in **86** afford the daughter molybdenum nitride complexes (Scheme 28). DFT calculations point to an increase in the Mo–N$_2$ σ-interaction as a result of the weaker Mo–amine vs. Mo-amide bonds.

Arashiba, *et al.* and Liao, *et al.* reported complexes **87^{tBu}** and **87^{Cy}**, respectively, using the all P donor atoms ligand (Figure 67).[161,162] From the solid state structure of **87^{Cy}**, a similar extent of N–N bond elongation as observed for the **83** complexes is seen. Vibrational data were used to infer the structure of **87^{tBu}**. In a follow-up article to the report of catalytic silylation effected by **87^{Cy}**, Liao *et al.*, showed that the reduction of the molybdenum

trichloride precursor with 3 equiv. Na/Hg in the presence of sodium iodide affords a Mo(IV) nitride complex with hypothesized intermediacy of a μ–1,2-dinitrogen transient **87$^{\text{Cy}}$-2I** (Scheme 29).[163] Shortly thereafter, Nishibayashi and coworkers demonstrated that (^{tBu}P$_2$N)MoI$_3$ (where ^{tBu}P$_2$N = 2,6-bis[(di-*tert*-butylphoshpino)methyl]pyridine) is an effective precatalyst for N$_2$ fixation to ammonia with yields, turnover frequency, and turnover numbers greater than those for **83^{tBu}-H**.[164] Given that the terminal nitride (^{tBu}P$_2$N)MoI(N) was observed in the reaction mixtures, the proposed mechanism invokes N$_2$ triple bond scission from a transient [(^{tBu}P$_2$N)MoI]$_2$(μ–1,2-N$_2$), which precedes ammonia formation from the daughter monometallic nitrides by a proton-coupled electron transfer pathway.[154] The same mechanism is proposed for (^{tBu}P$_2$C)MoCl$_3$ (where ^{tBu}P$_2$C = 2,6-bis[(di-*tert*-butylphoshpino)methyl]benzimidazolyl) reduction with SmI$_2$(OH$_2$) to yield 4350 equiv. of NH$_3$.[158]

Hexacoordinate bis(phosphine) complexes of chromium and Molybdenum (**88-M/R**, Figure 68 and Figure 69) were also reported in addition to the half-sandwich complexes (**69** and **70**) discussed above. Berben and Kozimor reported the dichromium-dinitrogen complex supported by bis(dimethylphosphino)ethane and trimethysilyl acetylide, **88-Cr/SiMe$_3$**.[165] From modeling of variable-temperature magnetic susceptibility data recorded on a solid sample of **88-Cr/SiMe$_3$**, the determined $\chi_{\text{M}}T$ (0.96 cm^{3}K/mol) is consistent with two magnetically isolated $S = \frac{1}{2}$ Cr^I centers. Formalisms then suggest a neutral and minimally-activated N$_2$ ligand. Curiously, electronic structure calculations on a simplified model of **88** [(dmpe)$_2$Cr(CCH)]$_2$(μ–1,2-N$_2$) (dmpe = bis(dimethylphosphino)ethane) proposed that the two SOMOs are M–N anti-bonding and N–N bonding in character, implying what would be an unusual oxidative enhancement of N–N bond activation.

To test this hypothesis, Shores and coworkers studied the series [**88-Cr/Si^{i}Pr$_3$**]$^{n+}$ in which n = 0, 1, and 2.[166] Magnetic susceptibility data evidence $S = 1$ and 2 ground states for [**88-Cr/Si^{i}Pr$_3$**]$^{0/2+}$, and a quartet-to-doublet spin equilibrium for [**88-Cr/Si^{i}Pr$_3$**]$^{1+}$ below 16 K. Despite the prior calculations, N–N bond lengths are within error and vibrational data indicate a marginal increase in N–N bond strength as one increases the metal formal oxidation state across the series. This trend suggests that oxidation is of a metal non-bonding d_δ orbital rather than the M–N$_2$ or N–N π^* orbital (Figure 68). The Mo analog, [(depe)(CO)Mo]$_2$(μ–1,2-N$_2$) or **88-Mo/CO**, features a short N–N bond length of 1.127(5) Å due to the *trans* influence of the CO, recapitulating the trend of π-acidic ligands disfavoring N$_2$ activation.[167] Masuda and coworkers identified the dimetallic complex without the CO ligands, [((depe)$_2$Mo)$_2$(μ-N$_2$)]$^{2+}$, by Raman spectra collected on mixtures for one-electron oxidation of *trans*-(depe)$_2$Mo(η^1-N$_2$)$_2$.[168] The $\nu_{\text{N–N}}$ of 1292 cm^{-1} is intermediate between that of hydrazine and diazene, evidencing the substantially greater activation despite the formally more oxidized Mo center as compared to **88-Mo/CO**. This transient species from Masuda ultimately affords two equivalents of the mononuclear nitride [(depe)$_2$MoN]$^+$.

3.3.2. Multimetallic chromium-dinitrogen complexes.—Sellman and Maisel reported the first example of a multinuclear chromium dinitrogen complex, [Cr(η^6-arene)(CO)$_2$](μ–1,2-N$_2$) where the arene is either hexamethylbenzene or mesitylene (**89-HMB** and **89-Mes**, respectively), from photolysis reactions of the related piano stool complex Cr(η^6-

arene)(CO)$_3$ under a N$_2$ atmosphere.[169] Solid state structures were not reported for **89-HMB** or **89-Mes**; however, Hunter and coworkers subsequently synthesized and crystallized the hexaethylbenzene congener, [Cr(η^6-C$_6$Et$_6$)(CO)$_2$]$_2$(μ–1,2-N$_2$) or **89-HEB** (Figure 70).[170] The N–N and Cr–N distances of 1.110(18) Å and 1.917(9) Å, respectively, in **89-HEB** agree with weaker metal-dinitrogen π-backbonding from competition with π-acidic CO and the arene ligand.

Yin, *et al.* recently reported the di- and trinuclear chromium-dinitrogen complexes **90-Cr$_n$/R** (n/R = 2/Cy, 3/Ph), generated by reduction of the monometallic chloride precursor with KBEt$_3$H under a dinitrogen atmosphere.[171] The substituents on phosphine donor dictate the product, with larger cone angle of Cy resulting in the dimetallic whereas Ph yields the trimetallic (Figure 71). The extent of activation of the μ–1,2-dinitrogen ligands are moderate with N–N bond lengths of 1.169 Å and 1.176 Å for **90-Cr$_2$/Cy** and **90-Cr$_3$/Ph**, respectively, consistent with the $\nu_{N–N}$ energies of 1751 and 1962 cm^{-1} (**90-Cr$_2$/Cy**) and 1739 and 1981 cm^{-1} (**90-Cr$_3$/Ph**). The higher energy vibration of each pair corresponds to the terminal N$_2$ donors in the complex. Reduction of **90-Cr$_2$/Cy** with excess K, Rb, or Cs yields the first examples of monometallic anionic Cr^0–N$_2$ compounds **91-M** where M = K, Rb, or Cs. Compound **91-K** reacts with trimethylsilyl chloride to produce the monometallic hydrazide complex—the first example of a chromium hydrazide—and the mono-chromium(II) chloride complex.

With respect to the lighter pnictogen, Theopold and coworkers synthesized a number of N-donor atom supported dinitrogen-bridged multichromium complexes (Figure 72), including the only example of η^2-coordination of N$_2$ to chromium.[172] Using the 2,6-diisopropylphenyl-substituted β-diketiminate, [^{Me}NacNac^{DIPP}]$^-$, metalation with Cr^{II} followed by reduction affords the [^{Me}NacNac^{DIPP}Cr]$_2$(μ-η^2:η^2-N$_2$), **92–2Cr**, in which the N–N bond distance of 1.249(5) Å is one of the longest in any chromium dinitrogen compound. The dinitrogen ligand is labile being readily replaced by stronger π-acid ligands (e.g., CO). Using the less encumbering 2,6-dimethylphenyl β-diketiminate [^{Me}NacNac^{Xyl}]$^-$ affords a mixture of products when the Cr(II)-hydride dimeric precursor is exposed to trimethylsilyl-diazomethane, from which the tri- and tetrachromium dinitrogen **92–3Cr** and **92–4Cr**, respectively, were isolated.[173] The solid state structures reveal the exclusive μ–1,2 coordination mode of the dinitrogen molecules in **92-nCr** (n = 3 and 4) with N–N bond lengths of 1.162 Å and 1.173 Å, and vibrational spectroscopy evidence N–N stretching frequencies of 2124–2244 cm^{-1} and 2063 cm^{-1}, respectively. Repeating the theme noted thus far, the change of coordination mode from μ-η^2:η^2 to μ–1,2 is accompanied by a shortening of the N–N bond distances.

In addition to the β-diketiminate complexes, Akturk *et al.* also reported a family of 4-coordinated dichromium dinitrogen complexes **93-R$_1$/R$_2$** in which the substituents on the supporting tris(pyrazolylborate) ligand, [^{R1,R2}Tp]$^-$, vary (Figure 73).[174] In all cases, the chromium centers are in a pseudotetrahedral geometry with a μ–1,2-dinitrogen bridge and N–N and Cr–N(N$_2$) bond lengths in the range of 1.213(5)–1.214(4) Å and 1.773(2)–1.838(3) Å, respectively. These bond distances are longer than the comparable tri- and tetrachromium complexes **92-nCr**.

3.3.3.   Multinuclear tungsten-dinitrogen compounds.—Fewer dinitrogen adducts have been reported for tungsten as compared to Mo and Cr with all examples comprising a μ−1,2-dinitrogen. Homo- or hetero-dimetallic complexes predominate; the sole tri- and tetra-metallic examples complexes **77-W$_3$** and **77-W$_4$** adopt chain-like topologies and were discussed above.

The first example of W$_2(\mu$−1,2-N$_2)$ complex was [(Et$_2$PhP)$_3$W(η^1-N$_2$)]$_2(\mu$−1,2-N$_2$), **94-Et**, followed shortly thereafter by the report of the P^{n}Pr$_2$Ph analog **94-^{n}Pr**, which were synthesized by reduction of WCl$_6$ with Mg in presence of the respective phosphine (Figure 74).[175,176] The structural solution was only able to confirm connectivity of the complex; the complex adopts a configuration analogous to that of the molybdenum PPP pincer complexes **87**. The IR spectra of **94-Et** suggest a comparable N–N vibrations for the bridging and terminal N$_2$ ligands due to the observed signals at 1890 and 1895 cm^{-1}. Subsequent to these reports, the bis(dichlorotungsten) analog [WCl$_2$(PMe$_3$)$_3$]$_2(\mu$−1,2-N$_2$) **95–2Cl**, the bis(trichlorotungsten) [WCl$_3$(PMe$_3$)$_2$]$_2(\mu$−1,2-N$_2$) **95–3Cl**, the bis(tricarbonyltungsten) [W(CO)$_3$(P^{i}Pr$_3$)$_2$]$_2(\mu$−1,2-N$_2$) **95-CO**, and [(PhN)Cl$_2$(PMe$_3$)$_2$W]$_2(\mu$-N$_2$) **95-NPh** were obtained (Figure 75). The first two were reported by Harvey, *et al.*, the carbonyl complex from Kubas and workers, and the imide by Harlan, *et al.*.[177–179] The long N–N bonds observed in **95–2Cl** (1.279(4) Å) and **95–3Cl** (1.24(2) Å) as compared to **95-CO** (1.136(6) Å with ν_{NN} = 1939cm^{-1}) bears strong resemblance with the greater N–N bond activation observed upon removal of CO ligand from **88-Mo/CO**. The N–N bond in **95-NPh** (1.19(2) Å) is of comparable length to that of **95-CO**, highlighting again the discounting effect of ancillary π-acids on N$_2$ activation. Indeed, this series of W complexes highlight the need to adopt a holistic electronic structure treatment of the metal fragment rather than overly relying on metal oxidation state.

A number of heterodimetallic compounds of W and a metal either from Group 4 or 5 have been reported by Hidai and coworkers (Figure 76).[180–182] Generally, these complexes have comparable W fragments with four P donor atoms in the square plane and an X-type donor *trans* to μ–1,2-dinitrogen. The heterometal fragment is variable as noted in Figure 76. Routes to these complexes typically arise from reaction of a bis- or mono-(dinitrogen) tungsten complex and a heterometal complex. As an example, reaction of *cis*-[W(PMe$_2$Ph)$_4(\eta^1$-N$_2)_2$] with titanocene dichloride and sodium iodide affords [Cl(PMe$_2$Ph)$_4$W(μ–1,2)TiCp$_2$Cl], **96–1**. In these complexes, the frequency of the N–N stretching mode is substantially lower than that of free N$_2$, ranging from 1408 cm^{-1} to 1545 cm^{-1} and in agreement with the formally low valent W center, the strong ligand field, and the push-pull effect of the W center and electropositive early transition metal. A related push-pull effect is proposed for N$_2$ fixation by nitrogenases in which the acidic amino acid side chains polarize the cofactor-bound dinitrogen ligand.[183,184] Here, the proximal Lewis acidic groups and the cofactor pull and push electron density, respectively, into the bound dinitrogen. Similar effects are noted in the **96** series of compounds with the protic Lewis acid replaced by the Gp 4 or 5 metal center. Protonolysis of **96–1** and [I(PMe$_2$Ph)$_4$W(μ-N2)ZrCp$_2$Cl], **96–2**, with excess sulfuric acid yields 0.86 mol of NH$_3$ and 0.08 mol of N$_2$H$_4$ per mole of **96–1**, and 0.33 mol of NH$_3$ and 0.16 mol of N$_2$H$_4$ per mole **96–2** with no observable N$_2$ evolution in either case. Further derivatization of these complexes is possible;

treatment of **96–2** with excess pyridine substitutes one of the phosphine ligands to yield **96–2Py** in which the bond metrics are comparable to those in **96–2**.

Comparisons between ligand field and the consequences on N_2 activation across the **96** series follows the trend that decreased π-acidity and increased electron donating ability of the ancillary ligands enhances N_2 activation. For $[Cl(PMe_2Ph)_4W(\mu–1,2)TiCpCl_2]$, **96–3**, vs. **96–1** in which the heterometal fragment is a $CpTiCl_2$ instead of Cp_2TiCl, one notes greater activation of the N–N bond (*viz.* $\nu_{N–N}$ = 1468 cm^{-1} and 1408 cm^{-1} in **96–1** and **96–3**, respectively). Similarly, the energy of N–N stretching mode for $[NCS(dppe)_2W(\mu–1,2-N_2)TiCp'Cl_2]$ (Cp′ = Cp for 96–4, Cp* for 96–5), is greater for **96–4** vs. **96–5** (1441 cm^{-1} vs. 1433 cm^{-1}). One also notes greater activation of the N_2 ligand for the Ta and Nb heterometallic complexes.

Reduction of $(\eta^5\text{-}Cp^*)W(Me)_3Cl$ with sodium-mercury amalgam in THF gave the first organometallic ditungsten dinitrogen complex **97-Me** (Figure 77).[185] This complex is analogous to reported dimolybdenum and heterodimetallic molybdenum-tungsten complexes for which the metal coordination environments are comparable. However, **97-Me** arises from incorporation of atmospheric N_2 whereas the Mo_2 and MoW compounds utilize hydrazine or the hydrazide complex in their syntheses. The N–N bond of 1.334(26) Å in **97-Me** is one of the longest reported for a $\mu–1,2$-dinitrogen complex, and longer than that of the Mo_2 and MoW analogs.[186] Building on this report, O'Regan, *et al.* developed a general methodology to replace methyl ligands in **97-Me** without dissolution of dimetallic.[187] Reaction of **97-Me** with two equiv. HX (X=Cl, OTf, $O_2CC_6F_5$, OC_6F_5 and SC_6F_5) affords a series of **97-X**, with the exchange of one methyl group per W center. Use of HBF_4 in the presence of acetonitrile instead of an acid with a coordinating conjugate base gives the dicationic solvent-adduct $[\textbf{97-ACN}]^{2+}$. Loss of the strongly donating methyl ligand results in a decrease in the N–N bond distance as evidenced in **97-OC$_6$F$_5$** with a N–N bond length of 1.26(2) Å. Reaction of **97-Me** with 6 equiv. HOTf or tetrabromocatechol leads to loss of two methyl groups per W center (**98-OTf** and **98-Br$_4$Cat**, respectively), with the tetrakis(triflate) complex providing a useful starting material to further derivatization. For example, thiolates can be incorporated into **98-OTf** to generate the corresponding $[Cp^*W(Me)_2(SR)]_2(\mu–1,2-N_2)$ (R = 2,4,6-$Me_3C_6H_2$ and 2,4,6-$^iPr_3C_6H_2$) complexes, which are inaccessible from **97-Me** with the respective thiol. As noted already, substitution of methyl leads to decreased π-backbonding from the W center to the N_2 ligand as reflected in the N–N bond distance.

3.4. Group 7: Mn, Tc, and Re

The dinitrogen coordination chemistry of Group 7 metals is substantially less than of the neighboring groups; arguably, the radioactivity of Tc has limited greater exploration of its coordination chemistry and the *s*-block like coordination chemistry of Mn (particularly Mn^{II}) have similarly contributed to its limited investigation in this arena by comparison to other mid-to-late first row transition metals. Consequently, the dinitrogen-related chemistry is dominated by that of Re for this group with few examples for Mn.

3.4.1. Manganese and Technetium Complexes.—The first example of a N_2-bridged dimanganese complex did not arise from coordination of atmospheric dinitrogen,

but rather from a diazoalkane. In 1976, Ziegler, *et al.* reported that addition of 2,2,2-trifluorodiazoethane to $[(C_5H_4R)(CO)_2(THF)Mn]$ afforded the N_2 bridged complex $[(C_5H_4R)(CO)_2Mn]_2(\mu-1,2-N_2)$ (R=H, Me).[188] These compounds exhibit IR absorptions attributable to the N_2 stretching mode at 1971–1975 cm^{-1}, which are consistent with the crystallographic N–N bond distance of 1.118(7) Å and the inclusion of π acidic CO ancillary ligands in the complex. In 1979, Sellman and coworkers reported the related MnCr heterodimetallic $[(C_5H_5)(CO)_2Mn](\mu-1,2-N_2)[Cr(CO)_5]$ utilizing $(C_5H_5)(CO)_2Mn(\eta^1-N_2)$ and $[Cr(CO)_5(THF)]$; the latter is formally a N_2 complex although generated by oxidation of the hydrazide precursor.[189]

The first multimanganese–dinitrogen complex arising from capture of atmospheric dinitrogen was $[N_2P_2]_2Mn(\mu-1,2-N_2)$ (**99**), which was synthesized by sodium naphthalenide reduction of the monometallic manganese chloride precursor (Figure 78).[78,190] Each Mn center in this complex adopts a pseudotetrahedral coordination sphere with the N–N bond length of 1.208(6) Å and ν_{N-N} stretching band from IR data at 1685 cm^{-1}. An analogous μ–1,2-dinitrogen complex with pseudotetrahedral metal centers was reported by Theopold and coworkers. Chemical reduction of $^{tBu,Me}TpMnCl$ under a dinitrogen atmosphere afforded the corresponding end-on/end-on bridged dimetallic $(^{tBu,Me}TpMn)_2(\mu-1,2-N_2)$, **100-Mn** (Figure 79).[191] The bond metrics are comparable to that of **99** with a d(N–N) of 1.196(5) Å.

Ziegler and coworkers obtained the only known example of a dinitrogen-bridged ditechnetium complex by photolysis of $[Tp'(CO)_3Tc]$ (Tp$'$ = tris(3,5-dimethyl-1-pyrazolyl)borate) in THF under N_2 (**100-Tc**, Figure 80).[192] The complex bears similarity to the Mn analog **100-Mn**. Given the presence of two CO donors per Tc center, the N–N bond distance (1.160(3) Å) is expectedly shorter than that for the Mn congener. We note here for comparison that Gunnoe, *et al.* reported the rhenium congener, $[Tp(CO)_2Re](\mu-1,2-N_2)$, **100-Re** (Figure 80).[193] The bond metrics for this complex are comparable to that of **100-Tc** with M–N and N–N bond lengths of 1.98(1) Å and 1.15(2) Å, respectively.

3.4.2. Rhenium Complexes.—The earliest examples of multimetallic-dinitrogen complexes containing Re were a series of heteronuclear complexes in which $(PhMe_2P)_4Re(N_2)Cl$ was used as a building block,[194–197] and a number of similar complexes have since been reported (Figure 81 and Scheme 30).[198–201] The general trend across the series is as noted for the heteronuclear molybdenum complexes from Schrock and coworkers; that is, higher nuclearity (1.154(29) for **101-Re$_2$Mo** to 1.18(3) for **101-ReMo-1**) results in decreased activation of the μ–1,2-dinitrogen donors whereas multiple Lewis acidic centers interacting with one N_2 donor lower the energy of the N–N stretching mode (1805 cm^{-1} for **101-ReTi-1** to 1622 cm^{-1} **101-ReTi$_2$**). Relatedly, heavier d^0 heterometals correlate with higher N–N stretching frequency as compared to their lighter counterparts, which again is related to the changes to Lewis acidity.

Schneider and coworkers have reported that reduction of a bis(phosphine)-amido (or $P^{(CH2)2}N^{(CH2)2}P^{tBu}$) rhenium dichloride, $(P^{(CH2)2}N^{(CH2)2}P^{tBu})ReCl_2$, by one electron with Na/Hg or CoCp*$_2$ under a N_2 atmosphere affords a mononuclear rhenium nitride product.[202] A dinitrogen-bridged dirhenium complex was the proposed intermediate with the reaction

traversing a mechanism similar to that proposed for Cummins'
tris(anilido)molybdenum(III). Subsequently, the complex [(P$^{(CH2)2}$N$^{(CH2)2}$P^{tBu})ReCl]$_2$(μ
−1,2-N$_2$) (**102**) was isolated and characterized (Figure 82).[203] X-ray data reveal a N–N bond
distance of 1.202(10) Å and short Re–N(N$_2$) bonds of 1.861(6) and 1.886(8) Å, consistent
with the N–N stretching mode observed in resonance Raman experiments at 1771 cm^{-1}.
Recently, the same group reported a slightly different system, (HPNP^{iPr})ReCl$_3$, which
effects the photochemical cleavage of N$_2$ to yield the corresponding nitride species.[204] The
analogous (μ–1,2-dinitrogen)dirhenium complex, **103**, could be synthesized by one-electron
reduction of (HPNP^{iPr})ReCl$_3$ with CoCp*$_2$ in the presence of N$_2$ (Figure 83). In contrast to
102, the pincer N-atoms are *trans* to the N$_2$ bridge in the solid-state structure of
[(HPNP^{iPr})ReCl$_2$]$_2$(μ–1,2-N$_2$). All metrics indicate less activation of the N–N bond in **103**
as compared to **102**; the N–N bond length and ν_{N-N} are 1.169(5) Å and 1733 cm^{-1},
respectively. This proton-dependent differences in N$_2$ activation are analogous to that for Mo
complex **86**.

3.5.   Group 8: Fe, Ru, and Os

The dinitrogen coordination chemistry of the Group 8 metals has primarily focused on iron-
based complexes, owing in large part to the use of Fe in the Mittasch catalyst and as the
common metal type across all forms of the nitrogenase enzymes. The reported compounds
presented below are primarily dimetallic complexes, with rare instances of higher nuclearity
complexes. The discussion below begins with arene and cyclopentadienyl complexes, and
subsequently treats examples with descending denticity of the supporting ligand.

3.5.1.   Arene and cyclopentadienyl complexes.—Few complexes of the Group 8
metals bearing arene or cyclopentadienyl moieties have been reported compared to other
ancillary ligands. Of these examples of Cp- (or Cp*) bearing dimetallic N$_2$ complexes, the
osmium compounds were accessed by methods beyond the scope of this review and will not
be discussed.[205,206]

The first crystallographically-characterized Fe–N$_2$ complex bearing a Cp* ligand was
reported in 2008 by Tatsumi and coworkers, **104** (Figure 84).[207] The experimentally-
determined N–N bond length of 1.132 Å and ν_{N-N} stretching frequency of 2126 cm^{-1} are
comparable to that of many of the reported mononuclear Fe^{II}–(η^1:N$_2$) compounds supported
by phosphine or related strong-field ligands (*vide infra*). Solution-phase UV/visible and ^{1}H-
NMR data evidence an equilibrium between the diiron species **104** and the related
monoiron-dinitrogen species.

Recently, Zhang *et al.,* reported a unique example of a dinitrogen bridged diiron compound
105 (Figure 84), which utilizes a bidentate phosphinothiolate as an ancillary ligand.[208] The
complex displays typical structural and spectroscopic parameters for end-on/end-on Fe^{II}–N$_2$
complexes with a N–N bond length of 1.130 Å and N$_2$ stretching frequency of 2016 cm^{-1}.

A mixed phosphorus chalcogenide chelate was also reported for Ru; that is, the two (k^2-
P,O-1-P^{i}Pr$_2$-2-indanone)Cp*Ru fragments bridged by N$_2$ in **106** (Figure 84).[209] The N–N
bond length of 1.131(8) Å and the resonance Raman active ν_{N-N} band observed at 2042 cm
$^{-1}$ are comparable to the data for **105**, which is somewhat surprising given the general trend

noted up to this point. One observes similar bond metrics and vibrational data for the $[(Cp(P)_2Ru)_2(\mu-1,2-N_2)])][BAr^4_F]_2$ $((P)_2$ = dippe, $(PEt_3)_2$, $(PMe^iPr_2)_2$, $(PPh_3)_2)$, **107** (Figure 84).[210,211] Specifically, the d(N–N) values vary from 1.114(5) Å for the bis-PEt_3 complex to 1.123 Å for bis-PPh_3 with the N–N stretching mode observed at 2050 cm^{-1} (dippe), 2062 cm^{-1} (PPh_3), and 2064 cm^{-1} (PEt_3) in resonance Raman spectra. No Raman data nor crystal structure were obtained for the bis-PMe^iPr_2 ligated derivative.

Moving to complexes with η^6-arene ligands, an amidinato diiron-dinitrogen complex $\{(Dipp)NC(^tBu)N(\eta^6$-Dipp)Fe]_2(\mu-1,2-N_2)\}$, **108**, was obtained from magnesium reduction of the diiron di(μ-bromide) precursor under N_2 (Figure 85).[212] The N–N and Fe–$N(N_2)$ bond distances of 1.124(6) and 1.834(3) Å, respectively, are consistent with the vibrational data (ν_{N-N} = 2005 cm^{-1}) and as one might anticipate for a formally lower valent Fe center as compared to **105**. Complex **108** can also be accessed by displacement of a η^6-toluene ligand by N_2 in a monometallic precursor.

The last arene examples are from Sunada and coworkers. The pair of half-sandwich bis-silyl diiron(II) dinitrogen complexes $[(\eta^6$-$C_6H_5R)Fe(Me_2SiC_6H_4SiMe_2)]_2(\mu-1,2-N_2)$ (**109-R**; **R** = H, Me) derived from reaction of $[Fe(mesityl)_2]_2$ with 1,2-bis(dimethylsilyl)benzene in benzene or toluene (Figure 85).[213] Again, we note that the N–N bond distances are unremarkable from the vantage of N_2 activation and functionalization with d(N–N) values of 1.119(3) Å and 1.126(3) Å for **109-H** and **109-Me**, respectively, which agree with the ~300 cm^{-1} bathochromic shift for the N–N vibration vs. free N_2 (*i.e.*, ν_{N-N} = 2035 cm^{-1} and 2022 cm^{-1} for R = H and Me, respectively). The dinitrogen ligand is readily displaced in this system by ligands, such as CO or PPh_3, and oxidative addition of H_2 is also reported.

3.5.2. Tetradentate ligands.—Collman *et al.* reported the earliest example of a complex in which a designed pocket was constructed to bind dinitrogen: the diruthenium(II) μ–1,2-dinitrogen complex, **110**, supported by a cofacial diporphyrin ligand (Figure 86).[214] The N–N distance of 1.1 Å in a partially refined structure is expected given the energy of the observed ν_{N-N} stretching mode at 2112 cm^{-1}, and both reflect the relatively weak π-backbonding afforded by the Ru^{II} centers.

Related to this report by Collman is that from Floriani and coworkers of a tetrapyrrolide diruthenium dinitrogen complex by utilizing a *meso*-octaalkylporphyrinogen tetraanion. Occupation of the fifth coordination site on the mononuclear Ru precursors by NaCCH affords $Na_6\{[(Me_8N_4)Ru]_2(\mu-1,2-N_2)\}$,[215] for which solvent results in differences to the acetylide moiety. When crystalized from DME the complex **111** is best described as containing an acetylide ligand with Ru–C and C–C distances of 1.875(3) Å and 1.185(4) Å, respectively, whereas the THF solvate, **111-THF**, evidences more vinylidene character with a contracted Ru–C (1.807(9) Å) and elongated C–C distances (1.31(1) Å) as compared with **111** (Figure 87). In both structures, however, the Ru_2N_2 core with d(N–N) = 1.28(1) Å is common with the end-on/end-on N_2 unit bridging the two ruthenium centers and interacting with four sodium cations. This bond length is the longest observed for a late transition metal with an end-on dinitrogen ligand. Notably, the Ru–$N(N_2)$ distance of 2.251(8) Å in **111-THF** is the longest of any dinuclear ruthenium dinitrogen complex, highlighting the effect of the Lewis acid interactions on N_2 activation.

Tetradentate ligands capable of imposing a trigonal coordination environment in analogous fashion to the previously discussed tren systems for Ti and Mo have also been employed for Group 8 metals. Beginning with the all phosphine examples, the dinuclear iron(II) dihydride dinitrogen complex $[((PP_3)HFe)_2(\mu–1,2\text{-}N_2)][BAr^F_4]_2$, **112–2H**, and the related mono-(**112–1H**) and di-deprotonated (**112-noH**) complexes were reported by Field and coworkers (Figure 88).[216] Although the N–N distances remain within error (1.129(4) Å for **112–2H** vs. 1.127(2) Å for **112–1H**) across the series, the Fe–N(N_2) markedly contracts with values of 1.905(2) Å and 1.798(2) Å for **112–2H** and **112–1H**, respectively, as anticipated for greater π-backdonation from the formally more reduced metal centers (Figure 88).

Building from the trigonal triphosphine ligands developed by their group (*vide infra*), Peters and coworkers developed a family of ligands wherein the apical unique P donor in **112** is replaced by a variety of donor atoms. Although these P_3X ligands do not afford multimetallic N_2 complexes, a subsequent iteration of this ligand design in which two of the meridional P donor atoms are replaced with thioether groups and the axial P donor substituted for a silicide allowed access to the diiron complex **113** by the one-electron reduction of the monometallic precursor under N_2 (Figure 89).[217] The structure was proposed based on vibration spectroscopic methods; $\nu_{N–N}$ stretching mode observed at 1881 cm^{-1} for **113** suggests a dimetallic system.

Related to **112** and the ligands developed by the Peters group is the alane-based system (Altraphos) from Lu and coworkers in which a tren-like pocket binds Al^{III} with a phosphine rimmed upper cavity for binding a second metal ion (Figure 90). The formally iron(0) complex of this alatrane binds N_2 in an end-on/end-on fashion to yield **114**,[218] for which IR spectra with the $\nu_{N–N}$ for the N–N stretching mode observed at 2010 cm^{-1} and an X-ray diffraction determined d(N–N) value of 1.146(7) Å. The lesser extent of activation of the N_2 ligand in **114** as compared to **112** and **113** can be attributed to the σ acidity of the Al^{III} center *trans* to the N_2 donor.

The final two tetradentate examples are the diruthenium polyamine complexes in which the metal centers are six-coordinate: The water-soluble dinitrogen-bridged diruthenium(II) polyamine complex **115** from Yoshimoto *et al.* and the N_2S_2-supported diruthenium compound **116** from Sellman and coworkers (Figure 91).[219,220] Both complexes exhibit similar N–N bond distances with values of 1.126(3) Å and 1.120(6) Å for **115** and **116**, respectively, and comparable to that for the Taube complex $\{[(NH_3)_5Ru](\mu–1,2\text{-}N_2)\}^{4+}$.[21] The $\nu_{N–N}$ stretch is observed by resonance Raman spectroscopy at 1994 cm^{-1} for **115** and is lower than the reported energy for this vibration in **116** (*viz.* 2047 cm^{-1}).

3.5.3. Tridentate ligands: meridional chelates.—The bis(imino)pyridine (PDI) derivatives are the only meridional chelating or pincer ligand for which N_2 complexes of more than one Group 8 metal have been reported. A number of iron examples have been reported by Chirik and coworkers of the general type $[(^{R1,R2}PDI)Fe(N_2)]_2(\mu–1,2\text{-}N_2)$ with R_1/R_2 = Me/Me, Et/Et, or Me/^iPr (**117-R$_1$,R$_2$**) or a bis(arylimidazol-2-ylidene)pyridine (^{Me}CNC), $[(^{Me}CNC)Fe(N_2)]_2(\mu–1,2\text{-}N_2)$, **117–2** (Figure 92).[221,222] In all cases, the bridging N_2 ligands are minimally activated based on spectroscopic data and single-crystal X-ray diffraction structures; for example, the N–N bond distances for the bridging N_2 in **117-**

Me,Me and **-Et,Et** are 1.137 and 1.123(3) Å, respectively, and Mößbauer data are consistent with formally iron(II) centers and reduced pincer ligands, rather than zero-valent metal centers.[223,224] Insofar as the bis(imino)pyridine ligand has an accessible LUMO, one anticipates such ligand-based reduction rather than population of N_2 π^* orbitals.

Related to **117** are ruthenium complexes **118** in which a similar PDI chelate is employed with minor differences to substituents on the pyridine ring and the aryl groups on the imine N atoms (Figure 93).[221,222,225,226] The long N–N bond distance, such as the 1.161(5) Å value determined for **118–1**, are consistent with more electron rich Ru centers as compared to the previously discussed complexes, and suggest Ru(I) or Ru(0) character for these compounds. ^{1}H-NMR spectroscopic data and computational methods suggest that the ground state is an admixture of an $S = 0$ state and low-lying electronic states of higher-spin multiplicities; this result was interpreted as reflecting the ligand non-innocence of the PDI chelate. **118–2** readily reacts with H_2 to afford the hydride derivative **118–2H**; the contraction of the N–N distance to 1.132(6) Å agrees with a more oxidized Ru center. One notes that extent of activation of the N_2 ligand based on structural metrics and vibrational data is comparable for Fe and Ru in analogous ligand sets.

Derivatives of the PDI architecture in which the imine arms are saturated have also been explored in the context of ruthenium dinitrogen coordination chemistry. Generally, the ligands utilized employ a pyridyl or phenylide ring with saturated pnictogen donor atoms in the flanking arms. One such series comprises the pincers bearing two dimethylamine arms, two di(*tert*-butyl)phosphine arms, and two di(*tert*-butyl)arsine arms as well as the NNP pincer in which one arm is a di(*tert*-butyl)phosphine and the other a dimethylamine (**119-X**, where **X** = **2N** for bis(dimethylamine), **NP** for (dimethylamine)(di(t-butyl)phosphine), **2P** for bis(di(t-butyl)phosphine), or **2As** for bis(di(t-butyl)arsine)); (Figure 94).[227–230] For these complexes, two chloride ligands complete the coordination sphere on each metal and the N_2 fragment adopts a μ–1,2 coordination mode with the two pyridyl planes being orthogonal, implying that each metal backbonds into a different dinitrogen π^* orbital. The N–N distances are comparable across the series with values of 1.110(3) Å, 1.119(4) Å, 1.121(6) Å, and 1.108(5) Å for **119–2N**, **–2P**, **-NP**, and **–2As**, respectively. The trend matches that of donor strength, although the observed changes are minimal. The crystallographic bond distances are consistent with the vibrational data where reported (*e.g.*, $\nu_{N–N} = 2099$ cm^{-1} for **119–2N**).

A diruthenium complex **120** ligated by a phenylide congener of **119–2P** was reported by Antipin and coworkers (Figure 95), although direct comparison to **119–2P** cannot be readily made as the ancillary ligands differ (*viz.* hydride and dinitrogen in **120** vs. two chlorides in **119–2P**).[231] The N–N bond distance of 1.134(6) Å in the solid state structure of **120** is comparable to that of the **119** complexes and provides a consistent picture of minimal backbonding in these ruthenium pincer complexes. Members of these pincer complexes with saturated arms are in equilibrium with monometallic species, evidenced in some cases by NMR and vibrational spectroscopies.

Nishibayashi and coworkers reported a diiron dinitrogen complex of a related NP$_2$ pincer ligand (**121**) as the pyridyl systems; however, the anionic carbazole N atom provides a

stronger donor than that of the pyridyl discussed above (Figure 96).[232] In contrast to the planar pyridine-based PNP-pincer Mo analogs ($\mathbf{83^R}$- $\mathbf{R'}$), the metal centers in **121** adopt a distorted tetrahedral geometry about the Fe center with solution magnetometry measurements indicating high spin d^7 metal centers. The observed spin state and geometry are attributed to the size and rigidity of the chelate ring of the complex as the greater rigidity of pyrrole-based complexes favor the square-planar geometry whereas the more flexible six-membered chelate rings of the carbazole complex allow access to the less-strained tetrahedral arrangement. Catalytic N_2 fixation to NH_3 was investigated, however, only minimal amounts of ammonia (0.5 equiv.) were obtained.

Expanding beyond the more typical pincer architectures, Suzuki, *et al.* used a tridentate iminophosphorane ligand to synthesize the diiron-dinitrogen complex **122** (Figure 97).[233] X-ray crystallography evidences each iron center in a distorted trigonal monopyramidal geometry ($\tau = 0.64$ and 0.65) with d(N–N) = 1.184(6) Å being comparable with other diiron systems discussed above. The Fe–N(N_2) distances of 1.800(4) and 1.814(4) Å, N–N stretching frequency of 1755 cm^{-1}, Mössbauer data with δ = 0.73 mm/s and E_Q = 1.83 mm/s, and DFT calculations are all consistent with substantial activation of the N_2 donor.

The final example of a Group 8 diiron-dinitrogen species employing a pincer ligand is the dinitrogen-bridged di(hydridoiron) complex **123** from Peters and coworkers (Figure 98).[17] Complex **123** was synthesized by reduction of the mononuclear iron(II) dibromide precursor with NaHBEt$_3$. The complex exhibits a singlet ground state arising from the anti-ferromagnetic coupling between the two $S = \frac{1}{2}$ iron centers, which is consistent with the strong ligand field on each metal center. Complex **123** is competent towards catalytic NH_3 formation from N_2 under photolytic conditions, despite a weakly activated N_2 ligand.

3.5.4. Tridentate ligands: pseudo-C_{3v} or *fac* chelates.—The tris(pyrazolyl)borate ligand family is the only *fac* ligand for which both iron and ruthenium dinitrogen species have been reported. Valerga, Puerta, and coworkers reported the dinuclear Ru complexes **124–1/R** (**R** = Me, iPr, and Ph; Figure 99) and **124–2** (Figure 100), in which the unsubstituted tris(pyrazolyl)borate is bound in a *fac* mode and an additional bidentate ligand and a μ-1,2-N_2 occupy the remaining three sites on each metal center.[234,235] The N–N bond distance is longer for **124–1/Me** as compared to **124–1/Ph**, but statistically equivalent to **124–2** (*i.e.*, 1.124(5) vs. 1.103(6) and 1.117(7) Å, respectively). The observed crystallographic changes in the Ru–N(N_2) distances (*viz.* 1.971(6) and 1.884(6) for **R** = Me, and 1.941 Å and 1.925 Å for **124–1/Ph** and **124–2**, respectively) suggest, however, that N_2 activation is increased in **124–1/Me**. For **124–1/Me** vs. **124–1/Ph**, the increased steric conflicts imposed by the Ph vs. Me substituents result in hindered approach of the two metal fragments disfavoring greater metal-dinitrogen π-backbonding and consequent N_2 activation; however, one notes that vibrational data indicate no major differences between the compounds with $\nu_{N–N}$ = 2091 cm^{-1} for **124–1/Me** and 2093 cm^{-1} for **124–1/iPr**. No N–N stretching band was observed for R = Ph due to the thermal decomposition of the complex by the laser.

One notable difference between Ru examples **124–1** and **124–2** and the iron congeners is that the latter complexes employ more sterically encumbering substituents on the pyrazolate

donors, thereby enforcing four coordinate Fe centers. The first report of such an iron species was by McSkimming, *et al.* of the dinuclear Fe–N_2 complex $(Tp^{Ph,Me}Fe)_2(\mu$–$1,2$-$N_2)$, **125–1** (Figure 101).[236] X-ray crystallographic values for d(N–N) of 1.180(2) Å and the short Fe–N(N_2) distance of 1.790 Å and the observed N–N stretching mode at 1779 cm^{-1} in resonance Raman spectra evidence the strong π-back donation from the iron(I) center to the dinitrogen ligand and suggesting a Fe^{II}–(N_2^{2-})–Fe^{II} formalism. The pyrazolate donors provide a weaker ligand field as compared to the phosphine donors from Peters (*vide infra* and to be discussed shortly), affording a solution magnetic moment of $\mu_{eff} = 6.9 \pm 0.2 \; \mu_B$ attributed to ferrimagnetism from two $S = 2 \; Fe^{II}$ centers antiferromagnetically coupled with the bridging $S = 1$ diazenide. Shortly following the report of **125–1**, Theopold and coworkers reported the dinculear iron-dinitrogen complex **125–2**, which is isostructural to **93-^{t}Bu/Me** and **100-Mn** (*vide supra*) and synthesized by reduction of the iron(II) iodide precursor with KC_8.[166] The N–N bond length reported is within error of **125–1** as one might anticipate given the comparable ligand fields as are the observed ground spin state for these complexes.

An asymmetric diiron-N_2 complex was prepared when $^{iPr2}TpFe(II)Cl$ was combined with $(depe)_2FeN_2$ resulting in the complex $[(depe)_2Fe](\mu$–$1,2$-$N_2)[FeTp^{iPr,iPr}]BAr^F_4$ (**126**) for which the IVCT band at 910 nm ($\varepsilon = 1700 \; M^{-1}cm^{-1}$) suggest the charge localization with formal Fe(0) and Fe(II) centers on the method timescales (Scheme 31).[237] The effect of adding an oxidized iron center instead of a reduced iron center is apparent when comparing the d(N–N) and N–N stretching frequency of **126** with that of **127**, which was reported by Ashley and coworkers.[238] The N–N bond distance is shorter and the N–N stretching mode observed at higher energy for **127** as compared to **126**. Thus, implying a push-pull effect wherein the more Lewis acidic Fe^{II} center aids in activation of the N_2 fragment. In the context of FeMoco, spatially resolved anomalous dispersion refinement (SpReAD) reported by Einsle and coworkers suggested unequal electron distribution within the resting state $S = 3/2$ of the cofactor. Should similar disparities in electron distribution be manifested in the E_4 state of the cofactor, which binds N_2, a similar push-pull effect may operate if dinitrogen coordinates in a bridging mode.[183,239,240]

Two mixed-ligand dinuclear clusters $(Cn*Ru)(\mu_2$-$H)_2(RuH(PR_3)_2)$ were bridged together by a dinitrogen bridge forming $[\{RuCn*(\mu_2$-$H)_2RuH(PR_3)_2\}_2(\mu$–$1,2$-$N_2)](PF_6)_2$ **128-R** where Cn* = 1,4,7-trimethyl-1,4,7-triazacyclononane and **R** = ^{i}Pr and Cyp or Cyclopentyl (Figure 102).[241] The cyclopentyl congener was structurally characterized with the observed distances of 1.135(5) Å and 1.937(3) Å for the N–N and Ru–N(N_2) bonds, respectively, being comparable to other dinuclear ruthenium dinitrogen complexes.

Continuing the theme of trigonal ligands, the metallo-ligand ruthenium dinitrogen complex $[(CpCo\{P(O)(OEt)_2\}_3)bpyRu](\mu$–$1,2$-$N_2)$ **129** was structurally characterized with N–N and Ru–N(N_2) bond distances of 1.130(6), and 1.890(5)–1.916(6) Å, respectively (Figure 103).[242] Together with resonance Raman data, which show the ν_{N-N} stretching band at 2000 cm^{-1}, **129** is one of the most activated diRu^{II}-dinitrogen complexes to date.

In 2003, Peters and coworkers synthesized a dimetallic four-coordinate iron complex by utilizing a tripodal, triphosphinoborate ligand $[PhB(CH_2CH_2P^iPr_2)_3]^-$. On treating

[PhBP$^{iPr}_3$]FeCl with 1 equiv of Na/Hg a dinuclear iron complex with end-on bound dinitrogen, ([PhB(P^{i}Pr)$_3$]Fe)$_2$(μ–1,2-N$_2$) (**130**; Figure 104) was formed.[243] This complex can also be prepared by reductive coupling between two Fe(IV) nitrides reminiscent of the high valent ruthenium and osmium complexes (*vide infra*).[244] The N–N and Fe–N(N$_2$) distances are 1.138(6) Å and 1.811(5)–1.818(5) Å, respectively, evidencing minimally activated N$_2$. The one-electron reduced mixed-valent congener is also accessible by reduction with Na/Hg (**130-red**). The N–N bond length increases to 1.171(4) Å as compared to **130**, as might be predicted given the more reducing nature of the metal ions.

Chomitz and Arnold reported the dinitrogen-diiron complex bearing a N$_2$P$_2$ ligand (**131**), which is structurally analogous to the tren ligands, but this ligand coordinates κ^3 with the apical N not coordinated to the metal centers (Figure 105).[78] Substituting a neutral phosphine in **130** for a more basic amide donor in **131** results in an elongation of the N–N distance (1.166(3) Å for **131**), which agrees with the energy for the N–N stretching mode (1760 cm^{-1}).

The dinitrogen-bridged diiron complex using the cyclohexyl-substituted derivative of the [PhBP$^{iPr}_3$]$^-$ scaffold (**132**) was prepared by Saouma, *et al.* (Figure 106). In contrast to the four coordinate Fe centers in **130**, the iron centers in **132** are six coordinate with a κ^2-acetate as a coligand. The μ–1,2-dinitrogen complex is in equilibrium with the dinitrogen-free monoiron species upon warming; together with the N–N bond length of 1.120 Å and a stretching frequency at 2083 cm^{-1}, this observation points to minimal activation of the N$_2$ donor. A series of related species to **132** were also reported, including the hydrazide, diazenide, and ammonia adducts; although the reactivity and interconversion of these species bears relevance to N$_2$ activation, such details are beyond our defined scope here.[245]

Peters and coworkers have developed a pair of tridentate ligand scaffolds redolent of their triphosphinoborane system in which the tridentate diphosphinoborane (or DPB) ligand has sufficient flexibility to adopt a facial coordination mode rather than the meridional mode of the typical pincer ligand family. Reduction of the isopropyl-substituted (DPB)FeBr complex with 1 equiv. Na/Hg yields the diiron-(μ–1,2-N$_2$) complex, **133** (Figure 107).[22] The solid-state structure of the compound displays the two Fe centers in pseudotetrahedral coordination geometries, with one Fe center interacting with the *ipso*-C of the phenyl substituent on B and the other Fe ion bound η^2 to the *ortho*- and *ipso*-C of the phenyl substituent; this Fe-BC interaction is highly flexible, however, as the ^{1}H NMR spectrum indicates the two Fe centers are equivalent. The N–N bond distance of 1.17 Å is comparable to that for **131** and elongated with respect to **130**; the latter comparison is complicated by the metal–B interaction which could be considered as a formal borane, boryl, or boride with an iron center in either the zero-, mono- or di-valent oxidation states.

3.5.5. Bidentate ligands.—β-diketiminates have been the most utilized with respect to iron-dinitrogen chemistry. The first such example was the three coordinate end-on/end-on dinitrogen complex [(^{Dipp}NacNac^{tBu})Fe]$_2$(μ–1,2-N$_2$), **134-^{t}Bu**, reported by Holland and coworkers, followed later by the two-electron reduced congeners M$_2${[(^{Dipp}NacNac^{tBu})Fe]$_2$(μ–1,2-N$_2$)}, **134-^{t}Bu/2M** (Figure 108).[246] Prior to reduction, the N–N bond is ~ 0.1 Å longer than that in free N$_2$ for **134-^{t}Bu** with a value of 1.182(5) Å, and

reduction to **134-^{t}Bu/2M** activates the bound N_2 with the bond distance elongated to 1.239(4) and 1.233(6) Å, for **M** = Na and K, respectively. Consistent with greater extent of π-backbonding, one notes that the Fe–N(N$_2$) shortens from 1.770(5)–1.779(5) Å to 1.763(6)–1.765(6) Å in **134-^{t}Bu/2K** as well as a decrease in the energy of the N–N stretching mode from 1778 cm^{-1} in **134-^{t}Bu** to 1583 cm^{-1} and 1589 cm^{-1} for **134-^{t}Bu/2Na** and **134-^{t}Bu/2K**, respectively. Indeed, the same trend is observed for the N–N and Fe–N(N$_2$) bond distances and the energy of the N–N vibration for the analogous methyl substituted congener: [(^{Dipp}NacNac^{Me})Fe]$_2$(μ–1,2-N$_2$) or **134-Me**; the one-electron reduced analog **134-Me/K,** wherein the K cation is chelated by a crown ether;[247] and the two-electron reduced complexes **134-Me/2M** (**M** = Na, K, Cs, Rb). Across these series of complexes, one notes that the N–N and Fe–N(N$_2$) bond distances and the energies for the N–N stretching modes exhibit minimal sensitivity to the alkali cation identity (Figure 108); encapsulation of that cation, however, afford structural metrics within error of that in **134-Me**, evidencing the added effect of the cation-N$_2$ interaction towards favoring π-backbonding. Taken together, the bonding picture evidenced from the structural and vibrational data are recapitulated in the magnetic, Mößbauer, and DFT results: **134-R** (**R** = ^{t}Bu, Me) is best described as being a ferrimagnet due to antiferromagnetic coupling between each Fe^{II} center and a triplet N$_2^{2-}$. A similar electronic structure was later proposed for the tris(pyrazolyl)borate complex **125**, mentioned above. Addition of pyridines to **134-R** increases the coordination number on each Fe center to yield **134-R/X** (Figure 109). Reaction of **134-^{t}Bu** with 4-*tert*-butylpyridine results in lengthening of the Fe–N(N$_2$) bond to 1.794(2)–1.804(2) Å and nominal contraction of the N–N bond distance to 1.161(4) Å.[248] The decreased π-backbonding upon increasing the coordination number of the Fe center is more clearly noted in the methyl congener, *viz.* [(^{Dipp}NacNac^{Me})Fe(^{t}BuPy)]$_2$(μ–1,2-N$_2$), for which these bond metrics are 1.816(2) and 1.151(3) Å, respectively. This correlation of reduced coordination number with N$_2$ activation on low valent iron centers is consistent with prior computational studies by Smith, *et al.*.[248]

Reduction of the diiron di(μ-chloride) complex for which the sterics of the β-diketiminate are reduced (specifically, the 2,6-diisopropylphenyl groups are replaced by 2,6-dimethylphenyl, and the backbone C–H of the chelate is replaced by a C–CH$_3$) results in cleavage of N$_2$ to give the tetra-iron di(μ-nitride) complex **135** (Scheme 32).[249] The large d(N–N) value of 2.799(2) Å in the solid-state structure agrees with a di(μ-nitride) formulation, as do the metal-ligand bond distances and the oxidation states (assigned from Mößbauer spectral simulations) of the iron centers. Each potassium cation interacts with one of the nitrides, two chlorides, and with an aryl group of one of the β-diketiminate ligands. DFT calculations provide insight into the reasons for the bifurcation in reactivity away from μ–1,2 coordination of N$_2$ as in the **134** series of complexes and towards N$_2$ scission. The reduced ligand sterics allow for approach of a third formally Fe^I center, resulting in a transient μ-η^1:η^2:η^1-dinitrogen ligand.[250] The minimum requirement for three iron centers to cleave N$_2$ was supported by the products arising from reduction of {[(^{DMePh}NacNac^{Me3})Fe]$_2$(μ_2-Cl)$_2$ with different alkali metal reductants (Na and MC$_8$, where M = K, Rb and Cs).[251] In the case of Na$^+$, K$^+$, and Rb$^+$ complete cleavage of N$_2$ was observed to generate analogous tetra- or tri-iron di(μ-nitride) products, whereas reduction with cesium yields {Cs$_2$[(^{DMePh}NacNac^{Me3})Fe(μ_2-Cl)(μ–1,2-N$_2$)$_2$} (**136–2N$_2$**, Figure 110).

These results are rationalized based on the alkali cation facilitating or templating the iron-dinitrogen interactions and allowing access to the reactive transient triiron-dinitrogen adduct; that is, the larger Cs^+ sterically precludes the close approach of the iron fragments. Upon increasing the number of reducing equivalents from two as in the instances above to four, the triiron tri(μ–1,2-dinitrogen) complexes **136–3N$_2$** (M = K, Rb, and Cs; Figure 110) are instead isolated, suggesting that the rate of reduction vs. aggregation or N_2 scission must be balanced appropriately.

Employing a variation on the β-diketiminate architecture, Fryzuk and coworkers reported the μ–1,2-dinitrogen diiron complex of an enamido-phosphinimine ligand **137-R** (**R** = Mes or DIPP, Figure 111).[252] The electronic asymmetry of the chelate was reasoned to limit the delocalization of charge as compared to the β-diketiminate, consequently affecting the extent of N_2 activation in the reduced polynuclear iron complexes. This hypothesis was later questioned based on comparable bond metrics within the ligand backbone of the iron(II) bromide complex of this enamido-phosphinimine ligand and that of (^{Dipp}NacNac^{tBu})FeCl. As one might anticipate then, the N–N bond distances in **137-R** of 1.186(3) and 1.183(6) Å for R = DIPP and Mes, respectively, are comparable to those observed in **134-R** as are the Fe–N(N_2) distances (1.776(2) and 1.764(3) Å for R = DIPP and Mes, respectively).

Although the *N,N*-chelates mentioned above have yet to be explored on Ru in the context of N_2 coordination and activation, acetylacetonate (acac) has been used and allows access to the μ–1,2-dinitrogen bis[bis(acac)-triisopropylphosphine)ruthenium] complex, **138** (Figure 112).[253] Two isomers are observed in solution spectra: the homochiral (/ΛΛ) and the heterochiral (Λ/Λ   ) isomers. The solid-state structure evidences a short N–N distance of 1.135(8) Å and a Ru–N(N_2) distance of 1.919(4) Å. These values, together with the ν_{N-N} stretching frequency of 2089 cm^{-1}, are comparable to others reported for formally Ru^{II} complexes.

3.5.6.   Monodentate ligands.—As noted in the introduction, Allen and Senoff's report of the [Ru(NH$_3$)$_5$(N$_2$)]$^{2+}$—the first transition-metal dinitrogen complex reported—was quickly followed by Taube's communication of the first dinitrogen-bridged dimetallic complex [(Ru(NH$_3$)$_5$)$_2$(μ–1,2-N$_2$)]$^{4+}$(**139**; Figure 113).[32,33] The product was characterized by UV/Vis spectroscopy, but one predicts similarly short N–N bond distances as compared to the other diruthenium(II)-dinitrogen complexes.

In contrast to the other Group 8 metals, osmium has few examples of multimetallic N_2 complexes, but related ammonia-ligated complex as **139** were reported by Magnuson and Taube in 1972.[254] Heating [(NH$_3$)$_5$Os(N$_2$)]$^{2+}$ with *cis*-[(NH$_3$)$_4$Os(N$_2$)$_2$]$^{2+}$ followed by an acid workup and aerial oxidation afforded [H$_2$O(NH$_3$)$_4$Os(μ–1,2-N$_2$)Os(NH$_3$)$_5$]$^{5+}$, **140–1**, and [Cl(NH$_3$)$_4$Os(μ–1,2-N$_2$)Os(NH$_3$)$_5$]$^{4+}$, **140–2**, (Figure 114).[254] [{Cl(NH$_3$)$_4$Os}$_2$(μ–1,2-N$_2$)]$^{3+}$, **140–3**, was also prepared using a similar protocol. Raman bands assigned as the ν_{N-N} stretching modes were observed at 1995 cm^{-1} and 1999 cm^{-1} for **140–2** and **140–3**, respectively, with spectroscopic data not reported for aqua-complex **140–1**.

The first example of a dinuclear iron-dinitrogen complex was reported in 1981 by Berke and coworkers who reported the diiron-μ–1,2-N$_2$ complex **141** by irradiation of

$Fe(CO)_3(P(OMe)_3)_2$ complex in diethyl ether at −80 °C under a N_2 atmosphere (Figure 115).[255] The presence of two π-acidic carbonyl ligands on each iron center in this complex diminishes iron to N_2 π-backbonding, which results in a N–N bond distance of 1.13 Å.

Our final species from Group 8 is **142**, which is bis(dihydridoruthenium)-dinitrogen complex supported by tris(isopropyl)phosphines (Figure 116).[256] Compound **142** is derived from reaction of the Kubas-type complex $Ru(H)_2(H_2)_2(P^iPr_3)_2$ with N_2 in solution, and exists in equilibrium with the monomeric congener $(^iPr_3)_2P(H)_2(N_2)_2Ru$.[257] Once again, one notes that the N–N bond distance is unremarkable in comparison to free N_2 with a value of 1.113(2) Å and the Ru-N(N_2) distances are expectedly long ranging from 2.051(1) to 2.049(1) Å. Indeed, an overall theme from Group 8 is that low valence provides the greatest extent of observed π-backbonding to N_2 and points to an inversion of the trend from earlier *d*-block metals in which the heavier and more reducing members of the group demonstrated greater proclivity to activate and cleave N_2.

3.6. Group 9: Co, Rh, and Ir

Fewer examples of multimetallic dinitrogen complexes have been reported for these metals as compared to prior groups. This observation results partly from the increasing electronegativity and consequent poorer π-backdonation by the metal centers to a bound dinitrogen as one moves across the periodic table as our survey. As for Group 8, the dinitrogen coordination here is dominated by cobalt, with fewer examples for Rh, and only two for Ir.

3.6.1. Tridentate ligands: pseudo C_{3v} or *fac* chelates.—Despite the first report of a cobalt dinitrogen complex being contemporary with those for other transition metals, [258–260] the coordination chemistry of dinitrogen at cobalt centers lay underexplored over the subsequent two decades. The first example of a polynuclear Co–N_2 complexes was the report by Cecconi *et al.* of the zero-valent dicobalt complex **143**, which was supported by 1,1,1-tris(diphenylphosphinomethyl)ethane or tppme (Figure 117).[261] Almost twenty years after **143** was reported, Betley and Peters communicated the dicobalt(I)-dinitrogen complex **144**, in which each metal center is ligated by a tris(diisopropylphosphinomethyl)borate (Figure 117).[243] Reduction of **144** by Na/Hg yielded the mixed-valent dicobalt(I/0) congener **144-red**; both **144** and **144-red** are isostructural with the iron analogs **130** and **130-red**. The scorpionate tris(pyrazolyl)borate enforces a similar trigonal environment on the Co centers and affords isostructural dicobalt dinitrogen compounds (**145-R/R′**; Figure 118) as **143** and **144**.[262] In contrast to **143** and **144**, which bear a stronger field arising from the P-donor set, the **145-R/R′** exhibit a slightly bent Co–N–N–Co fragment, which arises from a pseudo-Jahn-Teller effect. For the series **143**, **144-red**, and **145-R/R′** the N–N bond distances are all comparable and indicate a minimal metal-dinitrogen π-backbonding interaction with values of 1.18(2), 1.147(4), 1.14(3) (R/R′ = Np/H), and 1.154(9) Å (R/R′ = iPr/Me), respectively. These bond metrics are consistent with the vibrational data; for example, the $ν_{N–N}$ stretching mode is at 2056 cm^{-1} for **145-Np/H**. Despite similar bond distances as observed for the Fe^I congeners, one notes that the vibrational data indicate greater π-backbonding from Fe^I as compared to Co^I (*cf.* 1779 cm^{-1} for **125–1** and 2056 cm^{-1} for **145-Np/H**), in agreement with expectations based on changes in electronegativity.

The related tris(3,5-dimethylpyrazolyl)hydridoborate was reported as a ligand for a diiridium-dinitrogen complex, **146** (Figure 119).[263] Similar to the differences between the Ru vs. Fe tris(pyrazolyl)borate complexes, the Ir centers are not constrained to being four coordinate as is the case for Co; the metal centers are six coordinate with the scorpionate occupying three sites, the μ–1,2-dinitrogen bound in one, and two phenylides ligands in the remaining two coordination sites. The N–N and Ir–N(N$_2$) bond distances are as expected for a weakly bound N$_2$, with d(N–N) = 1.13(3) Å and d(Ir–N(N$_2$)) = 1.93(2) Å.

Wu *et al.* reported a heteronuclear Ti-Co tris(phosphinoamide) dinitrogen complex, which reacts with 1 equiv of azobenzene or 1,2-diphenylhydrazine resulting in the oxidation of one phosphinoamide arm and formation of the μ–1,2-dinitrogen complex **147** (Scheme 33).[264] The N–N bond distance of 1.065(4) Å, which is analogous to free N$_2$, agrees with the formal higher oxidation states for the metal centers as compared with **143** and **144**.

A sulfur ligated dinuclear cobalt complex was prepared electrochemically by Fernandez *et al.* by using a phenylphosphanyldithiolate and bipyridine in the presence of a Co electrode. Complex [(PhP(C$_6$H$_4$S)$_2$)(bipy)Co]$_2$(μ–1,2-N$_2$), **148** (Figure 120), was structurally characterized and revealed two octahedral Co(II) centers with the S$_2$P chelate binding in a *fac* coordination mode and N–N and Co–N(N$_2$) bond distances of 1.156(7) Å and 1.910(4) Å.[265]

3.6.2.   Tridentate ligands: meridional chelates.—Mindiola and coworkers reported a PNP-pincer ligated dicobalt(I)-dinitrogen complex [(^{iPr}PNP)Co]$_2$(μ–1,2-N$_2$) complex, **149-Co** (Figure 121), which is prepared by ^{t}Bu-Li reduction of the monometallic Co(II) precursor under N$_2$.[266] The N–N bond distance and stretching frequency observed (1.144(3) Å and 2024 cm^{-1}, respectively) are indicative of minimal backbonding to the N$_2$ donor. Comparison to the rhodium analog **149-Rh** evidences the greater activation afforded by the lighter metal with the N–N and Rh–N(N$_2$) bond lengths of 1.119(2) and 1.904(1) Å for **149-Rh**.[267]

In 2015, Nesbit *et al.* synthesized a dicobalt(0)-N$_2$ complex with a bis(phosphino)borane chelate, **150** (Figure 122), which is isostructural with diiron complex **133**.[268] The dicobalt complex cocrystallized with the monometallic congener, with the dimetallic-monometallic equilibrium lying towards the monocobalt complex. The solid state structure of **150** revealed each cobalt center as five-coordinate with a Co-C$_{ipso}$ interaction making up the fifth coordination site, analogous to **133**. The observed N–N bond distance of 1.129(3) Å is shorter than that for the Fe congener, reinforcing the effect of the changing electronegativity of the metal center on π backbonding.

A series of pincer-based dinitrogen complexes of Rh and Ir have been reported, the majority of which are from Milstein and coworkers (**151–1** to **151–8**; Figure 123 and Figure 124).[267,269–274] From the context of dinitrogen activation and potential functionalization, these complexes are unremarkable with N–N bond lengths ranging from 1.108(3)–1.130(7) Å, and Rh–N(N$_2$) distances from 1.912(2)–1.991(9) Å. These dimetallic species exist in equilibrium in solution with their mononuclear dinitrogen counterparts, with the exception of **151–7** and **151–8**.

3.6.3. Bidentate ligands.—The only bidentate ligand reported to afford polynuclear cobalt dinitrogen species is the β-diketiminate, reported exclusively by Holland and coworkers. Reduction of the cobalt(II) chloride complexes of the same β-diketiminate ligands as in **134** afforded the isostructural dicobalt(I)-dinitrogen complexes, **152-R** (R = ^{t}Bu, Me) (Figure 125).[275] As for the iron examples, further two-electron reduction of **152-^{t}Bu** can be effected to generate the di(potassium) or di(sodium) salts, in which the two alkali cations are tightly associated with the bridging N_2 and the aromatic rings of the diisopropylphenyl substituents. As with the Fe examples, the N–N bond and metal–N(N_2) bond distances evidence greater N_2 activation with reduction and association of the alkali cations, as well as nominally weaker metal-dinitrogen π-backbonding for Co as compared to Fe. Specifically, the N–N bond distance in **152-^{t}Bu** is 1.1390(15) Å, which lengthens to 1.220(2) Å and 1.211(3) Å in **152-^{t}Bu/2K**, **152-^{t}Bu/2Na**, respectively. The $\nu_{N–N}$ increases from 1589 cm^{-1} (**134-^{t}Bu/2K**) and 1583 cm^{-1} (**134-^{t}Bu/2Na**) to 1599 cm^{-1} for **152–2K** and 1598 cm^{-1} for **152–2Na**. Spitzer *et al.* reported the methyl congener, **152-Me/2K**, for which the N–N bond lengths of 1.215(3) and 1.220(4) Å (depending on crystallization conditions) are comparable to those in **152-^{t}Bu/2M**.[276] **152-^{t}Bu/2K** can also be prepared via a non-reductive approach. The dihydride congener [(^{Dipp}NacNac^{tBu})Co]$_2$(μ-H)$_2$ readily converts to the dinitrogen-bridged adduct upon exposure of the precursor solution to an atmosphere of N_2.[277] Counter to the general trend that the N_2 activation appears to be less for Co vs. Fe (albeit nominally in some cases), the N–N stretching frequency observed for **152-Me/2K** at 1568 cm^{-1} is notably lower in energy than the directly related Fe analog **134-Me/2K** for which ν_{NN} = 1625 cm^{-1}.[247]

3.6.4. Monodentate ligands.—Two final examples for Group 9 are presented here: the phosphine ligated di-cobalt and -rhodium dinitrogen complexes. Both examples show minimal lengthening of the N–N bond, but the lack of reported vibrational data prevents a more complete evaluation of N_2 activation. First, Klein *et al.* reported the isolation and characterization of [CoH(PMe$_3$)$_3$]$_2$(μ–1,2-N$_2$), **153** (Figure 126), with a comparable N–N bond length to many other penta-coordinate cobalt species discussed here.[278] Second, Yoshida *et al.* reported the solid-state structure of [(P^{i}Pr$_3$)$_2$HRh]$_2$(μ–1,2-N$_2$), **154** (Figure 126).[279] The experimentally-determined bond metrics are comparable to those for **142**, with N–N and Rh–N(N_2) bond lengths of 1.134(5) Å and 1.981(5)–l.973(5) Å, respectively.

3.7. Group 10: Ni, Pd, and Pt

The only examples of multimetallic dinitrogen complexes for Group 10 metals are of nickel. In 1971, Jolly, *et al.* reported the structure of the first multinuclear nickel dinitrogen complex, **155-Cy**, which was synthesized by the reaction of AlMe$_3$, Ni(acac)$_2$, and PCy$_3$.[280] The tris(isopropyl)phosphine congener **155-^{i}Pr** was reported more recently;[281] for both complexes, the N–N distances are minimally elongated relative to free dinitrogen with d(N–N) of 1.1285(2) and 1.158(5) Å for **155-Cy** and **-^{i}Pr**, respectively (Figure 127). Similarly, the metal–N distances do not suggest metal-dinitrogen multiple bonding character, which is consistent with a mild N_2 activation, evidenced by the N–N stretching band at 1908 cm^{-1} reported for **155-^{i}Pr**. The remainder of this survey is organized by decreasing ligand denticity as delineated for the preceding groups.

A repeated structural type in tridentate ligands is that of a *fac*-coordinating ligand comprised of two or three phosphorus donor atoms (Figure 128). The reported compounds herein employ a bis(phosphine)borane (**156-B**),[282] a tri-phosphine chelate (**156–3P**),[283] a ferrocenyl triphosphine ligand (**156-Fc3P**),[284] and the di-phosphine-phosphinite ligated compounds (**156–2P,PO^R**; R = Me and ^{i}Pr).[285] The synthetic route of these complexes follows a typical reduction of the nickel halide precursor or metalation with Ni(COD)$_2$ with the exception of **156–2P,PO^R**, which is accessed by reaction of the phosphide-chlorido-nickel(II) complex with an alkoxide source under a N$_2$ atmosphere (Scheme 34). In these complexes, the metal centers are in pseudotetrahedral environments, with N–N bond distances of 1.123(3), 1.124(3), 1.122(3), 1.112(5), and 1.133(4) Å for the **B**, **3P**, **Fc3P**, **2P,PO^{Me}**, and **2P,PO^{i}Pr** compounds, respectively. The donors in **156-B** differ from the other examples insofar as the third chelate donor is the π-type orbital at B–C$_{ipso}$. The comparison of the energies of the N–N stretching vibrations is more informative, however; as one notes the minimal difference between the 2045 vs. 2038 cm^{-1} values for **156–3P** vs. **156–2P,PO^{Me}**. The ligand field consequently appears to have minimal effect on the extent of N–N activation for Ni^0 species.

A related scorpionate or *fac*-coordinating ligand type as in **156–3P** wherein the P-Me is replaced by a silicide also accesses a dinitrogen-bridged complex (**157**), albeit by a slightly distinct route to the **156** complexes.[286] Reaction of the nickel-hydride precursor with N$_2$ results in reductive elimination of the silicide and hydride to afford the silane. The newly formed Si–H participates in an agostic interaction with the Ni^0 center and the dinitrogen binds in a μ–1,2 fashion. Compound **157** is in equilibrium in solution with the nickel hydride starting material and the mononuclear nickel-dinitrogen species (Scheme 35). The N–N bond distance is once again comparable to the **156** complexes with a value of 1.127(3) Å as is the ν$_{N–N}$ of 2050 cm^{-1}. The dinickel-dinitrogen complex, **158**, can be considered as **157** without the agostic interaction to the Si–H bond (Figure 129).[287] The longer N–N bond distance of 1.144(3) Å in **158** compared to the prior examples suggests greater activation, but supporting vibrational data is not available. As noted in instances previously, N–N bond distances may not be sufficient for ascertaining the extent of π-backbonding.

As was the case for chromium, iron, and cobalt, the bis(β-diketiminatonickel)dinitrogen complexes have also been reported (**159**, Figure 130).[288–290] The complexes are isostructural with the iron (**134**) and Co (**152**) congeners, with the neutral (**159**) and one-(**159–1K**) and two-electron reduced complexes (**159–2M** where **M** = Na or K, and **159-Na,K**) reported. Solution magnetometry suggests an *S* = 1 ground state for the dimetalic species (μ$_{eff}$ = 2.40 μ$_B$), which agrees with the DFT calculation wherein the ground state is comprised of two uncoupled or weakly coupled nickel *S* = ½ centers. The trend in N$_2$ bond activation with reduction of the complex is as noted before for the Fe and Co compounds, with the vibrational data evidencing less activation of N$_2$ as compared to Co and Fe. Starting with **159** for which the N–N bond distance and stretching frequency are 1.120(4) Å and 2164 cm^{-1}, these values trend towards further N$_2$ reduction in **159–1K** and **159–2K** for which these values are 1.143(8) Å and 1825 cm^{-1}, and 1.185(8) Å and 1698 cm^{-1}, respectively. The alkali cation identity has minimal effect on the extent of N$_2$ activation with **159–2Na** and **159-Na,K** having N–N bond distances and stretching frequencies of 1.192(3)

Å and 1685 cm^{-1}, and 1.195(4) Å and 1689 cm^{-1}, respectively. As one might expect, the Ni–N(N$_2$) bond distances contract with reduction. Calculations on the reduced complexes note accumulated spin density on the N$_2$ bridge being stabilized by the proximal alkali cations.

The first examples of dinitrogen coordination to a late transition metal in a side-on/side-on fashion was the phenylide cluster **160** (Figure 131). This cluster was accessed by reaction of Ni(CDT) (CDT: trans-1,5,9-cyclododecatriene) with phenyllithium ([(C$_6$H$_5$Li)$_6$Ni$_2$N$_2${(C$_2$H$_5$)$_2$O}$_2$]$_2$, **160–1**) or a mixture of phenyllithium and phenylsodium ({C$_6$H$_5$[Na.O(C$_2$H$_5$)$_2$]$_2$[(C$_6$H$_5$)$_2$Ni]$_2$N$_2$NaLi$_6$(OC$_2$H$_5$)$_4$.O(C$_2$H$_5$)$_2$}$_2$, **160–2**) under a dinitrogen atmosphere.[291–293] The clusters are best described as dimers in which [(Ph$_2$Ni)$_2$(N$_2$)] units are closely associated with the alkali countercations. The N–N bond axis is orthogonal to that of the Ni–Ni bond, reminiscent of the alkyne coordination to Co$_2$(CO)$_6$.[294] The formal metal oxidation states, association of many alkali cations with the reduced N$_2$ ligand, and side-on/side-on coordination of N$_2$ lead to substantial activation of the N–N bond, with the values of 1.36(2) Å for **160–1** and **–2** being among the longest reported for any late *d*-block metal.

3.8. Group 11: Cu, Ag, and Au

As has been stated a number of instances thus far, the increasing electronegativity of the *d*-block metals on moving from Group 4 to Group 11 results in poorer π-backbonding from the metal to π-acid ligands. Therefore, one notes fewer examples for Ni vs. Co or Fe. The changes to the reducing power of the 4*d* and 5*d* metals as one similarly traverses the table has a similar consequence on dinitrogen coordination chemistry with far fewer examples for Rh and Ir than Ta and Hf. Unsurprisingly then, molecular examples for Group 11 were absent from the literature until the last decade, and no examples of N$_2$ coordination to Au or Ag have been reported hitherto. We note that a gold hydrazide cluster was reported in which a N$_2$ ligand is present; however, the ligand likely arises from deprotonation of the hydrazine co-reactant rather than N$_2$ coordination and activation based on spectroscopic data reported.[295]

The two molecular examples for Group 11 are copper(I) complexes and the observed extent of N–N bond activation extends the trend observed from iron to nickel. The first example is a tricopper(I) complex of a tris(β-diketiminate) cyclophane (**161**, Figure 132) and the second is a dicopper(I) species supported by tris(pyrazolyl)borates (**162**; Figure 133).[296,297] In complex **161**, the dinitrogen coordinating in a μ-η^1:η^2:η^1 mode is the major contributor in the structural solution, which is rare in dinitrogen coordination chemistry with only two other examples (**1-Cp** and **1-Cp^{Me13}**) known.[47,48] Monocopper(I) β-diketiminate complexes were previously demonstrated to prefer coordination to solvent ligands, such as arenes, ethers, or nitriles, rather than N$_2$; one concludes, therefore, that the steric constraints of the cyclophane, which prevent solvent approach within the cavity, effectively select N$_2$ from the reaction milieu. The N–N bond distance of 1.0854(1) Å in **161** is comparable to that of free N$_2$, which is at odds with a substantial decrease in the N–N stretching frequency (1952 cm^{-1} for **161**). The solution-phase thermally-averaged symmetry of this complex is D_{3h}, however, and may point to liberation or other effects as influencing the solid state bond metrics. Comparison to other β-diketiminate complexes is challenging given the differences in

nuclearity; however, one notes the similarities to those effects of alkali cations on the N–N vibrational frequency for **134-Me/K** and **-Me/2K**. Consistent with this interpretation, DFT calculations including QTAIM analysis of the Cu–N_2 interactions suggest a primarily electrostatic interaction rather than substantial π-backbonding from Cu^I to N_2.

The second example is from Warren and coworkers wherein the tris(pyrazolyl)borate ligand enforces pseudo-tetrahedral coordination environments at each copper center in the dicopper(I)-(μ–1,2-dinitrogen) complex **162**.[296] Similar to **161**, N–N and Cu–N(N_2) bond distances of 1.112(5) Å and 1.829(3) Å, respectively, evidence minimal π-backbonding from Cu(I) to N_2, consistent with the resonance Raman active N–N stretching mode at 2130 cm^{-1}. Considered against the vibrational and structural data for **125** and **145**, the decreased activation of the bound N_2 is readily apparent; for example, the N–N stretching vibration is observed at 1779 cm^{-1} and 2056 cm^{-1} for **125–1** and **145-Np,H**. As expected from inclusion of a side-on bound Lewis acid, the N–N stretching frequency for **161** is substantially lower than that of **162** and on par with the effects noted for the β-diketiminate complexes of other late 3d transition metals.

3.9. Group 13: N_2 Activation by Boron

Beyond the lanthanides and actinides, the only other discrete complexes reported to activate dinitrogen are the boron complexes from Braunschweig and coworkers. In the reported examples, *in situ* formation of mononuclear borylene species by reduction of the dibromoborane under a N_2 atmosphere results in formation of the diboryl μ–1,2-dinitrogen adducts.[298,299] The transient borylene in both reports is stabilized by the cyclic alkylaminocarbene (or CAAC) 1-(2,6-diisopropylphenyl)-3,3,5,5-tetramethylpyrrolidin-2-ylidene, and an aryl donor, which is either duryl (Dur) or triisopropylphenyl (TIPP). For Dur(CAAC)BBr$_2$, a mixture of two species is observed: one arises from C–H activation of the isopropyl group on the CAAC and the other from capture of one equivalent of N_2 to generate [Dur(CAAC)B]$_2$(μ–1,2-N_2), **163–1** (Scheme 36). The bond metrics for the B$_2$N$_2$ fragment are indicative of a B=N=N=B formalism as the N–N and B–N distances are in the range of those in azo compounds (1.248(4) Å) and aminoboranes (1.423(4)–1.403(5) Å). In addition, the C$_{CAAC}$–B bond distances of 1.528(5)–1.541(4) Å are shorter than for the starting dihaloborane precursors or the monohaloboryl, supporting substantial π-backbonding from the B into the CAAC ligand. Indeed, one can approximate the C$_2$B$_2$N$_2$ core of the product as consisting of delocalized double bond character extended from the N-atom in one CAAC to that in the second carbene. The C$_2$B$_2$N$_2$ unit also adopts a zig-zag arrangement with ∠B–N–N = 146.1(2)° and ∠B–N–N = 131.9(2)°, which agrees with the partial double bond formalism and is distinct from the d-block compounds. DFT calculations are consistent with the bonding picture suggested by the X-ray structure. Related to **163–1**, is the two-electron reduced congener **163–2**, which can be accessed from the monobromoborane. One-electron reduction of Dur(CAAC)BBr$_2$ yields the radical Dur(CAAC)BBr, which reacts with excess KC$_8$ under a dinitrogen atmosphere to afford K$_2$[Dur(CAAC)B](μ–1,2-N_2), **163–2** (Scheme 37). The potassium cations interact with the N_2 fragment in an η^1 fashion, in contrast to the η^2 mode observed in Holland's and Limberg's reduced β-diketiminatometal compounds.[246,247,275,276,288,289] The N–N and B–N bond lengths in **163–2** of 1.304(3) Å and 1.484(4) Å, respectively, are longer as compared to

the metrics in **163–1** whereas the C_{CAAC}–B distance contracts to 1.470(4) Å. These changes imply weaker π-backbonding from B to N, consistent with reduction being primarily localized on the N_2 unit.

Varying the sterics on boron from duryl to triisopropylphenyl and executing similar reduction reactions starting from the chloroboryl results in an unexpected tetrazyl product **163–3** in which formal coupling of two N_2 fragments is observed (Scheme 38). Here the proposed mechanism involves formation of a transient borylene-dinitrogen anion, which dimerizes to afford the B_2N_4 core in **163–3**. As for **163–1** and **–2**, the bonding picture suggests delocalized double bond character across the ten-atom unit extending from one N_{CAAC} to the other. Arguably, the extent to which dimerization of the two purported borylene-dinitrogen anions is required to effectively trap the N_2 fixed species (*i.e.*, equilibrium constant for formation of the transient anion) would distinguish the process from mono- vs. di-boron. Inclusion here is intended to reflect this ambiguity.

3.10.   Rare Earth Elements and Actinides

Dinitrogen chemistry of the rare earth metals (REs) and actinides dates to the initial survey of catalysts for the Haber-Bosch process with cerium and uranium being reported as competent catalysts for ammonia production.[300] The REs exhibit bonding interactions reminiscent of the Group 4 and 5 metals; that is, the strongly reducing character leads to greater activation of N_2 through formal charge transfer. This survey for the rare earth metals begins with the cyclopentadienyl and related ligand systems and then proceeds through decreasing denticity of the supporting ligands. The only example of multimetallic N_2 activation by an actinide is for uranium; uranium complexes are considered at the end of this section.

Evans and coworkers reported the first example of a dinitrogen complex of an *f*-element with their report of the structure of $(Cp^*_2Sm)_2(\mu\text{-}\eta^2{:}\eta^2\text{-}N_2)$, **164-Sm**, which was synthesized from the formally Sm(II) species, Cp^*_2Sm.[301] X-ray crystallography data evidenced the side-on/side-on coordination of dinitrogen between the two metal centers and a planar M_2N_2 fragment, making this compound the first such example of this structural motif. Despite the N—N bond length of 1.09(1) Å is comparable to that of free N_2, the Sm—N bond distances (2.347(6) and 2.368(6) Å) are comparable to those for Sm^{III}—NR_2 complexes (*viz.* 2.3–2.4 Å) and the later report of the N–N stretching frequency of 1416 cm^{-1} implies significant backbonding or charge transfer from the Sm centers to the N_2 ligand.[302] This structure bears strong resemblance to the structure of the related Group 4 and 5 bis[bis(cyclopentadienyl)metal] dinitrogen compounds.

Building from this initial result, a few approaches were employed to generate additional members of this structure type, including reaction of divalent lanthanide salts with alkali cyclopentadienides or chemical reduction of the bis(cyclopentadienyl)RE(III) halides with alkali metals under a dinitrogen atmosphere. These approaches have led to reports for various substituted cyclopentadienyl complexes of La, Ce, Pr, Nd, Sm, Gd, Tb, Dy, Tm, Lu, and Y with Cp* (**164-M**), 1,2,3,4-tetramethylcyclopentadienyl or Cp′ (**165-M**), methylcyclopentadienyl (**166-M**), Cp (**167-M**), trimethylsilylcyclopentadienyl (**168-Tm**), 1,3-bis(trimethylsilyl)cyclopentadienyl (**169-M**), and 1,2,4-tri-*t*-butylcyclopentadienyl (**170-**

Nd) (Figure 134).[302–311] Steric constraints imposed by the cyclopentadienyl substituents dictate the coordination number of the RE, with less encumbered cyclopentadienyl ligands allowing for coordination of one solvent molecule to each metal center. Generally, these complexes exhibit similar N–N stretching vibrations from 1461 cm^{-1} in **164-Sm** to 1473 cm^{-1} in **165-Nd**. Greater variability is observed for the N–N bond distances although most are in the range of 1.24 Å; for example, the N–N bond in **164-Sm** and **164-Y** are unexpectedly short at 1.09(1) and 1.172(6) Å, respectively. One also notes that the extent of activation is relatively insensitive to the coordination number; inclusion of one THF donor per metal center in **165-Gd** affords similar bond metrics and N–N stretching frequency as **164-Gd** (e.g., 1457 vs. 1433 cm^{-1}, respectively). Arguably, the effects of sterics on precluding closer approach of the two metal fragments and incorporation of the additional ligand, which may have similar steric effect, likely lead the observed net similar outcome. The exception to this trend is the more encumbered *tert*-butyl substituted **170-Nd**, which has the least activated N–N bond based on vibrational spectra (ν_{NN} = 1622 cm^{-1}). Drawing parallels again to the Group 4 and 5 compounds discussed previously, one notes a similar trend wherein increasing ligand sterics disfavors close approach of the metal fragments and consequently lowers the extent of activation of N_2.

Demir, *et al.* then expanded on these series with the reports of the one-electron reduced congeners of **165-M** for M = Gd, Tb, and Dy (Figure 135).[308] The $[((C_5Me_4H)_2(THF)Ln)_2(\mu\text{-}\eta^2:\eta^2\text{-}N_2)]^-$ (Ln = Gd, Tb and Dy) –ate complexes retain the structure observed in **165-M** with the exception that the N–N bond is decidedly longer than the neutral **165-M** analogs with values ranging from 1.362(9) Å for **171-Gd**, which has a THF solvent molecule coordinated to the metal centers, to ~1.39(1) Å for the solvent-free complexes **172-Tb** and **172-Dy**. Formally these complexes are best described as containing N_2^{3-} ligands, which is consistent with the observed variable temperature magnetic susceptibility data. The bridging radical affords single molecule magnet behavior for these complexes. Loss of the solvent donor as in the **171-Tb** vs. **172-Tb** facilitated by dissolution of the THF solvate in 2-methyltetrahydrofuran increases the magnetic anisotropy, which raises the blocking temperature and coercive fields.

Metalation of fully deprotonated *meso*-octaethylporphyrinogen (OEP) with trivalent Sm, Nd, or Pr followed by reduction with alkali metal sources (Li for Sm, Na for Nd and Pr) resulted in complexes **173-M** (Figure 136). The core $[(OEP)M]_2(\mu\text{-}\eta^2:\eta^2\text{-}N_2)$ for these complexes is comparable with the OEP coordinated in either an $\eta^3:\eta^1:\eta^3:\eta^1$ for **173-Sm** or $\eta^5:\eta^1:\eta^5:\eta^1$ mode for **173-Nd** and **-Pr**. The more notable difference however is the number and coordination number of the alkali cations. The η^3 and η^5 coordination of two pyrrolide rings is reminiscent of the bis(cyclopentadienyl) complexes discussed above, with the *trans* orientation noted in all cases. In the structure of **173-Sm** from Gambarotta and coworkers, the N_2 ligand lies within the center of an octahedron defined by four equatorial lithium cations, of which two are η^2 and two are η^1 to the N_2 ligand, and two axial samarium centers with η^2 interactions. Given that the magnetic moment of 2.72 μ_B is consistent with two Sm^{III} centers, the charge balance for the complex (assuming Li$^+$ and Sm^{III}), and the elongated N–N bond of 1.525(4) Å, **173-Sm** approximates as two $[Li(OEt_2)][(\eta^3:\eta^1:\eta^3:\eta^1\text{-}OEP)Sm^{III}]$ bridged by a planar Li_4N_2 unit. In the report by Floriani and coworkers for **173-**

Nd and **-Pr**, the structure bears similarity to **173-Sm** when one considers the two fewer alkali cations. Two $[Na(solv)_2][(\eta^5:\eta^1:\eta^5:\eta^1\text{-}OEP)M^{III}]$ fragments (M/solv = Nd/1,4-dioxane, or Pr/DME) are bridged by $\{[Na(solv)]_2(\mu\text{--}1,2\text{-}N_2)\}$. Variable temperature magnetometry is consistent with the trivalent formalism provided above, and the observed N–N bond distances of 1.234(8) and 1.254(7) Å for **173-Nd** and **-Pr**, respectively. As for the cyclopentadienyl series, one notes minimal difference in the extent of activation (based on crystallography exclusively here) as the metal ion is varied, but rather with the extent of reduction as the oxidation state of the RE is held approximately constant.

Encouraged by the extent of N_2 activation achieved by these OEP or tetrapyrrolide complexes, Gambarotta and coworkers varied the sterics of the *meso* substituents in the smaller dipyrrole ligands to evaluate the consequence on N_2 activation.[312] The substituents on the methylene bridges of the dipyrrolide are either two phenyl groups (**174-Ph₂**) or a cyclohexyl (**174-Cy**); reduction of the Sm^{III} complexes of these dipyrrolides affords structurally homologous tetra-samarium(III) complexes, $[\{[\mu\text{-}RC(\eta^1:\eta^5\text{-}C_4H_3N)_2]Sm\}_4(\mu_4\text{-}\eta^2:\eta^2:\eta^1:\eta^1\text{-}N_2)]$ (Figure 137; R = Ph or Cy). As for **173-Nd** and **-Pr**, two pyrrolide rings coordinate η^5 to each Sm center and two others in an η^1 fashion. In both compounds, the N–N bond distances are within error with values of 1.41(2) Å for **174-Ph₂** and 1.39(2) Å for **174-Cy**. These results point to a cooperative activation of the bridging N_2 to afford a formally N_2^{4-} and four Sm^{III} centers. In an effort to effect complete N–N bond scission, **174-Cy** was reduced with excess sodium, yielding the structurally similar dianionic complex $[\{[\mu\text{-}CyC(\eta^1:\eta^5\text{-}C_4H_3N)_2]Sm\}_4(\mu_4\text{-}\eta^2:\eta^2:\eta^1:\eta^1\text{-}N_2)]^{2-}$ or **[174-Cy]²⁻**. For this complex, the N–N bond is retained and the bond length of 1.37(2) Å is within error of the unreduced starting species. Consequently, one concludes that reduction here is likely metal centered, which is unexpected. The proposed rationale for metal rather than N_2 reduction is that the rigidity of tetrametallic assembly limit sufficiently close approach of the metal centers to effect the complete cleavage of the N–N bond.

The only reported complexes with tetradentate ligands are the bis-O-alkylated calix[4]arene complexes, **175-M** where M = Sm or Pr from Floriani and coworkers (Figure 138).[313] Compound **175-Sm** was structurally characterized and is the only example of a $\mu_3\text{-}\eta^2:\eta^2:\eta^2$-dinitrogen complex. The structure shows the three Sm centers bridged by two oxygen atoms from a calix[4]arene unit and by the N_2 ligand coordinated in a $\mu_3\text{-}\eta^2:\eta^2:\eta^2$ fashion. The N—N bond length is sufficiently long at 1.62(2) Å, that one questions the extent to which a N–N bond is present, although a hydrazide type ligand is presumed. An analogous structure for M = Pr was suggested on the basis of elemental analysis and gas-volumetric measurements.

Amide and alkoxide constitute the monodentate ligands employed thus far for RE-dinitrogen compounds. Complexes $[X_2(THF)_yRE]_2(\mu\text{-}\eta^2:\eta^2\text{-}N_2)$ (**176-RE,X** where X = $(Me_3Si)_2N$ as NR_2 and 2,6-di(*t*-butyl)phenoxide as OAr) have been reported for which RE = Tm, Dy, Nd, Gd, Tb, Y, Ho, Er, and Lu, with X = $(Me_3Si)_2N$, 2,6-$^tBu_2$-OC_6H_3, and y = 1 or 2 (Figure 139). These complexes were prepared by treating the REX_3 precursor with alkali metal-based reductants or by reaction of the divalent diiodide with KX.[302,314–316] As for the cyclopentadienyl compounds the N–N bond distances and vibrational frequencies fall within a fairly narrow range with values of 1.264(7)–1.305(6) Å for the former and 1413–1447 cm

$^{-1}$ for the latter. The N–N stretching frequency decreases slightly as one moves to higher values of Z, which may arise from the increasing Lewis acidity of the metal ion. Again, recalling the cyclopentadienyl complexes, the RE centers here appear to be in the trivalent state, affording a formally diazenide bridging ligand.

In the initial report of the first members of the **176-RE,X** family, Evans and coworkers reported concomitant formation of the related one-electron reduced congeners of **176-Y,NR$_2$** and **176-Dy,OAr**. Two forms of these one-electron reduced species were characterized crystallographically: **[K(THF)$_6$][176-RE,X]** and **177-RE,X** in which the K$^+$ cation is associated with the X-type ligand and the bridging N$_2$ ligand (Scheme 39).[316] These two one-electron reduced complexes both formally comprise RE^{III} centers and a N$_2$$^{3-}$ bridge (*vide infra*), and are related by the loss or gain of THF, allowing for interconversion between the two species. As part of understanding the magnetic interactions mediated by the N$_2$$^{3-}$ radical bridge, targeted syntheses were developed for the one-electron reduced [**176-RE,X**]$^-$ and **177-RE,X** (Figure 140 and Figure 141).[317–319] The observed N–N bond distances in the [**176-RE,X**]$^-$ and **177-RE,X** series vary within error with an approximate value of 1.4 Å, which lies between those for N$_2$Ph$_2$ (1.25 Å) and hydrazine (1.47 Å) and is consistent with a N$_2$$^{3-}$ species.[320] This bond formalism was supported by DFT calculations in which the calculated structures and vibrational spectra—specifically, the N–N stretching vibrational frequency—were comparable. These calculations reveal a bonding picture wherein the π-donating orbitals on the RE fragment are nominally above the π* orbitals of the N$_2$ ligand; the SOMO of the [**176-RE,X**]$^-$ complexes is almost exclusively N$_2$ π* in character. These results predate the proposed similar electronic structures for previously discussed Group 6 complexes.

In contrast with the side-on/side-on coordination of N$_2$ prevalent in rare-earth metals, Woen *et al.*, reported the first example of an end-on/end-on dinitrogen coordination mode observed for a rare-earth metal (Figure 142).[321] Complex **178** or [K(2.2.2.-cryptand)]$_2$({[(Me$_3$Si)$_2$N]$_3$Sc}$_2$(μ–1,2-N$_2$)) was synthesized by the route described for **176-RE,X**. The N–N and Sc–N(N$_2$) bond lengths are 1.221(3) Å and 2.032(3) Å, respectively, with the former metric being noticeably shorter than that of the μ-η^2:η^2-dinitrogen complexes discussed above. This conclusion is consistent with the vibrational data, which evidence a N–N stretching mode of 1644 cm^{-1}. As for the majority of the RE dinitrogen complexes, the Sm centers are best described as trivalent ions with a formal diazenide bridging ligand for this system.

Scott, *et al.* reported the first example of a dinitrogen complex of uranium. The tren ligand bearing SiMe$_2$^{t}Bu substituents on the secondary amide donors (i.e., tren^{SiMe2tBu}) allowed access to the dinitrogen bridged compound [(tren^{SiMe2tBu})U]$_2$(μ-η^2:η^2-N$_2$) or **179** (Figure 143). The combination of the N–N bond distance of 1.109(7) Å in this compound being comparable to that of free N$_2$, the solution magnetic moment of 3.22 μ_B per uranium, and the solution phase UV/visible spectra—the latter two datasets are comparable to U^{III} complexes—imply that the complex is best described as two U^{III} centers with a bound N$_2$ ligand.[322] Cloke and coworkers subsequently reported the synthesis of a dinuclear uranium-dinitrogen complex, in which the N$_2$ ligand coordinates in a μ-η^2:η^2-N$_2$ fashion.[323] Reaction of (η^5-Cp*)[η^8-C$_8$H$_4$(1,4-Si^{i}Pr$_3$)$_2$]U with dinitrogen affords {(η^5-Cp*)[η^8-C$_8$H$_4$(1,4-

Si^{i}Pr$_3$)$_2$]U}$_2$(μ-η^2:η^2-N$_2$), **180** (Figure 144). The N–N and U–N(N$_2$) bond distances are 1.23(1) and 2.401(8)–2.423(8) Å, respectively; these crystallographic data are consistent with N–N double bond character and two formally U^{IV} centers, although additional spectroscopic data would be invaluable in corroborating the extent of π-backbonding.

Arnold and coworkers synthesized an unanticipated diuranium dinitrogen complex upon addition of 2,6-di-*tert*-butylphenol (HODtbp) or 2,4,6-tri-*tert*-butylphenol (HOTtbp) to U(N(SiMe$_3$))$_3$ under a dinitrogen atmosphere (Figure 145).[324] Solid-state structures of the crystallized products for the HODtbp reaction revealed two species: the first was the previously known but not structurally characterized monomeric U(ODtbp)$_3$ complex, and the second was the side-on/side-on diuranium-dinitrogen complex, [{U(ODtbp)$_3$}$_2$(μ-η^2:η^2-N$_2$)], **181-Di** (Figure 145). Three molecules are present in the asymmetric unit with N–N bond lengths of 1.16(2), 1.20(2), and 1.20(2) Å. Use of HOTtbp afforded the isostructural complex, [{U(OTtbp)$_3$}$_2$(μ-η^2:η^2-N$_2$)] **181-Tri**, with a comparable N–N bond length of 1.19(2) Å as in **181-Di**. The N–N stretching frequency is observed in resonance Raman spectra of **181-Tri** at 1451 cm^{-1}, suggesting substantial backbonding from the U centers to the N$_2$ bridge. These two diuranium-N$_2$ complexes are stable in solution and show no N$_2$ loss after several freeze-pump-thaw cycles.

Shortly after the report of the two **181** complexes, the synthesis of another example of a diuranium-dinitrogen complex was communicated by the same group (Figure 146). Reaction of trimesitylsilanol with U(N(SiMe$_3$)$_2$)$_3$ affords the side-on/side-on dinitrogen complex [U{OSi(Mes)$_3$}$_3$]$_2$(μ-η^2:η^2-N$_2$), **182**.[325] The Raman spectrum showed several signals in the unsaturated region making the assignment of ν_{N-N} inconclusive. The observed mode at 1437 cm^{-1} in the ^{14}N isotopolog is consistent with **181**, but the predicted frequency for the ^{15}N complex is obscured. The solid-state structure of **182** demonstrates that the complex exists in a staggered or in an eclipsed conformer, although both have similar N–N bond lengths with values of 1.12(1) Å and 1.08(1) Å for the eclipsed and staggered, respectively. These values are notably shorter to the N–N bond in **181** complexes; however, one notes throughout this survey that N–N bond distances cannot be used exclusively to make definitive judgements on extent of π-backbonding.

Recently, Mazzanti and coworkers reported a diuranium complex **183** in which the bridging N$_2$ approximates a N$_2$$^{4-}$ donor (Figure 147). Exposure of K$_3${[U(OR)$_3$]$_2$(μ-N)} to dinitrogen in the solid state or in solution affords the μ-η^2:η^2-dinitrogen species in which the U$_2$N$_2$ core adopts a butterfly rather than planar configuration.[326] The flexibility imparted by the siloxide donors plays a critical role by allowing the bridging nitride to be accommodated above the N$_2$ unit with the U–N–U angle and U–U distance decreasing from 173.7(8)° to 106.0(5)° and from 4.234(2) Å to 3.305(1) Å relative to the starting K$_3${[U(OR)$_3$]$_2$(μ-N)}. The N–N bond distance is surprisingly long at 1.52(2) Å, and comparable with that for a N–N single bond. Formally then, the bond metric suggests oxidation of the U^{III} to U^V upon N$_2$ coordination, which is indeed consistent with EPR and variable temperature magnetic susceptibility data. This complex features the longest N–N bond length compared to any other uranium complex and one of the longest for any metal complex (*vide supra*). Addition of 1 equiv. of 2,4,6-tri-*tert*-butylphenol to the dinitrogen complex resulted in the protonation of nitride to form a NH^{2-} species. The U$_2$N$_3$ core remain unchanged with no interaction

between the potassium cations and the N_2^{4-} or NH^{2-} moiety being the only major difference.

4. Outlook and Perspectives

Substantial progress has been made with respect to multimetallic systems competent for dinitrogen activation; however, limitations remain in the ability to functionalize N_2 by catalytic and stoichiometric methods. The identity of the metal ion and the N_2 coordination mode dictate the of cooperative N_2 activation in multimetallic systems; however, one challenge will be to develop systems that leverage this knowledge to favor activated N_2 species for nitrogen fixation to ammonia or equivalent molecules or as part of a N-atom transfer process from N_2 to organic substrates. Indeed, the latter could have a dramatic impact on current methodologies considering that N-atom incorporation typically relies on N_2 reduction and ammonia oxidation cycles to access desired reagents (*e.g.*, azide). One challenge is to access systems capable of greater formal reduction (*e.g.*, four- or six-electron reduction) of the bound N_2 without further addition of reducing agents will increase the possible options for N_2 functionalization; most reported examples result in formal one- or two-electron reduction of the bound N_2 and rely on further reduction to further activate the N_2 ligand. From this survey of multimetallic systems, we postulate the following foci as noteworthy and likely to advance N_2 activation, functionalization, and N-atom transfer.

Evaluating the effect of composition of polynuclear metal species on reactivity towards dinitrogen.

A number of examples presented here, such as the heteronuclear Mo_3Ti cubanes (**34-K$_2$/K$_3$**) or the various molybdenum-vanadium or -iron compounds (**76-V**, **79-V/Mo$_n$**, n = 2 or 3 and **79-Fe/Mo$_3$**, respectively) among many others, sought to evaluate the effect of metal compostion on N_2 activation. Generally, the effect of the heterometal on N_2 activation is consistent with the push-pull effect and these compounds are accessed by a spontaneous aggregation of monometallic species. However, the ability to design heterometallic complexes capable of binding dinitrogen upon reduction is an underexplored, but an important area of focus. Such systems can provide support for mechanisms for dinitrogen reduction in the Haber-Bosch process and by the nitrogenase cofactors; in the latter, the role of the heterometal as a possible N_2 coordination or functionalization site remains unresolved. In addition to metal ion composition, the effect of supporting donor atoms is topical and, in particular, systems that report on the possible function of the μ_6-carbide in the nitrogenase cofactors. A number of groups have reported non-carbene anionic C donor ligands and many more are likely targeting molecular clusters bearing an interstitial carbide. Broad comparison of reactivity of polynuclear metal species across periodic series (i.e., nitride, carbide, and boride) will be an important contribution in this regard.

Evaluating ligand-field effects on dinitrogen activation.

Most examples hitherto have employed ligands imposing intermediate or strong ligand fields. These compounds contrast the weaker ligand fields of the known industrial and biological catalysts. Recent work on iron-sulfur clusters suggests that the energy gaps between the ground and low lying excited spin states are relatively small, suggesting that

excited states may be critical for reactivity with dinitrogen, either by thermal population or by mixing of excited and ground states. Developing compounds that shed light on the properties that facilitate N_2 activation under ambient conditions with reasonably mild reductants—as compared to the ubiquitously employed alkali metal reductants—will have far reaching implications for N_2 utilization in future on-demand fixation technologies, chemical synthesis, and activation of other small molecule substrates.

Expanding coordination chemistry of late transition metals and utilizing weaker reducing agents.

The degree of activation of the N_2 fragment is strongly influenced by the coordination mode, as is apparent from work on the early transition metal ions in which all dimetallic-dinitrogen coordination modes have been reported. Contrastingly, bridging modes other than μ–1,2 remain exceptionally rare for late transition metals.[327] Late d-block complexes that access these rare bridging modes will mirror the diverse reactivities noted in the early metal compounds (*e.g.*, hydrogenation, nucleophilic attack), but require weaker reducing agents given the relative electronegativities of metal centers. Rational approaches wherein metal-metal separation and relative orientation of the frontier orbitals can be tuned to favor one of these modes remains underexplored. More generally, polynuclear metal complexes for N_2 activation—even for early transition metals—primarily arises from aggregation of monometallic species, resulting in serendipitous access to the various observed coordination modes. Rational and designed approaches to polynuclear early metal species would complement these seminal contributions, and allow one to experimentally describe the parameters that dictate such coordination preferences.

Accessing designed polynuclear RE and Ac complexes.

Broadly, few systems have been reported for dinitrogen activation in which polynuclear metal complexes are templated by multinucleating ligands, with the most common examples being for the late first row transition metals. A plethora of multimetallic RE and actinide (specifically, uranium) compounds are known in which N_2 binding or activation results in sponateneous aggregation of monometallic precursors. Thus, a fruitful future direction in which multinucleating ligands afford predictable polynuclear RE or Ac complexes for the targeted activation of small molecule species, such as N_2. Specifically, U with its reasonably accessible oxidation states would hold particular promise in a multimetallic context.

Coupling multiple metals with secondary coordination sphere effects.

Incorporating secondary sphere effects in monometallic complexes has strong precedent, and primarily in the arena of O_2 activation and H^+/CO_2 reduction,[328–332] with recent work expanding the concept to dinitrogen activation.[333–335] Unsurprisingly then, one envisions similar possibilities with respect to multimetallic systems, leading to systems that more closely mimic multimetallic active sites in metalloproteins.[336–339] Indeed, realizing such an approach will require creative solutions to afford reasonably facile access to conceptually complex ligand architectures.

To conclude, continued exploration of mutlimetallic N_2 activation and coupling this cooperativity to other reactive functionalities (*e.g.*, push-pull effects with Lewis acids or

hydrogen bonding interactions) will enhance our understanding of the biological and industrial processes as well as effecting as-yet-realized reactions utilizing dinitrogen (*e.g.*, N-atom transfer). Such systems and particularly designed complexes that can be readily tuned will also access unique and unexpected reactivity manifolds that extend beyond dinitrogen activation, but to small molecule activation in general (*e.g.*, O_2 reduction and O-atom transfer, H_2O oxidation, and CO_2 reduction).

ACKNOWLEDGMENT

Biographies

Leslie J. Murray was born in Trinidad & Tobago (1980) and received his undergraduate education at Swarthmore College. While an undergraduate student, he conducted research on resonance Raman spectroscopy, the electronic effects of solid-phase resins, the synthesis of small molecule agonists, and synthetic methodology. Subsequently, he attended and then received his Ph.D. from M.I.T under Stephen Lippard, where his thesis focused on mechanistic studies of dioxygen activation by toluene/o-xylene monooxygenase. After a postdoctoral appointment in Jeffrey Long's group (UC, Berkeley) where he evaluated metal-organic frameworks for gas storage and separation, he began his independent career at the University of Florida in 2010 and is currently an Associate Professor.

Devender Singh is a Ph.D. candidate in the Department of Chemistry at the University of Florida. He received his Master's degree in chemistry from Indian Institute of Technology, Bombay, India. His research focuses on small molecule activation by low coordinate iron clusters in a weak-ligand field regime.

William Buratto is a Ph.D. candidate in the Department of Chemistry at the University of Florida. He received his Bachelor's degree in chemistry from the University of California, Santa Barbara. His research focuses on the synthesis and reactivity studies of novel iron-sulfur clusters, and their ability to activate small molecules.

Juan Felipe Torres Gonzalez is a Ph.D. candidate in the Department of Chemistry at the University of Florida. He received his Bachelor's degrees in chemistry and environmental engineering from the Universidad de los Andes in Bogotá, Colombia. His research focuses on N_2 activation by triiron complexes in a weak-ligand field regime.

REFERENCES

(1). Murray R; Smith DC The Activation of Molecular Nitrogen. Coord. Chem. Rev. 1968, 3, 429–470.

(2). Shilov A; Denisov N; Efimov O; Shuvalov N; Shuvalova N; Shilova A New Nitrogenase Model for Reduction of Molecular Nitrogen in Protonic Media. Nature 1971, 231, 460–461. [PubMed: 4931606]

(3). Shilov AE Catalytic Reduction of Molecular Nitrogen in Solutions. Russ. Chem. Bull. 2003, 52, 2555–2562.

(4). Pople JA; Curtiss LA The Energy of N_2H_2 and Related Compounds. J. Chem. Phys. 1991, 95, 4385–4388.

(5). Zhan CG; Nichols JA; Dixon DA Ionization Potential, Electron Affinity, Electronegativity, Hardness, and Electron Excitation Energy: Molecular Properties from Density Functional Theory Orbital Energies. J. Phys. Chem. A 2003, 107, 4184–4195.

(6). Jia HP; Quadrelli EA Mechanistic Aspects of Dinitrogen Cleavage and Hydrogenation to Produce Ammonia in Catalysis and Organometallic Chemistry: Relevance of Metal Hydride Bonds and Dihydrogen. Chem. Soc. Rev. 2014, 43, 547–564. [PubMed: 24108246]

(7). Curley JJ; Cook TR; Reece SY; Müller P; Cummins CC Shining Light on Dinitrogen Cleavage: Structural Features, Redox Chemistry, and Photochemistry of the Key Intermediate Bridging Dinitrogen Complex. J. Am. Chem. Soc. 2008, 130, 9394–9405. [PubMed: 18576632]

(8). Laplaza CE; Johnson MJA; Peters JC; Odom AL; Kim E; Cummins CC; George GN; Pickering IJ Dinitrogen Cleavage by Three-Coordinate Molybdenum(III) Complexes: Mechanistic and Structural Data. J. Am. Chem. Soc. 1996, 118, 8623–8638.

(9). Laplaza CE; Cummins CC Dinitrogen Cleavage by a Three-Coordinate Molybdenum(III) Complex. Science 1995, 268, 861–863. [PubMed: 17792182]

(10). Thompson NB; Green MT; Peters JC Nitrogen Fixation via a Terminal Fe(IV) Nitride. J. Am. Chem. Soc. 2017, 139, 15312–15315. [PubMed: 28992418]

(11). Yandulov DV; Schrock RR. Studies Relevant to Catalytic Reduction of Dinitrogen to Ammonia by Molybdenum Triamidoamine Complexes. Inorg. Chem. 2005, 44, 1103–1117. [PubMed: 15859292]

(12). Yandulov DV; Schrock RR Reduction of Dinitrogen to Ammonia at a Well-Protected Reaction Site in a Molybdenum Triamidoamine Complex. J. Am. Chem. Soc. 2002, 124, 6252–6253. [PubMed: 12033849]

(13). Yandulov DV; Schrock RR Catalytic Reduction of Dinitrogen to Ammonia at a Single Molybdenum Center. Science 2003, 301, 76–78. [PubMed: 12843387]

(14). Anderson JS; Rittle J; Peters JC Catalytic Conversion of Nitrogen to Ammonia by an Iron Model Complex. Nature 2013, 501, 84–87. [PubMed: 24005414]

(15). Creutz SE; Peters JC Catalytic Reduction of N_2 to NH_3 by an Fe-N_2 Complex Featuring a C-Atom Anchor. J. Am. Chem. Soc. 2014, 136, 1105–1115. [PubMed: 24350667]

(16). Anderson JS; Cutsail GE; Rittle J; Connor BA; Gunderson WA; Zhang L; Hoffman BM; Peters JC Characterization of an Fe≡N-NH_2 Intermediate Relevant to Catalytic N_2 Reduction to NH_3. J. Am. Chem. Soc. 2015, 137, 7803–7809. [PubMed: 26000443]

(17). Buscagan TM; Oyala PH; Peters JC N_2-to-NH_3 Conversion by a Triphos–Iron Catalyst and Enhanced Turnover under Photolysis. Angew. Chem., Int. Ed. 2017, 56, 6921–6926.

(18). Chalkley MJ; Del Castillo TJ; Matson BD; Roddy JP; Peters JC Catalytic N2-to-NH3 Conversion by Fe at Lower Driving Force: A Proposed Role for Metallocene-Mediated PCET. ACS Cent. Sci. 2017, 3, 217–223. [PubMed: 28386599]

(19). Del Castillo TJ; Thompson NB; Peters JC A Synthetic Single-Site Fe Nitrogenase: High Turnover, Freeze-Quench ^{57}Fe Mössbauer Data, and a Hydride Resting State. J. Am. Chem. Soc. 2016, 138, 5341–5350. [PubMed: 27026402]

(20). Rittle J; Peters JC An Fe-N_2 Complex That Generates Hydrazine and Ammonia via Fe=NNH_2: Demonstrating a Hybrid Distal-to-Alternating Pathway for N2 Reduction. J. Am. Chem. Soc. 2016, 138, 4243–4248. [PubMed: 26937584]

(21). Anderson JS; Moret ME; Peters JC Conversion of Fe-NH_2 to Fe-N_2 with Release of NH_3. J. Am. Chem. Soc. 2013, 135, 534–537. [PubMed: 23259776]

(22). Suess DLM; Peters JC H-H and Si-H Bond Addition to Fe≡NNR_2 Intermediates Derived from N_2. J. Am. Chem. Soc. 2013, 135, 4938–4941. [PubMed: 23472709]

(23). Fryzuk MD; Johnson SA The Continuing Story of Dinitrogen Activation. Coord. Chem. Rev. 2000, 200–202, 379–409

(24). Burford RJ; Fryzuk MD Examining the Relationship between Coordination Mode and Reactivity of Dinitrogen. Nat. Rev. Chem. 2017, 1, 0026.

(25). MacLachlan EA; Fryzuk MD Synthesis and Reactivity of Side-on-Bound Dinitrogen Metal Complexes. Organometallics. 2006, 25, 1530–1543.

(26). Gambarotta S; Scott J Multimetallic Cooperative Activation of N_2. Angew. Chem., Int. Ed. 2004, 43, 5298–5308.

(27). Burford RJ; Yeo A; Fryzuk MD Dinitrogen Activation by Group 4 and Group 5 Metal Complexes Supported by Phosphine-Amido Containing Ligand Manifolds. Coord. Chem. Rev. 2017, 334, 84–99.

(28). Hidai M; Mizobe Y Recent Advances in the Chemistry of Dinitrogen Complexes. Chem. Rev. 1995, 95, 1115–1133.

(29). Schneider et al. Chem. Rev. 2020.

(30). Chirik et al. Chem. Rev. 2020.

(31). Tuczek F; Lehnert N New Developments in Nitrogen Fixation. Angew. Chem., Int. Ed. 1998, 37, 2636–2638.

(32). Allen AD; Senoff CV Nitrogenopentammineruthenium(II) Complexes. Chem. Commun. 1965, 156, 621.

(33). Harrison DF; Weissberger E; Taube H Binuclear Ion Containing Nitrogen as a Bridging Group. Science 1968, 159, 320–322. [PubMed: 5634502]

(34). Fryzuk MD; Haddad TS; Mylvaganam M; McConville DH; Rettig SJ End-On Versus Side-On Bonding of Dinitrogen to Dinuclear Early Transition-Metal Complexes. J. Am. Chem. Soc. 1993, 115, 2782–2792.

(35). Fryzuk MD; Johnson SA; Patrick BO; Albinati A; Mason SA; Koetzle TF New Mode of Coordination for the Dinitrogen Ligand: Formation, Bonding, and Reactivity of a Tantalum Complex with a Bridging N_2 Unit That Is Both Side-on and End-On. J. Am. Chem. Soc. 2001, 123, 3960–3973. [PubMed: 11457146]

(36). Van Tamelen EE Design and Development of an Organic-Inorganic System for the Chemical Modification of Molecular Nitrogen under Mild Conditions. Acc. Chem. Res. 1970, 3, 361–367.

(37). Bercaw JE; Marvich RH; Bell LG; Brintzinger HH Titanocene as an Intermediate in Reactions Involving Molecular Hydrogen and Nitrogen. J. Am. Chem. Soc. 1972, 94, 1219–1238.

(38). Brintzinger H; Marvich RH Metastable Form of Titanocene. Formation from a Hydride Complex and Reactions with Hydrogen, Nitrogen, and Carbon Monoxide. J. Am. Chem. Soc. 1971, 93, 2046–2048.

(39). Bercaw JE Bis(Pentamethylcyclopentadienyl)Titanium(II) and Its Complexes with Molecular Nitrogen. J. Am. Chem. Soc. 1974, 96, 5087–5095.

(40). Sanner RD; Duggan DM; McKenzie TC; Marsh RE; Bercaw JE Structure and Magnetism of μ-Dinitrogen-Bis(Bis(Pentamethylcyclopentadienyl)Titanium(II)), {(η5-C5(CH3)5)2Ti}2N2. J. Am. Chem. Soc. 1976, 98, 8358–8365.

(41). Hanna TE; Keresztes I; Lobkovsky E; Bernskoetter WH; Chirik PJ Synthesis of a Base-Free Titanium Imido and a Transient Alkylidene from a Titanocene Dinitrogen Complex. Studies on Ti=NR Hydrogenation, Nitrene Group Transfer, and Comparison of 1,2-Addition Rates. Organometallics 2004, 23, 3448–3458.

(42). Hanna TE; Bernskoetter WH; Bouwkamp MW; Lobkovsky E; Chirik PJ Bis(Cyclopentadienyl) Titanium Dinitrogen Chemistry: Synthesis and Characterization of a Side-on Bound Haptomer. Organometallics 2007, 26, 2431–2438.

(43). de Wolf JM; Blaauw R; Meetsma A; Teuben JH; Gyepes R; Varga V; Mach K; Veldman N; Spek AL Bis(Tetramethylcyclopentadienyl)Titanium Chemistry. Molecular Structures of [(C5HMe4) (μ-η1:η5-C5Me4)Ti]2 and [(C5HMe4)2Ti]2N2. Organometallics 1996, 15, 4977–4983.

(44). Hanna TE; Lobkovsky E; Chirik PJ Dinitrogen Complexes of Bis(Cyclopentadienyl) Titanium Derivatives: Structural Diversity Arising from Substituent Manipulation. Organometallics 2009, 28, 4079–4088.

(45). Scherer A; Kollak K; Lützen A; Friedemann M; Haase D; Saak W; Beckhaus R Low-Valent Titanium-Pentafulvene Complexes - Formation of Dinuclear Titanium-Nitrogen Complexes. Eur. J. Inorg. Chem. 2005, 2005, 1003–1010.

(46). Oswald T; Frey A; Schmidtmann M; Beckhaus R Crystal Structure of an Isomeric Bis[(η5:η1–6,6-Di-p-Tolylpentafulvene)(η5-Pentamethylcyclopentadienyl)Titanium(III)]-μ2,η1:η1-

Dinitrogen Complex, C60H66N2Ti2. Zeitschrift fur Krist. - New Cryst. Struct. 2016, 231, 1095–1097.

(47). Semproni SP; Milsmann C; Chirik PJ Side-on Dinitrogen Complexes of Titanocenes with Disubstituted Cyclopentadienyl Ligands: Synthesis, Structure, and Spectroscopic Characterization. Organometallics 2012, 31, 3672–3682.

(48). Pez GP; Apgar P; Crissey RK Reactivity of [μ-(η1:η5-C5H4)](η-C5H5)3Ti2 with Dinitrogen. Structure of a Titanium Complex with a Triply-Coordinated N2 Ligand. J. Am. Chem. Soc. 1982, 104, 482–490.

(49). Carlotti M; Johns JWC; Trombetti A The ν 5 Fundamental Bands of N_2H_2 and N_2D_2. Can. J. Phys. 1974, 52, 340–344.

(50). Craig NC; Levin IW Vibrational Assignment and Potential Function for Trans-Diazene (Diimide): Predictions for Cis-Diazene. J. Chem. Phys. 1979, 71, 400–407.

(51). Braibaxti A; Dallavalle F; Nghelli MAP; Leporati E The Nitrogen-Nitrogen Stretching Band in Hydrazine Derivatives and Complexes. Inorg. Chem. 1968, 7, 1430–1433.

(52). Pool JA; Lobkovsky E; Chirik PJ Hydrogenation and Cleavage of Dinitrogen to Ammonia with a Zirconium Complex. Nature 2004, 427, 527–530. [PubMed: 14765191]

(53). Bernskoetter WH; Olmos AV; Lobkovsky E; Chirik PJ N2 Hydrogenation Promoted by a Side-on Bound Hafnocene Dinitrogen Complex. Organometallics 2006, 25, 1021–1027.

(54). Semproni SP; Lobkovsky E; Chirik PJ Dinitrogen Silylation and Cleavage with a Hafnocene Complex. J. Am. Chem. Soc. 2011, 133, 10406–10409. [PubMed: 21682285]

(55). Bernskoetter WH; Lobkovsky E; Chirik PJ Kinetics and Mechanism of N2 Hydrogenation in Bis(Cyclopentadienyl) Zirconium Complexes and Dinitrogen Functionalization by 1,2-Addition of a Saturated C-H Bond. J. Am. Chem. Soc. 2005, 127, 14051–14061. [PubMed: 16201827]

(56). Pool JA; Lobkovsky E; Chirik PJ Cyclopentadienyl Substituent Effects on Reductive Elimination Reactions in Group 4 Metallocenes: Kinetics, Mechanism, and Application to Dinitrogen Activation. J. Am. Chem. Soc. 2003, 125, 2241–2251. [PubMed: 12590553]

(57). Margulieux GW; Semproni SP; Chirik PJ Photochemically Induced Reductive Elimination as a Route to a Zirconocene Complex with a Strongly Activated N_2 Ligand. Angew. Chem., Int. Ed. 2014, 53, 9189–9192.

(58). Pool JA; Bernskoetter WH; Chirik PJ On the Origin of Dinitrogen Hydrogenation Promoted by [(η5- C5Me4H)2Zr]2(μ2, η2, η2-N2). J. Am. Chem. Soc. 2004, 126 (44), 14326–14327. [PubMed: 15521731]

(59). Hanna TE; Keresztes I; Lobkovsky E; Chirik PJ Diazene Dehydrogenation Follows H_2 Addition to Coordinated Dinitrogen in an Ansa-Zirconocene Complex. Inorg. Chem. 2007, 46, 1675–1683. [PubMed: 17266302]

(60). Knobloch DJ; Lobkovsky E; Chirik PJ Dinitrogen Cleavage and Functionalization by Carbon Monoxide Promoted by a Hafnium Complex. Nat. Chem. 2010, 2, 30–35. [PubMed: 21124377]

(61). Chirik PJ; Henling LM; Bercaw JE Synthesis of Singly and Doubly Bridged Ansa-Zirconocene Hydrides. Formation of an Unusual Mixed Valence Trimeric Hydride by Reaction of H2 with {(Me2Si)2(η5-C5H3)2}Zr(CH3)2 and Generation of a Dinitrogen Complex by Reaction of N2 with a Zirconocene Dihydride. Organometallics 2001, 20, 534–544.

(62). Zeinstra JD; Teuben JH; Jellinek F Structure of μ-Dinitrogenbis[p-Tolyldicyclopentadienyl-Titanium(III)], [(C5H5)2Ti(p-CH3C6H4)]2N2. J. Organomet. Chem. 1979, 170, 39–50.

(63). Berry DH; Procopio LJ; Carroll PJ Molecular Structure of {Cp2TI(PMe3)}2(μ-N2), a Titanocene Dinitrogen Complex. Organometallics 1988, 7, 570–572.

(64). Semproni SP; Knobloch DJ; Milsmann C; Chirik PJ Redox-Induced N_2 Hapticity Switching in Zirconocene Dinitrogen Complexes. Angew. Chem., Int. Ed. 2013, 52, 5372–5376.

(65). Benito-Garagorri D; Bernskoetter WH; Lobkovsky E; Chirik PJ 1,4-Addition of Alkyl Halides to a Side-on Bound Bafnocene Dinitrogen Complex. Organometallics 2009, 28, 4807–4813.

(66). Knobloch DJ; Benito-Garagorri D; Bernskoetter WH; Keresztes I; Lobkovsky E; Toomey H; Chirik PJ Addition of Methyl Triflate to a Hafnocene Dinitrogen Complex: Stepwise N_2 Methylation and Conversion to a Hafnocene Hydrazonato Compound. J. Am. Chem. Soc. 2009, 131, 14903–14912. [PubMed: 19785422]

(67). Pun D; Lobkovsky E; Chirik PJ Indenyl Zirconium Dinitrogen Chemistry: N_2 Coordination to an Isolated Zirconium Sandwich and Synthesis of Side-on, End-on Dinitrogen Compounds. J. Am. Chem. Soc. 2008, 130, 6047–6054. [PubMed: 18399632]

(68). Pun D; Bradley CA; Lobkovsky E; Keresztes I; Chirik PJ N2 Hydrogenation from Activated End-on Bis(Indenyl) Zirconium Dinitrogen Complexes. J. Am. Chem. Soc. 2008, 130, 14046–14047. [PubMed: 18826309]

(69). Fontaine PP; Yonke BL; Zavalij PY; Sita LR Dinitrogen Complexation and Extent of N-N Activation within the Group 6 "End-On-Bridged" Dinuclear Complexes, {(η5-C 5Me5)M[N(i-Pr)C(Me)N(i-Pr)]}2(μ-η1:η1-N2) (M = Mo and W). J. Am. Chem. Soc. 2010, 132, 12273–12285. [PubMed: 20707320]

(70). Hirotsu M; Fontaine PP; Zavalij PY; Sita LR Extreme N≡N Bond Elongation and Facile N-Atom Functionalization Reactions within Two Structurally Versatile New Families of Group 4 Bimetallic "Side-on-Bridged" Dinitrogen Complexes for Zirconium and Hafnium. J. Am. Chem. Soc. 2007, 129, 12690–12692. [PubMed: 17902670]

(71). Bai G; Wei P; Stephan DW Reductions of β-Diketiminato-Titanium (III) Complexes. Organometallics 2006, 25, 2649–2655.

(72). Sekiguchi Y; Meng F; Tanaka H; Eizawa A; Arashiba K; Nakajima K; Yoshizawa K; Nishibayashi Y Synthesis and Reactivity of Titanium- and Zirconium-Dinitrogen Complexes Bearing Anionic Pyrrole-Based PNP-Type Pincer Ligands. Dalt. Trans. 2018, 47, 11322–11326.

(73). Shima T; Hu S; Luo G; Kang X; Luo Y; Hou Z Dinitrogen Cleavage and Hydrogenation by a Trinuclear Titanium Polyhydride Complex. Science 2013, 340, 1549–1552. [PubMed: 23812710]

(74). Fryzuk MD; Love JB; Rettig SJ; Young VG Transformation of Coordinated Dinitrogen by Reaction with Dihydrogen and Primary Silanes. Science 1997, 275, 1445–1447.

(75). Morello L; Yu P; Carmichael CD; Patrick BO; Fryzuk MD Formation of Phosphorus-Nitrogen Bonds by Reduction of a Titanium Phosphine Complex under Molecular Nitrogen. J. Am. Chem. Soc. 2005, 127, 12796–12797. [PubMed: 16159262]

(76). Yates BF; Basch H; Musaev DG; Morokuma K Reaction of H2 with a Binuclear Zirconium Dinitrogen Complex - Evaluation of Theoretical Models and Hybrid Approaches. J. Chem. Theory Comput. 2006, 2, 1298–1316. [PubMed: 26626838]

(77). Studt F; Morello L; Lehnert N; Fryzuk MD; Tuczek F Side-on Bridging Coordination of N2: Spectroscopic Characterization of the Planar Zr2N2 Core and Theoretical Investigation of Its Butterfly Distortion. Chem. - Eur. J. 2003, 9, 520–530. [PubMed: 12532302]

(78). Chomitz WA; Arnold J Transition Metal Dinitrogen Complexes Supported by a Versatile Monoanionic [N2P2] Ligand. Chem. Commun. 2007, 4797–4799.

(79). Luo Y; Nishiura M; Wang B; Shima T; Hou Z; Luo G; Hu S Dinitrogen Activation by Dihydrogen and a PNP-Ligated Titanium Complex. J. Am. Chem. Soc. 2017, 139, 1818–1821. [PubMed: 28134522]

(80). Baumann R; Stumpf R; Davis WM; Liang LC; Schrock RR Titanium and Zirconium Complexes That Contain the Tridentate Diamido Ligands [(i-PrN-o-C6H4)2O]2- ([i-PrNON] 2-) and [(C6H11N-o-C6H4)2O]2- ([CyNON]2-). J. Am. Chem. Soc. 1999, 121, 7822–7836.

(81). Fryzuk MD; Haddad TS; Rettig SJ Reduction of Dinitrogen by a Zirconium Phosphine Complex To Form a Side-On-Bridging N2 Ligand. Crystal Structure of {[(Pri2PCH2SiMe2)2N]ZrCl}2(μ-η2:η2-N2). J. Am. Chem. Soc. 1990, 112, 8185–8186.

(82). Cohen JD; Fryzuk MD; Loehr TM; Mylvaganam M; Rettig SJ Synthesis and Structure of a Zirconium Dinitrogen Complex with a Side-On Bridging N2 Unit. Inorg. Chem. 1998, 37, 112–119. [PubMed: 11670268]

(83). Duchateau R; Gambarotta S; Beydoun N; Bensimon C Side-on versus End-on Coordination of Dinitrogen to Titanium(II) and Mixed-Valence Titanium(I)/Titanium(II) Amido Complexes. J. Am. Chem. Soc. 1991, 113, 8986–8988.

(84). Doyle LR; Wooles AJ; Jenkins LC; Tuna F; McInnes EJL; Liddle ST Catalytic Dinitrogen Reduction to Ammonia at a Triamidoamine–Titanium Complex. Angew. Chem., Int. Ed. 2018, 57, 6314–6318.

(85). Nakanishi Y; Ishida Y; Kawaguchi H Nitrogen–Carbon Bond Formation by Reactions of a Titanium–Potassium Dinitrogen Complex with Carbon Dioxide, Tert-Butyl Isocyanate, and Phenylallene. Angew. Chem., Int. Ed. 2017, 56, 9193–9197.

(86). Ohki Y; Uchida K; Tada M; Cramer RE; Ogura T; Ohta T N2 Activation on a Molybdenum–Titanium–Sulfur Cluster. Nat. Commun. 2018, 9, 3200. [PubMed: 30097563]

(87). Mullins SM; Duncan AP; Bergman RG; Arnold J Reactivity of a Titanium Dinitrogen Complex Supported by Guanidinate Ligands: Investigation of Solution Behavior and a Novel Rearrangement of Guanidinate Ligands. Inorg. Chem. 2001, 40, 6952–6963. [PubMed: 11754277]

(88). Grant LN; Kurogi T; Carroll ME; Manor BC; Carroll PJ; Mindiola DJ; Pinter B; Wu G Molecular Titanium Nitrides: Nucleophiles Unleashed. Chem. Sci. 2017, 8, 1209–1224. [PubMed: 28451262]

(89). Kurogi T; Ishida Y; Kawaguchi H Synthesis of Titanium and Zirconium Complexes Supported by a *p*-Terphenoxide Ligand and Their Reactions with N2, CO2 and CS2. Chem. Commun. 2013, 49, 11755–11757.

(90). Turner HW; Fellmann JD; Rocklage SM; Schrock RR; Churchill MR; Wasserman HJ Tantalum Complexes Containing Diimido Bridging Dinitrogen Ligands. J. Am. Chem. Soc. 1980, 102(26), 7809–7811.

(91). Keane AJ; Yonke BL; Hirotsu M; Zavalij PY; Sita LR Fine-Tuning the Energy Barrier for Metal-Mediated Dinitrogen N≡N Bond Cleavage. J. Am. Chem. Soc. 2014, 136, 9906–9909. [PubMed: 24960112]

(92). Hirotsu M; Fontaine PP; Epshteyn A; Zavalij PY; Sita LR Dinitrogen Activation at Ambient Temperatures: New Modes of H2 and PhSiH3 Additions for an "End-on-Bridged" [Ta(IV)]2(μ-η1:η1-N2) Complex and for the Bis(μ-Nitrido) [Ta(V)(μ-N)]2 Product Derived from Facile N≡N Bond Cleavage. J. Am. Chem. Soc. 2007, 129, 9284–9285. [PubMed: 17625853]

(93). Caselli A; Solari E; Scopelliti R; Floriani C; Re N; Rizzoli C; Chiesi-Villa A Dinitrogen Rearranging over a Metal-Oxo Surface and Cleaving to Nitride: From the End-on to the Side-on Bonding Mode, to the Stepwise Cleavage of the N≡N Bonds Assisted by Nb(III)-Calix[4]Arene. J. Am. Chem. Soc. 2000, 122, 3652–3670.

(94). Kozak CM; Rettig SJ; Patrick BO; Fryzuk MD; Bowdridge MR Nitride Formation by Thermolysis of a Kinetically Stable Niobium Dinitrogen Complex. J. Am. Chem. Soc. 2002, 124, 8389–8397. [PubMed: 12105920]

(95). Yonke BL; Keane AJ; Zavalij PY; Sita LR Mononuclear Tantalum(IV, d1) Imido Complexes Supported by the Monocyclopentadienyl, Amidinate and Guanidinate Ligand Sets as Models to Explore Dinitrogen Fixation by "End-on-Bridged" Dinuclear {[Ta(IV, d1)]}2(μ-η1:η1-N2)Complexes. Organometallics 2012, 31, 345–355.

(96). Horrillo-Martinez P; Patrick BO; Schafer LL; Fryzuk MD Oxygen Extrusion from Amidate Ligands to Generate Terminal TaO Units under Reducing Conditions. How to Successfully Use Amidate Ligands in Dinitrogen Coordination Chemistry. Dalt. Trans. 2012, 41, 1609–1616.

(97). Song J-I; Berno P; Gambarotta S Dinitrogen Fixation, Ligand Dehydrogenation, and Cyclometalation in the Chemistry of Vanadium(III) Amides. J. Am. Chem. Soc. 1994, 116, 6927–6928.

(98). Kilgore UJ; Sengelaub CA; Pink M; Fout AR; Mindiola DJ A Transient V^III-Alkylidene Complex: Oxidation Chemistry Including the Activation of N2 to Afford a Highly Porous Honeycomb-like Framework. Angew. Chem., Int. Ed. 2008, 47, 3769–3772.

(99). Kilgore UJ; Sengelaub CA; Fan H; Tomaszewski J; Karty JA; Baik MH; Mindiola DJ A Transient Vanadium(III) Neopentylidene Complex. Redox Chemistry and Reactivity of the V=CH^*t*Bu Functionality. Organometallics 2009, 28, 843–852.

(100). Kilgore UJ; Yang X; Tomaszewski J; Huffman JC; Mindiola DJ Activation of Atmospheric Nitrogen and Azobenzene N=N Bond Cleavage by a Transient Nb(III) Complex. Inorg. Chem. 2006, 45, 10712–10721. [PubMed: 17173427]

(101). Fryzuk MD; Johnson SA; Rettig SJ New Mode of Coordination for the Dinitrogen Ligand: A Dinuclear Tantalum Complex with a Bridging N2 Unit That is Both Side-On and End-On. J. Am. Chem. Soc. 1998, 120, 11024–11025.

(102). Berno P; Gambarotta S Formation of a Metalaaziridine Ring and Dinitrogen Fixation Promoted by a Niobium Amide Complex. Organometallics 1995, 14, 2159–2161.

(103). Groysman S; Villagrán D; Freedman DE; Nocera DG Dinitrogen Binding at Vanadium in a Tris(Alkoxide) Ligand Environment. Chem. Commun. 2011, 47, 10242–10244.

(104). Hulley EB; Williams VA; Hirsekorn KF; Wolczanski PT; Lancaster KM; Lobkovsky EB Application of 93Nb NMR Spectroscopy to (Silox)3Nb(Xn/Lm) Complexes (Silox = TBu3SiO): Where Does (Silox)3Nb(NN)Nb(Silox)3 Appear? Polyhedron 2016, 103, 105–114

(105). Liu G; Liang X; Meetsma A; Hessen B Synthesis and Structure of an Aminoethyl-Functionalized Cyclopentadienyl Vanadium(I) Dinitrogen Complex. Dalt. Trans. 2010, 39, 7891.

(106). Kokubo Y; Yamamoto C; Tsuzuki K; Nagai T; Katayama A; Ohta T; Ogura T; Wasada-Tsutsui Y; Kajita Y; Kugimiya S; Masuda H Dinitrogen Fixation by Vanadium Complexes with a Triamidoamine Ligand. Inorg. Chem. 2018, 57, 11884–11894. [PubMed: 30199244]

(107). Desmangles N; Jenkins H; Ruppa KB; Gambarotta S Preparation and Characterization of a Vanadium (III) Dinitrogen Complex Supported by a Tripodal Anionic Amide Ligand. Inorg. Chim. Acta 1996, 250, 1–4.

(108). Clentsmith GKB; Bates VME; Hitchcock PB; Cloke FGN Reductive Cleavage of Dinitrogen by a Vanadium Diamidoamine Complex: The Molecular Structures of [V(Me3SiN{CH2CH2NSiMe3}2)(μ-N)]2 and K[V(Me3SiN{CH2CH2NSiMe3}2)(μ-N)]2. J. Am. Chem. Soc. 1991, 121, 10444–10445.

(109). Holland PL Metal-Dioxygen and Metal-Dinitrogen Complexes: Where Are the Electrons? Dalton Trans 2010, 39, 5415–5425 [PubMed: 20361098]

(110). Vidyaratne I; Gambarotta S; Korobkov I; Budzelaar PHM Dinitrogen Partial Reduction by Formally Zero- and Divalent Vanadium Complexes Supported by the Bis-Iminopyridine System. Inorg. Chem. 2005, 44, 1187–1189. [PubMed: 15732953]

(111). Milsmann C; Turner ZR; Semproni SP; Chirik PJ Azo N=N Bond Cleavage with a Redox-Active Vanadium Compound Involving Metal-Ligand Cooperativity. Angew. Chem., Int. Ed. 2012, 51, 5386–5390.

(112). Vidyaratne I; Crewdson P; Lefebvre E; Gambarotta S Dinitrogen Coordination and Cleavage Promoted by a Vanadium Complex of a σ,π,σ-Donor Ligand. Inorg. Chem. 2007, 46, 8836–8842. [PubMed: 17883267]

(113). Sekiguchi Y; Arashiba K; Tanaka H; Eizawa A; Nakajima K; Yoshizawa K; Nishibayashi Y Catalytic Reduction of Molecular Dinitrogen to Ammonia and Hydrazine Using Vanadium Complexes. Angew. Chem., Int. Ed. 2018, 57, 9064–9068.

(114). Berno P; Hao S; Minhas R; Gambarotta S Dinitrogen Fixation versus Metal-Metal Bond Formation in the Chemistry of Vanadium(II) Amidinates. J. Am. Chem. Soc. 1994, 116, 7417–7418.

(115). Tran BL; Pinter B; Nichols AJ; Konopka FT; Thompson R; Chen CH; Krzystek J; Ozarowski A; Telser J; Baik MH; Meyer K; Mindiola DJ A Planar Three-Coordinate Vanadium(II) Complex and the Study of Terminal Vanadium Nitrides from N2: A Kinetic or Thermodynamic Impediment to N-N Bond Cleavage? J. Am. Chem. Soc. 2012, 134, 13035–13045. [PubMed: 22694364]

(116). Edema JJH; Meetsma A; Gambarotta S Divalent Vanadium and Dinitrogen Fixation: The Preparation and X-Ray Structure of (μ-N2){[(o-Me2NCH2)C6H4]2V(Py)}2(THF)2. J. Am. Chem. Soc. 1989, 111, 6878–6880.

(117). Buijink JKF; Meetsma A; Teuben JH Electron-Deficient Vanadium Alkyl Complexes: Synthesis and Molecular Structure of the Vanadium(III) Dinitrogen Complex [(Me3CCH2)3V]2(μ-N2). Organometallics 1993, 12, 2004–2005.

(118). Ferguson R; Solari E; Floriani C; Osella D; Ravera M; Re N; Chiesi-Villa A; Rizzoli C Stepwise Reduction of Dinitrogen Occurring on a Divanadium Model Compound: A Synthetic, Structural, Magnetic, Electrochemical, and Theoretical Investigation on the [V=N=N=N](n+) [n = 4–6] Based Complexes. J. Am. Chem. Soc. 1997, 119, 10104–10115.

(119). Connor GP; Holland PL Coordination Chemistry Insights into the Role of Alkali Metal Promoters in Dinitrogen Reduction. Catal. Today 2017, 286, 21–40. [PubMed: 28344387]

(120). Fryzuk MD; Kozak CM; Patrick BO Dinuclear Organometallic Dinitrogen Complexes of Niobium. Inorg. Chim. Acta 2003, 345, 53–62.

(121). Zanotti-Gerosa A; Solari E; Giannini L; Floriani C; Chiesi-Villa A; Rizzoli C Stepwise Reduction of Dinitrogen to Nitride Assisted by Niobium Bonded to Oxygen Donor Atoms: The Potential of Reduced Forms of Niobium Calix[4]Arene. J. Am. Chem. Soc. 1998, 120, 437–438.

(122). Dilworth JR; Henderson RA; Hills A; Hughes DL; MacDonald C; Stephens AN; Walton DRM The Chemistry of Niobium and Tantalum Dithiocarbamato-Complexes. Part 1. Synthesis, Structure, and Protonation of Dinitrogen-Bridged Complexes. J. Chem. Soc. Dalt. Trans 1990, 0, 1077–1085.

(123). Bregel DC; Oldham SM; Lachicotte RJ; Eisenberg R A New Tantalum Dinitrogen Complex and a Parahydrogen-Induced Polarization Study of Its Reaction with Hydrogen. Inorg. Chem. 2002, 41, 4371–4377. [PubMed: 12184753]

(124). Lee T-Y; Wooten AJ; Luci JJ; Swenson DC; Messerle L Four-Electron Reduction of Dinitrogen during Solution Disproportionation of the Organodimetallic (η-C5Me4R)2Ta2(μ-Cl)4 (R = Me, Et) to a New μ-η1:η1-N2 Complex and Odd-Electron Organotrimetallic Cluster. Chem. Commun. 2005, No. 43, 5444.

(125). Takada R; Hirotsu M; Nishioka T; Hashimoto H; Kinoshita I Sulfur-Bridged Ta-M (M = Mo, Cr) Multinuclear Complexes Bearing a Four-Electron-Reduced Dinitrogen Ligand. Organometallics 2011, 30, 4232–4235.

(126). Sperry CK; Cotter WD; Lee RA; Lachicotte RJ; Bazan GC Tantalum Borollide Trichloride: A Versatile Entry into Tantalum Borollide Complexes. J. Am. Chem. Soc. 1998, 120, 7791–7805.

(127). Schrock RR; Wesolek M; Liu AH; Wallace KC; Dewan JC Thiolato Dinitrogen (or Hydrazido(4-)) Complexes, [Ta(SAr)3(THF)]2(μ-N2) (Ar = 2,6-C6H3-i-Pr2, 2,4,6-C6H2-i-Pr3), and Phenoxide Analogues. Structural Comparison of [Ta(S-2,6-C6H3-i-Pr2)3(THF)]2(μ-N2) and [Ta(o-2,6-C6H3-i-Pr2)3(THF)]2(μ-N2). Inorg. Chem. 1988, 27, 2050–2054.

(128). Bulen WA; Keeler RF; Varner JE Distribution of Molybdenum99 in Cell-Free Preparations of Azotobacter Vinelandii.[1] J. Bacteriol. 1956, 72, 394–396. [PubMed: 13366934]

(129). Burema SJ; Wieringa KT Molybdenum as a Growth Factor of Azotobacter Chroococcum. Antonie Van Leeuwenhoek 1942, 8, 123–133.

(130). Forder RA; Prout K μ-Dinitrogen-Bis-{(π-Mesitylene)[1,2-Bis(Dimethylphosphino)Ethane]Molybdenum}. Acta Crystallogr. 1974, 30, 2778–2780.

(131). Mork BV; Tilley TD Synthons for Coordinatively Unsaturated Complexes of Tungsten, and Their Use for the Synthesis of High Oxidation-State Silylene Complexes. J. Am. Chem. Soc. 2004, 126, 4375–4385. [PubMed: 15053627]

(132). Buss JA; Vandervelde DG; Agapie T Lewis Acid Enhancement of Proton Induced CO_2 Cleavage: Bond Weakening and Ligand Residence Time Effects. J. Am. Chem. Soc. 2018, 140, 10121–10125. [PubMed: 30032606]

(133). Miyazaki T; Tanaka H; Tanabe Y; Yuki M; Nakajima K; Yoshizawa K; Nishibayashi Y Cleavage and Formation of Molecular Dinitrogen in a Single System Assisted by Molybdenum Complexes Bearing Ferrocenyldiphosphine. Angew. Chem., Int. Ed. 2014, 53, 11488–11492.

(134). Keane AJ; Farrell WS; Yonke BL; Zavalij PY; Sita LR Metal-Mediated Production of Isocyanates, R3EN=C=O from Dinitrogen, Carbon Dioxide, and R3ECl. Angew. Chem., Int. Ed. 2015, 54, 10220–10224.

(135). Duman LM; Farrell WS; Zavalij PY; Sita LR Steric Switching from Photochemical to Thermal Reaction Pathways for Enhanced Efficiency in Metal-Mediated Nitrogen Fixation. J. Am. Chem. Soc. 2016, 138, 14856–14859. [PubMed: 27779843]

(136). Peters JC; Cherry JPF; Thomas JC; Baraldo L; Mindiola DJ; Davis WM; Cummins CC Redox-Catalyzed Binding of Dinitrogen by Molybdenum N-Tert-Hydrocarbylanilide Complexes: Implications for Dinitrogen Functionalization and Reductive Cleavage. J. Am. Chem. Soc. 1999, 121, 10053–10067.

(137). Odom AL; Arnold PL; Cummins CC Heterodinuclear Uranium/Molybdenum Dinitrogen Complexes. J. Am. Chem. Soc 1998, 120, 5836–5837

(138). Mindiola DJ; Meyer K; Cherry J-PF; Baker TA; Cummins CC Dinitrogen Cleavage Stemming from a Heterodinuclear Niobium/Molybdenum N2 Complex: New Nitridoniobium Systems Including a Niobazene Cyclic Trimer. Organometallics 2000, 19, 1622–1624.

(139). Figueroa JS; Piro NA; Clough CR; Cummins CC A Nitridoniobium(V) Reagent That Effects Acid Chloride to Organic Nitrile Conversion: Synthesis via Heterodinuclear (Nb/Mo) Dinitrogen Cleavage, Mechanistic Insights, and Recycling. J. Am. Chem. Soc. 2006, 128, 940–950. [PubMed: 16417385]

(140). Cozzolino AF; Silvia JS; Lopez N; Cummins CC Experimental and Computational Studies on the Formation of Cyanate from Early Metal Terminal Nitrido Ligands and Carbon Monoxide. Dalton Trans. 2014, 43, 4639–4652. [PubMed: 24492850]

(141). Solari E; Da Silva C; Iacono B; Hesschenbrouck J; Rizzoli C; Scopelliti R; Floriani C Photochemical Activation of the N≡N Bond in a Dimolybdenum-Dinitrogen Complex: Formation of a Molybdenum Nitride. Angew. Chem., Int. Ed. 2001, 40, 3907–3909.

(142). Solari E; Hesschenbrouck J; Scopelliti R; Floriani C; Re N From Oligomers to Conducting Polymers of the Metal-Dinitrogen Functionality. Angew. Chem., Int. Ed. 2001, 40, 932–934.

(143). Kol M; Kempe R; Davis WM; Schrock RR Synthesis of Molybdenum and Tungsten Complexes That Contain Triamidoamine Ligands of the Type (C6F5NCH2CH2)3N and Activation of Dinitrogen by Molybdenum. J. Am. Chem. Soc. 1994, 116, 4382–4390.

(144). Shih KY; Kempe R; Schrock RR Synthesis of Molybdenum Complexes That Contain Silylated Triamidoamine Ligands. A μ-Dinitrogen Complex, Methyl and Acetylide Complexes, and Coupling of Acetylides. J. Am. Chem. Soc. 1994, 116, 8804–8805.

(145). Greco GE; Schrock RR Synthesis, Structure, and Electrochemical Studies of Molybdenum and Tungsten Dinitrogen, Diazenido, and Hydrazido Complexes That Contain Aryl-Substituted Triamidoamine Ligands. Inorg. Chem. 2001, 40, 3861–3878. [PubMed: 11466043]

(146). Scheer M; Müller J; Schiffer M; Baum G; Winter R Pnictides as Symmetrically Bridging Ligands in Novel Neutral Complexes. Chem. - Eur. J. 2000, 6, 1252–1257. [PubMed: 10785812]

(147). O'Donoghue MB; Davis WM; Schrock RR; Reiff WM Heterobimetallic Dinitrogen Complexes That Contain the {[N3N]Mo-N=N}⁻ Ligand. Inorg. Chem. 1999, 38, 243–252.

(148). Margulieux GW; Turner ZR; Chirik PJ Synthesis and Ligand Modification Chemistry of a Molybdenum Dinitrogen Complex: Redox and Chemical Activity of a Bis(Imino)Pyridine Ligand. Angew. Chem., Int. Ed. 2014, 53, 14211–14215.

(149). Joannou MV; Bezdek MJ; Al-Bahily K; Korobkov I; Chirik PJ Synthesis and Reactivity of Pyridine(Diimine) Molybdenum Olefin Complexes: Ethylene Dimerization and Alkene Dehydrogenation. Organometallics 2017, 36, 4215–4223.

(150). Vidyaratne I; Scott J; Gambarotta S; Budzelaar PHM Dinitrogen Activation, Partial Reduction, and Formation of Coordinated Imide Promoted by a Chromium Diiminepyridine Complex. Inorg. Chem. 2007, 46, 7040–7049. [PubMed: 17649991]

(151). Bezdek MJ; Guo S; Chirik PJ Terpyridine Molybdenum Dinitrogen Chemistry: Synthesis of Dinitrogen Complexes That Vary by Five Oxidation States. Inorg. Chem. 2016, 55, 3117–3127. [PubMed: 26959702]

(152). Arashiba K; Miyake Y; Nishibayashi Y A Molybdenum Complex Bearing PNP-Type Pincer Ligands Leads to the Catalytic Reduction of Dinitrogen into Ammonia. Nat. Chem. 2011, 3, 120–125. [PubMed: 21258384]

(153). Kuriyama S; Arashiba K; Nakajima K; Tanaka H; Kamaru N; Yoshizawa K; Nishibayashi Y Catalytic Formation of Ammonia from Molecular Dinitrogen by Use of Dinitrogen-Bridged Dimolybdenum-Dinitrogen Complexes Bearing Pnp-Pincer Ligands: Remarkable Effect of Substituent at Pnp-Pincer Ligand. J. Am. Chem. Soc. 2014, 136, 9719–9731. [PubMed: 24896850]

(154). Tanaka H; Arashiba K; Kuriyama S; Sasada A; Nakajima K; Yoshizawa K; Nishibayashi Y Unique Behaviour of Dinitrogen-Bridged Dimolybdenum Complexes Bearing Pincer Ligand towards Catalytic Formation of Ammonia. Nat. Commun. 2014, 5, 3737. [PubMed: 24769530]

(155). Kinoshita E; Arashiba K; Kuriyama S; Miyake Y; Shimazaki R; Nakanishi H; Nishibayashi Y Synthesis and Catalytic Activity of Molybdenum-Dinitrogen Complexes Bearing Unsymmetric PNP-Type Pincer Ligands. Organometallics 2012, 31, 8437–8443.

(156). Arashiba K; Kuriyama S; Nakajima K; Nishibayashi Y Preparation and Reactivity of a Dinitrogen-Bridged Dimolybdenum-Tetrachloride Complex. Chem. Commun. 2013, 49, 11215–11217.

(157). Eizawa A; Arashiba K; Tanaka H; Kuriyama S; Matsuo Y; Nakajima K; Yoshizawa K; Nishibayashi Y Remarkable Catalytic Activity of Dinitrogen-Bridged Dimolybdenum Complexes Bearing NHC-Based PCP-Pincer Ligands toward Nitrogen Fixation. Nat. Commun. 2017, 8, 14874. [PubMed: 28374835]

(158). Ashida Y; Arashiba K; Nakajima K; Nishibayashi Y Molybdenum-Catalysed Ammonia Production with Samarium Diiodide and Alcohols or Water. Nature. 2019, 568, 536–540. [PubMed: 31019315]

(159). Brown KA; Harris DF; Wilker MB; Rasmussen A; Khadka N; Hamby H; Keable S; Dukovic G; Peters JW; Seefeldt LC; King PW Light-Driven Dinitrogen Reduction Catalyzed by a CdS:Nitrogenase MoFe Protein Biohybrid. Science 2016, 352, 448–450. [PubMed: 27102481]

(160). Silantyev GA; Förster M; Schluschaß B; Abbenseth J; Würtele C; Volkmann C; Holthausen MC; Schneider S Dinitrogen Splitting Coupled to Protonation. Angew. Chem., Int. Ed. 2017, 56, 5872–5876.

(161). Arashiba K; Kinoshita E; Kuriyama S; Eizawa A; Nakajima K; Tanaka H; Yoshizawa K; Nishibayashi Y Catalytic Reduction of Dinitrogen to Ammonia by Use of Molybdenum-Nitride Complexes Bearing a Tridentate Triphosphine as Catalysts. J. Am. Chem. Soc. 2015, 137, 5666–5669. [PubMed: 25879994]

(162). Liao Q; Saffon-Merceron N; Mézailles N N2 Reduction into Silylamine at Tridentate Phosphine/Mo Center: Catalysis and Mechanistic Study. ACS Catal. 2015, 5, 6902–6906.

(163). Liao Q; Cavaillé A; Saffon-Merceron N; Mézailles N Direct Synthesis of Silylamine from N$_2$ and a Silane: Mediated by a Tridentate Phosphine Molybdenum Fragment. Angew. Chem., Int. Ed. 2016, 55, 11212–11216.

(164). Arashiba K; Eizawa A; Tanaka H; Nakajima K; Yoshizawa K; Nishibayashi Y Catalytic Nitrogen Fixation via Direct Cleavage of Nitrogen-Nitrogen Triple Bond of Molecular Dinitrogen under Ambient Reaction Conditions. Bull. Chem. Soc. Jpn. 2017, 90, 1111–1118.

(165). Berben LA; Kozimor SA Dinitrogen and Acetylide Complexes of Low-Valent Chromium. Inorg. Chem. 2008, 47, 4639–4647. [PubMed: 18459723]

(166). Hoffert WA; Rappé AK; Shores MP Unusual Electronic Effects Imparted by Bridging Dinitrogen: An Experimental and Theoretical Investigation. Inorg. Chem. 2010, 49, 9497–9507. [PubMed: 20843076]

(167). Luo XL; Kubas GJ; Burns CJ; Butcher RJ; Bryan JC Synthesis and X-Ray Crystal Structures of {Mo(CO)(Et2PC2H4PEt2)2}2(μ-N2) with an End-On Bridging Dinitrogen Ligand and Mo(CO)(Bui2PC2H4PBui2)2 Containing an Agostic Mo···H-C Interaction. Inorg. Chem. 1995, 34, 6538–6545.

(168). Katayama A; Ohta T; Wasada-Tsutsui Y; Inomata T; Ozawa T; Masuda H A Dinitrogen Molybdenum Complex Induces Dinitrogen Cleavage by One-Electron Oxidation. Angew. Chem., Int. Ed. 2019, 58, 11279–11284.

(169). Sellmann D; Maisel G Notizen: Systematische Synthese von N2-Komplexen: Weitere N2-Komplexe Des Chroms/ Systematic Synthesis of N2-Complexes: Further N2-Complexes of Chromium. Zeitschrift für Naturforsch. B 1972, 27, 718–719.

(170). Denholm S; Hunter G; Weakley TJR Dinitrogen Complexes Derived from Tricarbonyl(η6-Hexaethylbenzene)Chromium(0): Crystal and Molecular Structure of μ-Dinitrogen-Bis[Dicarbonyl(η6-Hexaethylbenzene)Chromium(0)]-Toluene (1/1). J. Chem. Soc. Dalton Trans. 1987, 2789–2791.

(171). Yin J; Li J; Wang GX; Yin ZB; Zhang WX; Xi Z Dinitrogen Functionalization Affording Chromium Hydrazido Complex. J. Am. Chem. Soc. 2019, 141, 4241–4247. [PubMed: 30817140]

(172). Monillas WH; Yap GPA; MacAdams LA; Theopold KH Binding and Activation of Small Molecules by Three-Coordinate Cr(I). J. Am. Chem. Soc. 2007, 129, 8090–8091. [PubMed: 17567016]

(173). Hung YT; Yap GPA; Theopold KH Unexpected Reactions of Chromium Hydrides with a Diazoalkane. Polyhedron 2019, 157, 381–388.

(174). Akturk ES; Yap GPA; Theopold KH Mechanism-Based Design of Labile Precursors for Chromium(I) Chemistry. Chem. Commun. 2015, 51, 15402–15405.

(175). Anderson SN; Richards RL; Hughes DL Dinitrogen Complexes of Tungsten with Bulky Phosphine Co-Ligands: Preparation and Crystal Structures of [{W(N2)2(PEt2Ph)3} 2(μ-N2)],Trans-[W(N2)2(PEt2,Ph)4].C4H8O, and [W(η6-C6H6PPrn2)(N2)(PPrn2Ph)2] and Their Reactions to Give Hydrazine and Ammonia. J. Chem. Soc. Dalt. Trans. 1986, 245–252.

(176). Anderson SN; Richards RL; Hughes DL Preparation and Crystal Structure of [{W(N2)2(PEt2Ph)3}2(μ-N2)]. J. Chem. Soc. Chem. Commun. 1982, 1291–1292.

(177). Harvey BG; Arif AM; Ernst RD Syntheses and Characterization of the W(II) and W(III) N2 Complexes, [WCl2(PMe3)3]2N2 and [WCl3(PMe3)2]2N2. Inorg. Chim. Acta 2010, 363, 221–224.

(178). Butts MD; Bryan JC; Luo X-L; Kubas GJ Comparison of H–H versus Si–H σ-Bond Coordination and Activation on 16e Metal Fragments. Organosilane, N2, and Ethylene Addition to the Agostic Complex W(CO)3(PR3)2 and Dynamic NMR Behavior of the Latter. Inorg. Chem. 1997, 36, 3341–3353. [PubMed: 11670001]

(179). Harlan CJ; Jones RA; Koschmieder SU; Nunn CM Reduction of Tungsten Complexes with Primary Phosphines and Lithium Dialkyl Phosphides. X-Ray Crystal Structures of [(Cp*WCl2)2·(t-Bu2PPt-Bu2)2], [(Cp*WCl4)(H2PPh)], [{(PhN)WCl2(PMe3)2}2(μ-N2)] and Trans-WCl4(H2Pt-Bu)2 (Cp* = η5-C5Me5). Polyhedron 1990, 9, 669–679.

(180). Mizobe Y; Yokobayashi Y; Oshita H; Takahashi T; Hidai M Preparation of Heterobimetallic Complexes with a Bridging Dinitrogen Ligand, [WX(PMe2Ph)4(μ-N2)MCp2Cl] (M = Ti, X = Cl; M = Zr, and Hf, X = I), and X-Ray Structure of [WI(PMe2Ph)3(Py)(μ-N2)ZrCp2Cl] (Py = Pyridine). Organometallics 1994, 13, 3764–3766.

(181). Ishino H; Nagano T; Kuwata S; Yokobayashi Y; Ishii Y; Hidai M; Mizobe Y Syntheses, Structures, and Reactivities of Heterobimetallic Bridging Dinitrogen Complexes Containing Group 6 and Group 4 or 5 Transition Metals 1. Organometallics 2002, 20, 188–198.

(182). Ishino H; Takemoto S; Hirata K; Kanaizuka Y; Hidai M; Nabika M; Seki Y; Miyatake T; Suzuki N Olefin Polymerization Catalyzed by Titanium-Tungsten Heterobimetallic Dinitrogen Complexes. Organometallics 2004, 23, 4544–4546.

(183). Hoffman BM; Lukoyanov D; Yang ZY; Dean DR; Seefeldt LC Mechanism of Nitrogen Fixation by Nitrogenase: The next Stage. Chem. Rev. 2014, 114, 4041–4062. [PubMed: 24467365]

(184). Hoffman BM; Lukoyanov D; Dean DR; Seefeldt LC Nitrogenase: A Draft Mechanism. Acc. Chem. Res. 2013, 46, 587–595. [PubMed: 23289741]

(185). Murray RC; Schrock RR Preparation of an Unsubstituted Hydrazido(1-) Complex and an Authentic High Oxidation State Ditungsten Dinitrogen Complex. J. Am. Chem. Soc. 1985, 107, 4557–4558.

(186). Churchill MR; Li Y-J The W(μ-N2)W System. J. Organomet. Chem. 1986, 301, 49–59.

(187). O'Regan MB; Liu AH; Finch WC; Schröck RR; Davis WM A Study of High Oxidation State Complexes of the Type [W(η5-C5Me5)Me2X]2(μ-N2), Including X-Ray Structures of [W(η5-C5Me5)Me2(OC6F5)]2(μ-N2) and [W(η5-C5Me5)Me2(S-2,4,6-C6H2Me3)]2(μ-N2). J. Am. Chem. Soc. 1990, 112, 4331–4338.

(188). Ziegler ML; Weidenhammer K; Zeiner H; Skell PS; Herrmann WA Nitrogen Transfer from a Diazoalkane to a Metal Center. Angew. Chem., Int. Ed. 1976, 15, 695–696.

(189). Sellman D; Gerlach R; Jödden K Reaktionen an Komplexgebundenen Liganden. XXXII. Synthese und Eigenschaften von heteronuklearen Mangan-Chrom-Komplexen mit Distickstoff-Diazen- und Hydrazin-Briickenl iganden J. Organomet. Chem. 1979, 178, 433–447.

(190). Chomitz WA; Arnold J Synthesis and Characterization of Manganese and Iron Complexes Supported by Multidentate [N2P2] Ligands. J. Chem. Soc. Dalt. Trans. 2009, 1714–1720.

(191). Cummins DC; Yap GPA; Theopold KH Scorpionates of the "Tetrahedral Enforcer" Variety as Ancillary Ligands for Dinitrogen Complexes of First Row Transition Metals (Cr-Co). Eur. J. Inorg. Chem. 2016, 2016, 2349–2356.

(192). Joachim JE; Apostolidis C; Kanellakopulos B; Maier R; Meyer D; Rebizant J; Ziegler ML Metallorganische Chemie Des Technetiums. J. Organomet. Chem. 1993, 455, 137–141.

(193). Gunnoe TB; Sabat M; Harman WD Reactions of TpRe(CO)2(THF) with Aromatic Molecules (Tp = Hydridotris(Pyrazolyl)Borate). J. Am. Chem. Soc. 1998, 120, 8747–8754.

(194). Chatt J; Dilworth JR; Leigh GJ; Richards RL Polynuclear Dinitrogen Complexes. J. Chem. Soc. D Chem. Commun. 1970, 955–956.

(195). Chatt J; Dilworth JR; Richards RL; Sanders JR Chemical Evidence Concerning the Function of Molybdenum in Nitrogenase. Nature 1969, 224, 1201–1202. [PubMed: 5358340]

(196). Zhang QF; Chim JLC; Lai W; Wong WT; Leung WH Bridged Dinitrogen Complexes of Iron and Chromium Porphyrins. Inorg. Chem. 2001, 40, 2470–2471. [PubMed: 11350218]

(197). Seymore SB; Brown SN Kinetic Effects in Heterometallic Dinitrogen Cleavage. Inorg. Chem. 2006, 45, 9540–9550. [PubMed: 17083256]

(198). Robson R Lewis Base Behavior of Dinitrogen and Carbonyl Complexes of Rhenium toward Titanium Tetrachloride and Related Species. Inorg. Chem. 1974, 13, 475–479.

(199). Mercer M; Crabtree RH; Richards RL A μ-Dinitrogen Complex with a Long N-N Bond. X-Ray Crystal Structure of [(PMe2Ph)4ClReN2MoCl4(OMe)]. J. Chem. Soc. Chem. Commun. 1973, 808–809.

(200). Mercer M Crystal Structure of a Dinuclear Dinitrogen Complex: Tetrachloro-{chlorotetrakis[Dimethyl(Phenyl)Phosphine]Rhenium(I)}-μ- Dinitrogen-Methoxymolybdenum(V)-Methanol-Hydrochloric Acid. J. Chem. Soc. Dalt. Trans. 1974, 1637–1640.

(201). Cradwick PD Crystal Structure of a Trinuclear Dinitrogen-Bridged Complex: Di-μ-Di-Nitrogen-Tetrachlorobis[Chlorotetrakis(Dimethylphenylphosphine)Rhenio]Molybdenum–Dichloromethane (1/1). J. Chem. Soc., Dalt. Trans. 1976, 1934–1936.

(202). Klopsch I; Finger M; Würtele C; Milde B; Werz DB; Schneider S Dinitrogen Splitting and Functionalization in the Coordination Sphere of Rhenium. J. Am. Chem. Soc. 2014, 136, 6881–6883. [PubMed: 24779407]

(203). Lindley BM; Van Alten RS; Finger M; Schendzielorz F; Würtele C; Miller AJM; Siewert I; Schneider S Mechanism of Chemical and Electrochemical N_2 Splitting by a Rhenium Pincer Complex. J. Am. Chem. Soc. 2018, 140, 7922–7935. [PubMed: 29856611]

(204). Schendzielorz F; Finger M; Abbenseth J; Würtele C; Krewald V; Schneider S Metal-Ligand Cooperative Synthesis of Benzonitrile by Electrochemical Reduction and Photolytic Splitting of Dinitrogen. Angew. Chem., Int. Ed. 2019, 58, 830–834.

(205). Albertin G; Antoniutti S; Castro J; Ganz V; Sibilla F Preparation and Reactivity of Half-Sandwich Organic Azide Complexes of Osmium. Dalton Trans. 2018, 47, 11658–11668. [PubMed: 30095833]

(206). Glaser PB; Wanandi PW; Tilley TD Synthesis, Structure, and Reactivity of Osmium Silyl and Silylene Complexes Cp*(Me3P)2OsSiR2X and [Cp*(Me3P)2OsSiR2][B(C6F5)4] (R = Me, iPr; X = Cl, OTf). Organometallics 2004, 23, 693–704.

(207). Ohki Y; Hatanaka T; Tatsumi K C-H Bond Activation of Heteroarenes Mediated by a Half-Sandwich Iron Complex of N-Heterocyclic Carbene. J. Am. Chem. Soc. 2008, 130, 17174–17186. [PubMed: 19007215]

(208). Zhang F; Song H; Zhuang X; Tung CH; Wang W Iron-Catalyzed 1,2-Selective Hydroboration of N-Heteroarenes. J. Am. Chem. Soc. 2017, 139, 17775–17778. [PubMed: 29192777]

(209). Rankin MA; Hesp KD; Schatte G; McDonald R; Stradiotto M Reactivity of a Coordinatively Unsaturated Cp*Ru(K2- P,O) Complex. Chem. Commun. 2008, 250–252.

(210). Aneetha H; Jiménez-Tenorio M; Puerta MC; Valerga P; Mereiter K Bridging and Terminal Half-Sandwich Ruthenium Dinitrogen Complexes and Related Derivatives: A Structural Study. Organometallics 2002, 21, 628–635.

(211). Vidovic D; Addy DA; Krämer T; McGrady J; Aldridge S Probing the Intrinisic Structure and Dynamics of Aminoborane Coordination at Late Transition Metal Centers: Mono(σ-BH) Binding in [CpRu(PR3)2(H2BNCy2)]+. J. Am. Chem. Soc. 2011, 133, 8494–8497. [PubMed: 21563831]

(212). Rose RP; Jones C; Schulten C; Aldridge S; Stasch A Synthesis and Characterization of Amidinate-Iron(I) Complexes: Analogies with β-Diketiminate Chemistry. Chem. - Eur. J. 2008, 14, 8477–8480. [PubMed: 18698573]

(213). Sunada Y; Imaoka T; Nagashima H Half-Sandwich (η6-Arene)Iron(II) Dinitrogen Complexes Bearing a Disilaferracycle Skeleton as a Precursor for Double Silylation of Ethylene and Alkynes. Organometallics 2010, 29, 6157–6160.

(214). Collman JP; Hutchison JE; Lopez MA; Guilard R A Stable Dinitrogen Complex of a Ruthenium Cofacial Diporphyrin. J. Am. Chem. Soc. 1992, 114, 8066–8073.

(215). Bonomo L; Stern C; Solari E; Scopelliti R; Floriani C Acetylenes Rearranging on Ruthenium-Porphyrinogen and Leading to Vinylidene and Carbene Functionalities. Angew. Chem., Int. Ed. 2001, 40, 1449–1452.

(216). Field LD; Guest RW; Turner P Mixed-Valence Dinitrogen-Bridged Fe(0)/Fe(II) Complex. Inorg. Chem. 2010, 49, 9086–9093. [PubMed: 20815362]

(217). Takaoka A; Mankad NP; Peters JC Dinitrogen Complexes of Sulfur-Ligated Iron. J. Am. Chem. Soc. 2011, 133, 8440–8443. [PubMed: 21574618]

(218). Liu S; Gagliardi L; Rudd PA; Lu CC; Young VG Metal–Alane Adducts with Zero-Valent Nickel, Cobalt, and Iron. J. Am. Chem. Soc. 2011, 133, 20724–20727. [PubMed: 22122804]

(219). Yoshimoto K; Yatabe T; Matsumoto T; Robertson A; Nakai H; Tanaka H; Kamachi T; Shiota Y; Yoshizawa K; Asazawa K; Tanaka H; Ogo S Synthesis and Structure of a Water-Soluble μ-$\eta^1 : \eta^1$-N_2 Dinuclear Ru^{II} Complex with a Polyamine Ligand. Chem. Lett. 2016, 45, 149–151.

(220). Sellmann D; Hille A; Heinemann FW; Moll M; Rösler A; Sutter J; Brehm G; Reiher M; Hess BA; Schneider S Metal Thiolate Complexes Binding Molecular Nitrogen under Mild Conditions: [μ-N2{Ru(PiPr3)(N2Me2S2)}2], the First Dinuclear Example. Inorg. Chim. Acta 2003, 348, 194–198.

(221). Darmon JM; Margulieux GW; Turner ZR; Yu RP; Hoyt JM; Chirik PJ High-Activity Iron Catalysts for the Hydrogenation of Hindered, Unfunctionalized Alkenes. ACS Catal. 2012, 2, 1760–1764. [PubMed: 26229734]

(222). Russell SK; Darmon JM; Lobkovsky E; Chirik PJ Synthesis of Aryl-Substituted Bis(Imino) Pyridine Iron Dinitrogen Complexes. Inorg. Chem. 2010, 49, 2782–2792. [PubMed: 20143847]

(223). Bart SC; Chłopek K; Bill E; Bouwkamp MW; Lobkovsky E; Neese F; Wieghardt K; Chirik PJ Electronic Structure of Bis(Imino)Pyridine Iron Dichloride, Monochloride, and Neutral Ligand Complexes: A Combined Structural, Spectroscopic, and Computational Study. J. Am. Chem. Soc. 2006, 128, 13901–13912. [PubMed: 17044718]

(224). Bart SC; Lobkovsky E; Bill E; Wieghardt K; Chirik PJ Neutral-Ligand Complexes of Bis(Imino)Pyridine Iron: Synthesis, Structure, and Spectroscopy. Inorg. Chem. 2007, 46, 7055–7063. [PubMed: 17655227]

(225). Wieder NL; Gallagher M; Carroll PJ; Berry DH Evidence for Ligand Non-Innocence in a Formally Ruthenium(I) Hydride Complex. J. Am. Chem. Soc. 2010, 132, 4107–4109. [PubMed: 20199024]

(226). Gallagher M; Wieder NL; Dioumaev VK; Carroll PJ; Berry DH Low-Vaient Ruthenium Complexes of the Non-Innocent 2, 6-Bis(Imino)Pyridine Ligand. Organometallics 2010, 29, 591–603.

(227). Tanabe Y; Kuriyama S; Arashiba K; Nakajima K; Nishibayashi Y Synthesis and Reactivity of Ruthenium Complexes Bearing Arsenic-Containing Arsenic-Nitrogen-Arsenic-Type Pincer Ligand. Organometallics 2014, 33, 5295–5300.

(228). Abbenhuis RATM; Del Río I; Bergshoef MM; Boersma J; Veldman N; Spek AL; Van Koten G 16- And 18-Electron Ruthenium(II) Complexes of the Neutral, Potentially Tridentate Triamine Ligand 2,6-[Bis(Dimethylamino)Methyl]Pyridine (NN'N). Inorg. Chem. 1998, 37, 1749–1758.

(229). Zhang J; Gandelman M; Shimon LJW; Milstein D Electron-Rich, Bulky PNN-Type Ruthenium Complexes: Synthesis, Characterization and Catalysis of Alcohol Dehydrogenation. J. Chem. Soc. Dalt. Trans. 2006, No. 1, 107–113.

(230). Zhang J; Gandelman M; Shimon LJW; Rozenberg H; Milstein D Electron-Rich, Bulky Ruthenium PNP-Type Complexes. Acceptorless Catalytic Alcohol Dehydrogenation. Organometallics 2004, 23, 4026–4033.

(231). Gusev DG; Dolgushin FM; Antipin MY Hydride, Borohydride, and Dinitrogen Pincer Complexes of Ruthenium. Organometallics 2000, 19, 3429–3434.

(232). Higuchi J; Kuriyama S; Eizawa A; Arashiba K; Nakajima K; Nishibayashi Y Preparation and Reactivity of Iron Complexes Bearing Anionic Carbazole-Based PNP-Type Pincer Ligands toward Catalytic Nitrogen Fixation. Dalt. Trans. 2018, 47, 1117–1121.

(233). Suzuki T; Wasada-Tsutsui Y; Ogawa T; Inomata T; Ozawa T; Sakai Y; Fryzuk MD; Masuda H N_2 Activation by an Iron Complex with a Strong Electron-Donating Iminophosphorane Ligand. Inorg. Chem. 2015, 54, 9271–9281. [PubMed: 26135343]

(234). Fernández FE; Puerta MC; Valerga P Picolyl-NHC Hydrotris(Pyrazolyl)Borate Ruthenium(II) Complexes: Synthesis, Characterization, and Reactivity with Small Molecules. Inorg. Chem. 2013, 52, 4396–4410. [PubMed: 23530454]

(235). Jiménez-Tenorio M; Puerta MC; Valerga P Activation of Propargyl Alcohols by TpRu Complexes Bearing a Bidentate NHC Ligand. Organometallics 2016, 35, 388–399.

(236). McSkimming A; Harman WH A Terminal N2 Complex of High-Spin Iron(I) in a Weak, Trigonal Ligand Field. J. Am. Chem. Soc. 2015, 137, 8940–8943. [PubMed: 26135639]

(237). Geri JB; Shanahan JP; Szymczak NK Testing the Push-Pull Hypothesis: Lewis Acid Augmented N_2 Activation at Iron. J. Am. Chem. Soc. 2017, 139, 5952–5956. [PubMed: 28414226]

(238). Doyle LR; Hill PJ; Wildgoose GG; Ashley AE Teaching Old Compounds New Tricks: Efficient N2 Fixation by Simple Fe(N2)(Diphosphine)2 Complexes. Dalt. Trans. 2016, 45, 7550–7554.

(239). Sippel D; Rohde M; Netzer J; Trncik C; Gies J; Grunau K; Djurdjevic I; Decamps L; Andrade SLA; Einsle O A Bound Reaction Intermediate Sheds Light on the Mechanism of Nitrogenase. Science 2018, 359, 1484–1489. [PubMed: 29599235]

(240). Seefeldt LC; Hoffman BM; Dean DR Mechanism of Mo-Dependent Nitrogenase. Annu. Rev. Biochem. 2009, 78, 701–722. [PubMed: 19489731]

(241). Namura K; Suzuki H Synthesis, Structure, and Reactivity of Mixed-Ligand Dinuclear Ruthenium Polyhydrido Complexes Supported by 1,4,7-Trimethyl-1,4,7-Triazacyclononane and Bulky Phosphine Ligands. Organometallics 2014, 33, 2968–2983.

(242). Ip HF; Yi XY; Wong WY; Williams ID; Leung WH Synthesis, Structures and Reactivity of Ruthenium Nitrosyl Complexes Containing Kläui's Oxygen Tripodal Ligand. Dalt. Trans. 2011, 40, 11043–11050.

(243). Betley TA; Peters JC Dinitrogen Chemistry from Trigonally Coordinated Iron and Cobalt Platforms. J. Am. Chem. Soc. 2003, 125, 10782–10783. [PubMed: 12952446]

(244). Betley TA; Peters JC A Tetrahedrally Coordinated L_3Fe-N_x Platform That Accommodates Terminal Nitride (FeIV≡N) and Dinitrogen (FeI-N2-FeI) Ligands. J. Am. Chem. Soc. 2004, 126, 6252–6254. [PubMed: 15149221]

(245). Saouma CT; Moore CE; Rheingold AL; Peters JC A Five-Coordinate Phosphino/Acetate Iron(II) Scaffold That Binds N2, N2H2, N2H4, and NH3 in the Sixth Site. Inorg. Chem. 2011, 50, 11285–11287. [PubMed: 22004139]

(246). Smith JM; Lachicotte RJ; Pittard KA; Cundari TR; Lukat-Rodgers G; Rodgers KR; Holland PL Stepwise Reduction of Dinitrogen Bond Order by a Low-Coordinate Iron Complex. J. Am. Chem. Soc. 2001, 123, 9222–9223. [PubMed: 11552855]

(247). McWilliams SF; Bunting PC; Kathiresan V; Mercado BQ; Hoffman BM; Long JR; Holland PL Isolation and Characterization of a High-Spin Mixed-Valent Iron Dinitrogen Complex. Chem. Commun. 2018, 54, 13339–13342.

(248). Smith JM; Sadique AR; Cundari TR; Rodgers KR; Lukat-Rodgers G; Lachicotte RJ; Flaschenriem CJ; Vela J; Holland PL Studies of Low-Coordinate Iron Dinitrogen Complexes. J. Am. Chem. Soc. 2006, 128, 756–769. [PubMed: 16417365]

(249). Rodriguez MM; Bill E; Brennessel WW; Holland PL N_2 Reduction and Hydrogenation to Ammonia by a Molecular Iron-Potassium Complex. Science 2011, 334, 780–783. [PubMed: 22076372]

(250). Figg TM; Holland PL; Cundari TR Cooperativity between Low-Valent Iron and Potassium Promoters in Dinitrogen Fixation. Inorg. Chem. 2012, 51, 7546–7550. [PubMed: 22734966]

(251). Grubel K; Brennessel WW; Mercado BQ; Holland PL Alkali Metal Control over N-N Cleavage in Iron Complexes. J. Am. Chem. Soc. 2014, 136, 16807–16816. [PubMed: 25412468]

(252). Hein NM; Suzuki T; Ogawa T; Fryzuk MD Low Coordinate Iron Derivatives Stabilized by a β-Diketiminate Mimic. Synthesis and Coordination Chemistry of Enamidophosphinimine Scaffolds

to Generate Diiron Dinitrogen Complexes. Dalton Trans. 2016, 45, 14697–14708. [PubMed: 27273745]

(253). Bennett MA; Byrnes MJ; Chung G; Edwards AJ; Willis AC Bis(Acetylacetonato)Ruthenium(II) Complexes Containing Bulky Tertiary Phosphines. Formation and Redox Behaviour of Ru(Acac)2(PR3) (R = iPr, Cy) Complexes with Ethene, Carbon Monoxide, and Bridging Dinitrogen. Inorg. Chim. Acta 2005, 358, 1692–1708.

(254). Magnuson RH; Taube H Mixed Oxidation States in Osmium Ammine Dinitrogen Complexes. J. Am. Chem. Soc. 1972, 94, 7213–7214.

(255). Berke H; Bankhardt W; Huttner G; v. Seyerl, J.; Zsolnai, L. Eisenkomplexe Als Modellverbindungen Zur Homogenen Hydrierung von Kohlenmonoxid. Chem. Ber. 1981, 114, 2754–2768.

(256). Abdur-Rashid K; Gusev DG; Lough AJ; Morris RH Synthesis and Characterization of RuH2(H2)2(PiPr3)2 and Related Chemistry. Evidence for a Bis(Dihydrogen) Structure. Organometallics 2000, 19, 1652–1660.

(257). Abdur-Rashid K; Gusev DG; Lough AJ; Morris RH Synthesis and Characterization of RuH2(H2)2(PiPr3)2 and Related Chemistry. Evidence for a Bis(Dihydrogen) Structure. Organometallics 2002, 19, 1652–1660.

(258). Misono A; Uchida Y; Saito T Preparation of a Cobalt Complex Coordinated by Molecular Nitrogen and Triphenylphosphine. Bull. Chem. Soc. Jpn. 1967, 40, 700–700.

(259). Yamamoto A; Kitazume S; Pu LS; Ikeda S Study of the Fixation of Nitrogen. Isolation of Tris(Triphenylphosphine)Cobalt Complex Co-Ordinated with Molecular Nitrogen. Chem. Commun. 1967, 2, 79–80.

(260). Sacco A; Rossi M Hydride and Nitrogen Complexes of Cobalt. Chem. Commun. 1967, 316.

(261). Cecconi F; Ghilardi CA; Midollini S; Moneti S; Orlandini A; Bacci M Synthesis, Characterization, and Crystal Structure of the Dimeric, Paramagnetic Cobalt(0) Complex {[MeC(CH2PPh2)3Co]2(μ-N2)}. J. Chem. Soc. Chem. Commun. 1985, No. 11, 731–733.

(262). Detrich JL; Konečný R; Vetter WM; Doren D; Rheingold AL; Theopold KH Structural Distortion of the TpCo-L Fragment (Tp = Tris(Pyrazolyl)Borate). Analysis by X-Ray Diffraction and Density Functional Theory. J. Am. Chem. Soc. 1996, 118, 1703–1712.

(263). Gutierrez E; Monge A; Nicasio MC; Poveda ML; Carmona E An Iridium(III) Compound That Thermally Activates Two Molecules of Benzene and Forms a Stable Dinitrogen Complex. J. Am. Chem. Soc. 1994, 116, 791–792.

(264). Wu B; Gramigna KM; Bezpalko MW; Foxman BM; Thomas CM Heterobimetallic Ti/Co Complexes That Promote Catalytic N-N Bond Cleavage. Inorg. Chem. 2015, 54, 10909–10917. [PubMed: 26492046]

(265). Fernández P; Sousa-Pedrares A; Romero J; Dnrán ML; Sousa A; Pérez-Lourido P; García-Vázquez JA Synthesis and Structural Characterization of Cobalt, Nickel and Copper Phosphanylthiolato Complexes. Eur. J. Inorg. Chem. 2010, 2010, 814–823.

(266). Fout AR; Basuli F; Fan H; Tomaszewski J; Huffman JC; Baik MH; Mindiola DJ A Co2N2 Diamond-Core Resting State of Cobalt(I): A Three-Coordinate CoI Synthon Invoking an Unusual Pincer-Type Rearrangement. Angew. Chemie - Int. Ed. 2006, 45, 3291–3295.

(267). Gatard S; Guo C; Foxman BM; Ozerov OV Thioether, Dinitrogen, and Olefin Complexes of (PNP)Rh: Kinetics and Thermodynamics of Exchange and Oxidative Addition Reactions. Organometallics 2007, 26, 6066–6075.

(268). Nesbit MA; Suess DLM; Peters JC E-H Bond Activations and Hydrosilylation Catalysis with Iron and Cobalt Metalloboranes. Organometallics 2015, 34, 4741–4752.

(269). Cohen R; Rybtchinski B; Gandelman M; Rozenberg H; Martin JML; Milstein D Metallacarbenes from Diazoalkanes: An Experimental and Computational Study of the Reaction Mechanism. J. Am. Chem. Soc. 2003, 125, 6532–6546. [PubMed: 12785793]

(270). Salem H; Ben-David Y; Shimon LJW; Milstein D Exclusive C-C Activation and an Apparent α-H Elimination with a Rhodium Phosphinite Pincer Complex. Organometallics 2006, 25, 2292–2300.

(271). Hasegawa M; Segawa Y; Yamashita M; Nozaki K Isolation of a PBP-Pincer Rhodium Complex Stabilized by an Intermolecular C-H σ Coordination as the Fourth Ligand. Angew. Chemie - Int. Ed. 2012, 51, 6956–6960.

(272). Van Der Boom ME; Liou SY; Ben-David Y; Shimon LJW; Milstein D Alkyl- and Aryl-Oxygen Bond Activation in Solution by Rhodium(I), Palladium(II), and Nickel(II). Transition-Metal-Based Selectivity. J. Am. Chem. Soc. 1998, 120, 6531–6541.

(273). Göttker-Schnetmann I; White PS; Brookhart M Synthesis and Properties of Iridium Bis(Phosphinite) Pincer Complexes (p-XPCP)IrH2, (p-XPCP)Ir(CO), (p-XPCP)Ir(H)(Aryl), and {(p-XPCP)Ir}H2{μ-N2} and Their Relevance in Alkane Transfer Dehydrogenation. Organometallics 2004, 23, 1766–1776.

(274). Ghosh R; Kanzelberger M; Emge TJ; Hall GS; Goldman AS Dinitrogen Complexes of Pincer-Ligated Iridium. Organometallics 2006, 25, 5668–5671.

(275). Ding K; Pierpont AW; Brennessel WW; Lukat-Rodgers G; Rodgers KR; Cundari TR; Bill E; Holland PL Cobalt-Dinitrogen Complexes with Weakened N-N Bonds. J. Am. Chem. Soc. 2009, 131, 9471–9472. [PubMed: 19537787]

(276). Spitzer F; Graßl C; Balázs G; Mädl E; Keilwerth M; Zolnhofer EM; Meyer K; Scheer M Nacnac-Cobalt-Mediated P4 Transformations. Chem. - Eur. J 2017, 23, 2716–2721. [PubMed: 28032678]

(277). Ding K; Brennessel WW; Holland PL Three-Coordinate and Four-Coordinate Cobalt Hydride Complexes That React with Dinitrogen. J. Am. Chem. Soc. 2009, 131, 10804–10805. [PubMed: 19621923]

(278). Klein HF; Beck H; Hammerschmitt B; Koch U; Koppert S; Cordier G; Paulus H Synthesis, Properties, and Structure of a Dinitrogen Bridged Dinuclear Hydridocobalt Complex and Its Reactions with 1-Alkynes. Zeitschrift fur Naturforsch. - Sect. B J. Chem. Sci. 1991, 46, 147–156.

(279). Yoshida T; Okano T; Thorn DL; Tulip TH; Otsuka S; Ibers JA Preparations and Reactions of Some Hydridodinitrogentrialkylphosphine Complexes of Rhodium(I). The Structure of a Dinitrogen-Bridged Rhodium(I) Dimer, [RhH(P(i-Pr)3)2]2(μ-N2). J. Organomet. Chem. 1979, 181, 183–201.

(280). Jolly PW; Jonas K; Krüger C; Tsay YH The Preparation, Reactions and Structure of Bis[Bis(Tricyclohexylphosphine)Nickel] Dinitrogen, {[(C6H11)3P]2Ni}2N2. J. Organomet. Chem. 1971, 33, 109–122.

(281). Beck R; Shoshani M; Krasinkiewicz J; Hatnean JA; Johnson SA Synthesis and Chemistry of Bis(Triisopropylphosphine) Nickel(I) and Nickel(0) Precursors. J. Chem. Soc. Dalt. Trans. 2013, 42, 1461–1475.

(282). Harman WH; Lin TP; Peters JC A d10 Ni-(H2) Adduct as an Intermediate in H-H Oxidative Addition across a Ni-B Bond. Angew. Chem., Int. Ed. 2014, 53, 1081–1086.

(283). Kim YE; Kim J; Lee Y Formation of a Nickel Carbon Dioxide Adduct and Its Transformation Mediated by a Lewis Acid. Chem. Commun. 2014, 50, 11458–11461.

(284). Cowie BE; Emslie DJH Nickel and Palladium Complexes of Ferrocene-Backbone Bisphosphine-Borane and Trisphosphine Ligands. Organometallics 2015, 34, 4093–4101.

(285). Kim YE; Oh S; Kim S; Kim O; Kim J; Han SW; Lee Y Phosphinite-Ni(0) Mediated Formation of a Phosphide-Ni(II)-OCOOMe Species via Uncommon Metal-Ligand Cooperation. J. Am. Chem. Soc. 2015, 137, 4280–4283. [PubMed: 25798737]

(286). Charboneau DJ; Balcells D; Hazari N; Lant HMC; Mayer JM; Melvin PR; Mercado BQ; Morris WD; Repisky M; Suh HW Dinitrogen-Facilitated Reversible Formation of a Si-H Bond in a Pincer-Supported Ni Complex. Organometallics 2016, 35, 3154–3162.

(287). Diccianni JB; Katigbak J; Hu C; Diao T Mechanistic Characterization of (Xantphos)Ni(I)-Mediated Alkyl Bromide Activation: Oxidative Addition, Electron Transfer, or Halogen-Atom Abstraction. J. Am. Chem. Soc. 2019, 141, 1788–1796. [PubMed: 30612428]

(288). Horn B; Pfirrmann S; Limberg C; Herwig C; Braun B; Mebs S; Metzinger R N2 Activation in NiI-NN-NiI Units: The Influence of Alkali Metal Cations and CO Reactivity. Zeitschrift fur Anorg. und Allg. Chemie 2011, 637, 1169–1174.

(289). Pfirrmann S; Limberg C; Herwig C; Stößer R; Ziemer B A Dinuclear Nickel(I) Dinitrogen Complex and Its Reduction in Single- Electron Steps. Angew. Chem., Int. Ed. 2009, 48, 3357–3361.

(290). Pfirrmann S; Yao S; Ziemer B; Stösser R; Driess M; Limberg C β-Diketiminato Nickel(I) Complexes with Very Weak Ligation Allowing for H2 and N2 Activation. Organometallics 2009, 28, 6855–6860.

(291). Krüger C; Tsay Y-H. Molecular Structure of a π-Dinitrogen-Nickel-Lithium Complex. Angew. Chem., Int. Ed. 1973, 12, 998–999.

(292). Jonas K; Brauer DJ; Krüger C; Roberts PJ; Tsay YH "Side-on" Dinitrogen-Transition Metal Complexes. The Molecular Structure of {C6H5[Na·O(C2H5)2]2[(C6H5)2Ni]2N2NaLi6(OC2H5)4·O(C2H5)2}2. J. Am. Chem. Soc. 1976, 98, 74–81.

(293). Jonas K π-Bonded Nitrogen in a Crystalline Nickel-Lithium Complex. Angew. Chem., Int. Ed. 1973, 12, 997–998.

(294). Cotton FA; Jamerson JD; Stults BR Metal-Metal Multiple Bonds in Organometallic Compounds. I. (Di-Tert-Butylacetylene)Hexacarbonyldiiron and -Dicobalt. J. Am. Chem. Soc. 1976, 98, 1774–1779.

(295). Shan H; Yang Y; James AJ; Sharp PR Dinitrogen Bridged Gold Clusters. Science 1997, 275, 1460–1462.

(296). Zhang S; Fallah H; Gardner EJ; Kundu S; Bertke JA; Cundari TR; Warren TH A Dinitrogen Dicopper(I) Complex via a Mixed-Valence Dicopper Hydride. Angew. Chem., Int. Ed. 2016, 55, 9927–9931.

(297). Murray LJ; Weare WW; Shearer J; Mitchell AD; Abboud KA Isolation of a (Dinitrogen)Tricopper(I) Complex. J. Am. Chem. Soc. 2014, 136, 13502–13505. [PubMed: 25238198]

(298). Légaré MA; Rang M; Bélanger-Chabot G; Schweizer JI; Krummenacher I; Bertermann R; Arrowsmith M; Holthausen MC; Braunschweig H The Reductive Coupling of Dinitrogen. Science 2019, 363, 1329–1332. [PubMed: 30898929]

(299). Légaré MA; Bélanger-Chabot G; Dewhurst RD; Welz E; Krummenacher I; Engels B; Braunschweig H Nitrogen Fixation and Reduction at Boron. Science 2018, 359, 896–900. [PubMed: 29472479]

(300). Haber F Über Die Synthetische Gewinnung Des Ammoniaks. Zeitschrift für Angew. Chemie 1914, 27, 473–477.

(301). Evans WJ; Ulibarri TA; Ziller JW Isolation and X-Ray Crystal Structure of the First Dinitrogen Complex of an f-Element Metal, [(C5Me5)2Sm]2N2. J. Am. Chem. Soc. 1988, 110, 6877–6879.

(302). Fieser ME; Woen DH; Corbey JF; Mueller TJ; Ziller JW; Evans WJ Raman Spectroscopy of the N-N Bond in Rare Earth Dinitrogen Complexes. Dalton Trans. 2016, 45, 14634–14644. [PubMed: 26940691]

(303). Evans WJ; Allen NT; Ziller JW Facile Dinitrogen Reduction via Organometallic Tm(II) Chemistry. J. Am. Chem. Soc. 2001, 123, 7927–7928 [PubMed: 11493075]

(304). Evans WJ; Allen NT; Ziller JW Expanding Divalent Organolanthanide Chemistry: The First Organothulium(II) Complex and the in Situ Organodysprosium(II) Reduction of Dinitrogen. Angew. Chem., Int. Ed. 2002, 41, 359–361.

(305). Demir S; Lorenz SE; Fang M; Furche F; Meyer G; Ziller JW; Evans WJ Synthesis, Structure, and Density Functional Theory Analysis of a Scandium Dinitrogen Complex, [(C5Me4H)2Sc]2μ-η2:η2-N2). J. Am. Chem. Soc. 2010, 132, 11151–11158. [PubMed: 20698681]

(306). Evans WJ; Lee DS; Johnston MA; Ziller JW The Elusive (C5Me4H)3Lu: Its Synthesis and LnZ3/K/N2 Reactivity. Organometallics 2005, 24, 6393–6397.

(307). Evans WJ; Rego DB; Ziller JW Synthesis, Structure, and ^{15}N NMR Studies of Paramagnetic Lanthanide Complexes Obtained by Reduction of Dinitrogen. Inorg. Chem. 2006, 45, 10790–10798. [PubMed: 17173438]

(308). Demir S; Gonzalez MI; Darago LE; Evans WJ; Long JR Giant Coercivity and High Magnetic Blocking Temperatures for N23– Radical-Bridged Dilanthanide Complexes upon Ligand Dissociation. Nat. Commun. 2017, 8, 2144. [PubMed: 29247236]

(309). Lorenz SE; Schmiege BM; Lee DS; Ziller JW; Evans WJ Synthesis and Reactivity of Bis(Tetramethylcyclopentadienyl) Yttrium Metallocenes Including the Reduction of Me3SiN3 to [(Me3Si)2N] with [(C5Me4H)2Y(THF)]2(μ-η2:η2-N2). Inorg. Chem. 2010, 49, 6655–6663. [PubMed: 20545319]

(310). Evans WJ; Lee DS; Lie C; Ziller JW Expanding the LnZ$_3$/Alkali-Metal Reduction System to Organometallic and Heteroleptic Precursors: Formation of Dinitrogen Derivatives of Lanthanum. Angew. Chem., Int. Ed. 2004, 43, 5517–5519.

(311). Jaroschik F; Momin A; Nief F; Le Goff XF; Deacon GB; Junk PC Dinitrogen Reduction and C-H Activation by the Divalent Organoneodymium Complex [(C5H2tBu3)2Nd(μ-I)K([18]Crown-6)]. Angew. Chem., Int. Ed. 2009, 48, 1117–1121.

(312). Dubé T; Conoci S; Gambarotta S; Yap GPA; Vasapollo G Tetrametallic Reduction of Dinitrogen: Formation of a Tetranuclear Samarium Dinitrogen Complex. Angew. Chem., Int. Ed. 1999, 38, 3657–3659.

(313). Guillemot G; Castellano B; Prangé T; Solari E; Floriani C Use of Calix[4]Arenes in the Redox Chemistry of Lanthanides: The Reduction of Dinitrogen by a Calix[4]Arene-Samarium Complex. Inorg. Chem. 2007, 46, 5152–5154. [PubMed: 17542578]

(314). Evans WJ; Lee DS; Ziller JW Reduction of Dinitrogen to Planar Bimetallic M2(μ-η2:η2-N2) Complexes of Y, Ho, Tm, and Lu Using the K/Ln[N(SiMe3)2]3 Reduction System. J. Am. Chem. Soc. 2004, 126, 454–455. [PubMed: 14719928]

(315). Evans WJ; Lee DS; Rego DB; Perotti JM; Kozimor SA; Moore EK; Ziller JW Expanding Dinitrogen Reduction Chemistry to Trivalent Lanthanides via the LnZ3/Alkali Metal Reduction System: Evaluation of the Generality of Forming Ln2(μ-η2:η2-N2) Complexes via LnZ$_3$/K. J. Am. Chem. Soc. 2004, 126, 14574–14582. [PubMed: 15521778]

(316). Evans WJ; Fang M; Zucchi GL; Furche F; Ziller JW; Hoekstra RM; Zink JI Isolation of Dysprosium and Yttrium Complexes of a Three-Electron Reduction Product in the Activation of Dinitrogen, the (N2)3- Radical. J. Am. Chem. Soc. 2009, 131, 11195–11202. [PubMed: 19610635]

(317). Rinehart JD; Fang M; Evans WJ; Long JR Strong Exchange and Magnetic Blocking in N23-- Radical-Bridged Lanthanide Complexes. Nat. Chem. 2011, 3, 538–542. [PubMed: 21697874]

(318). Fang M; Bates JE; Lorenz SE; Lee DS; Rego DB; Ziller JW; Furche F; Evans WJ (N2)3- Radical Chemistry via Trivalent Lanthanide Salt/Alkali Metal Reduction of Dinitrogen: New Syntheses and Examples of (N2)2- and (N2)3- Complexes and Density Functional Theory Comparisons of Closed Shell Sc3+, Y 3+, and Lu3+ versus 4f9 Dy3$^+$. Inorg. Chem. 2011, 50, 1459–1469. [PubMed: 21204570]

(319). Rinehart JD; Fang M; Evans WJ; Long JR A N23- Radical-Bridged Terbium Complex Exhibiting Magnetic Hysteresis at 14 K. J. Am. Chem. Soc. 2011, 133, 14236–14239. [PubMed: 21838285]

(320). Allen FH; Kennard O; Watson DG; Brammer L; Orpen AG; Taylor R Tables of Bond Lengths Determined by X-Ray and Neutron Diffraction. Part 1. Bond Lengths in Organic Compounds. J. Chem. Soc. Perkin Trans. 2 1987, S1–S19.

(321). Woen DH; Chen GP; Ziller JW; Boyle TJ; Furche F; Evans WJ End-On Bridging Dinitrogen Complex of Scandium. J. Am. Chem. Soc. 2017, 139, 14861–14864. [PubMed: 28957628]

(322). Roussel P; Errington W; Kaltsoyannis N; Scott P Back Bonding without σ-Bonding: A Unique π-Complex of Dinitrogen with Uranium. J. Organomet. Chem. 2001, 635, 69–74.

(323). Cloke FGN; Hitchcock PB Reversible Binding and Reduction of Dinitrogen by a Uranium(III) Pentalene Complex. J. Am. Chem. Soc. 2002, 124, 9352–9353. [PubMed: 12167012]

(324). Mansell SM; Kaltsoyannis N; Arnold PL Small Molecule Activation by Uranium Tris(Aryloxides): Experimental and Computational Studies of Binding of N2, Coupling of CO, and Deoxygenation Insertion of CO_2 under Ambient Conditions. J. Am. Chem. Soc. 2011, 133, 9036–9051. [PubMed: 21591662]

(325). Mansell SM; Farnaby JH; Germeroth AI; Arnold PL Thermally Stable Uranium Dinitrogen Complex with Siloxide Supporting Ligands. Organometallics 2013, 32, 4214–4222.

(326). Falcone M; Chatelain L; Scopelliti R; Živkovi I; Mazzanti M Nitrogen Reduction and Functionalization by a Multimetallic Uranium Nitride Complex. Nature 2017, 547, 332–335. [PubMed: 28726827]

(327). a)Liu T; Gau MR; Tomson NC Mimicking the Constrained Geometry of a Nitrogen-Fixation Intermediate. J. Am. Chem. Soc. 2020 DOI: 10.1021/jacs.0c01861,b)Sorsche D; Miehlich ME; Searles K; Gouget G; Zolnhofer EM; Fortier S; Chen C-H; Gau M; Carroll PJ; Murray C; Caulton K-NG; Khusniyarov MM; Meyer K; Mindiola DJ Unusual Dinitrogen Binding and Electron Storage in Dinuclear Iron Complexes. J. Am. Chem. Soc. 2020 DOI: 10.1021/jacs.0c01488.

(328). Shook RL; Borovik AS Role of the Secondary Coordination Sphere in Metal-Mediated Dioxygen Activation. Inorg. Chem. 2010, 49, 3646–3660. [PubMed: 20380466]

(329). MacBeth CE; Golombek AP; Young J; Yang C; Kuczera K; Hendrich MP; Borovik AS O2 Activation by Nonheme Iron Complexes: A Monomeric Fe(III)-Oxo Complex Derived from O_2. Science 2000, 289, 938–941. [PubMed: 10937994]

(330). Dubois DL Development of Molecular Electrocatalysts for Energy Storage. Inorg. Chem. 2014, 53, 3935–3960. [PubMed: 24555579]

(331). Rakowski Dubois M; Dubois DL The Roles of the First and Second Coordination Spheres in the Design of Molecular Catalysts for H_2 Production and Oxidation. Chem. Soc. Rev. 2009, 38, 62–72. [PubMed: 19088965]

(332). Costentin C; Drouet S; Robert M; Savéant JM A Local Proton Source Enhances CO_2 Electroreduction to CO by a Molecular Fe Catalyst. Science 2012, 338, 90–94. [PubMed: 23042890]

(333). Bhattacharya P; Prokopchuk DE; Mock MT Exploring the Role of Pendant Amines in Transition Metal Complexes for the Reduction of N_2 to Hydrazine and Ammonia. Coord. Chem. Rev. 2017, 334, 67–83

(334). Sickerman NS; Peterson SM; Ziller JW; Borovik AS Synthesis, Structure and Reactivity of $Fe^{II}/^{III}$-NH_3 Complexes Bearing a Tripodal Sulfonamido Ligand. Chem. Commun. 2014, 50, 2515–2517.

(335). Creutz SE; Peters JC Exploring Secondary-Sphere Interactions in Fe-NxHy Complexes Relevant to N2 Fixation. Chem. Sci. 2017, 8, 2321–2328. [PubMed: 28451336]

(336). Rosenzweig AC; Frederick CA; Lippard SJ; Nordlund P Crystal Structure of a Bacterial Non-Haem Iron Hydroxylase That Catalyses the Biological Oxidation of Methane. Nature 1993, 366, 537–543. [PubMed: 8255292]

(337). Nicolet Y; Piras C; Legrand P; Hatchikian CE; Fontecilla-Camps JC Desulfovibrio Desulfuricans Iron Hydrogenase: The Structure Shows Unusual Coordination to an Active Site Fe Binuclear Center. Structure 1999, 7, 13–23. [PubMed: 10368269]

(338). Dobbek H; Svetlitchnyi V; Gremer L; Huber R; Meyer O Crystal Structure of a Carbon Monoxide Dehydrogenase Reveals a [Ni-4Fe-5S] Cluster. Science 2001, 293, 1281–1285. [PubMed: 11509720]

(339). Logan DT; Su XD; Åberg A; Regnström K; Hajdu J; Eklund H; Nordlund P Crystal Structure of Reduced Protein R2 of Ribonucleotide Reductase: The Structural Basis for Oxygen Activation at a Dinuclear Iron Site. Structure 1996, 4, 1053–1064. [PubMed: 8805591]
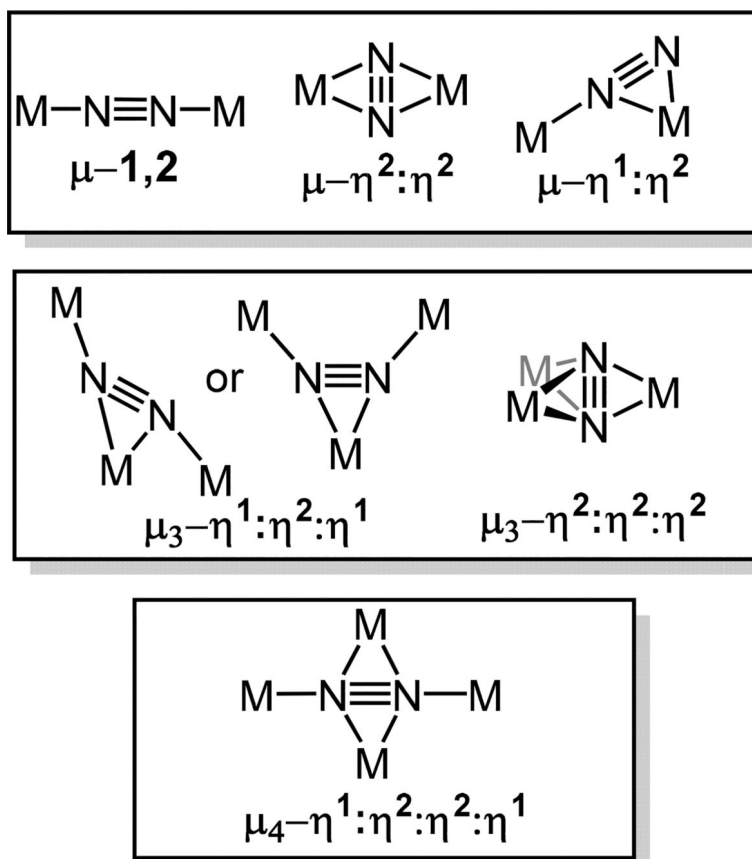
Figure 1.
Binding modes of N_2. The dinitrogen ligand is depicted as N≡N for simplicity as the extent of activation varies depending on metal ion type and oxidation state. Associated s-block elements (e.g., Li+, K+) are not included in this treatment.
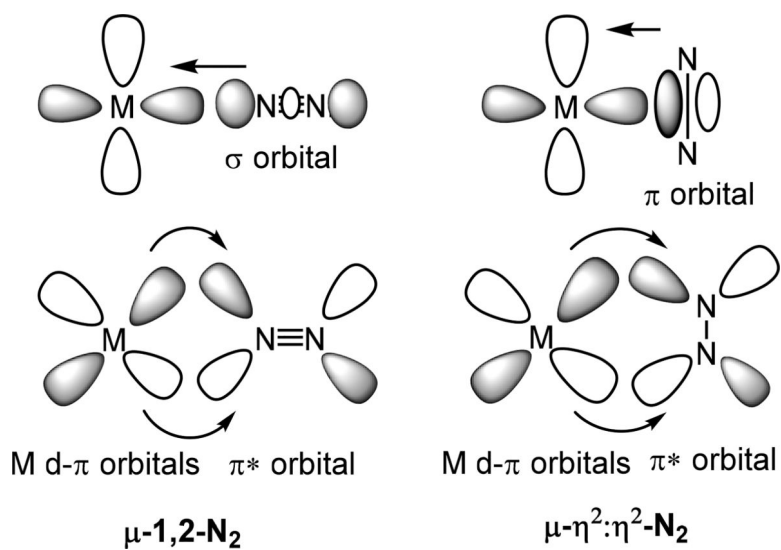
Figure 2.
Bonding interactions for end-on/end-on and side-on/side-on dinitrogen complexes wherein the interactions of only one metal center with dinitrogen are depicted.
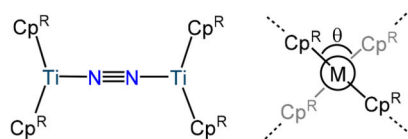
θ: Angle between the planes defined by the centroid-M-centroid of the metalocene unit

Name	CpR	d(N–N) (Å)	θ
1-Cp*		1.165	ave. ~90°
1-Cp'		1.170(4)	0°
1-CpMe4,Xyl	R = 3,5-Me$_2$-C$_6$H$_3$	1.1574(11)	85.9°
1-CpMe12iPr4 / 1-CpMe12tBu4	R = ^{i}Pr or ^{t}Bu	1.168(3)	0°
1-CpTMS13	SiMe$_3$ / SiMe$_3$	1.164(5)	9.6°
2-(p-tol)$_2$		1.216(3)	3.2°
2-(Ad)	CR$_2$ = C(p-tol)$_2$; CR$_2$ = C(Ad)	1.216(5)	19.1°

Figure 3.
Type A complexes: the (μ–1,2-dinitrogen)bis(titanocene) compounds.

1-Cp^{Me13}
d(N−N): 1.320(3) Å

1-Cp
d(N−N): 1.301(12) Å
ν(N−N): 1282 cm^{-1}
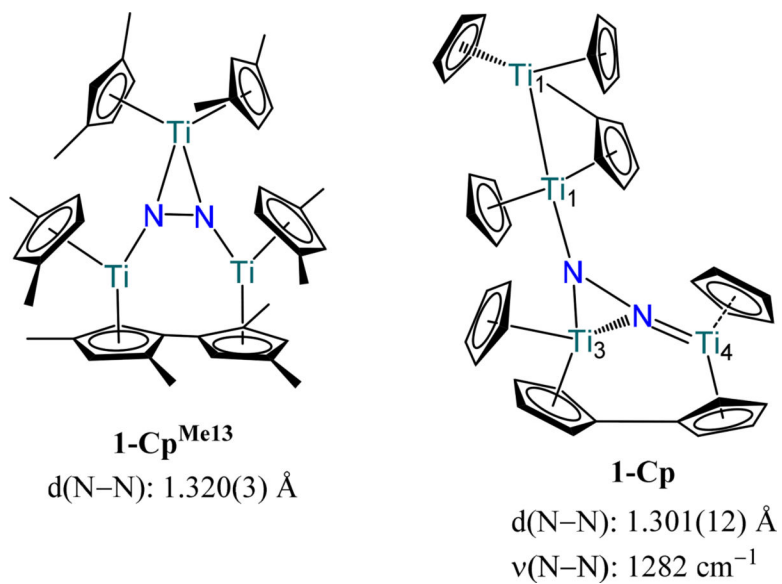
Figure 4.
Titanocene complexes (1-Cp^{Me13} and 1-Cp) featuring a μ_3-dinitrogen coordination mode.
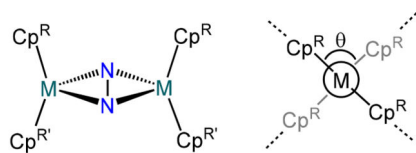
θ: Angle between the planes defined by the centroid-M-centroid of the metalocene unit

Name	CpR, CpR'	d(N−N) (Å) ν_{N-N} (cm^{-1})	θ
1-Cp^{Me124} M = Ti	CpR = CpR' =	1.216(3)	12.2°
1-Cp^{Me1iPr3} M = Ti 1-Cp^{iPr13} M = Ti	CpR = CpR' =	1.226(5) 1742 1.216(5) 1747	0° 0°
3-Cp', M = Zr	CpR = CpR' =	1.377(3)	65.3°
3-Cp*/Cp^{Me12Ph4} M = Zr	CpR = CpR' =	1.3787(19)	72.9°
3-Cp^{TMS13} M = Zr	CpR = CpR' =	1.47(3)	0°
4-Cp' M = Hf	CpR = CpR' =	1.423(11)	65.3°
4-Cp^{Me124} M = Hf	CpR = CpR' =	1.457(5) 818	49.3°

Figure 5.
Type B complexes: the (μ-(η^2:η^2)-dinitrogen)bis(metallocene) compounds
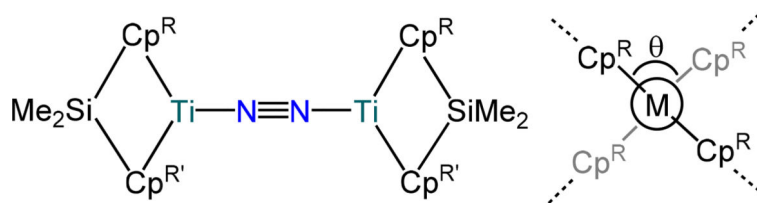
θ: Angle between the planes defined by the centroid-M-centroid of the metalocene unit

Name	Cp^R, Cp$^{R'}$	d(N–N) (Å)	θ
5-1	Me$_3$Si / ^{t}Bu	1.174(3) Å	43.2°
5-2	Cp^R = (pentamethyl); Cp$^{R'}$ = (^{t}Bu)	1.165(3) Å	36.7°

Figure 6.

(μ–1,2-dinitrogen)bis(ansa-titanocene) compounds (5).
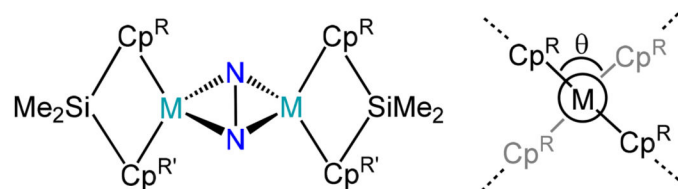
θ: Angle between the planes defined by the centroid-M-centroid of the metalocene unit

Name	CpR, CpR'	d(N−N) (Å)	θ
6-1, M = Zr	(Me₃Si / ᵗBu substituted Cp)	1.241(3) Å	46.4°
6-2, M = Zr	CpR = (permethyl Cp); CpR' = (ᵗBu substituted Cp)	1.406(4) Å	54.1°
7, M = Hf		1.457(5) Å	54°

Figure 7.
(μ-(η^2:η^2)-dinitrogen)bis(*ansa*-metallocene) compounds (6 and 7).

Name	CpR	d(N−N) (Å)	ν_{N-N} (cm^{-1})	θ
8-Cp*, M = Ti			1711	
9-Cp*, M = Zr		1.182(5)	1578	
8-Cp^{Me4Et} M = Ti		1.150(2)	1719	78.6°
8-Cp^{Me4,Ph} M = Ti			1603	
8-Cp^{Me4,xyl} M = Ti			1603	

Ar = 3,5-Me$_2$-C$_6$H$_3$

Figure 8.
Type C complexes: the (μ–1,2-dinitrogen)bis(metallocene) compounds.
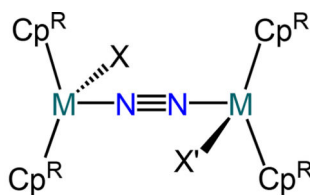
Name	Cp^R	d(N–N) (Å)	ν_{N-N} (cm^{-1})
8-Cp,X; M = Ti, X=X'=PMe$_3$		1.191(8)	1711
8-Cp,X; M = Ti, X =X'=p-CH$_3$C$_6$H$_4$		1.162(12)	
9-Cp,X, M = Zr X=X'= CH(SiMe$_3$)$_2$		1.175(4)	
Na[9-Cp,X]		1.182(5)	1578
11-X/X', M = Hf X= Me, X' = I		1.181(9)	
11-X/X', M = Hf X = X' = OTf$_2$		1.189(8)	

Figure 9.
Additional type C complexes: (μ–1,2-dinitrogen)bis(metallocene) compounds containing X-type donor ligands.
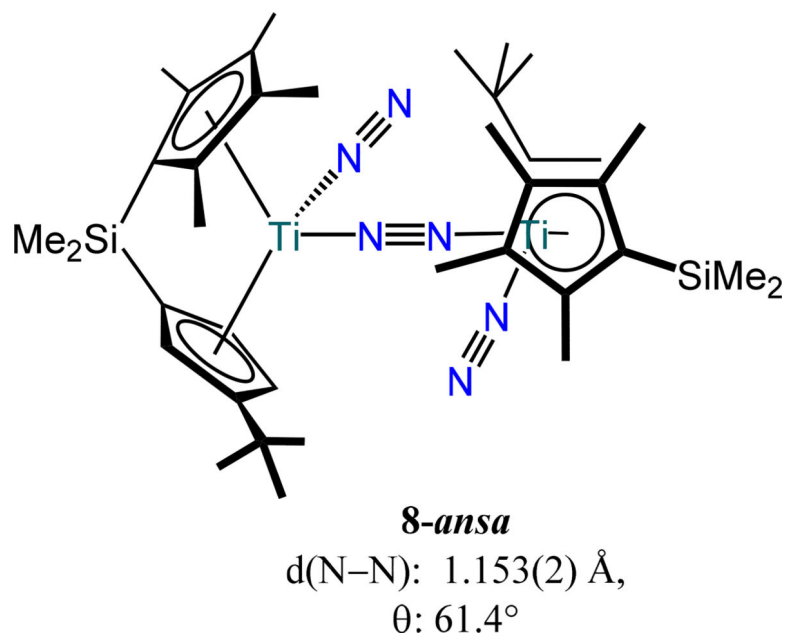
Figure 10.
An *ansa*-titanocene type C complex (8-*ansa*).

12
$d(\text{N–N})$ (Å): 1.39(2) Å
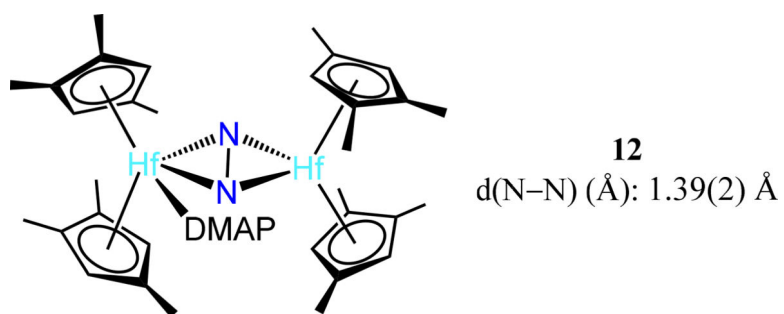
Figure 11.
A μ-η^2:η^2-N_2-bis(hafnocene) DMAP-adduct.

16
d(N–N): 1.270(2) Å
d(Ti–N): 1.775 Å
Ti-N-N angles of 166.71°
and 166.97°
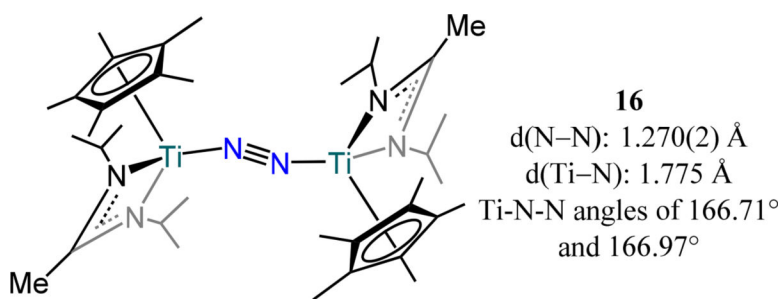
Figure 12.
Bis[Cp*(amidinato)titanium]-dinitrogen complex, 16.
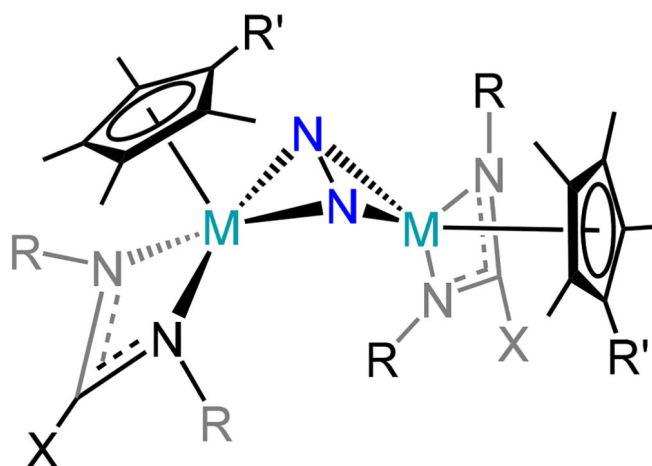
Name, M	X, R, R'	d(N−N) (Å)
17-Zr	NMe_2, ^{i}Pr, Me	1.518
17-A, Hf	NMe_2, ^{i}Pr, Me	1.581(4)
17-B, Hf	NMe_2, ^{i}Pr, H	1.600(6)
17-C, Hf	Me, ^{i}Pr, Me	1.611(4)
17-D, Hf	Me, ^{i}Pr, H	1.630(4)
17-E, Hf	Me, Et, Me	1.635(5)

Figure 13.
Bis[Cp*(amidinato or guanidinato)-zirconium or -hafnium)-N_2 compounds (17-Zr and 17-A-E) featuring side-on/side-on N_2 coordination mode.

Ar: 2,6-diisopropylphenyl
18
d(N−N): 1.273(6) Å
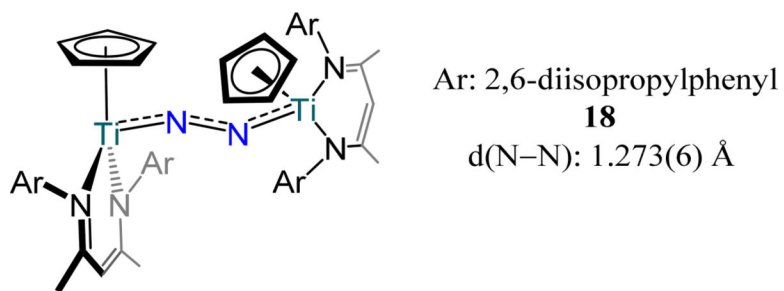
Figure 14.
Piano stool bis[(Cp)(β-diketiminato)tititanium](μ–1,2-N$_2$) complex, 18.
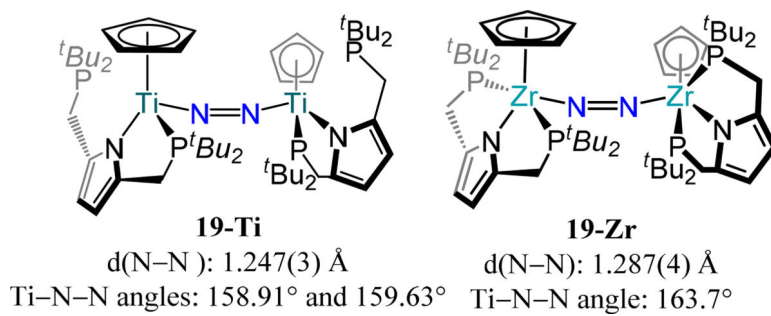
Figure 15.
Three- and four-legged piano stool dinuclear Ti- or Zr- μ–1,2-N_2-bridged complexes, 19-Ti and 19-Zr.

21

d(N−N): 1.255(7) Å
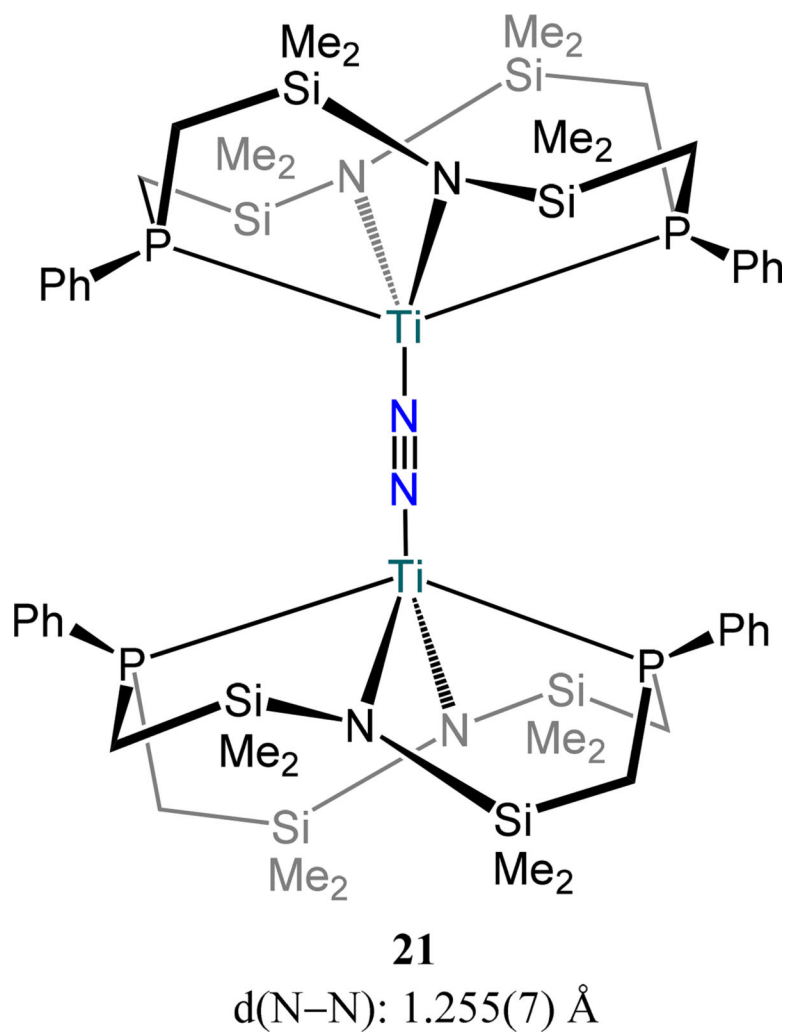
Figure 16.
Titanium-dinitrogen complex 21 supported by a tetranucleating PPh2N$_2$ ligand.
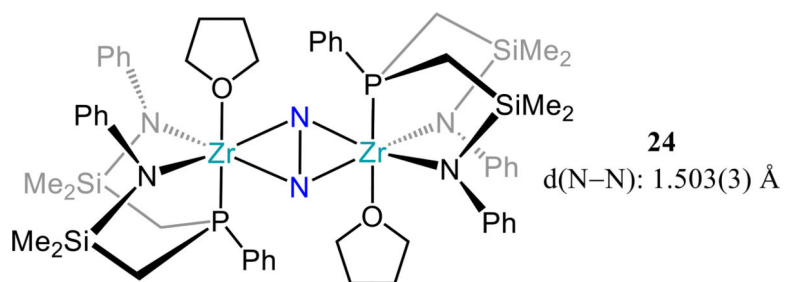
Figure 17.
Side-on/side-on dizirconium-N_2 complex 24 supported by a diamido phosphine ligand
($P^{Ph}N^{Ph}_2$).
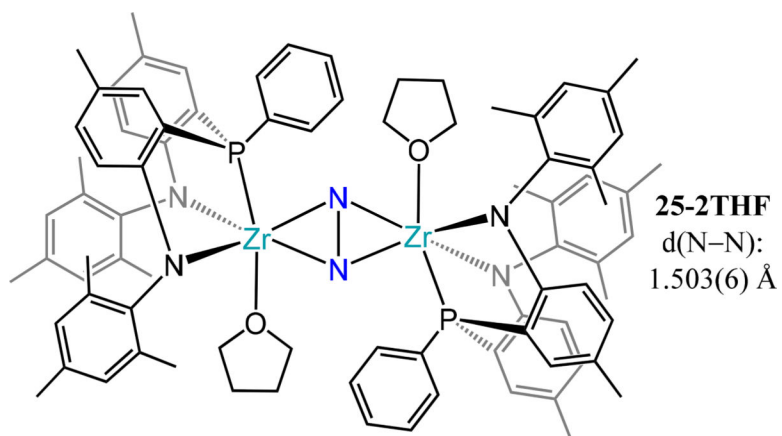
Figure 18.
Side-on/side-on dizirconium-dinitrogen complex 25–2THF employing a diamidophosphine chelate (P^{tol}N$^{Mes}_2$).
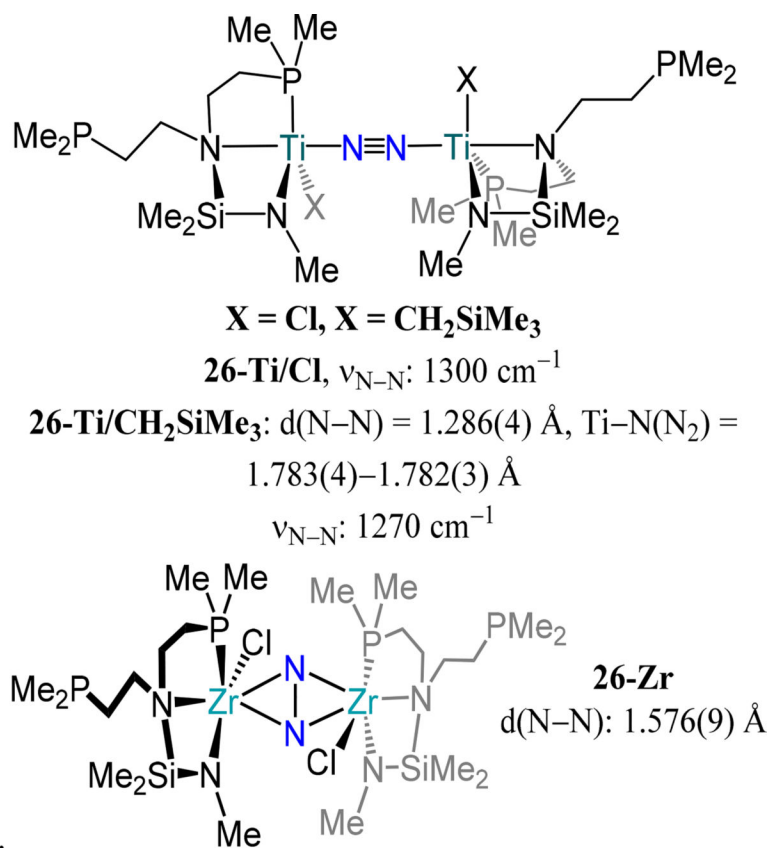
Figure 19.
Complexes 26-Ti/CH$_2$SiMe$_3$ and 26-Zr with end-on/end-on and side-on/side-on dinitrogen modes, respectively.
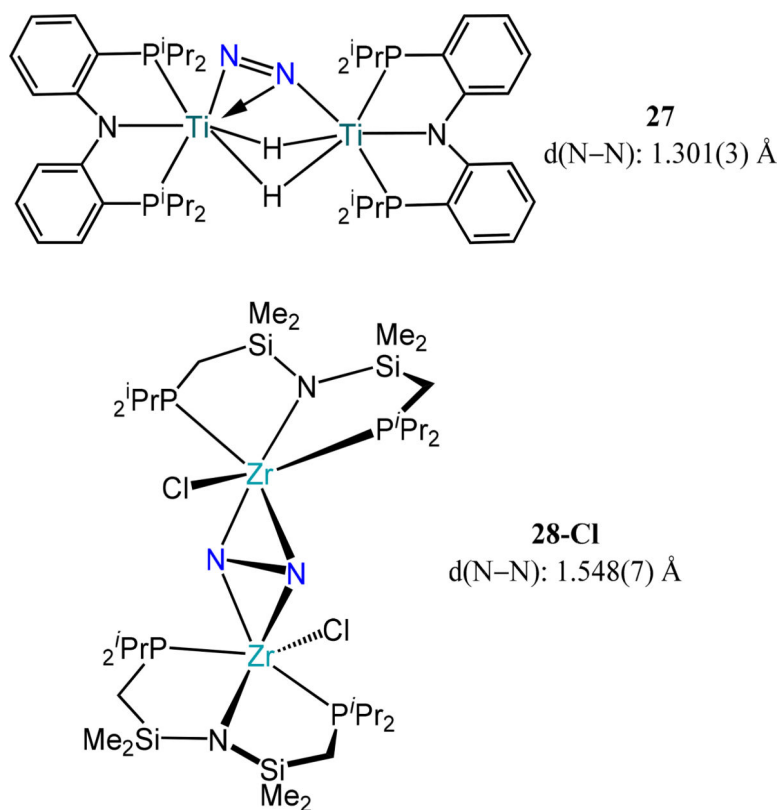
Figure 20.
Dititanium- and dizirconium-dinitrogen compounds (27 and 28-Cl, respectively) supported by amidodiphosphine (PNP) pincer type ligands. Complex 27 exhibits a rare $\mu\text{-}\eta^1\text{:}\eta^2$-dinitrogen mode.

29
d(N−N): 1.264(8) Å
Ti−N(N$_2$): 1.811(4) Å
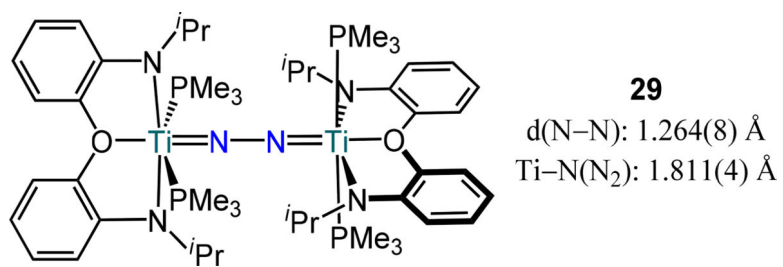
Figure 21.
Complex [(^{iPr}NON)Ti(PMe$_3$)$_2$]$_2$(μ−1,2-N$_2$), 29.
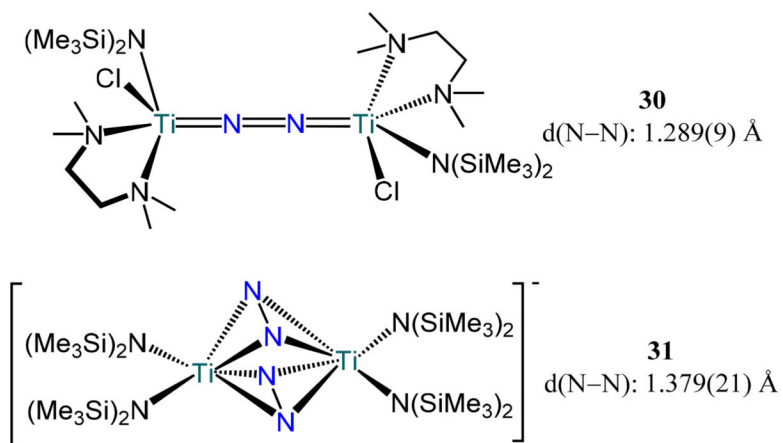
Figure 22.
Compounds [Ti(TMEDA)(N(Me$_3$Si)$_2$)Cl]$_2$(μ–1,2-N$_2$) (30) and [Li(TMEDA)$_2$]
[{(Me$_3$Si)$_2$N]$_2$Ti}$_2$(μ-η^2:η^2-N$_2$)$_2$] (31).

33
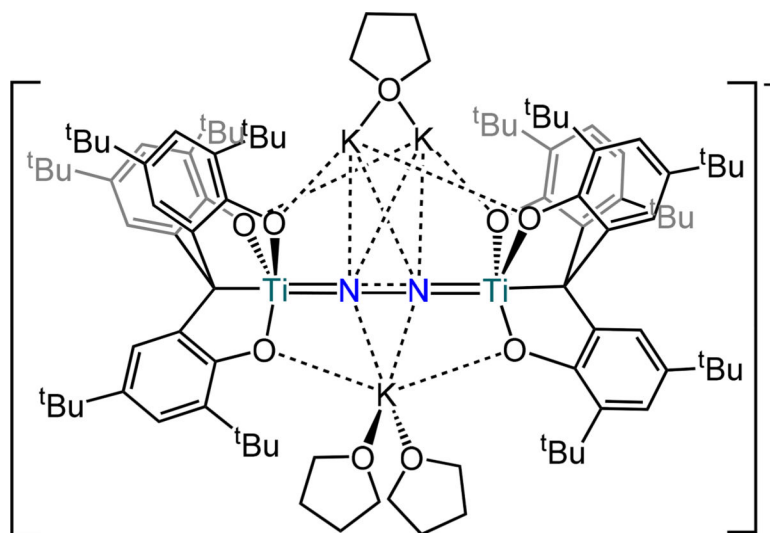
d(N−N): 1.320(5) Å, ν_{N-N}: 1265 cm^{-1}

Figure 23.
Bis(titanatrane)-N$_2$ complex 33, [[K(THF)$_2$][K$_2$(μ-THF)]{[O$_3$C]Ti)$_2$(μ–1,2-N$_2$)}]$^-$.

$[K(THF)]_2\{[Mo_3S_4Ti]_2(\mu\text{-}1,2\text{-}N_2)\}$, **34-K$_2$**
d(N–N): 1.294(7) Å, ν_{N-N}: 1240 cm^{-1}

$K_3(THF)_5\{[Mo_3S_4Ti]_2(\mu\text{-}1,2\text{-}N_2)\}$, **34-K$_3$**
d(N–N): 1.293(5) Å
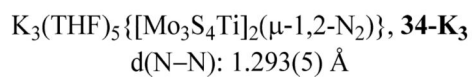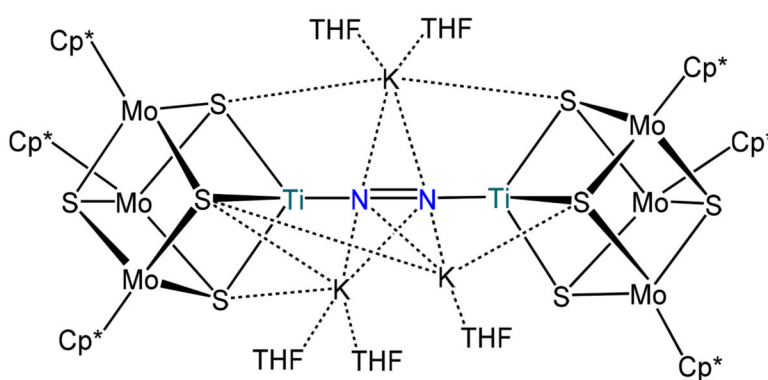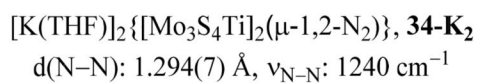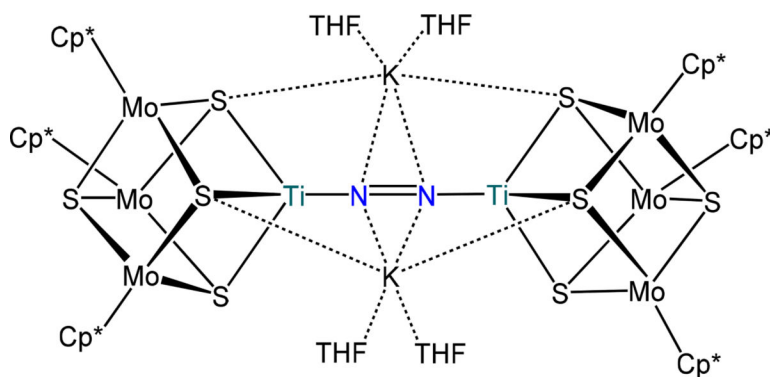
Figure 24.
Subsite-differentiated hetero-cubane Mo$_3$Ti clusters 34-K$_2$ and 34-K$_3$ bridged by a linear N$_2$
donor.
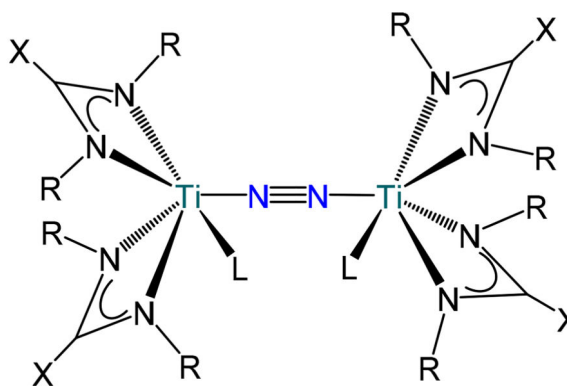
Name	X, R, L	d(N–N) Å
35-Ph/SiMe₃	Ph, SiMe₃, L = none	1.275(6)
35-NMe₂/ⁱPr	NMe₂, ⁱPr, L = none	1.28(1)
35-Ph/SiMe₃/THF	Ph, SiMe₃, L = THF	
35-Ph/SiMe₃/py	Ph, SiMe₃, L = Py	1.264(5)

Figure 25.
[Bis(amidinato or guanidinato)titanium](μ–1,2-N$_2$) complexes, 35-X/R.

36
d(N–N): 1.252(8) Å
Ti–N(N$_2$): 1.832(3) Å
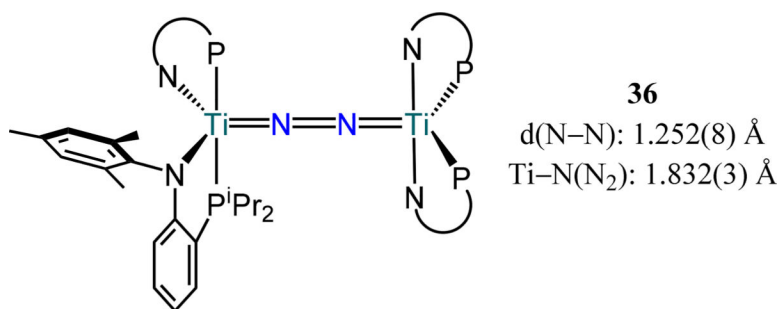
Figure 26.
Complex [(P^{iPr}N^{tol})$_2$Ti]$_2$(μ–1,2-N$_2$), 36.
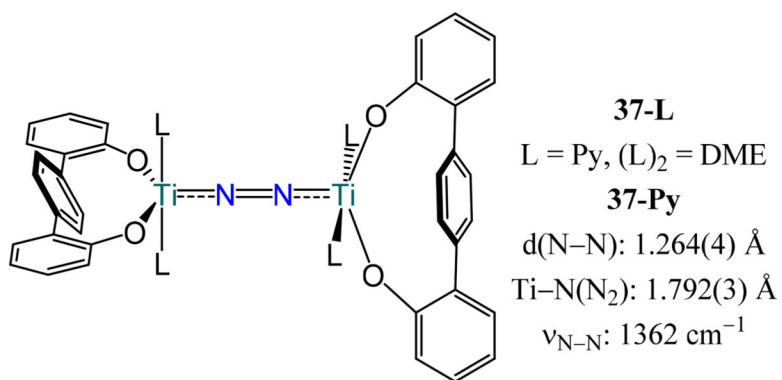
Figure 27.
Compounds [(OO)Ti(L)]$_2$(μ–1,2-N$_2$) bearing bidentate *p*-terphenoxide ligands, 37-L.
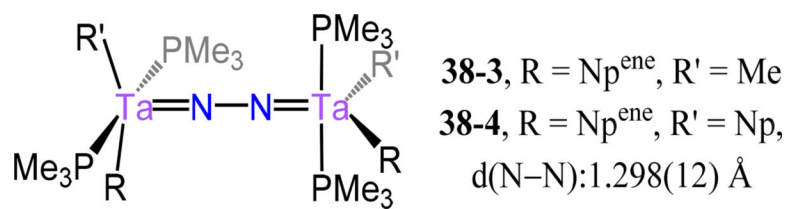
Figure 28.
Organometallic ditantalum-N_2 complexes 38–3 and 38–4.
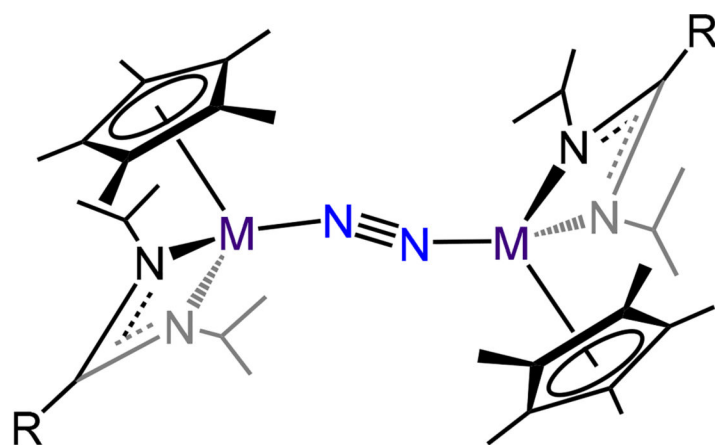
Name	R	d(N−N) Å
39-V/Me	Me	1.225(2)
39-Nb/Me	Me	
39-Nb/Ph	Ph	1.300(3)
39-Ta/Me	Me	1.313(4)
39-Ta/Ph	Ph	1.308(5)
39-Ta/NMe₂	NMe₂	1.306(5)

Figure 29.
Bis[Cp*(amidinato or guanidinato)metal]-dinitrogen compounds 39-M/R where M = V, Nb, and Ta.
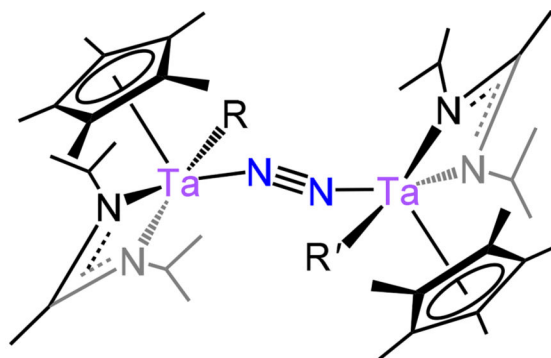
41-R/R′, R = R′ = H, d(N–N): 1.307(6) Å
41-R/R′, R = SiH$_2$Ph, R′ = H, d(N–N): 1.284(4) Å
41-R/R′, R = R′ = SPh, d(N–N): 1.297(3) Å

Figure 30.
Bis[Cp*(amidinato)tantalum](μ–1,2-dinitrogen) compounds (41-R/R′).
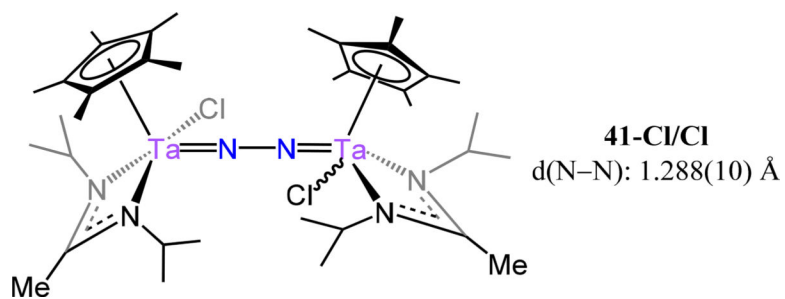
41-Cl/Cl
d(N−N): 1.288(10) Å

Figure 31.
Bis[Cp*(amidinato)tantalum](μ–1,2-N$_2$) compound, 41-Cl/Cl.
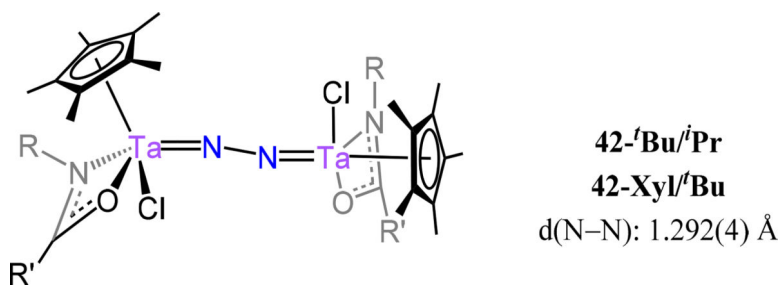
Figure 32.
Bis[Cp*(amidato)tantalum](μ–1,2-dinitrogen) compounds, 42-R/R′.
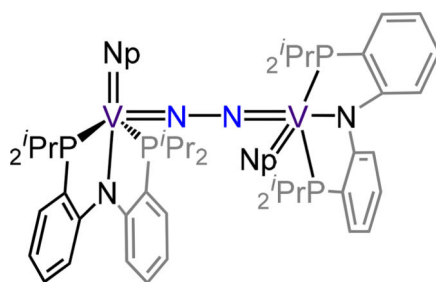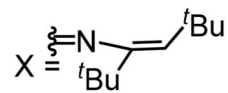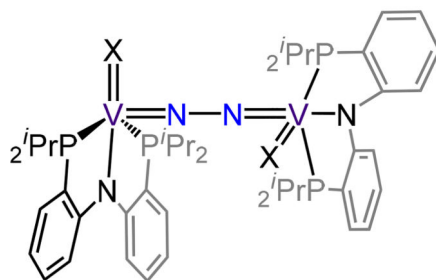
Figure 33.
Compounds 43-V/Np and 43-V/X supported by meridional PNP pincer ligands.
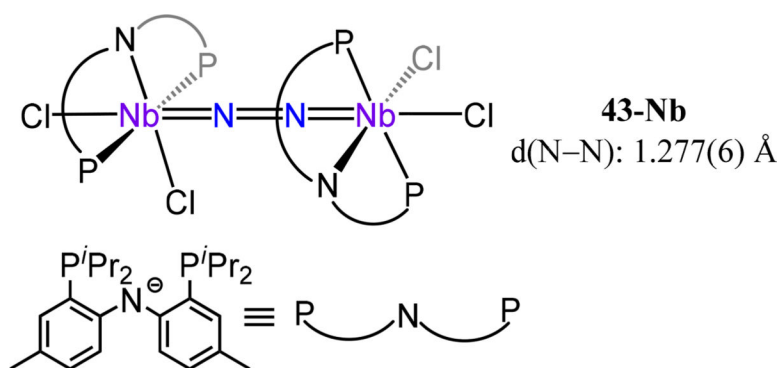
Figure 34.
Diniobium-dinitrogen complex 43-Nb.
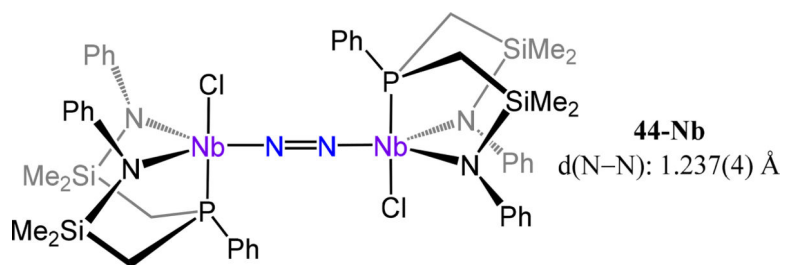
Figure 35.
Complex 44-Nb in which a dianionic diamidophosphine ligand, NPN^{Ph}, adopts a *fac* coordination mode.

45-V/Cy
45-V/ⁱPr d(N–N): 1.27(1) Å
45-Nb/Cy d(N–N): 1.34(1) Å
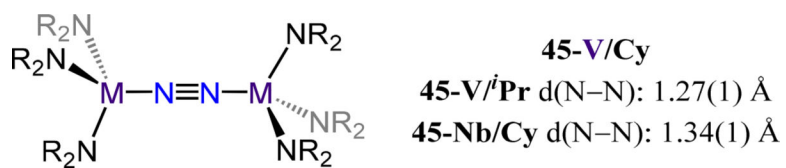
Figure 36.
Bis[tris(dialkylamido)-vanadium or -niobium](μ–1,2-dinitrogen) complexes 45-V/R and 45-Nb/Cy.
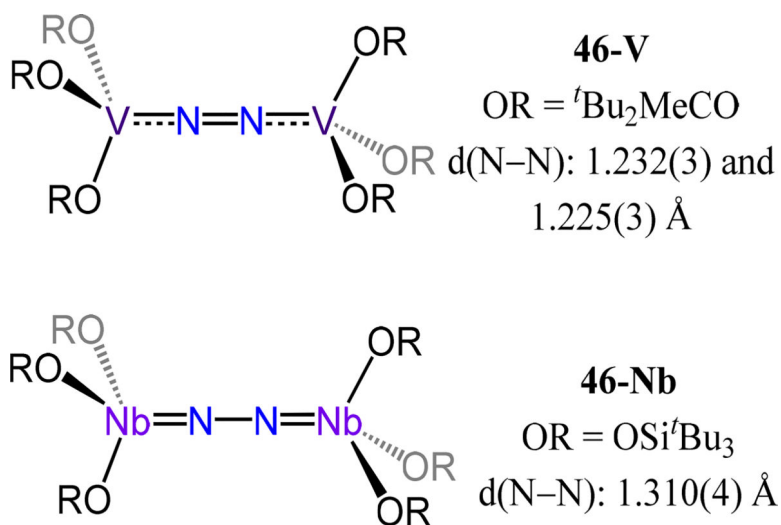
Figure 37.
Bis[tris(alkoxy)vanadium] and bis[tris(siloxy)niobium] dinitrogen complexes 46-M.
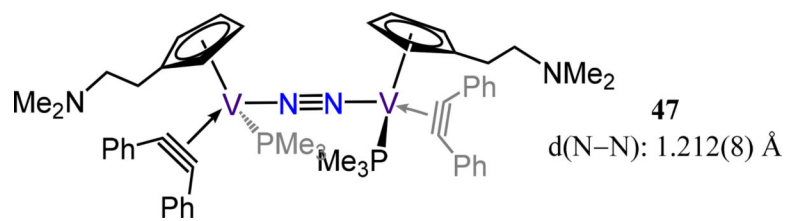
Figure 38.
Piano stool divanadium-dinitrogen complex, 47.
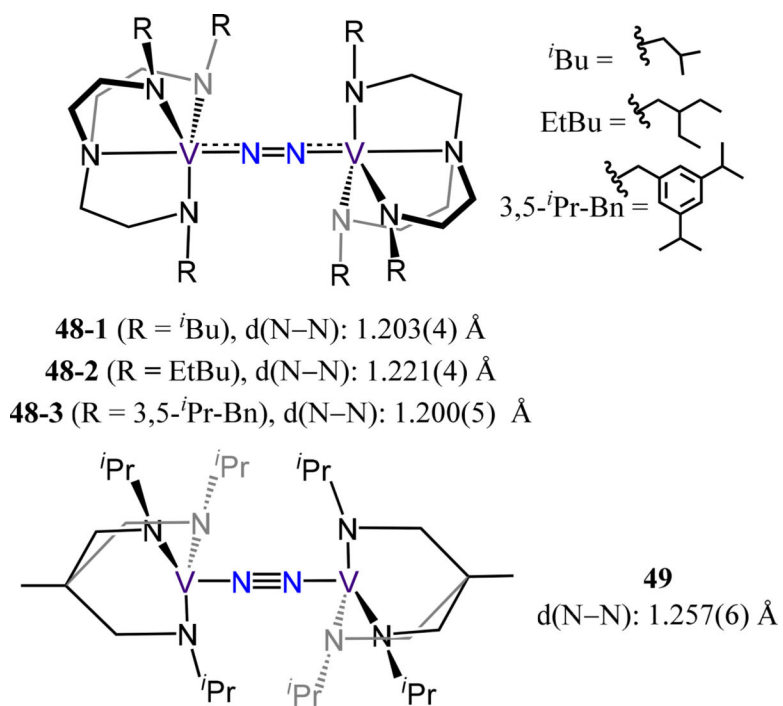
Figure 39.
Dinitrogen-bridged bis(triamidovanadium) complexes 48-X and 49.

51-1 (R = Me)
d(N–N): 1.259(6) Å
51-3 (R = Ph)
d(N–N): 1.242(5) Å
Ar = 2,6-diisopropylphenyl

51-2
Ar = 2,6-diisopropylphenyl
d(N–N) = 1.242(5) Å
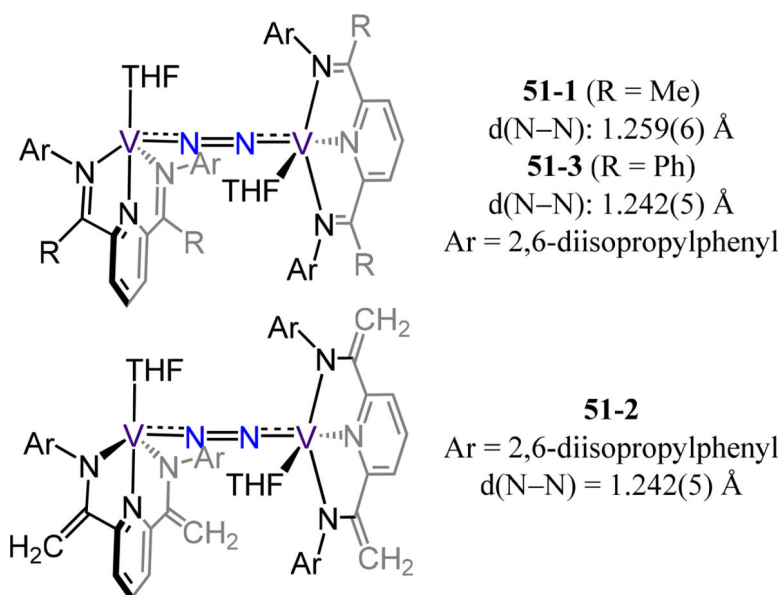
Figure 40.
Dinitrogen-bridged bis[bis(imino)pyridine-vanadium] complexes 51.

53

d(N−N): 1.235(4) Å
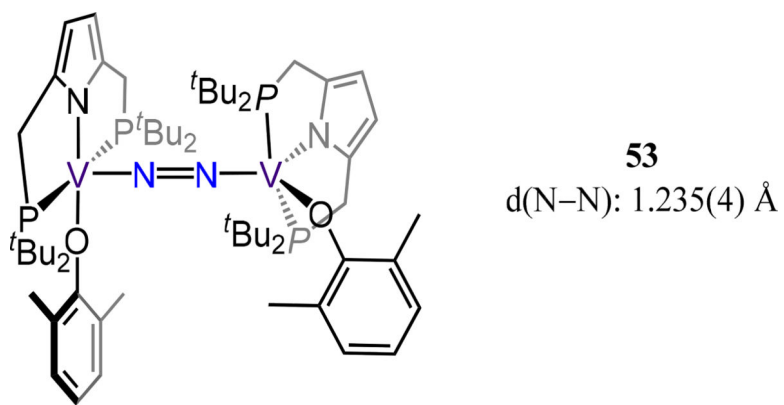
Figure 41.
Divanadium-μ–1,2-dinitrogen complex 53 wherein each V is ligated by a diphosphinopyrrolide pincer ligand and a phenoxide.

54-1 (R = Cy, R' = Me)
54-2 (R = SiMe$_3$, R' = Ph)
54-2 d(N−N) = 1.235(6) Å
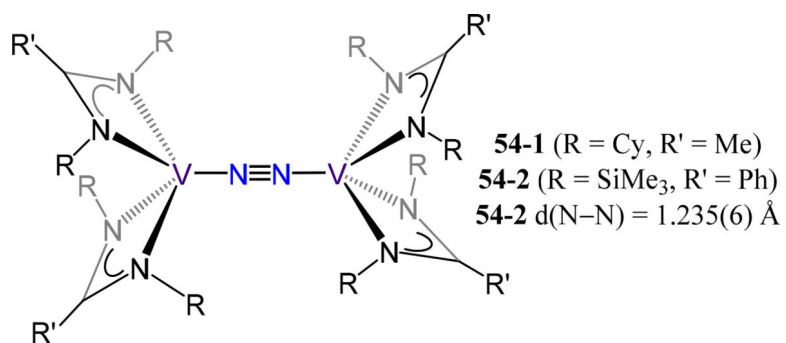
Figure 42.
Bis[bis(amidinato)vanadium](μ−1,2-dinitrogen) 54.

55

Ar = 2,6-diisopropylphenyl

$\nu_{N-N} = 1374$ cm^{-1}
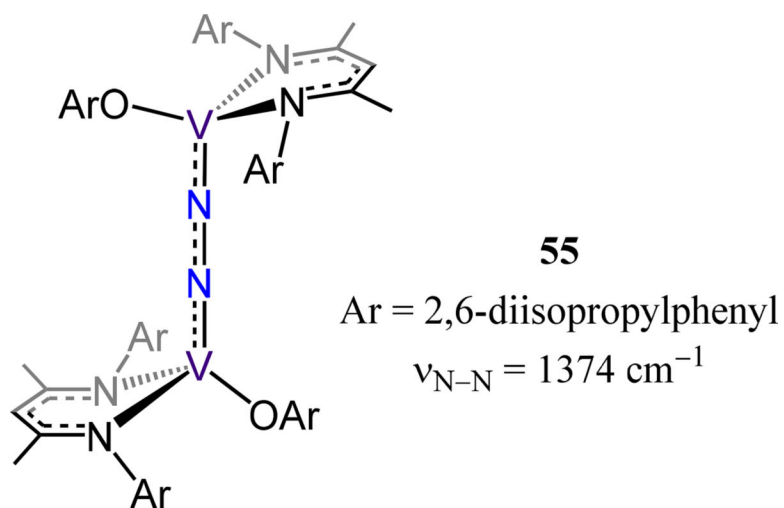
Figure 43.
Bis[(*β*-diketiminato)(phenoxy)vanadium](μ–1,2-N$_2$) compound 55.

56
d(N−N): 1.228(4) Å, V−
N(N$_2$): 1.833(3) Å
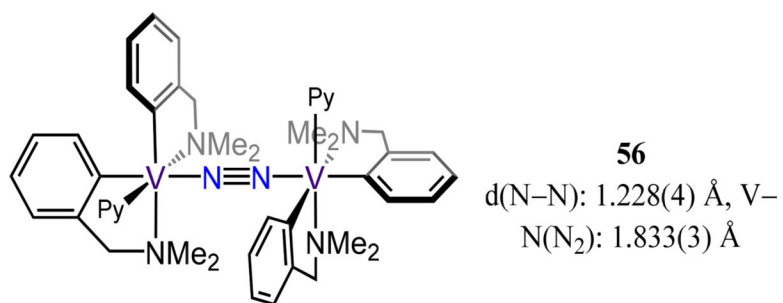
Figure 44.
Divanadium-dinitrogen complex 56.
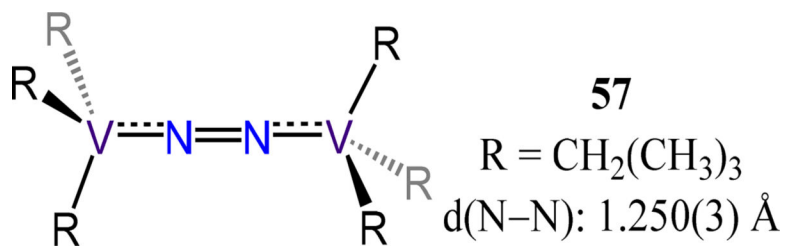
Figure 45.
Bis[tris(neopentyl)vanadium](dinitrogen), 57.

Figure 46.
Diniobium-μ–1,2-N$_2$ complexes 59.
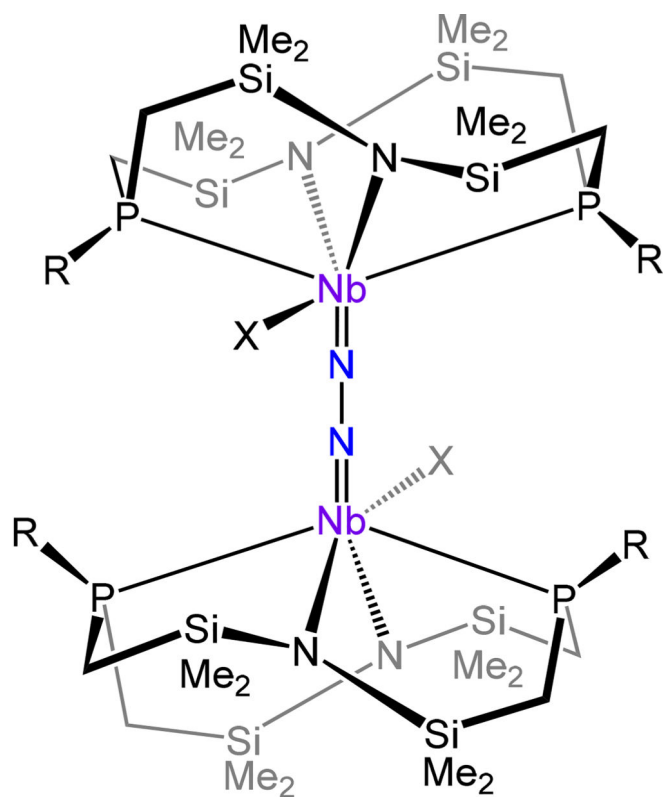
Name	R, X	d(N−N) Å
59-1	R = Ph, X = none	1.272(5)
59-2	R = Ph, X = Me	1.280(7)
59-3	R = Cy, X = Me	1.250(3)
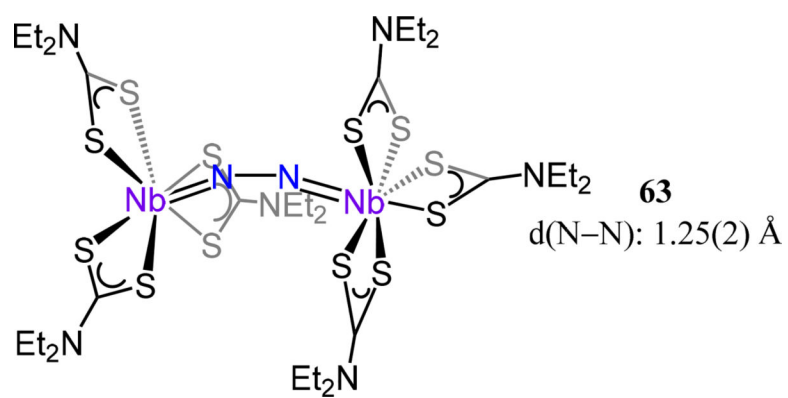
Figure 47.
Bis[tris(dithiocarbamatoniobium)](μ–1,2-dinitrogen) complex 63.
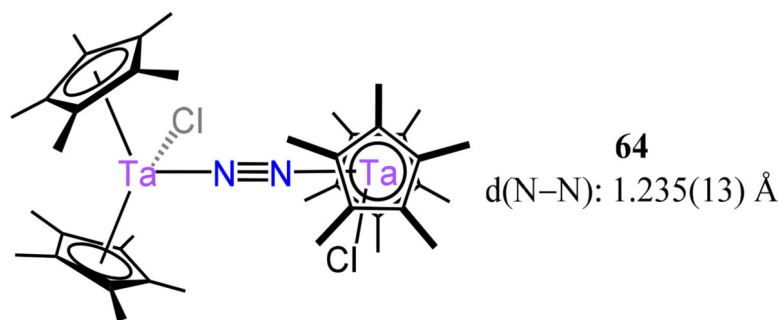
Figure 48.
Bis[chloro-bis(Cp*)-tantalum](μ–1,2-N$_2$) 64.
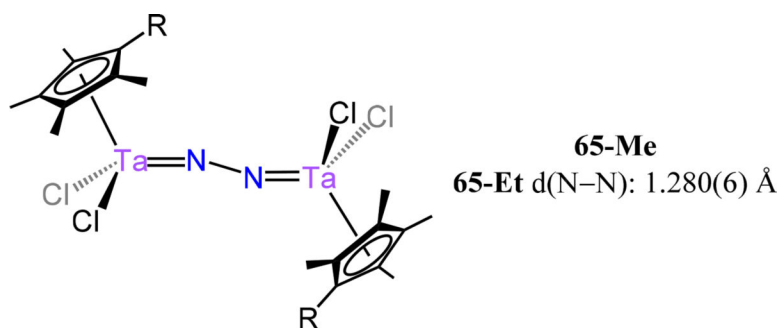
Figure 49.
Half-sandwich ditantalum-dinitrogen complexes 65-Me and 65-Et.
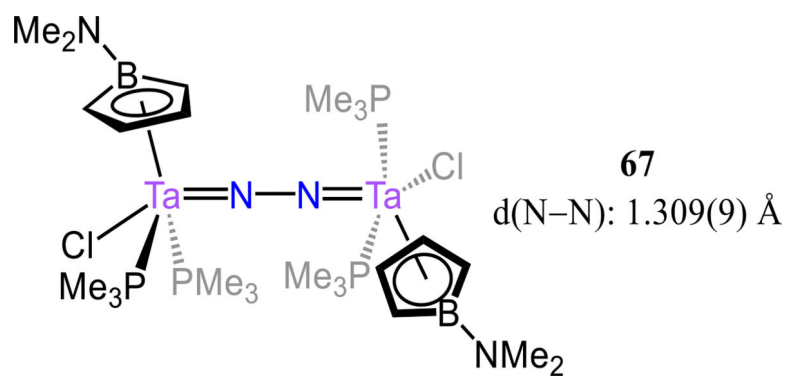
Figure 50.
Ditantalum-dinitrogen with an η^5-borrolide analog of Cp coordinated to each Ta center (67).
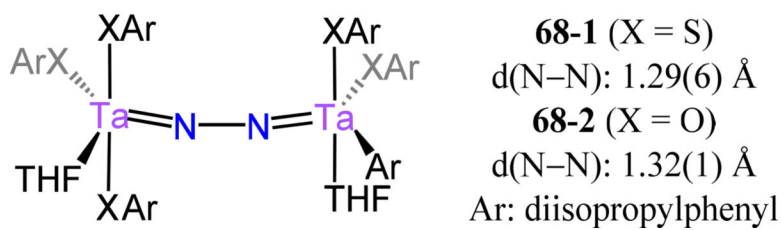
Figure 51.
Ditantalum-μ–1,2-N_2 complexes 68 with thiophenolates or phenolates as ancillary ligands.
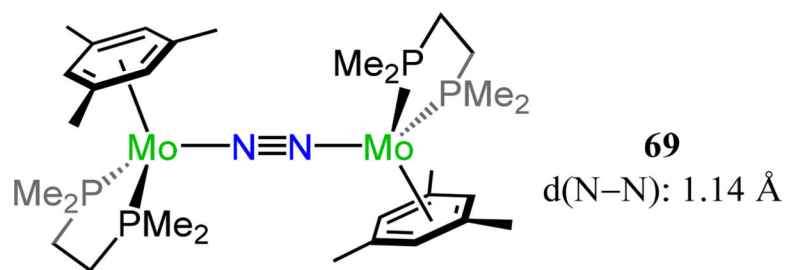
Figure 52.
[Mo(dmpe)(η^6-mesitylene)]$_2$(μ–1,2-N$_2$), 69.
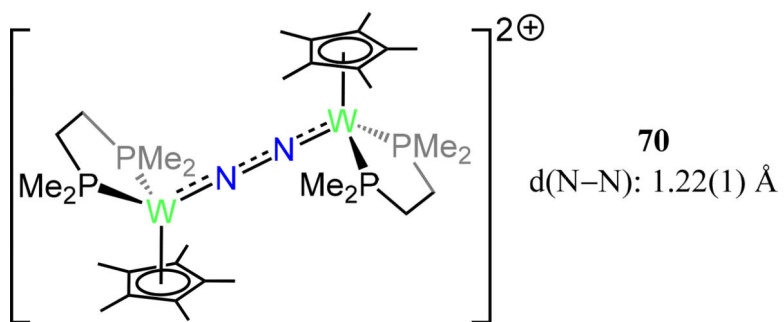
Figure 53.
Dinuclear tungsten end-on/end-on dinitrogen piano stool complex, 70.
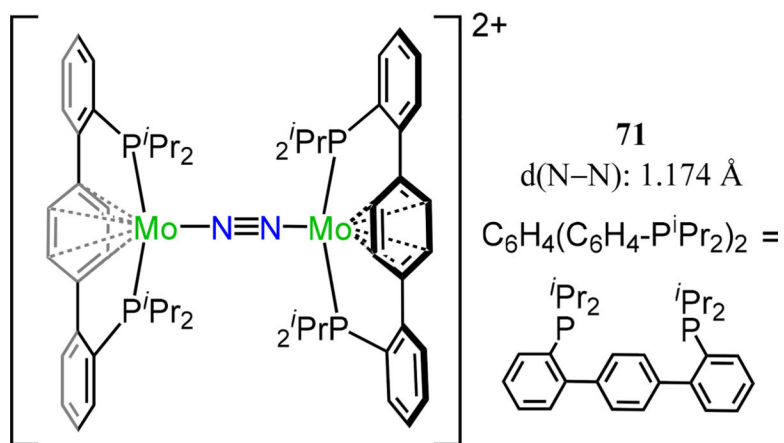
Figure 54.

Bis(diphosphino-(η^6-arene)-molybdenum)(μ–1,2-N_2) complex, 71.

72
d(N−N): 1.182(5) Å
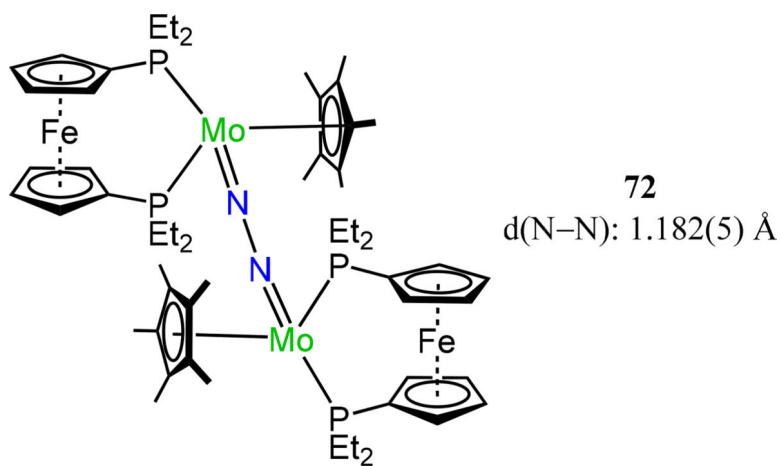
Figure 55.
Dinitrogen adduct of [Cp*(dpef)Mo], 72.
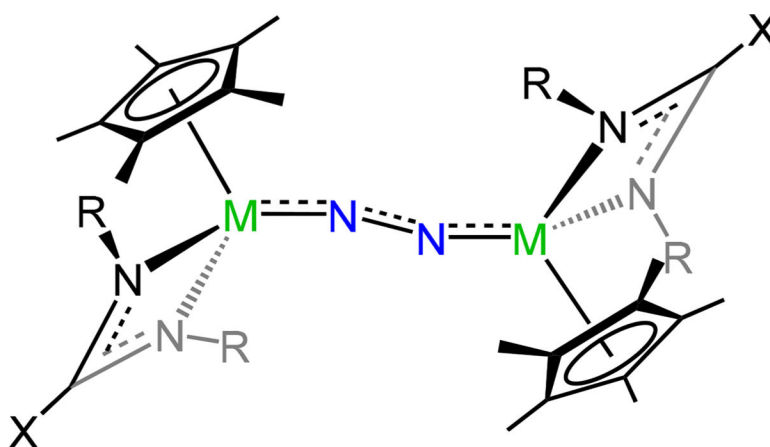
73-M/N^R,X	d(N−N) (Å)
73-Mo/N^{iPr},Me	
73-Mo/N^{iPr},NMe$_2$	1.267(2)
73-Mo/N^{Et},Ph	1.288(3)
73-W/N^{iPr},Me	1.277(8)
73-W/N^{Et},Ph	1.299(5)

Figure 56.
Dinitrogen-bridged bis[Cp*(amidinato or guanidinato)metal] compounds of Mo and W, 73-M/N^R,X.

74
d(N–N): 1.189(4) Å
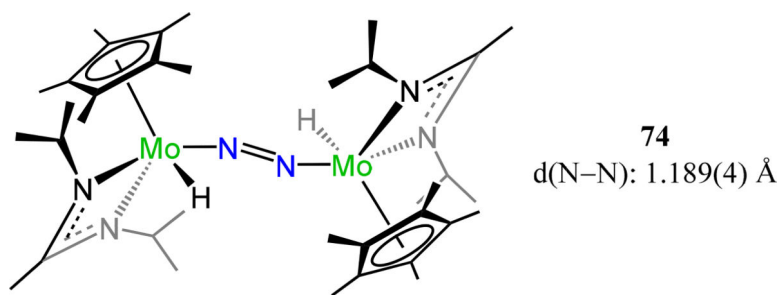
Figure 57.
Bis[Cp*(amidinato)molybdenum](*μ*-dinitrogen), 74.
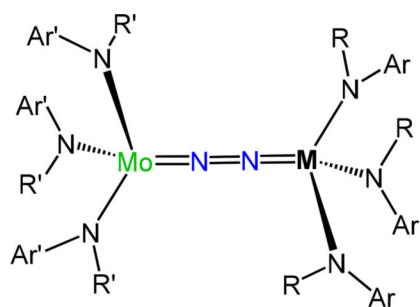
Name	R, R'	d(N–N) Å	ν_{N-N} cm^{-1}
76-Ti	R = ^{t}Bu, R' = C(CD$_3$)$_2$CH$_3$ Ar = Ph, Ar' = 3,5-C$_6$H$_3$Me$_2$	1.229(4)	1575
76-U-1	R = ^{t}Bu, R' = ^{t}Bu Ar' = Ph, Ar = 3,5-C$_6$H$_3$Me$_2$	1.232(11)	
76-U-2	R = ^{t}Bu, R' = 1-adamantyl Ar' = Ar = 3,5-C$_6$H$_3$Me$_2$	1.23(2)	1568
76-Nb-1	R = ^{i}Pr, R' = ^{t}Bu Ar = 3,5-C$_6$H$_3$Me$_2$	1.235(10)	1583
76-Nb-2	R = Np, R' = ^{t}Bu Ar = 3,5-C$_6$H$_3$Me		
76-Nb-3	R = R' = Np Ar = 3,5-C$_6$H$_3$Me$_2$		

Figure 58.
Heterodimetallic-μ–1,2-dinitrogen complexes (76-M) utilizing the tris(anilido)molybdenum-dinitrogen fragment.
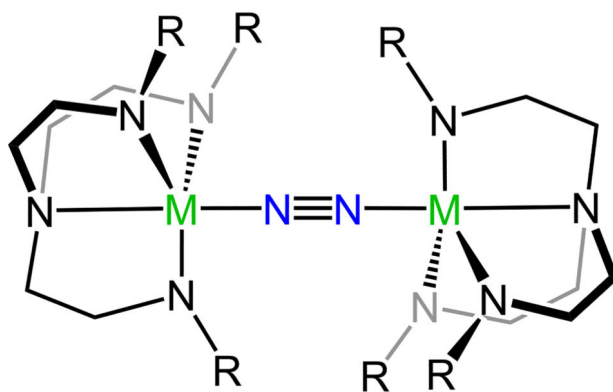
Name	R	d(N−N) Å	d(M−N) Å
78-1, **Mo**	C_6F_5		
78-2, **Mo**	$^tBuMe_2Si$	1.20(2)	1.907(8)
78-3, **Mo**	$4\text{-}^tBuC_6H_4$	1.186(7)	1.930(4)
78-4, **W**	Np	1.39(2)	1.845(11)

Figure 59.
Tren^{3-} ligated dinuclear molybdenum or tungsten dinitrogen complexes, 78.
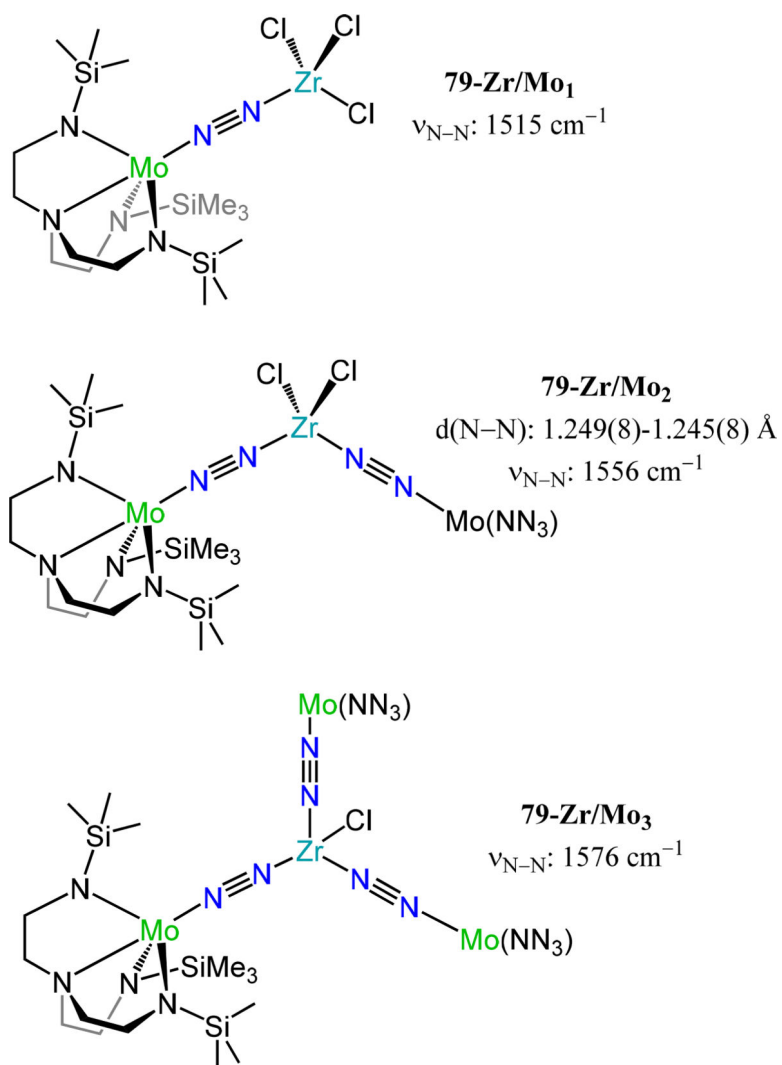
Figure 60.
Heteronuclear Mo_nZr dinitrogen complexes, 79-M/Mo_n.
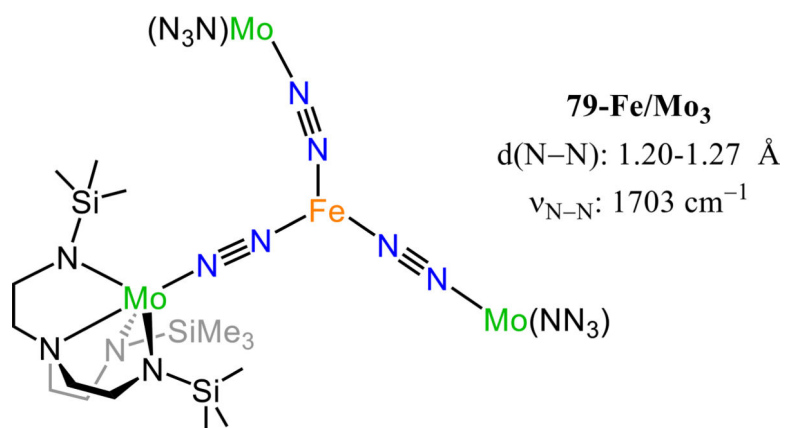
Figure 61.
Heteronuclear Mo_3Fe dinitrogen complex, 79-Fe/Mo_3.

Figure 62.
Compounds 81-N_2 and 81-diene.
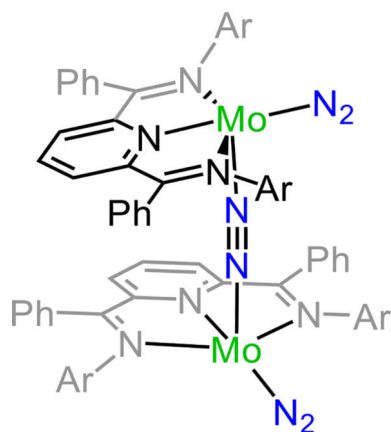
81-N_2
Ar = 2,6-^{i}Pr$_2$Ph
d(N−N): 1.246(4) Å
Mo−N(N_2): 1.819(3)-
1.823(3) Å
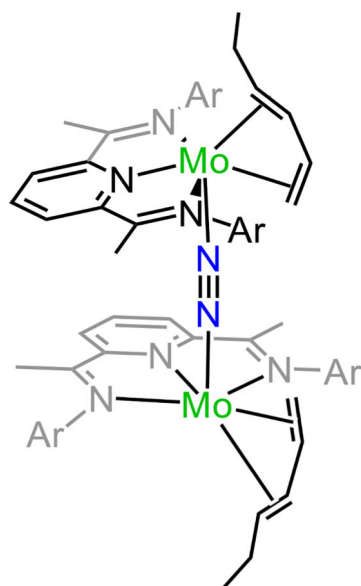
81-diene
Ar = 2,6-^{i}Pr$_2$Ph
d(N−N): 1.145(4) Å
Mo−N(N_2): 2.031(4) Å

[82]²⁺, d(N−N): 1.203(3) Å
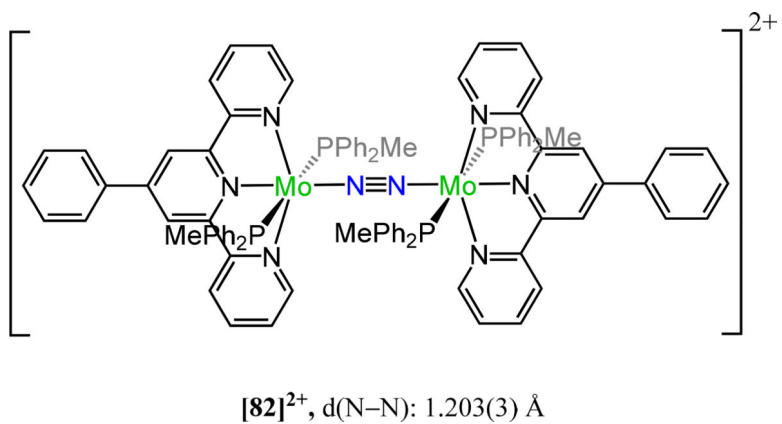
Figure 63.
Dinuclear molybdenum-dinitrogen complex with redox-active phenyl-substituted terpyridine ligands, [82]²⁺.
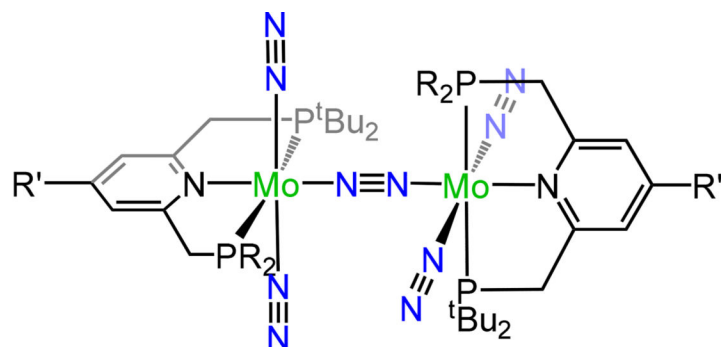
R=^{t}Bu, Ad, Ph   R'=H
R=^{t}Bu   R'= Ph, SiMe$_3$, tBu, Me, OMe
R=^{t}Bu   R'= Fc, Et^{Fc}, Ph^{Fc}, Rc

83^R-R'	d(N−N) (Å)	ν_{N-N}(μ-N$_2$)
R = ^{t}Bu, R' = H	1.146(4)	1890 cm^{-1}
R = Ph, R' = H	1.131(4)	
R = ^{t}Bu, R' = Ph	1.140(4)	
R = ^{t}Bu, R' = ^{t}Bu	1.155(4)	
R = ^{t}Bu, R' = Me	1.143(6)	
R = ^{t}Bu, R' = OMe	1.139(4)	
R = ^{t}Bu, R' = Fc	1.146(4)	
R = ^{t}Bu, R' = Rc	1.139(4)	

Figure 64.
Dinuclear molybdenum-μ–1,2-dinitrogen complexes (83^R-R′) chelated by [PNP] pincer-type ligands with *trans-trans* stereochemistry.
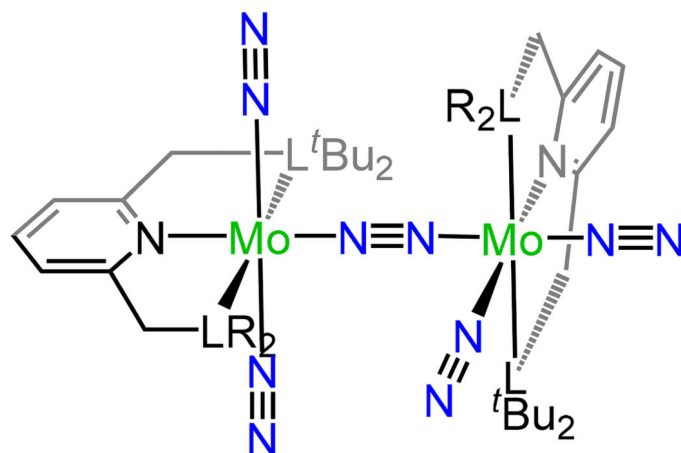
Figure 65.
Dinuclear molybdenum-μ–1,2-dinitrogen complexes (83^R-H and 84) in the *cis-trans* configuration chelated by PNP pincer-type ligands.
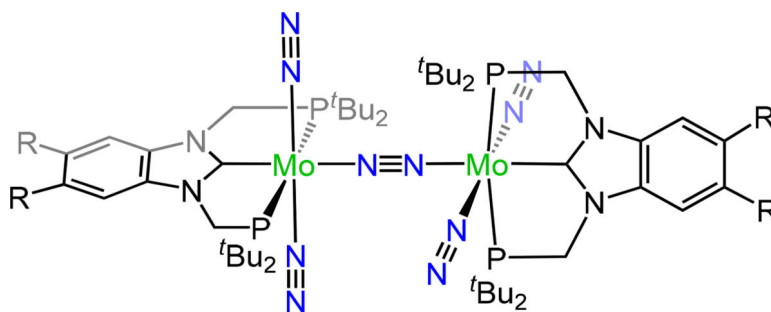
85-1, R = H, d(N–N): 1.130(2) Å
85-2, R = Me, d(N–N): 1.134(2) Å
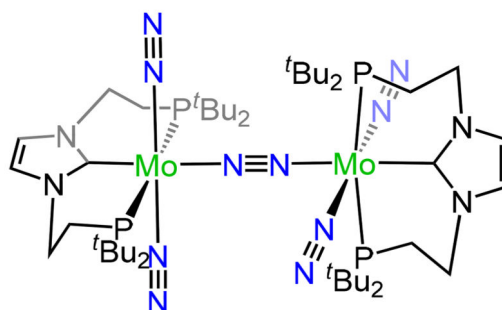
85-3, d(N–N): 1.154(4) Å

Figure 66.
PCP-ligated $Mo_2(\mu–1,2-N_2)$ complexes, 85.

87^{tBu}
87^{Cy}: d(N–N): 1.120(6) Å,
ν_{N-N}: 1946 cm^{-1}
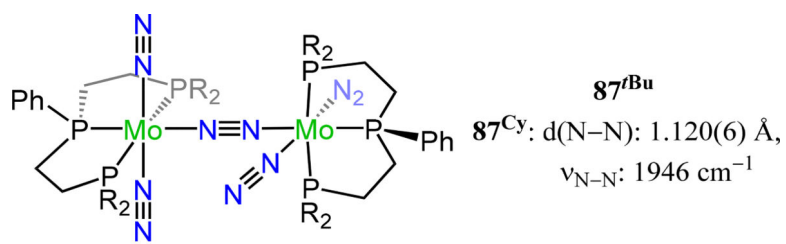
Figure 67.
PPP-ligated $Mo_2(\mu–1,2-N_2)$ complexes, 87^R.
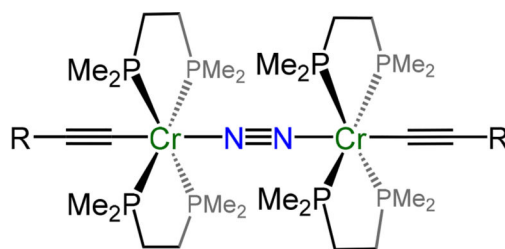
Name	d(Cr–N) (Å)	d(N–N) (Å)	ν_{N-N} (cm^{-1})
88-Cr/SiMe$_3$	1.870(10)	1.177(10)	-
88-Cr/Ph	1.885	1.177	1685
[88-Cr/Si^{i}Pr$_3$]^0	1.881(2)	1.187(5)	1680
[88-Cr/Si^{i}Pr$_3$]$^{1+}$	1.857(7)	1.195(5)	-
[88-Cr/Si^{i}Pr$_3$]$^{2+}$	1.88(1)	1.181(8)	1710

Figure 68.
Bis(dimethylphosphino)ethane ligated chromium complexes 88-M/R.
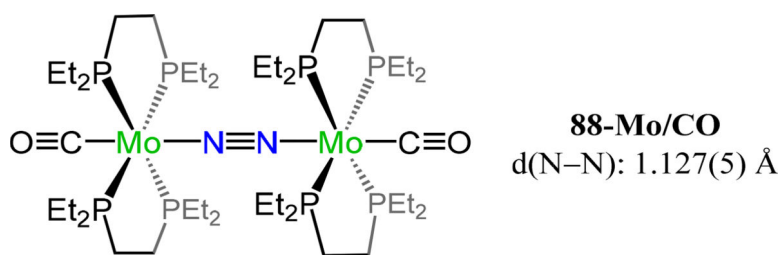
88-Mo/CO
d(N–N): 1.127(5) Å

Figure 69.
Complex 88-Mo/CO.
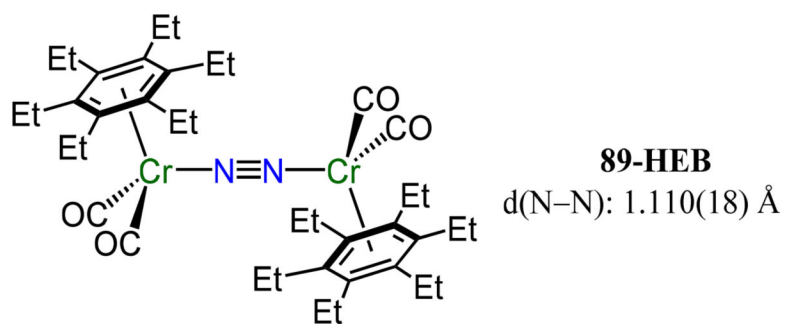
Figure 70.
Compound 89-HEB, $[Cr(\eta^6\text{-arene})(CO)_2](\mu\text{--}1,2\text{-}N_2)$.
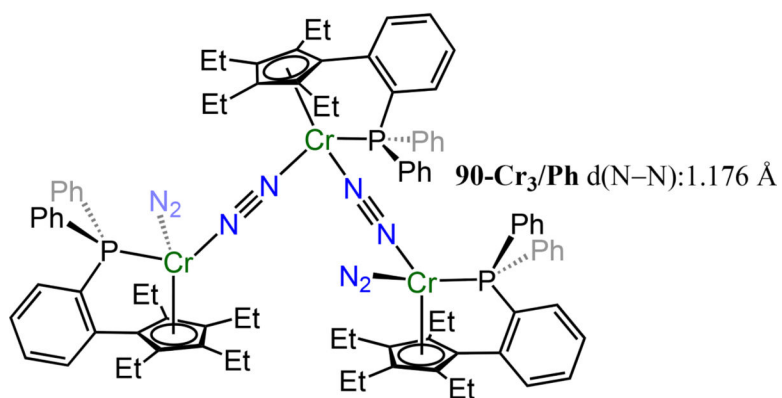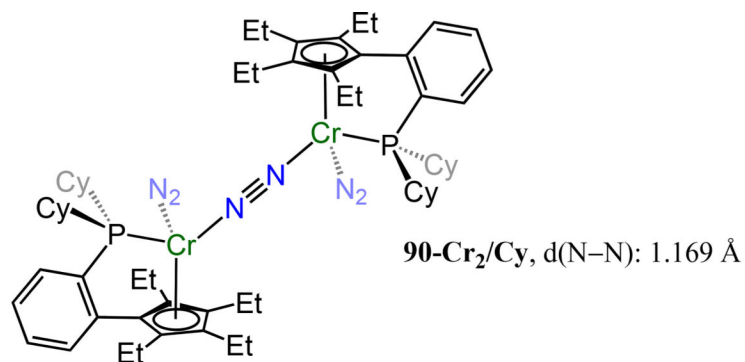
Figure 71.
Polynuclear chromium-dinitrogen adducts, 90-Cr$_n$/R.
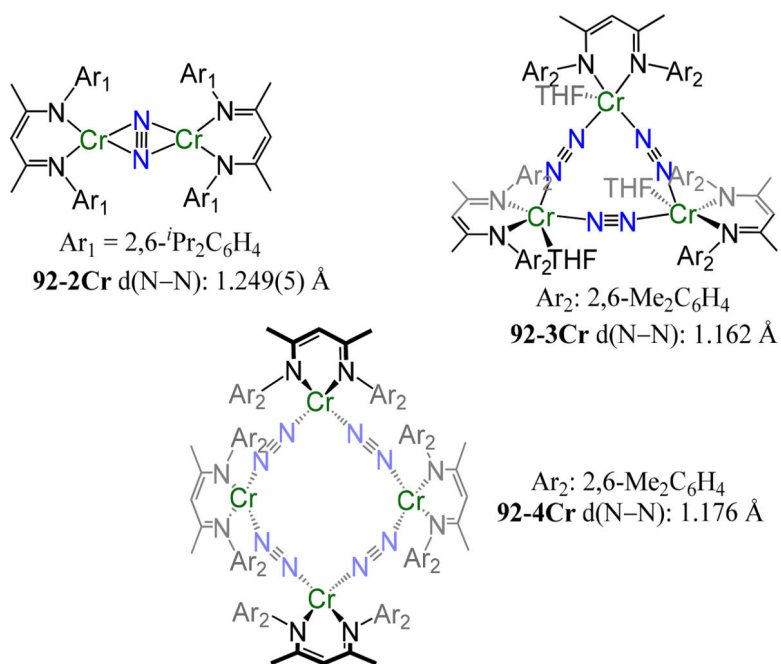
Figure 72.
(β-diketiminatochromium)-dinitrogen complexes of varying nuclearities, 92-nCr. The side-on/side-on coordination mode observed for 92–2Cr is rare for Gp 6 complexes.
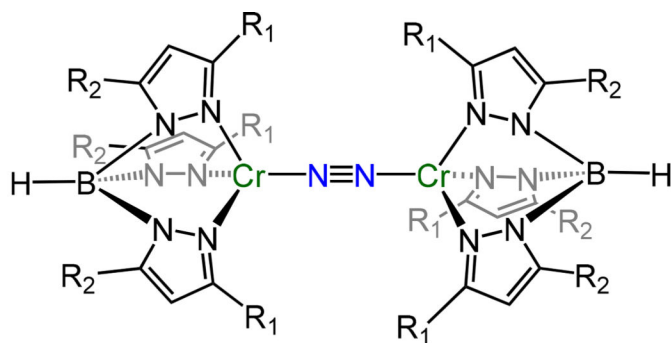
93-R$_1$/R$_2$, R$_1$ = ^{t}Bu, R$_2$ = Me

93-R$_1$/R$_2$, R$_1$ = ^{i}Pr, R$_2$ = ^{i}Pr

93-R$_1$/R$_2$, R$_1$ = ^{t}Bu, R$_2$ = ^{i}Pr; d(N–N) = 1.213(5)–1.214(4) Å

Figure 73.
Tris(pyrazolylborate)-supported dinuclear chromium- μ–1,2-dinitrogen complexes, 93
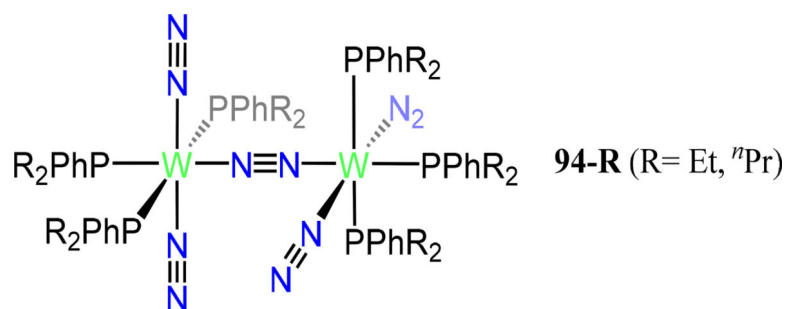
Figure 74.
Compounds $[(R_2PhP)_3W(\eta^1\text{-}N_2)]_2(\mu\text{--}1,2\text{-}N_2)$, 94-R.

Figure 75.
[W(CO)$_3$(P^{i}Pr$_3$)$_2$]$_2$(μ–1,2-N$_2$) (95-CO) and [(PhN)Cl$_2$(PMe$_3$)$_2$W]$_2$(μ–1,2-N$_2$) (95-NPh).

X=Cl	P=PMe$_2$Ph,dppe
X=NCS	P=dppe
X=NCS	P=dppe
X=Cl	P=PMe$_2$Ph
X=I	P=PMe$_2$Ph
X=NCS	P=dppe
X=Cl	P=dppe
X=Cl, Me	P=depe

96

$$\text{M} \begin{cases} \text{TiCpCl}_2, \text{TaMe}_3\text{Cl} \\ \text{MCp}_2\text{Cl (M=Ti, Zr, Hf)} \\ \text{TiCp'Cl}_2 \text{ (Cp'=Cp,Cp*)} \\ \text{MCp'Cl}_3 \text{ (M=Nb,Ta; Cp'=Cp, Cp*)} \\ \text{ZrCp}_2\text{Me, ZrCpCl}_2 \\ \text{NbMe}_2\text{Cl}_2 \\ \text{TiCpS}_5 \\ \text{TiCp*Me}_2 \end{cases}$$
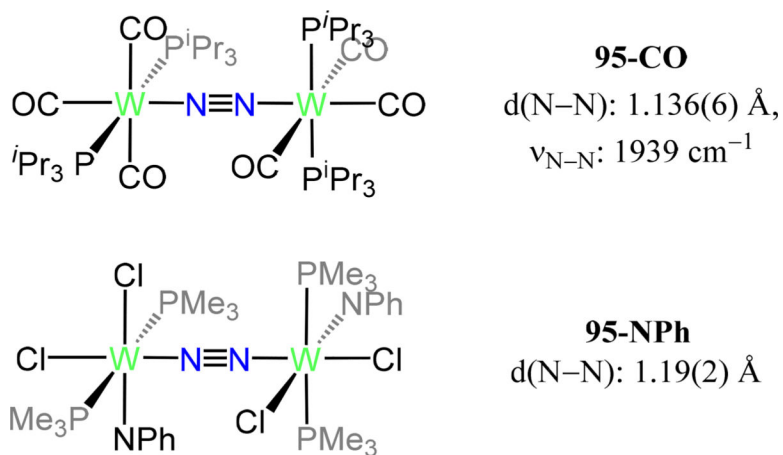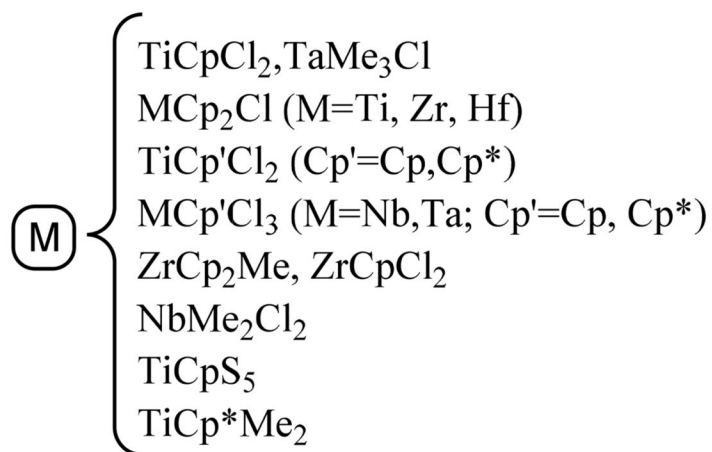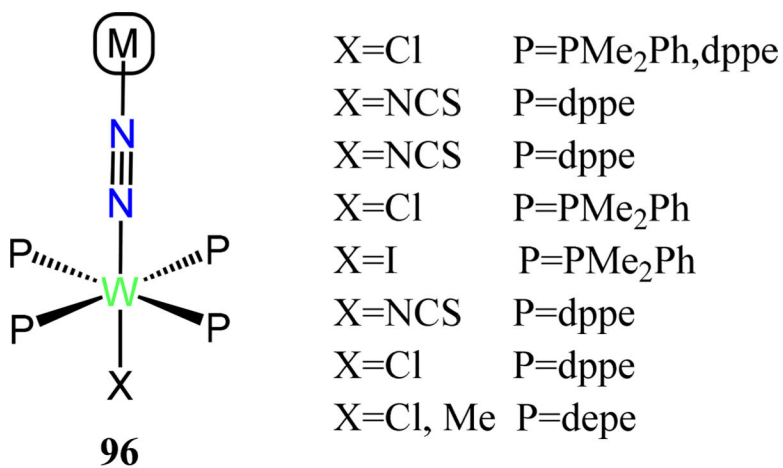
Figure 76.
Heterodimetallic complexes 96 derived from similar [W(PR$_3$)X] fragments and a Gp 4 or 5 fragment.
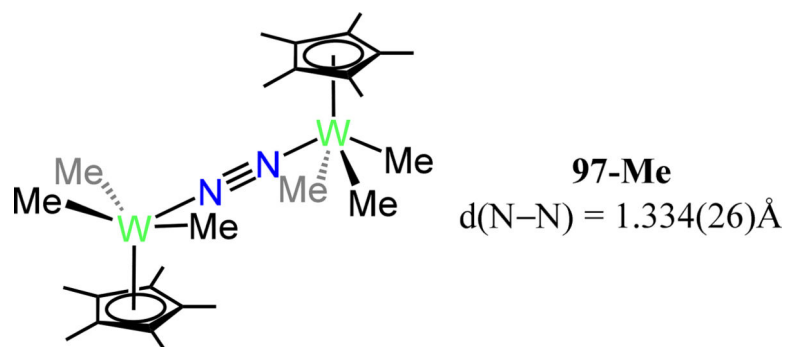
97-Me
d(N–N) = 1.334(26)Å

Figure 77.
Bis[Cp*(Me)$_3$W](μ–1,2-N$_2$), 97-Me.
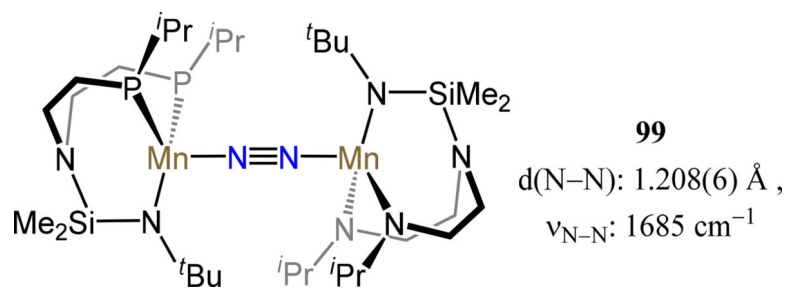
Figure 78.
The first dimanganese-μ–1,2-N_2 complex (99) synthesized from atmospheric N_2.

Figure 79.
Bis(TpMn)(μ–1,2-N$_2$), 100-Mn.

100-Tc
d(N–N):
1.160(3) Å
d(Tc–N(N$_2$)):
1.94(2) Å

100-Re
d(N–N): 1.15(2) Å
d(Tc–N(N$_2$)): 1.98(1) Å
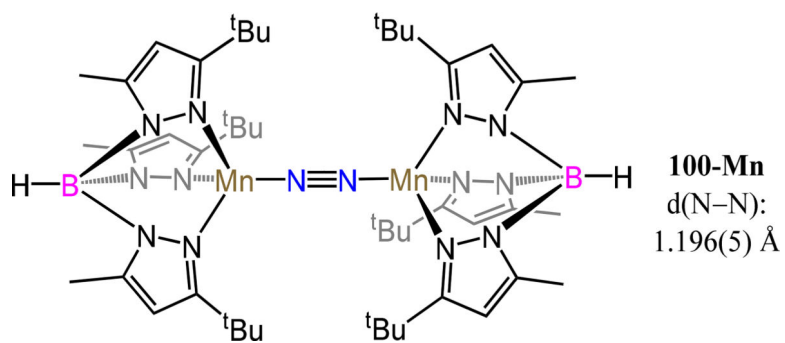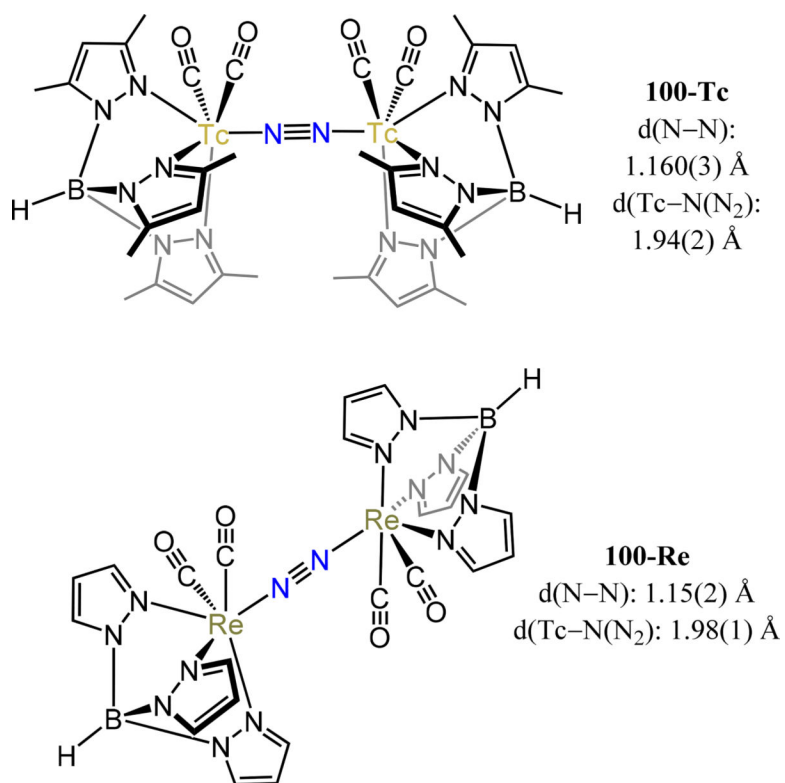
Figure 80.
Tp-ligated dimetallic Tc- and Re-μ–1,2- dinitrogen complexes, 100-Tc/Re.

$$Ti \left(N \equiv N - Re \right)_x$$

$$Ti \begin{cases} = TiCl_3, \ x = 1, \ \textbf{101-ReTi-1}, \ \nu_{N-N} = 1805 \ cm^{-1} \\ = TiCl_4, \ x = 2, \ \textbf{101-ReTi-2}, \nu_{N-N} = 1800 \ cm^{-1} \\ = TiCl_4CH_2Cl_2, \ \textbf{101-ReTi-3}, \ x = 2, \ \nu_{N-N} = 1812 \ cm^{-1} \\ = Ti_2Cl_6O(Et_2O), \ x = 1, \ \textbf{101-ReTi_2}, \nu_{N-N} = 1622 \ cm^{-1} \end{cases}$$

Re ≡≡≡

PhMe₂P,,,,, Re ,,,,,PMe₂Ph
PhMe₂P   PMe₂Ph
              Cl
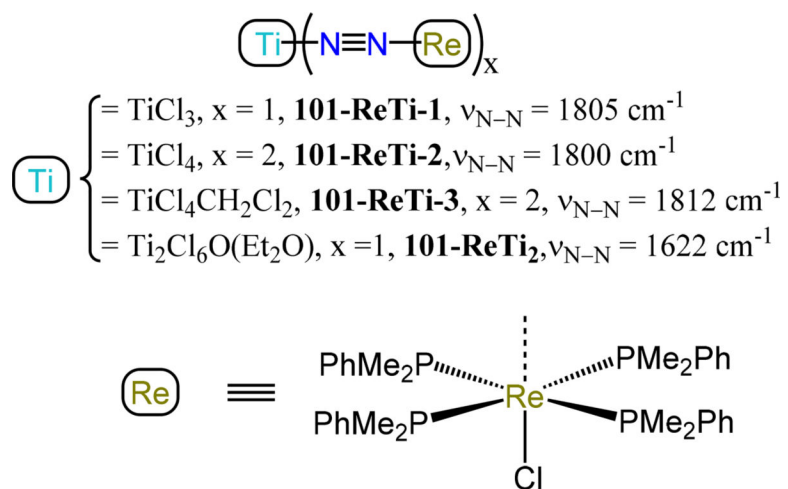
Figure 81.
Heterometallic TiRe and TiRe$_2$ dinitrogen compounds, 101-ReTi and 101-ReTi$_2$.
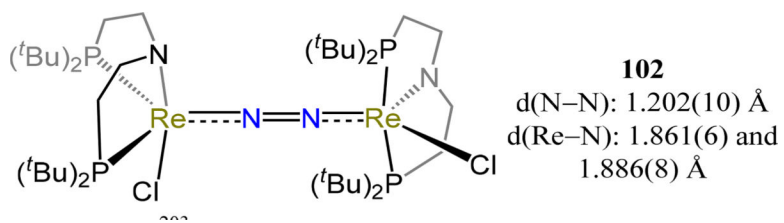
Figure 82.
Dirhenium complex 102 supported by a bis(phosphine)-amido ligand, [P$^{(CH2)2}$N$^{(CH2)2}$P^{tBu}]$^-$.

103
d(N–N): 1.169(5) Å
ν_{N-N}: 1733 cm^{-1}
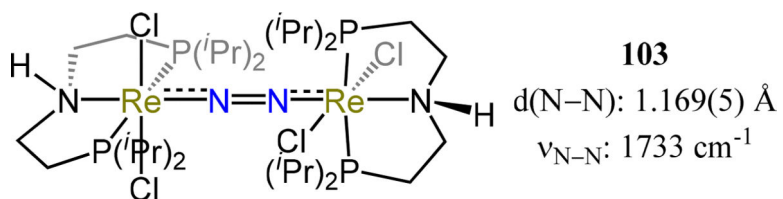
Figure 83.
[(HPNP^{iPr})ReCl$_2$]$_2$(μ–1,2-N$_2$), 103. Protonation of the ligand backbone in 102 decreases activation of the coordinated N$_2$ in 103.

104
d(N–N): 1.132 Å
$v_{N–N}$: 2126 cm^{-1}

105
d(N–N): 1.130 Å
$v_{N–N}$: 2016 cm^{-1}

106
d(N–N): 1.131(8) Å
$v_{N–N}$: 2042 cm^{-1}

107-dippe
d(N–N): 1.124(6) Å
$v_{N–N}$: 2050 cm^{-1}

107-R
R = Et, d(N–N): 1.114(5) Å,
$v_{N–N}$: 2064 cm^{-1}
R = Ph$_3$, d(N–N): 1.123 Å,
$v_{N–N}$: 2062 cm^{-1}
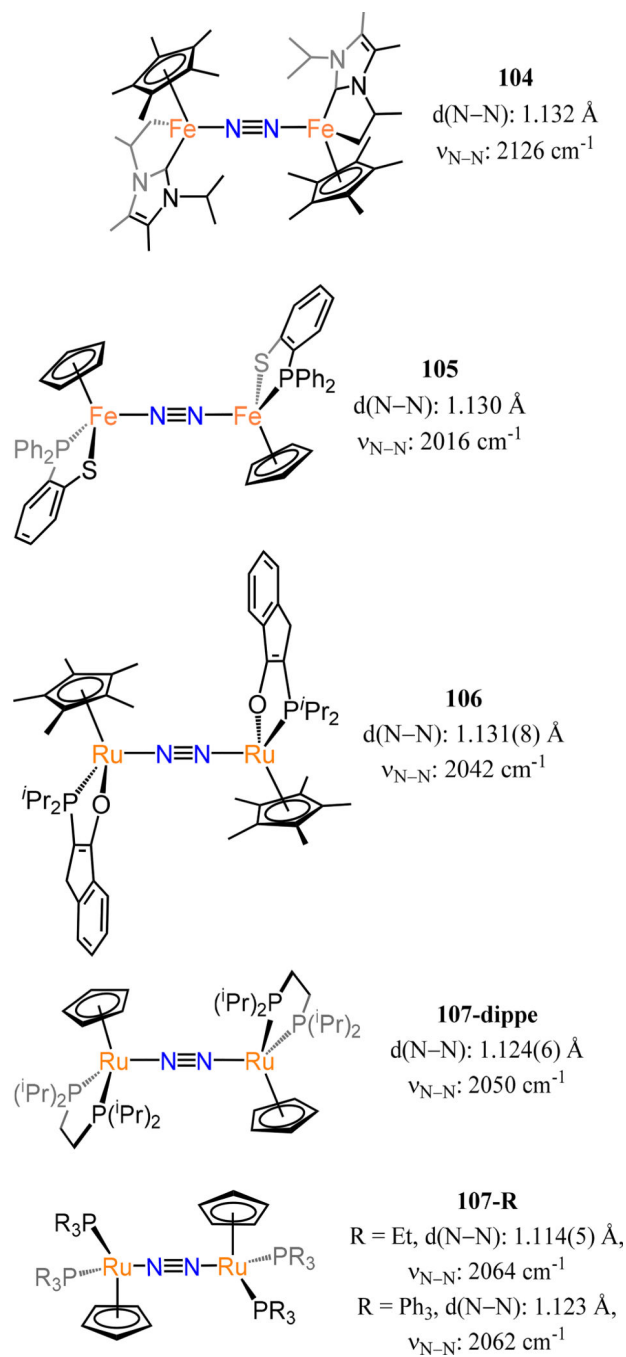
Figure 84.
Group 8 dimetallic-μ–1,2-N$_2$ complexes 104–107.
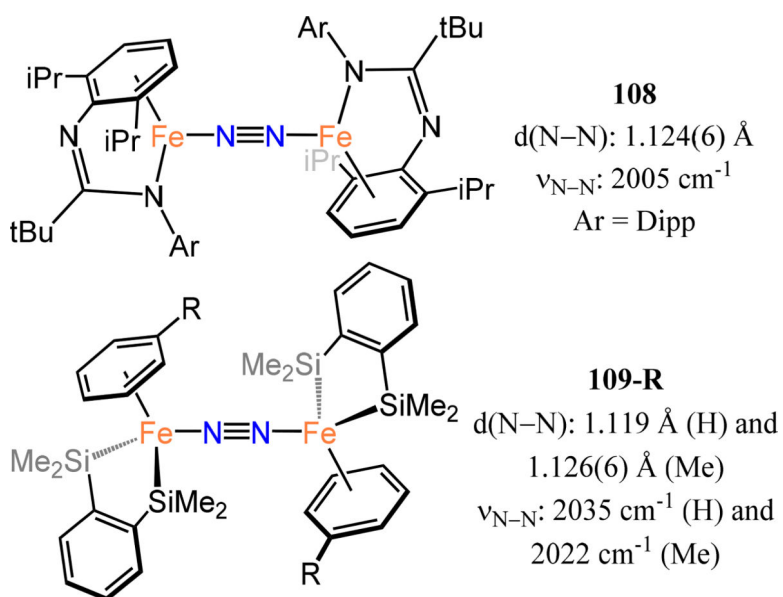
Figure 85.

Coordination of N_2 by η^6-arene-bound Fe centers in complexes 108 and 109-R.

Author Manuscript

Author Manuscript

Author Manuscript

Author Manuscript

110
d(N–N): 1.1 Å
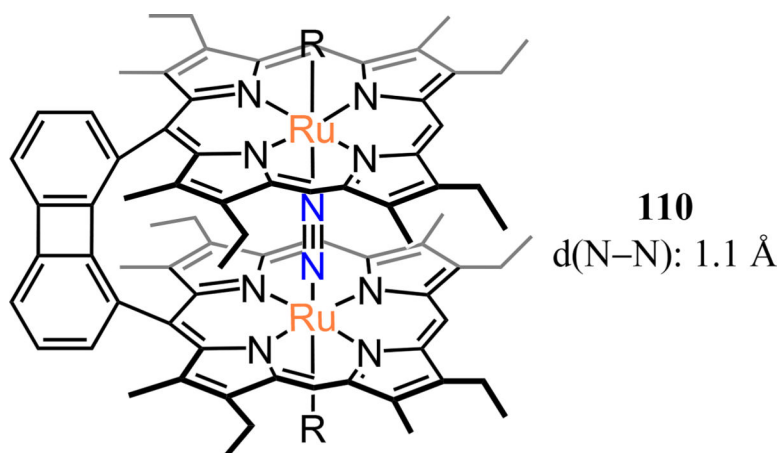
Figure 86.
Diruthenium complex 110.
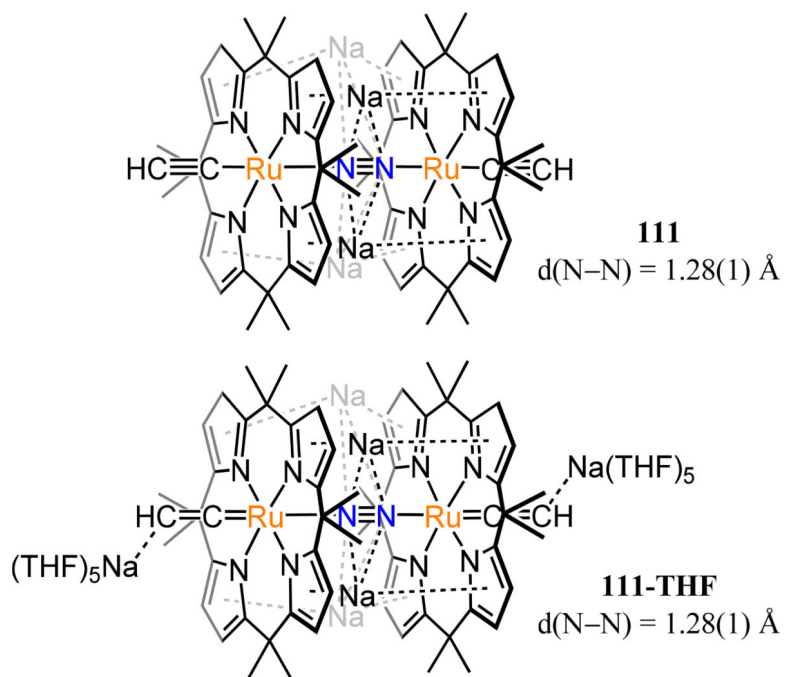
Figure 87.
Bis(*meso*-octaalkylporphyrinatoruthenium) complexes 111 and 111-THF.
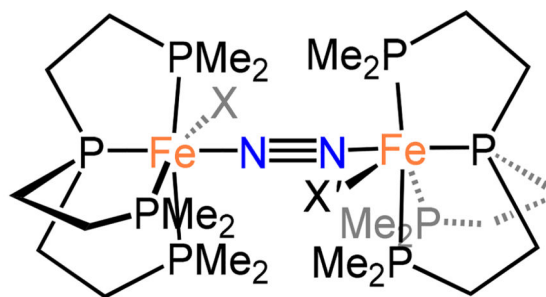
Name	X, X′	d(N–N) (Å)
112-2H	X = H, X′ = H	1.129(4)
112-1H	X = H, X′ = none	1.121(6)
112-noH	X = none, X′ = none	

Figure 88.
Diiron-dinitrogen complexes 112.
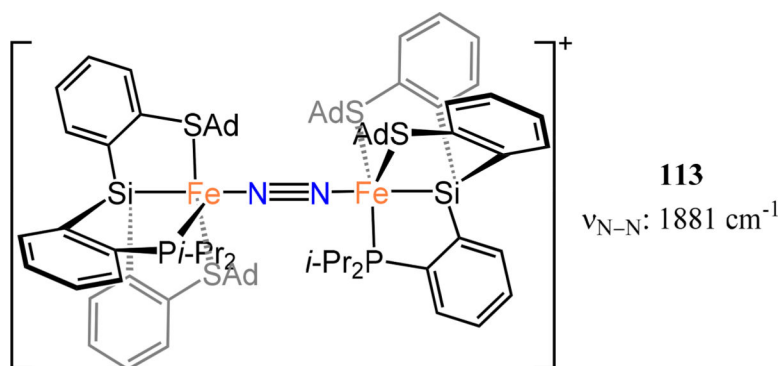
Figure 89.
Diiron-dinitrogen complex (113) employing a bis-thioether tripodal ligand.

114

d(N−N): 1.146(7) Å

ν_{N-N}: 2010 cm^{-1}
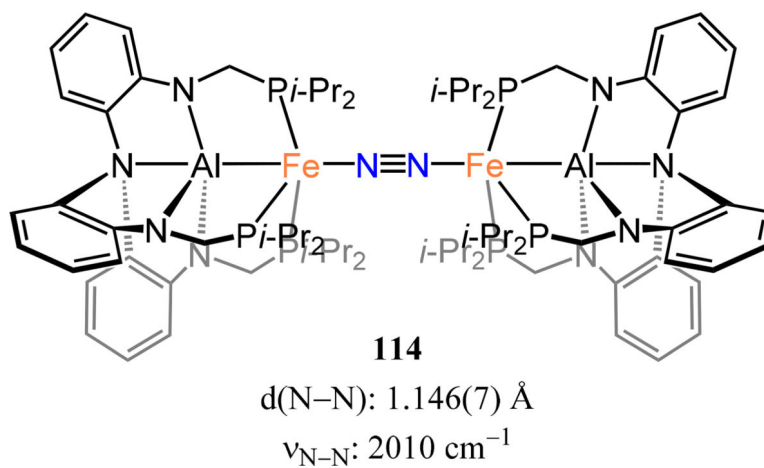
Figure 90.
Alane-supported diiron-dinitrogen complex 114.
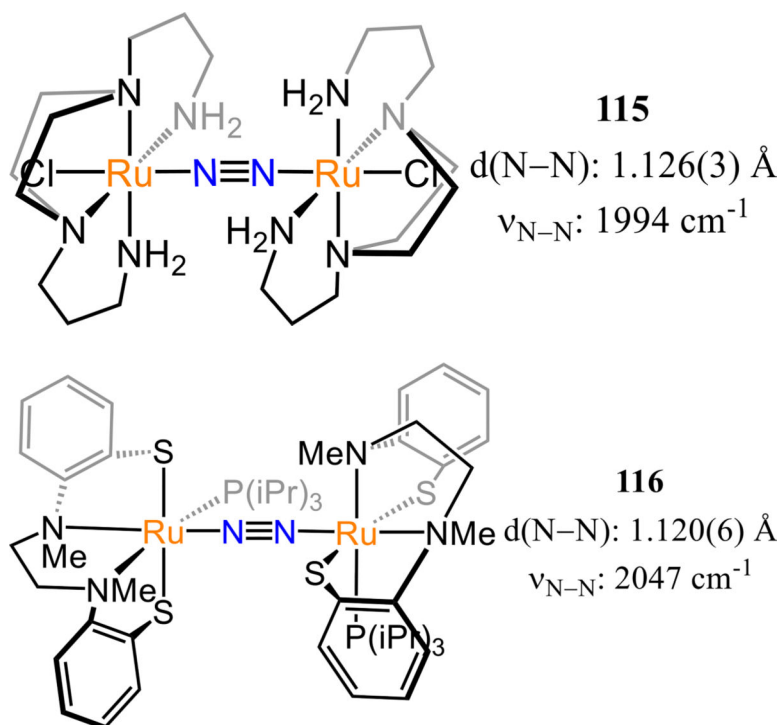
Figure 91.
Tetraamine and diamine-dithiolate ligated diruthenium-dinitrogen adducts, 115 and 116, respectively.

117-Me,Me
d(N−N): 1.137 Å
ν_{N-N}: 2100 cm^{-1} (ave.)

117-Et,Et
d(N−N): 1.123(3) Å
ν_{N-N}: 2090 cm^{-1} (ave.)

117-R$_1$,R$_2$
Ar = $C_6H_4R_1R_2$

117-2
d(N-N): 1.118(5) (terminal)
and 1.140(5) (bridging) Å
ν_{N-N}: 2100, 2030 cm^{-1}
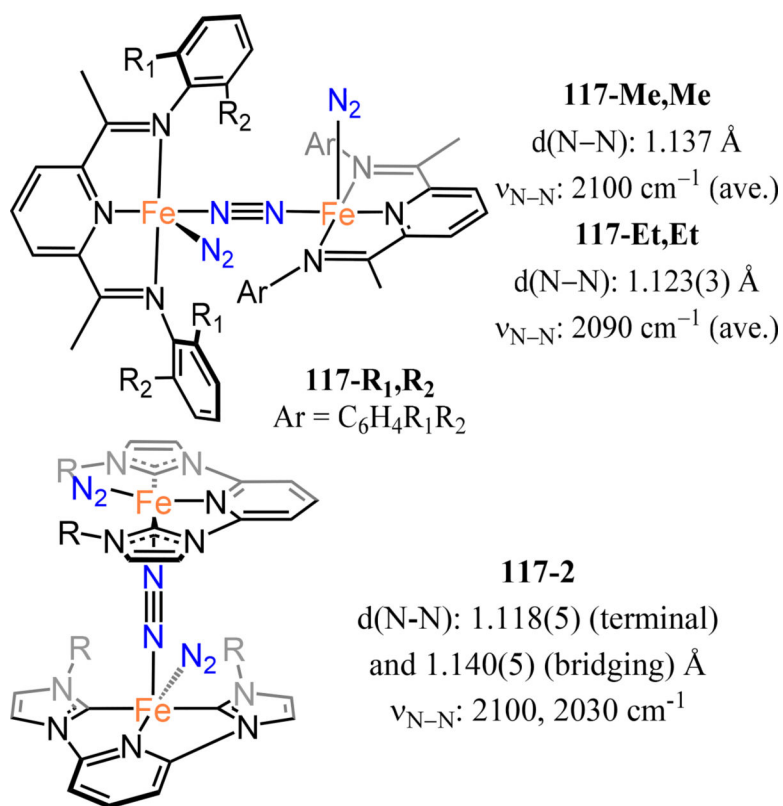
Figure 92.
PDI and bis(NHC)-pyridine diiron-dinitrogen complexes, 117.
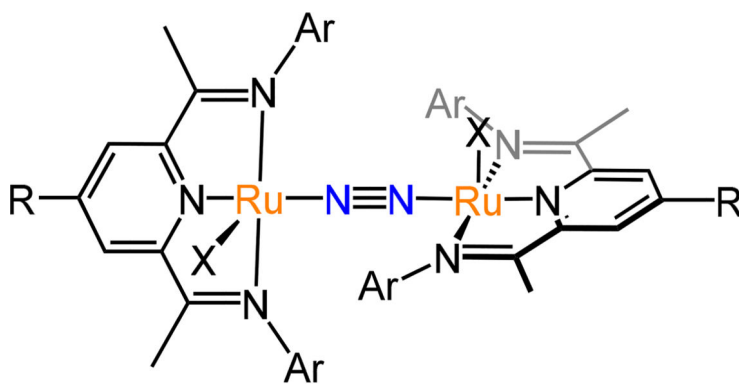
Name	R, Ar, X	d(N−N) Å
118-1	^{t}Bu, Mes, none	1.161(5)
118-2	H, Xyl, none	
118-3	H, Mes, none	
118-2H	H, Xyl, H	1.132(6)

Figure 93.
Diruthenium-dinitrogen complexes utilizing PDI chelates, 118.
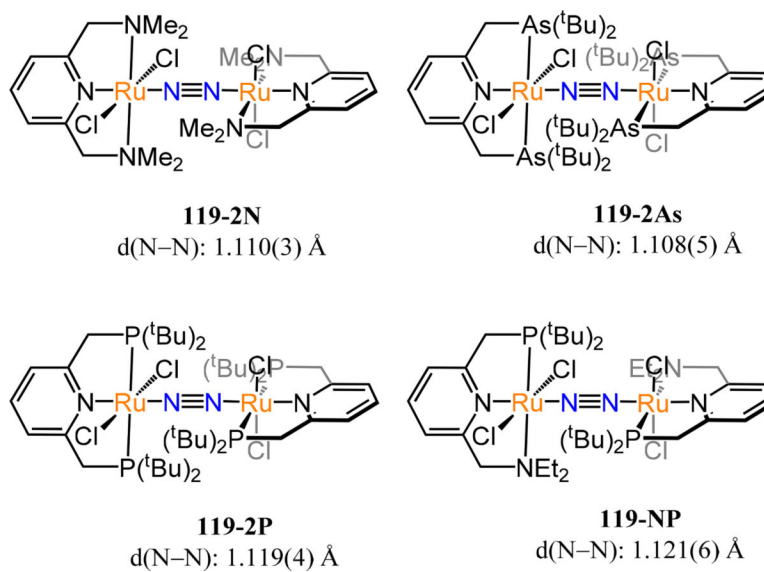
Figure 94.
ENE-type (E = N, P, or As) pincer diruthenium-dinitrogen complexes 119-X.
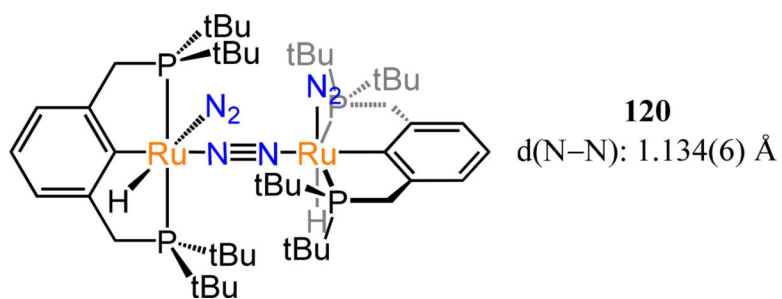
Figure 95.
PCP pincer-type diruthenium-dinitrogen complex 120.
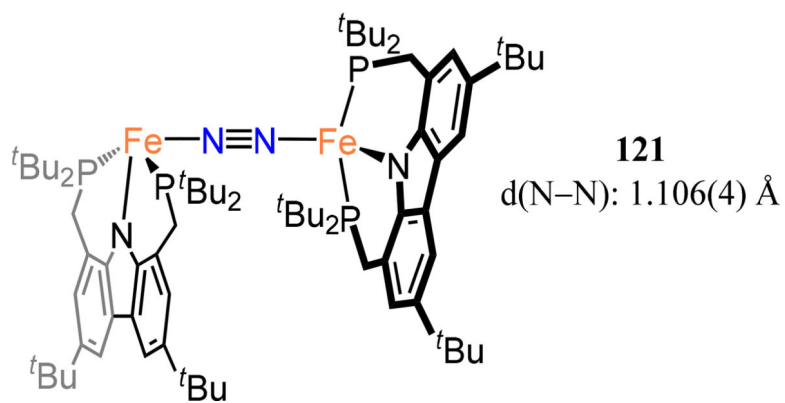
Figure 96.
Diiron-dinitrogen complex 121 in which the PNP pincer ligand employs a carbazole backbone.
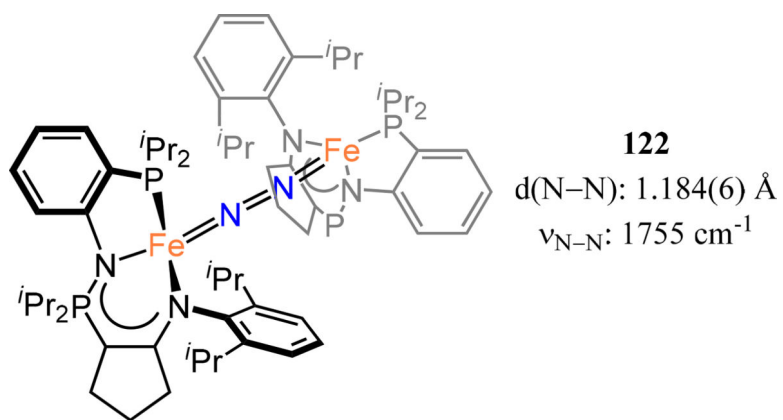
Figure 97.
Diiron-μ–1,2-dinitrogen complex 122 in which each Fe center is coordinated to an iminophospharane ligand.
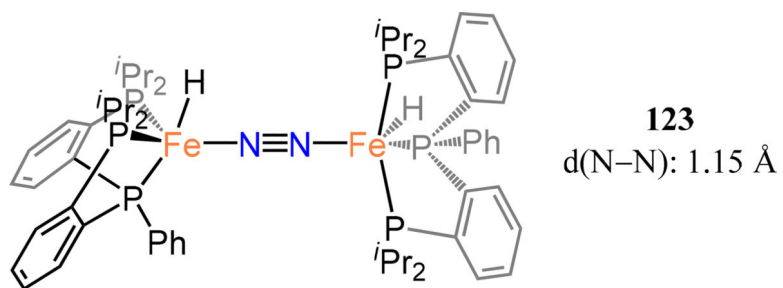
Figure 98.
DPB-based diiron-μ–1,2-N_2 complex (123).

124-1

d(N–N): 1.124(5) Å (Me), 1.103(6) Å (Ph)

ν_{N-N}: 2091 cm^{-1} (Me), 2093 cm^{-1} (^{i}Pr)
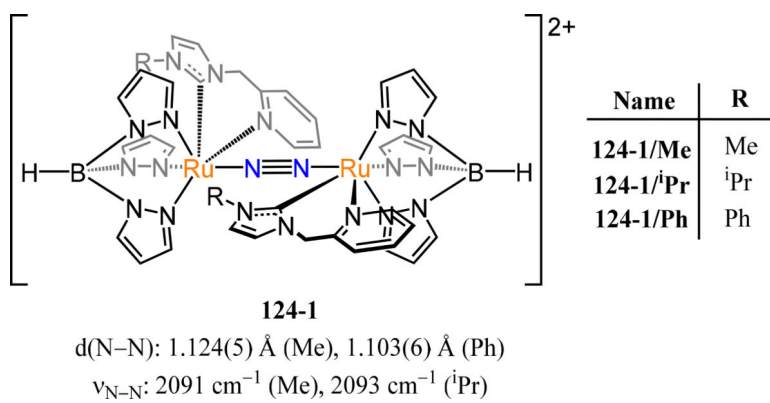
Figure 99.

Diruthenium-dinitrogen complex 124–1/R in which both chelating pyridyl-carbenes and Tp ligands are employed.

124-2
d(N–N): 1.117(7) Å
ν_{N-N}: 2106 cm^{-1}
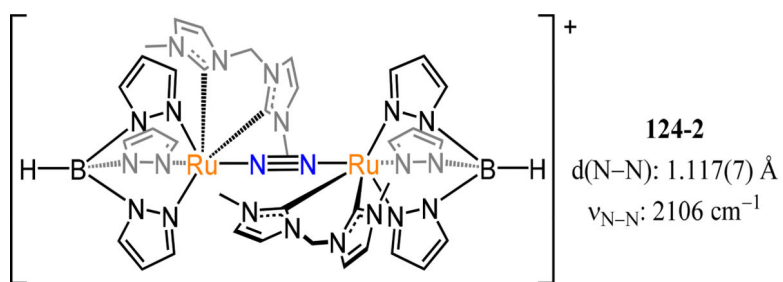
Figure 100.
Diruthenium-dinitrogen complex 124–2 in which both chelating bisNHC and Tp ligands are employed.

Figure 101.
Tp-based diiron-μ–1,2-dinitrogen complexes (125).
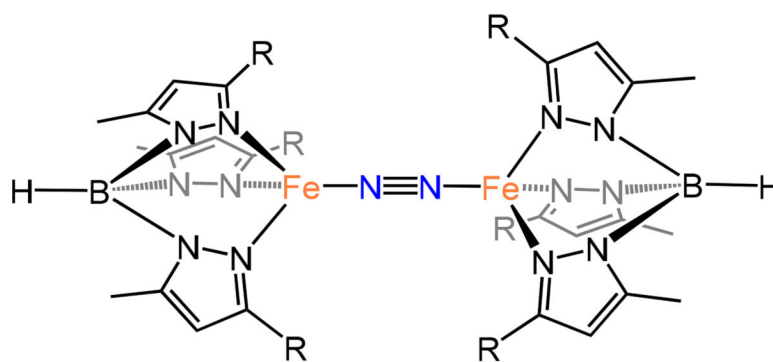
Name	R	d(N–N) (Å)
125-1	Ph	1.1804(19)
125-2	^{t}Bu	1.184(7)

128-Cyp
d(N−N): 1.135(5) Å
Cyp = cyclopentyl
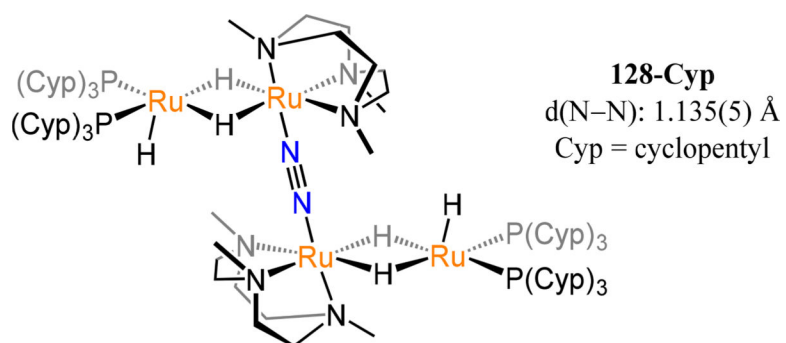
Figure 102.
Complex 128-Cyp featuring two (Cn*Ru)(μ_2-H)$_2$(RuH(PR$_3$)$_2$) units bridged together by an end-on/end-on N$_2$.
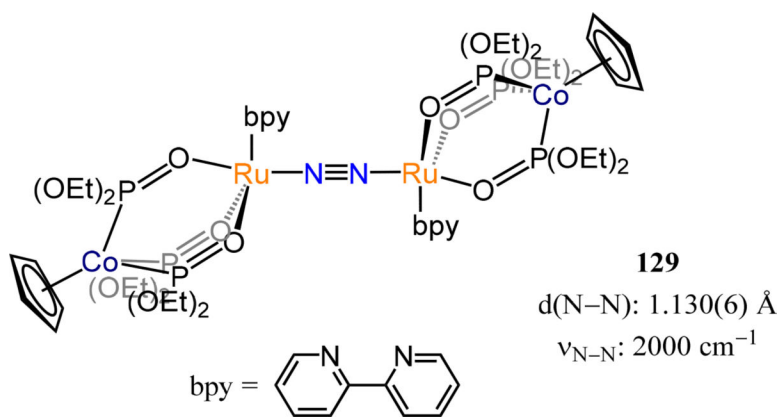
Figure 103.
Diruthenium-dinitrogen complex 129 bearing Co-based metalloligand.
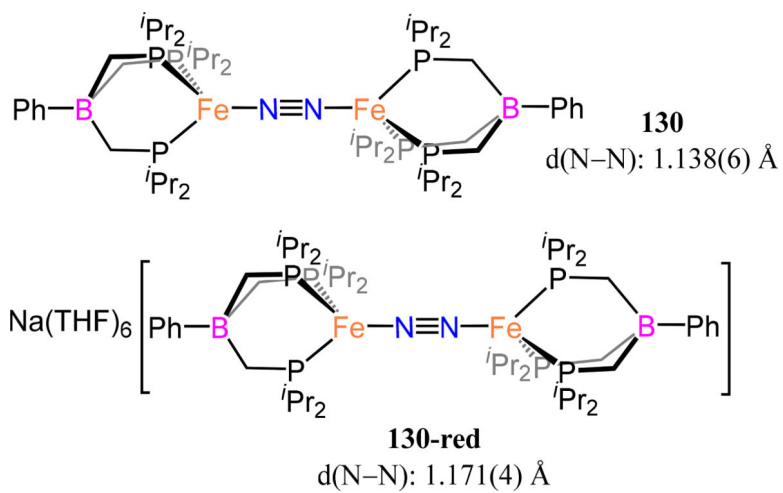
Figure 104.
Triphosphinoborate-coordinated diiron-μ–1,2-dinitrogen complexes 130 and 130-red.
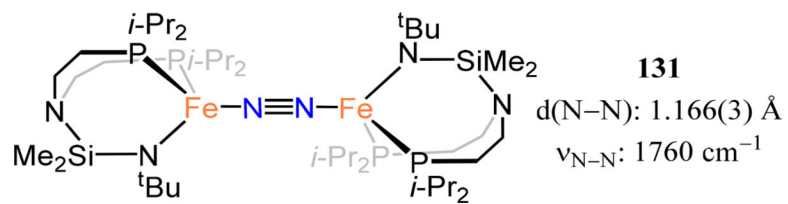
Figure 105.
$[N_2P_2]_2Fe(\mu–1,2-N_2)$, 131.
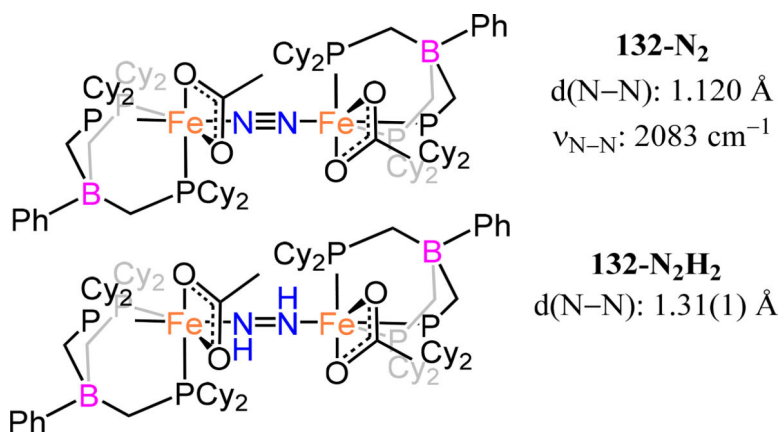
Figure 106.
Triphosphinoborate diiron-μ–1,2-dinitrogen or hydrazine complexes 132-N_2 and 132-N_2H_2.
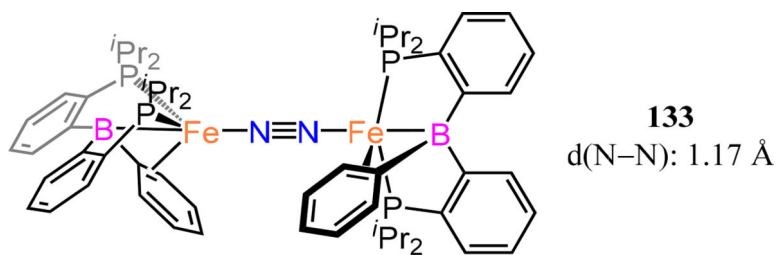
Figure 107.
Dinitrogen adduct of (DPB)Fe, 133.

134-R, R = ^tBu

d(N–N): 1.182(5) Å

ν_{N-N}: 1778 cm^{-1}

134-R, R = Me

d(N–N): 1.186(7) Å

ν_{N-N}: 1810 cm^{-1}
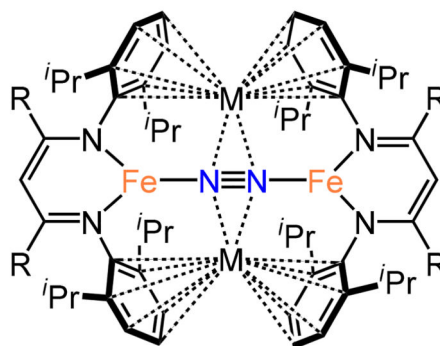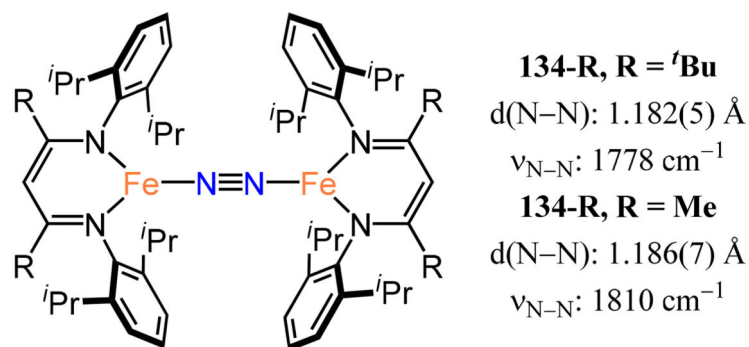
134-R/2M	d(N–N) (Å)	ν(N–N)(cm^{-1})
134-^tBu/2Na	1.239(4)	1583
134-^tBu/2K	1.233(6)	1589
134-Me/2Na	1.253(6)	1612
134-Me/2K	1.215(6)	1625
134-Me/2Rb	1.257(8)	1621
134-Me/2Cs	1.33(2)	1613

134-Me/K

d(N–N): 1.186(6) Å

ν_{N-N}: 1749 cm^{-1}
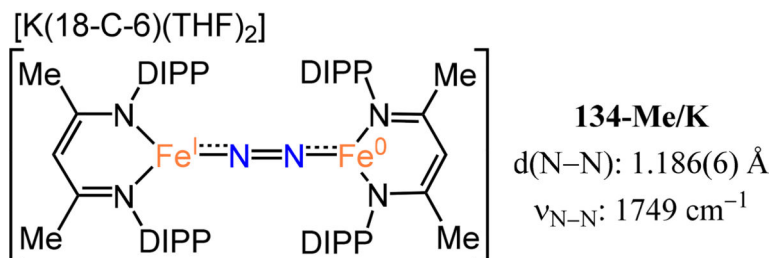
Figure 108.

Bis(β-diketiminatoiron)(μ–1,2-dinitrogen) complexes, 134.

134-*t*Bu/X

Ar = Dipp
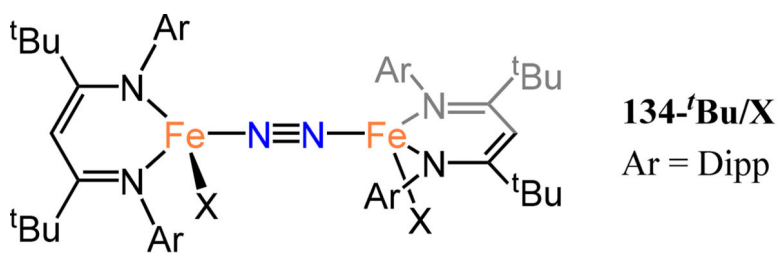
X = Pyridine
X = 4-(dimethylamino)pyridine
X = 4-*tert*-butylpyridine; d(N−N): 1.161(4) Å

134-Me/X
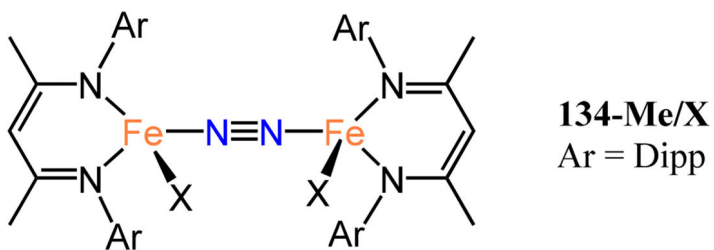
Ar = Dipp

X = Pyridine
X = 4-(dimethylamino)pyridine
X = 4-*tert*-butylpyridine; d(N−N): 1.151(3) Å

Figure 109.
NacNac-ligated diiron-dinitrogen complexes 143-R/X.

Author Manuscript

Author Manuscript

Author Manuscript

Author Manuscript

136-2N$_2$
d(N−N): 1.234(11) Å

136-3N$_2$
d(N−N): 1.191(14) Å (Rb),
1.200(9) Å (Cs)
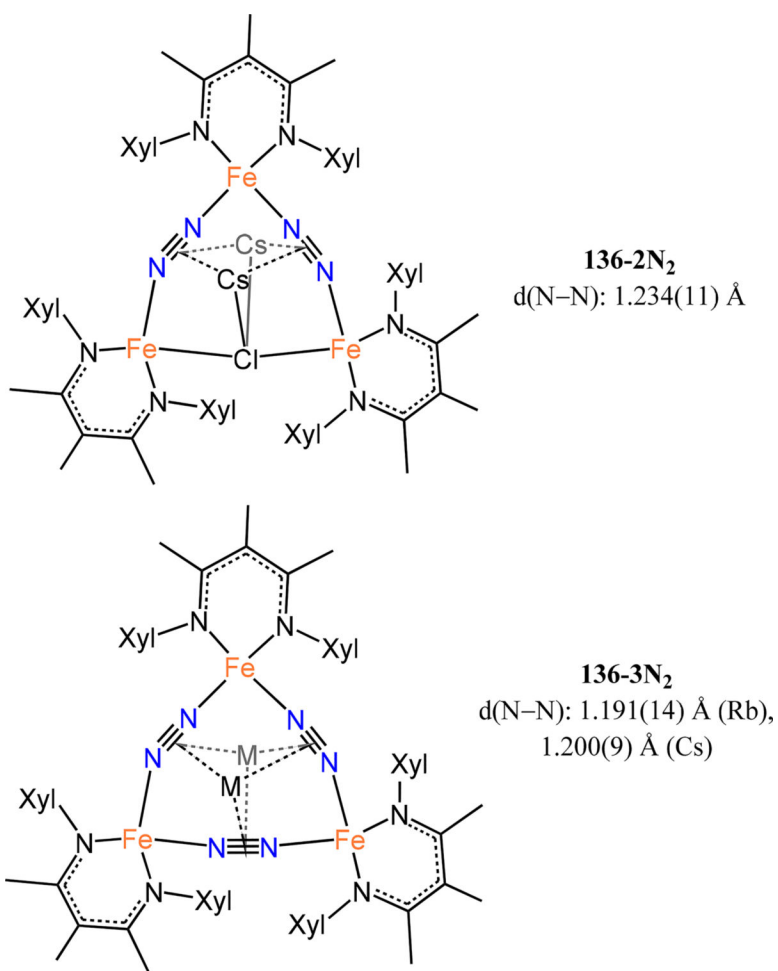
Figure 110.
Trimetallic iron-dinitrogen complexes utilizing β-diketiminate ligands.
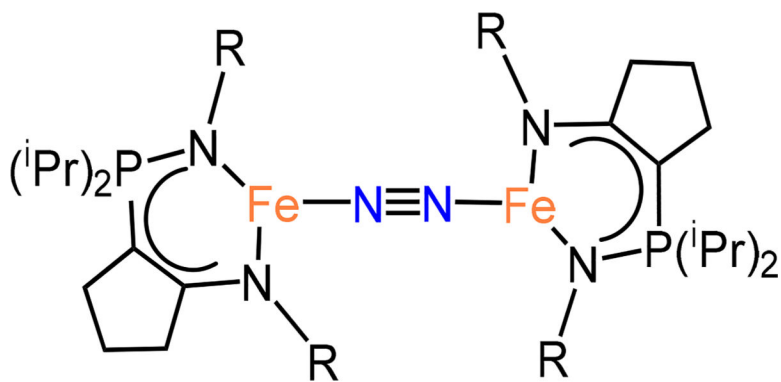
137-R
R = Dipp; d(N−N): 1.186(3) Å
R = Mes, d(N−N): 1.183 Å

Figure 111.
Diiron-dinitrogen complexes 137-R supported by enamido-phosphinimine donors.

138
d(N−N): 1.135(8) Å
ν_{N-N}: 2089 cm^{-1}
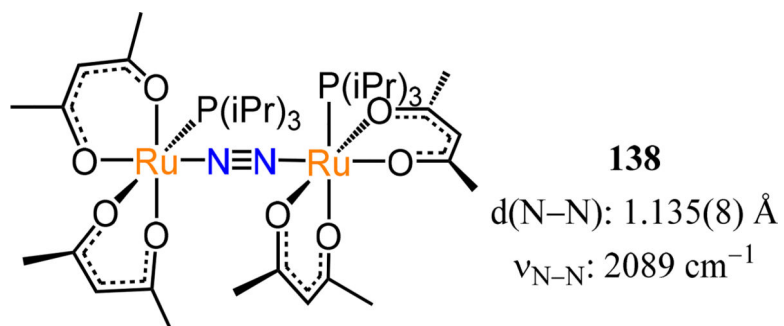
Figure 112.
Diruthenium-dinitrogen complex 138.
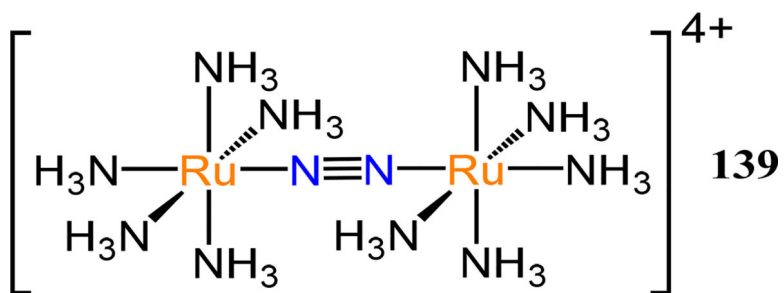
Figure 113.
Complex $[(Ru(NH_3)_5)_2(\mu-1,2-N_2)]^{4+}$ (139).
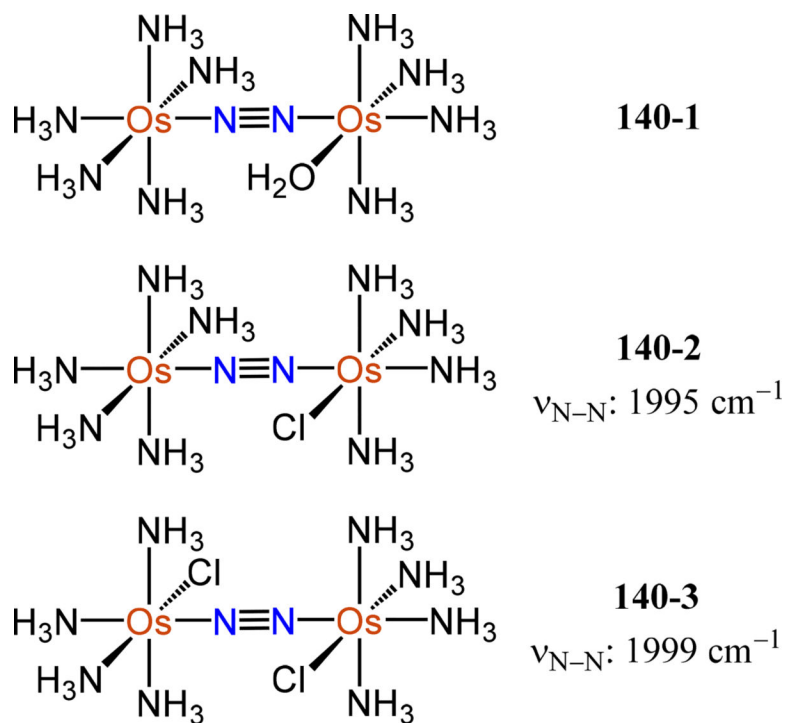
Figure 114.
Dimetallic osmium-dinitrogen complexes, 140.
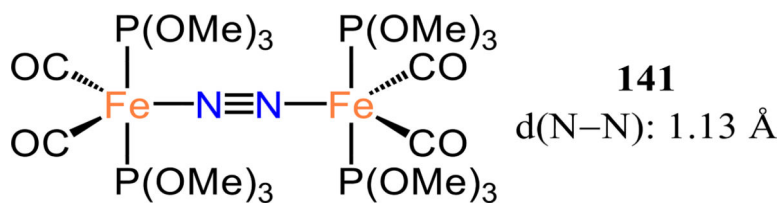
Figure 115.
Bis(dicarbonyl-bis(phosphite)iron)-dinitrogen complex 141.
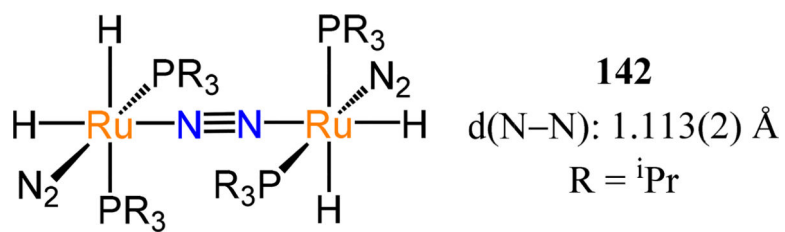
Figure 116.
Dinitrogen-bridged ruthenium dihydride complex 142.

143

d(N–N): 1.18(2) Å

144

144-red

d(N–N): 1.147(4) Å
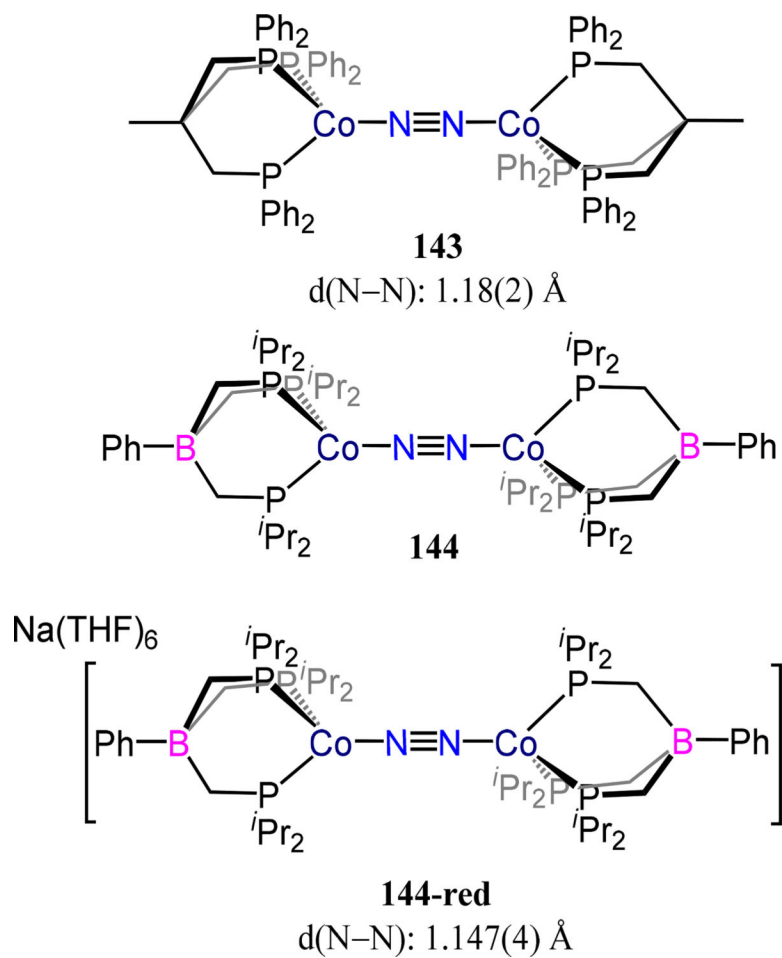
Figure 117.
Triphosphinoborate-coordinated dinuclear cobalt-dinitrogen complexes 143, 144, and 144-red.
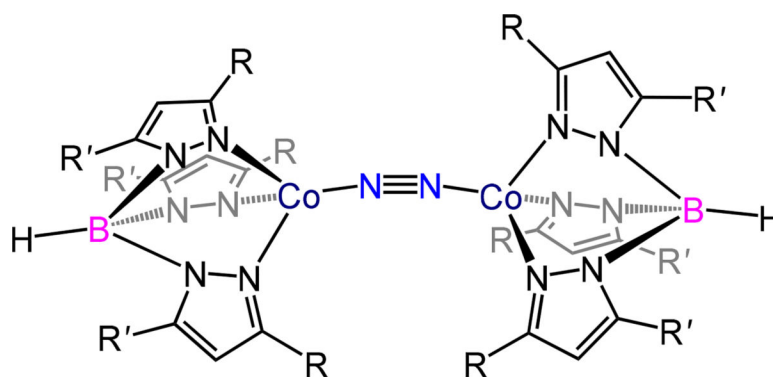
145-R/R′

R = Np, **R′** = H; d(N–N): 1.141(30) Å, ν_{N-N}: 2056 cm^{-1}

R = ^{i}Pr, **R′** = Me; d(N–N): 1.154(9) Å

Figure 118.
Dicobalt-dinitrogen complexes 145-R/R′.
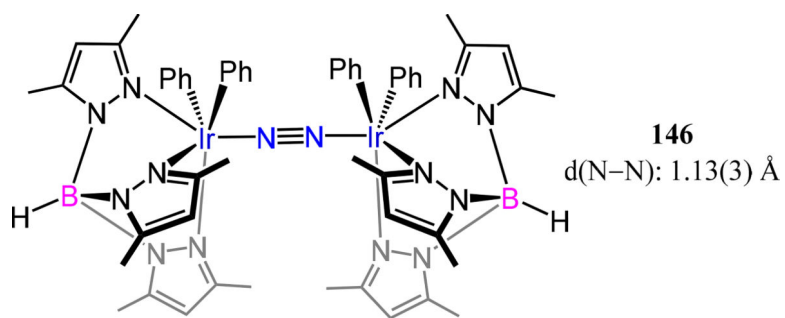
Figure 119.
Tp-ligated dinuclear iridium-dinitrogen complex 146.

148
d(N−N): 1.156(7) Å

N‿N = bipyrdine
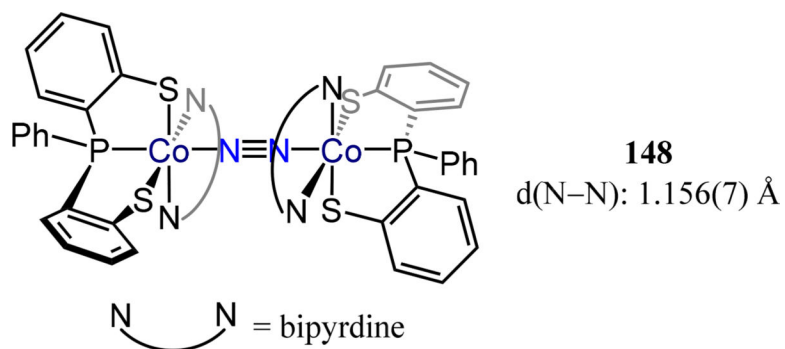
Figure 120.
Tridentate phosphanyldithiolato-based dicobalt end-on/end-on dinitrogen complex 148.
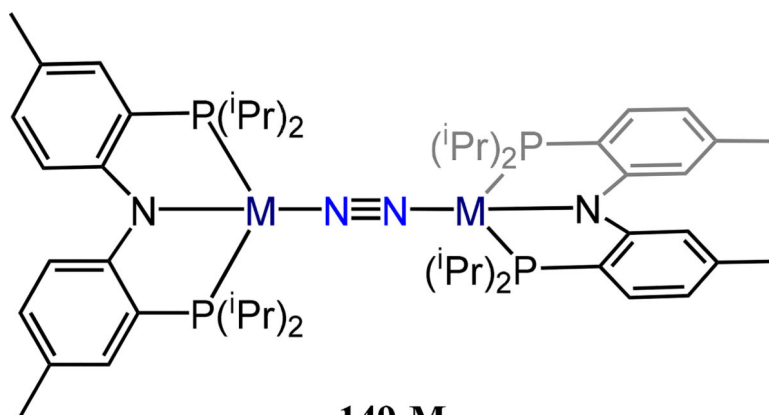
149-M

M = Co; d(N–N): 1.144(3) Å, ν_{N-N}: 2024 cm^{-1}

M = Rh; d(N–N): 1.119(2) Å

Figure 121.
Dinuclear Co and Rh dinitrogen adducts, 149-M, wherein each metal is ligated by a PNP-pincer chelate.
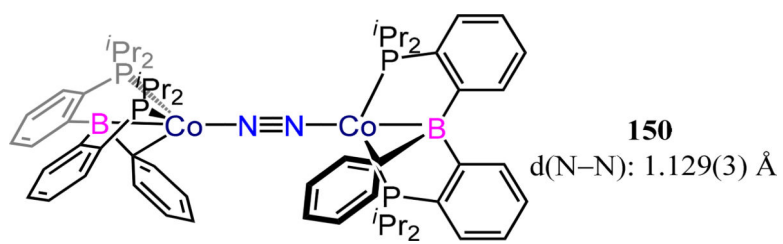
Figure 122.
Bis(phosphino)borane-ligated dicobalt(0)-dinitrogen complex, 150.
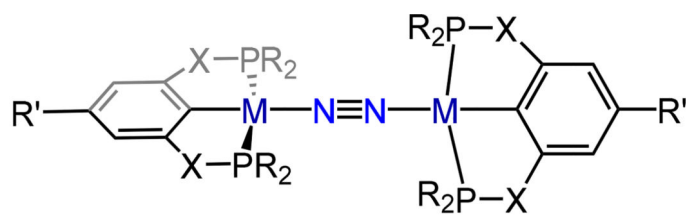
Name, M	R, X, R'	d(N−N)(Å)	ν_{N-N} (cm^{-1})
151-1, Rh	^{i}Pr, O, H	1.122(11)	
151-2, Ir	^{t}Bu, O,	1.119(6)	
151-3, Rh	^{i}Pr, CH$_2$, H	1.108(3)	
151-4, Ir	^{t}Bu, CH$_2$, H	1.134(2)	1979

Figure 123.
PCP-pincer dinuclear rhodium- or iridium-dinitrogen complexes, 151–1 to −4.
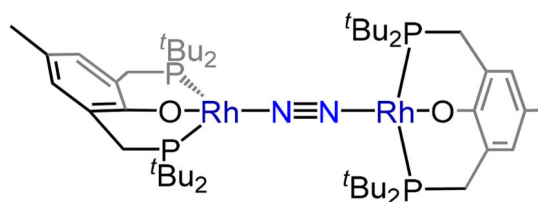
151-5
d(N−N): 1.129(4) Å
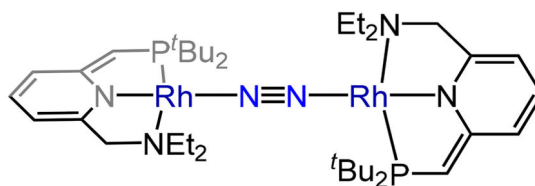
151-6
d(N−N): 1.124(3) Å
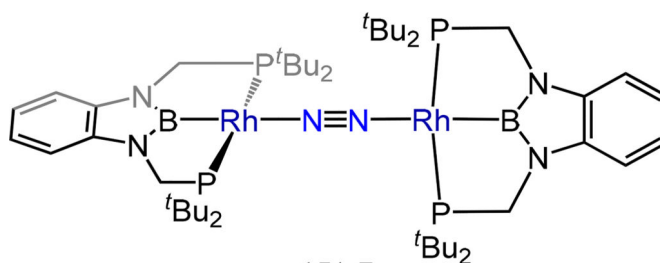
151-7
d(N−N): 1.106(4) Å, ν_{N-N}: 2063 cm^{-1}
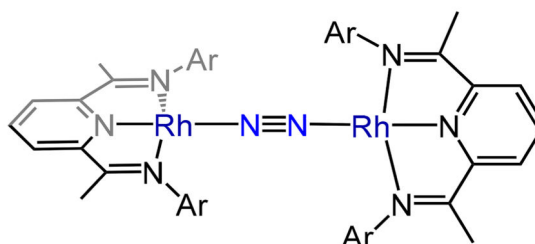
151-8
d(N−N):1.130(7) Å
Ar = 2,6-dimethylphenyl

Figure 124.
Pincer-based dirhodium-dinitrogen compounds, 151–5 to −8.
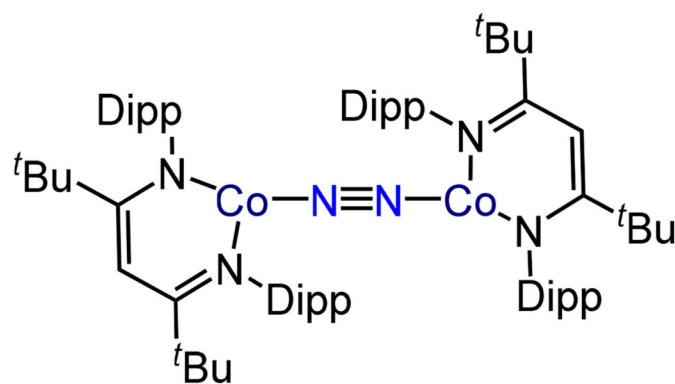
152-^{t}Bu

d(N−N): 1.1390(15) Å
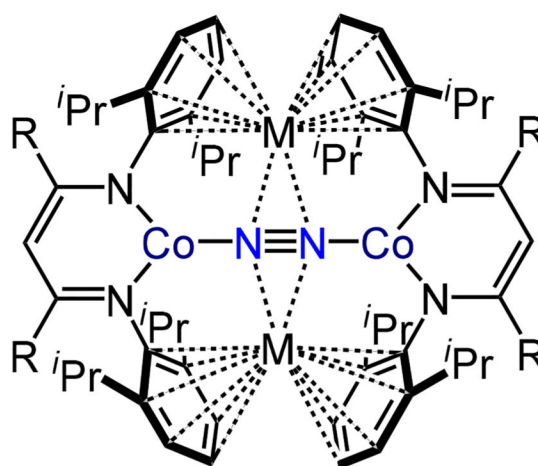
152-R/2M	d(N−N) (Å)	ν_{N-N}(cm^{-1})
152-^{t}Bu/2Na	1.211(3)	1598
134-^{t}Bu/2K	1.220(2)	1599
134-Me/2K	1.215(3) 1.220(4)	1568

Figure 125.
Bis(β-diketiminatocobalt)(μ–1,2-dinitrogen) complexes, 152.
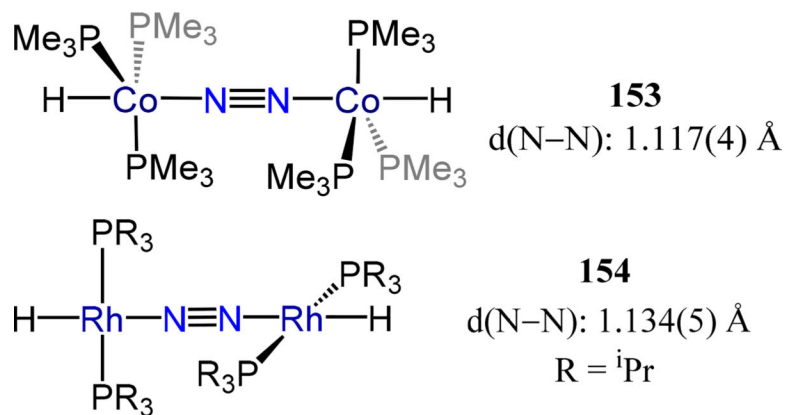
Figure 126.
Bis[hydrido-tris(trimethylphosphine)cobalt](μ–1,2-dinitrogen), 153 and bis[*trans*-hydrido-bis(triisopropylphosphine)rhodium](μ–1,2-dinitrogen), 154.
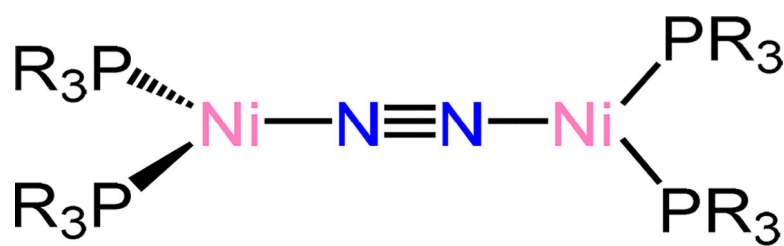
155-R

R = Cy

d(N–N): 1.1285(2) Å

R = ^{i}Pr

d(N–N) = 1.158(5) Å

ν_{N-N} = 1908 cm^{-1}

Figure 127.
Dinickel-dinitrogen complexes, 155-R.
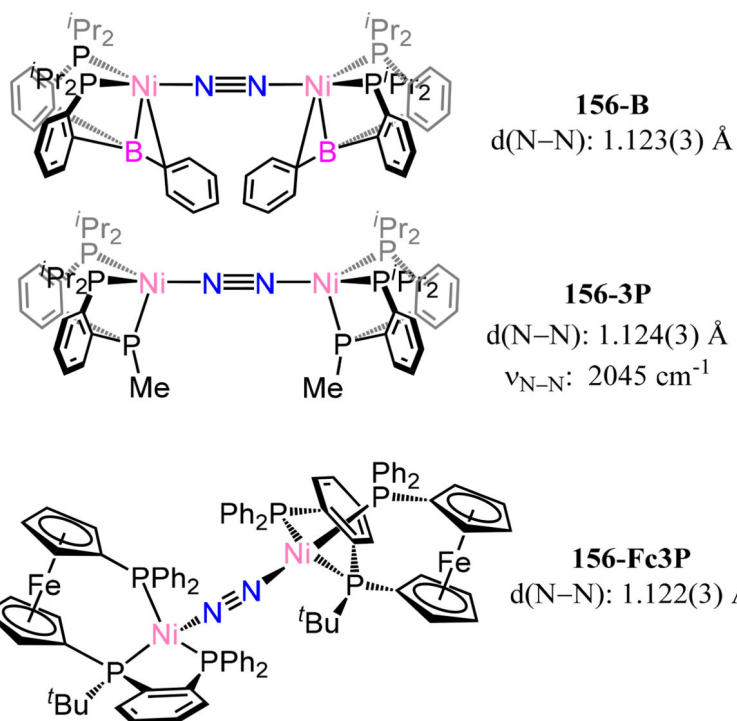
Figure 128.
Dinuclear nickel-dinitrogen adducts 156 bearing *fac*-coordinating tridentate ligands.

158

d(N−N): 1.144(3) Å
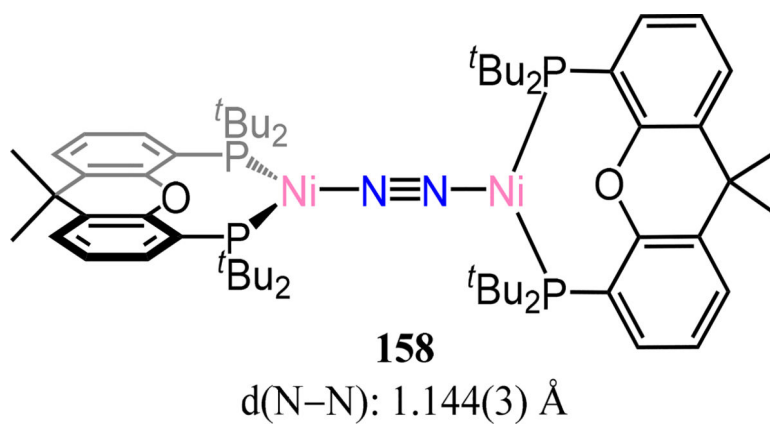
Figure 129.
Xantphos-ligated dinickel-*μ*–1,2-dinitrogen complex, 158.

159
d(N−N): 1.120(4) Å
ν_{N-N}: 2164 cm^{-1}

159-1K
d(N−N): 1.143(8) Å
ν_{N-N}: 1825 cm^{-1}
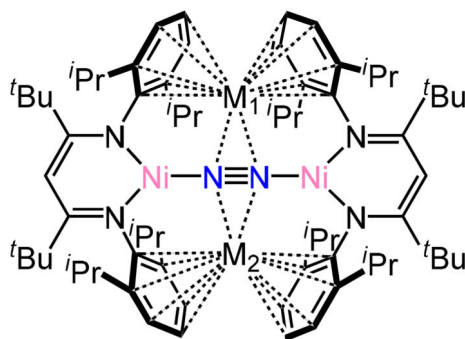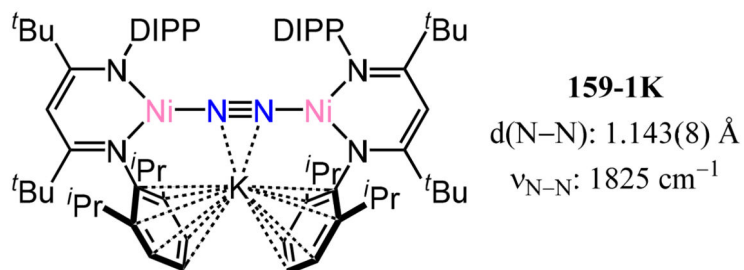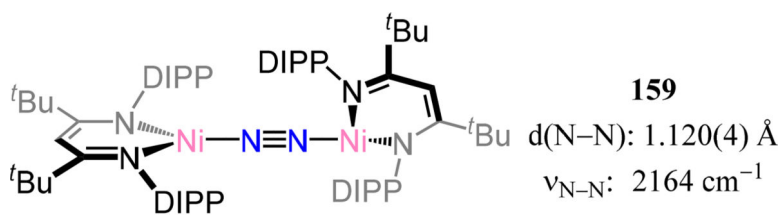
Name	d(N−N) Å	ν_{N-N} (cm^{-1})
159-2K	1.185(8)	1698
159-Na,K	1.195(4)	1689
159-2Na	1.192(3)	1685

Figure 130.
[Bis(β-diketiminatonickel)](μ–1,2-N$_2$) complexes 159.
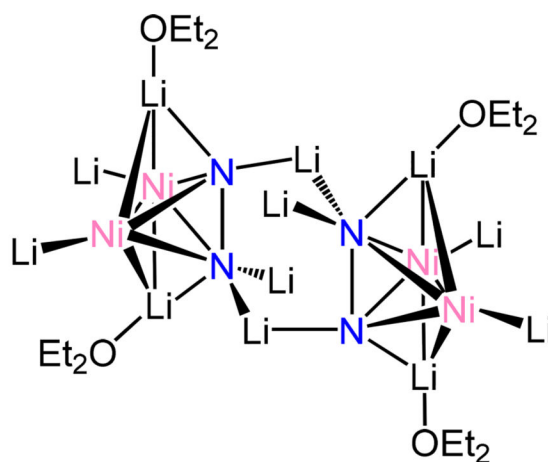
Internal skeleton of complex **160-1**
d(N−N): 1.35 Å
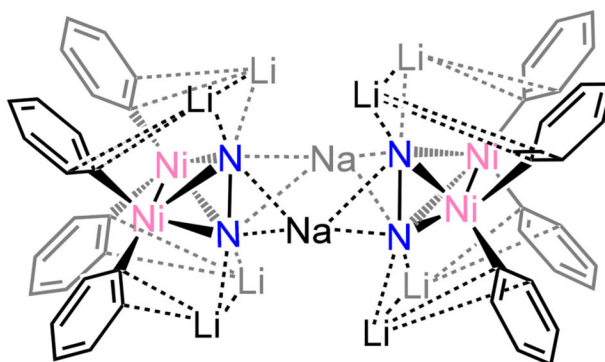
*Some Li atoms and solvent molecules are omitted
for clarity
160-2
d(N−N): 1.359(18) Å

Figure 131.
Side-on/side-on coordinated N_2 in phenylide Ni clusters (160).

161
d(N−N): 1.0854(1) Å
ν_{N-N}: 1952 cm^{-1}
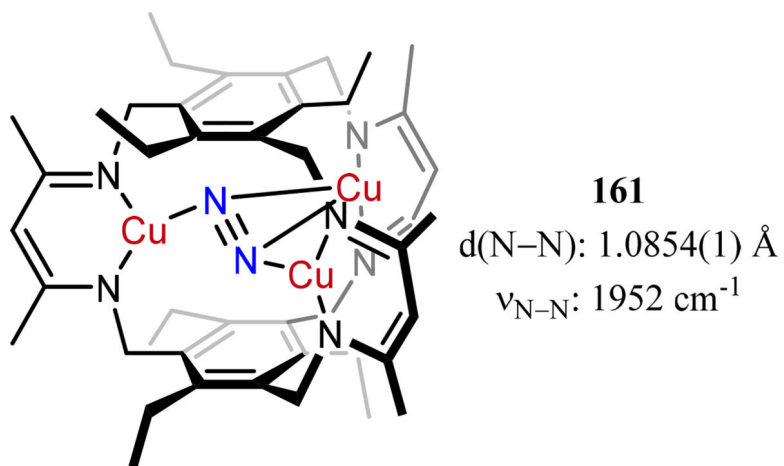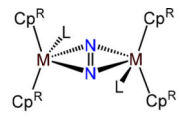
Figure 132.
Tricopper(I)-μ-η^1:η^2:η^1-N$_2$ unit housed in a tris(β-diketiminato)cyclophanate ligand scaffold.

162
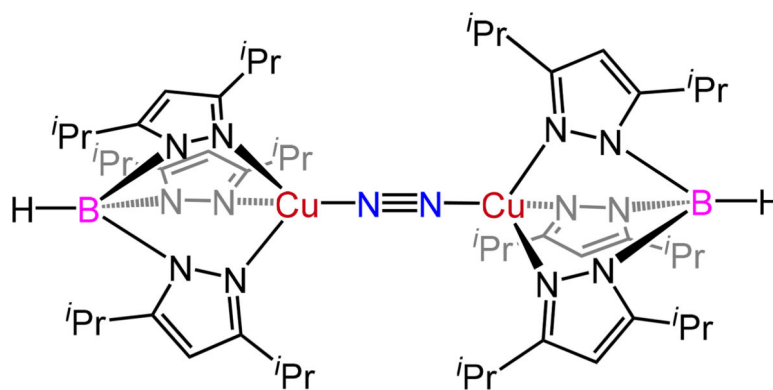
d(N–N): 1.112(5) Å

ν_{N-N}: 2130 cm^{-1}

Figure 133.
Dicopper(I)-μ–1,2-dinitrogen complex supported by tris(pyrazolyl)borates.
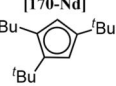
	CpR	d(N–N) Å	ν_{N-N} (cm⁻¹)
M = Y, L = none	[164-M]	1.172(6)	1428
M = Sm, L = none		1.088(12)	1416
M = Gd, L = none		1.236(5)	1432
M = Tb, L = none		1.238(4)	1433
M = Tm, L = none			
M = Lu, L = none		1.111(5)–1.239(12)	1406
M = Sc, L = none	[165-M]	1.239(3)	
M = Y, L = THF		1.252(5)	
M = La, L = THF		1.243	
M = Ce, L = THF		1.235(6)	
M = Pr, L =THF			1461
M = Nd, L = THF		1.243	1473
M = Gd, L = THF		1.247(3)	1457
M = Tb, L = THF		1.247 Å	
M = Dy, L = THF		1.243(7)	1454
M = Lu, L = THF		1.243(12)	
M = Y, L = THF	[166-M]	1.250(2)	1454
M = Dy, L = THF		1.250(4)	1453
M = Tm, L = THF	[168-Tm]	1.236(8)	
M = Tm, L = none	[169-M]	1.259(4)	
M = Dy, L = none			
M = Nd, L = none	[170-Nd]	1.226(12)	1622
M = La, L = THF	[167-M]	1.243	
M = Ce, L = THF		1.258(9)	
M = Pr, L = THF		1.242(9)	

Figure 134.
$[(Cp^R)_2RE](\mu\text{-}\eta^2\text{:}\eta^2\text{-}N_2)$ complexes 164–167.
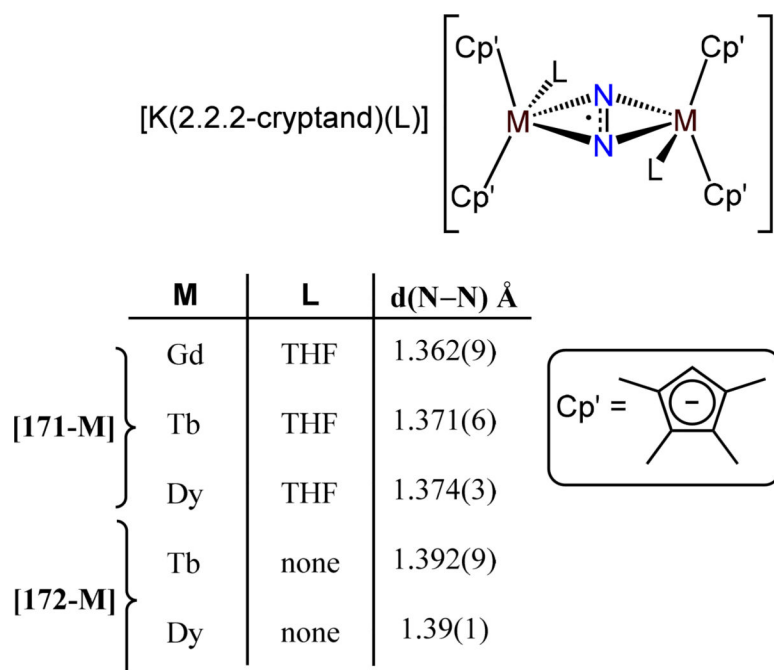
Figure 135.
Reduced bis[bis(tetramethylcyclopentadienyl)RE](μ-η^2:η^2-N$_2$) complexes 171 and 172 with formal N$_2^{3-}$ ligands.
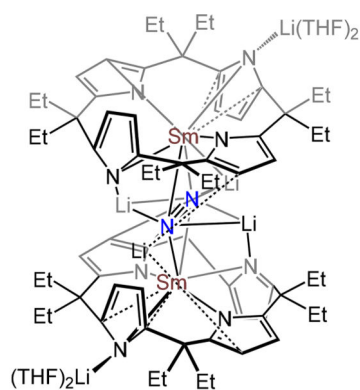
173-Sm
d(N−N): 1.525(4) Å
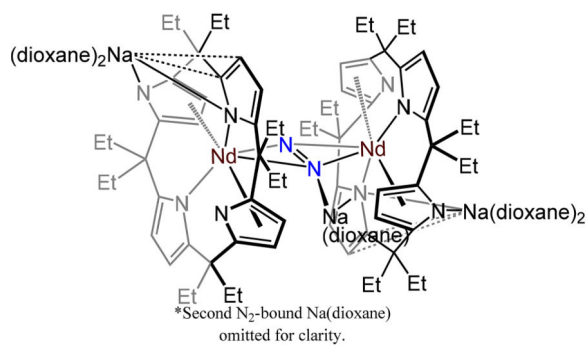
173-Nd
d(N−N): 1.234(8) Å
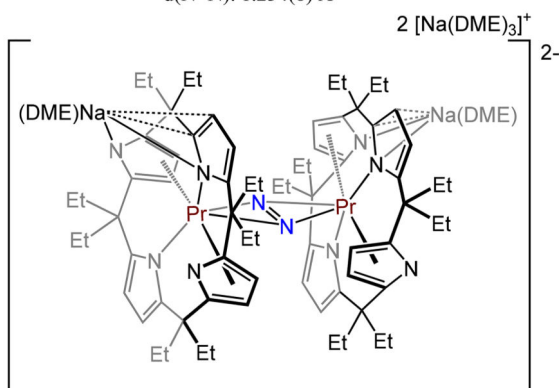
173-Pr
d(N−N): 1.254(7) Å

Figure 136.
Dinuclear Sm-, Nd-, or Pr-(μ-η^2:η^2-N$_2$) adducts (173-M) supported by *meso*-octaethylporphyrinogen (OEP) ligands.
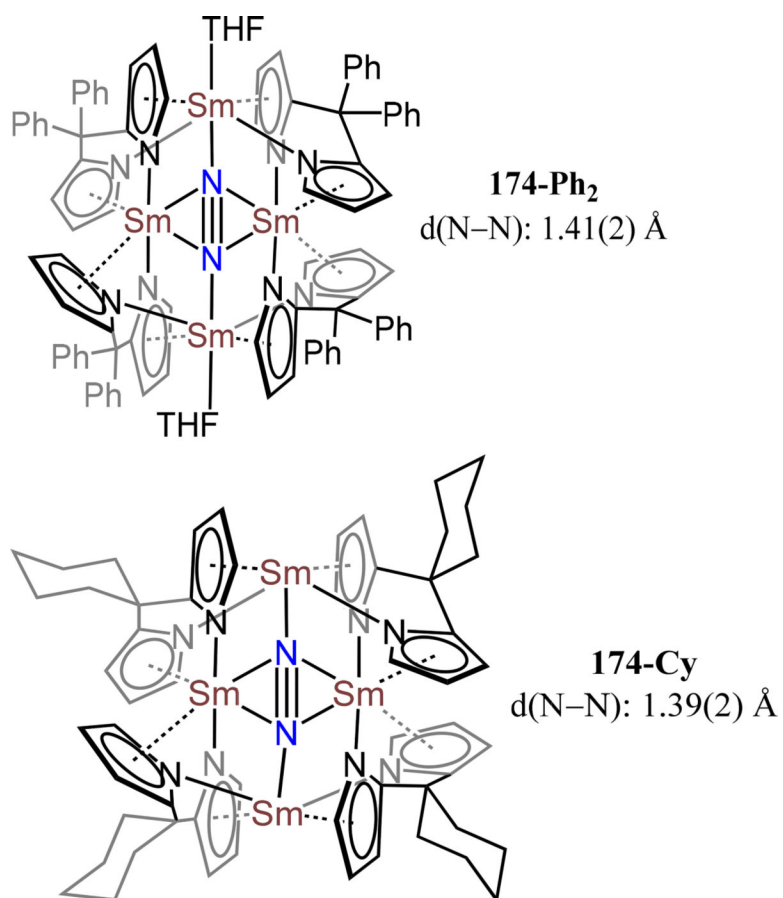
Figure 137.
Tetranuclear samarium-(μ_4-η^2:η^2:η^1:η^1-N$_2$) complexes 174 supported by dipyrrolide ligands.

175-Pr
175-Sm, d(N–N) = 1.62(2) Å
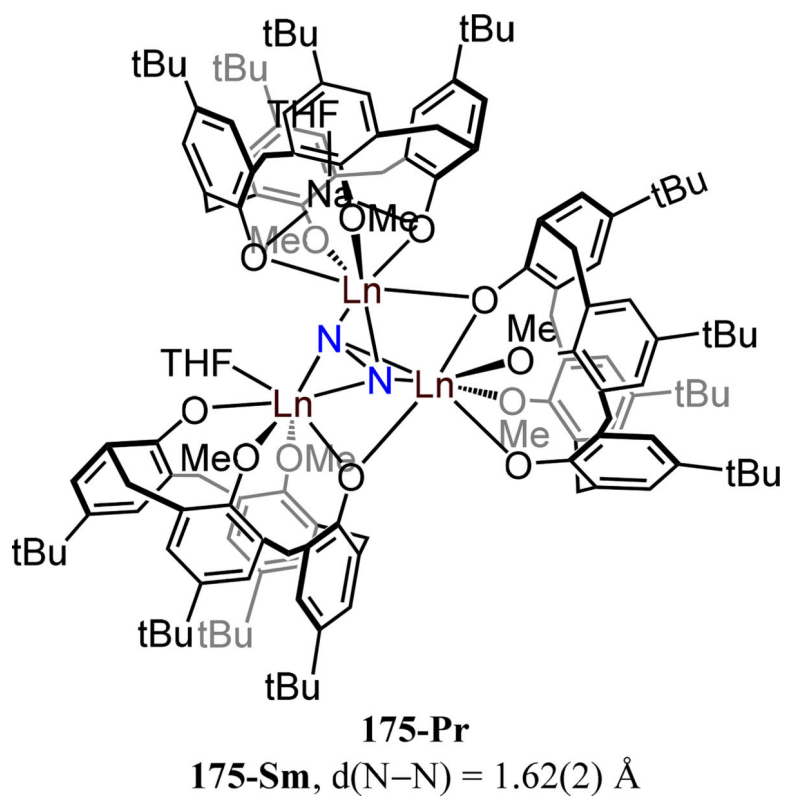
Figure 138.
Trinuclear Ln-(μ_3-η^2:η^2:η^2-N$_2$) complexes 175-M.

X = (Me₃Si)₂N y = 1		
RE	**d(N–N) Å**	ν_{N-N} (cm⁻¹)
Y	1.268(3)	1425
Nd	1.258(3)	1447
Gd	1.278(4)	1432
Tb	1.271(4)	1428
Dy	1.305(6)	1425
Ho	1.264(4)	1421
Er	1.276(5)	1417
Tm	1.264(7)	1413
Lu	1.285(4)	

176-RE,X

X = 2,6-ᵗBu₂-OC₆H₃ y = 2	
RE	**d(N–N) Å**
Nd	1.242(7)
Dy	1.257(7) 1.256(9)

Figure 139.
Amide and alkoxide dimetallic RE-dinitrogen adducts 176-RE,X.

$$\left[\text{THF} \cdots X \cdots \underset{X}{\overset{X}{RE}} \cdots \underset{N}{\overset{N}{\cdots}} \cdots \underset{\text{THF}}{\overset{X}{RE}} \cdots X \right]^{-} \quad \mathbf{[176\text{-}RE,X]^{-}}$$

$$X = N(SiMe_3)_2$$
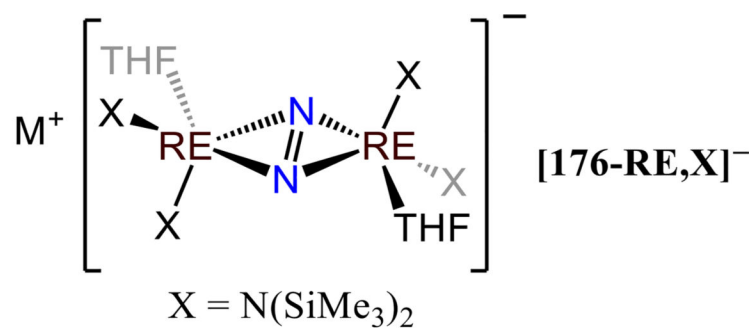
RE	M	d(N–N) Å
Y	K(18c6)(THF)$_2$	1.396(3)
Y	Na(THF)$_6$	1.393(7)
Y	K(THF)$_6$	1.401(6)
Gd	K(18c6)(THF)$_2$	1.400(2)
Tb	K(18c6)(THF)$_2$	1.394(3)
Dy	K(18c6)(THF)$_2$	1.400(2)
Ho	K(18c6)(THF)$_2$	1.405(3)
Er	K(18c6)(THF)$_2$	1.409(3)
Er	Na(THF)$_6$	1.403(4)
Lu	K(THF)$_6$	1.414(8)

18c6 = 18-crown-6

Figure 140.
Anionic dimetallic rare-earth dinitrogen complexes [176-RE,X]⁻ featuring a side-on/side-on coordinated N2^{3-} ligand.

177-RE,X
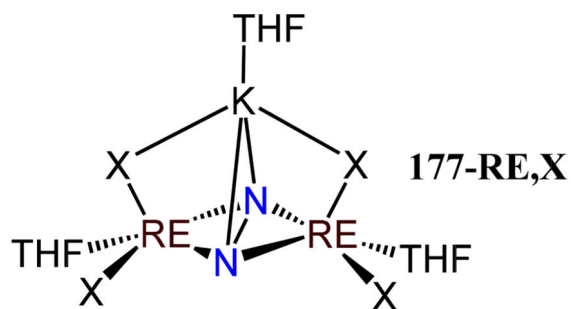
X = $(Me_3Si)_2N$	
RE	**d(N−N) Å**
Y	1.405(X)
Gd	1.395(X)
Tb	1.401(X)
Dy	1.403(X)

X = 2,6-$^tBu_2$-OC_6H_3	
RE	**d(N−N) Å**
Dy	1.401(X)

Figure 141.
Complexes 177-RE,X.

{K(2.2.2-cryptand)}$_2$

$$\left[\begin{array}{c} (Me_3Si)_2N \quad\quad N(SiMe_3)_2 \\ (Me_3Si)_2N \diagdown\quad\quad\quad\diagup N(SiMe_3)_2 \\ Sc-N{=}N-Sc \\ (Me_3Si)_2N \quad\quad\quad N(SiMe_3)_2 \end{array} \right]$$

178
d(N−N): 1.221(3) Å
ν_{N-N}: 1644 cm^{-1}
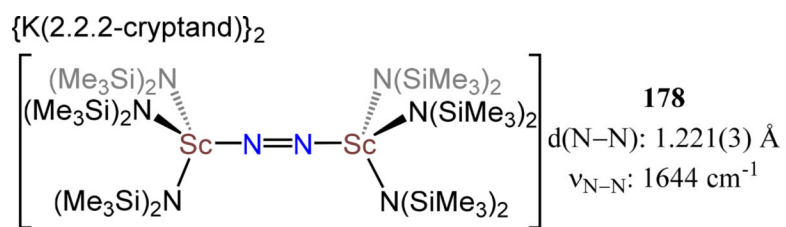
Figure 142.
Bis[tris(hexamethyldisilazido)scandium](μ−1,2-dinitrogen), 178.
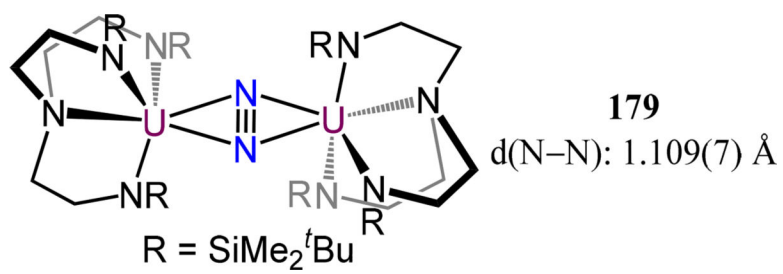
Figure 143.
Tren^{3-}-chelated diuranium-μ-η^2:η^2-dinitrogen complex, 179.
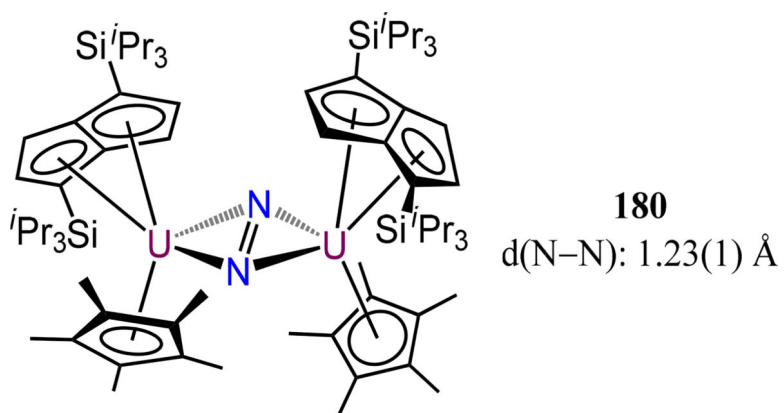
Figure 144.
Diuranium-μ-η^2:η^2-dinitrogen complex 180.

181-Di
Ar = 2,6-^{t}Bu$_2$C$_6$H$_4$
d(N−N): 1.16(2), 1.20(2), 1.20(2) Å

181-Tri
Ar = 2,4,6-^{t}Bu$_3$-C$_6$H$_3$
d(N−N): 1.19(2) Å
ν_{N-N}: 1451 cm^{-1}
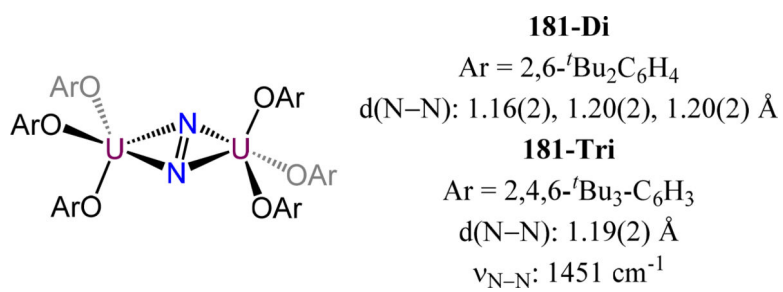
Figure 145.
Aryloxide-supported diuranium-μ-η^2:η^2-dinitrogen complexes, 181.
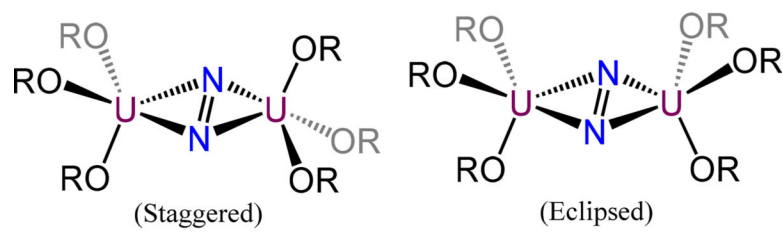
182

Staggered d(N-N): 1.08(1) Å
Eclipsed d(N-N): 1.12(1) Å
R = Si(2,4,6-Me$_3$C$_6$H$_2$)

Figure 146.
Isomers of [U{OSi(Mes)$_3$}$_3$]$_2$(μ-η^2:η^2-N$_2$), 182.
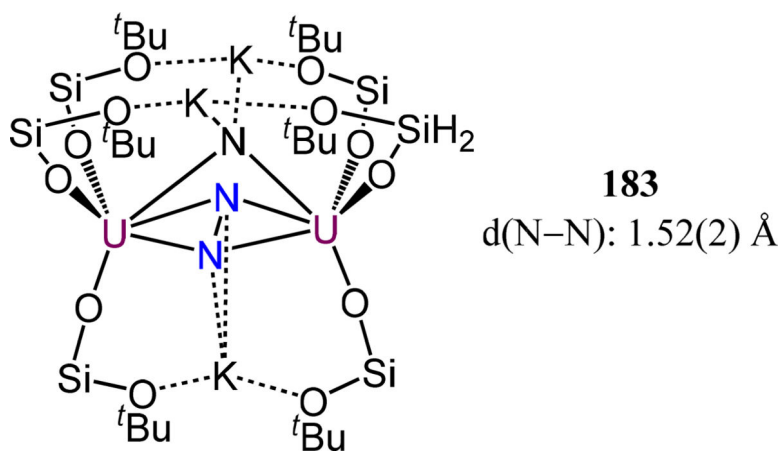
Figure 147.
Siloxide-supported diuranium-μ-η^2:η^2-N$_2$ complex 183 with a butterfly U$_2$N$_2$ core and a μ-N^{3-}.

$$N_2 + e^- \rightleftharpoons N_2^- \qquad E^o = -4.16 \text{ V}$$

$$N_2 + H^+ + e^- \rightleftharpoons N_2H \qquad E^o = -3.20 \text{ V}$$

$$N_2 + 2H^+ + 2e^- \rightleftharpoons N_2H_2 \qquad E^o = -1.10 \text{ V}$$

$$N_2 + 4H^+ + 4e^- \rightleftharpoons N_2H_4 \qquad E^o = -0.33 \text{ V}$$

$$N_2 + 6H^+ + 6e^- \rightleftharpoons 2 NH_3 \qquad E^o = -0.148 \text{ V}$$
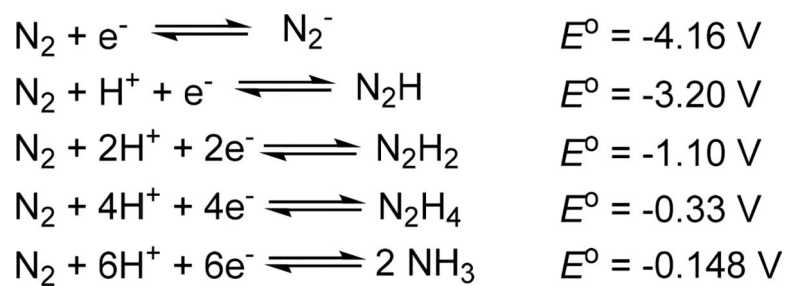
Scheme 1.
Reduction Potentials for N_2 vs. NHE
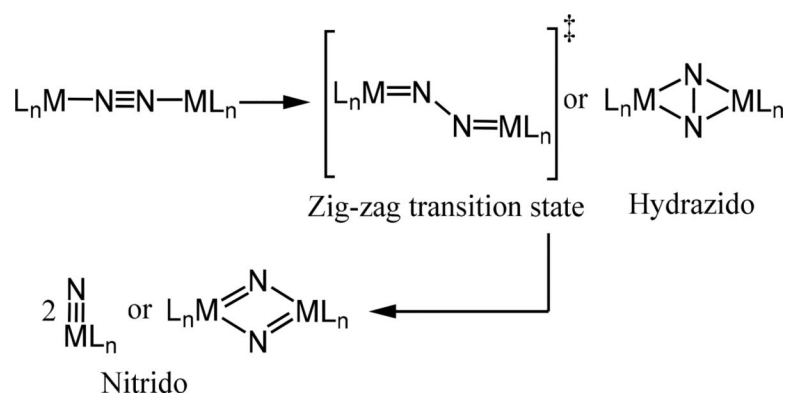
Scheme 2.
Proposed Dimetallic N_2 Scission Mechanism
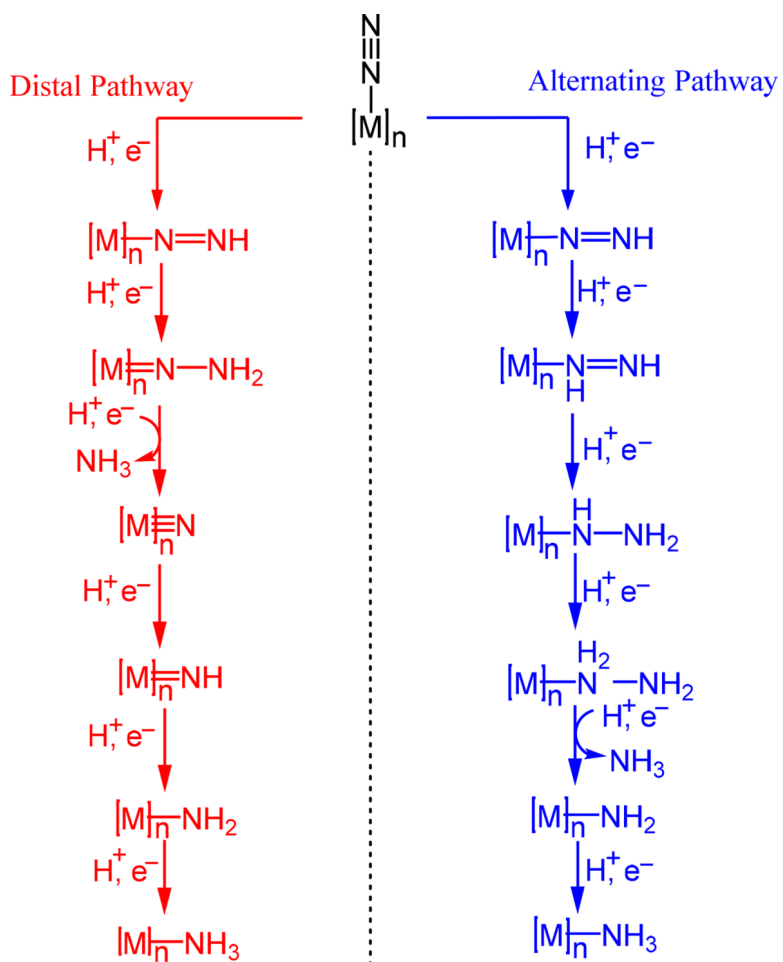
Scheme 3.

Possible PCET Pathways for N_2 to NH_3 Conversion.

Note: The scheme does not define the number of metal centers nor the coordination mode of N_2

10-A

KC$_8$ | AgBPh$_4$

10-B, L = Et$_2$O
d(N−N): 1.223(9) Å
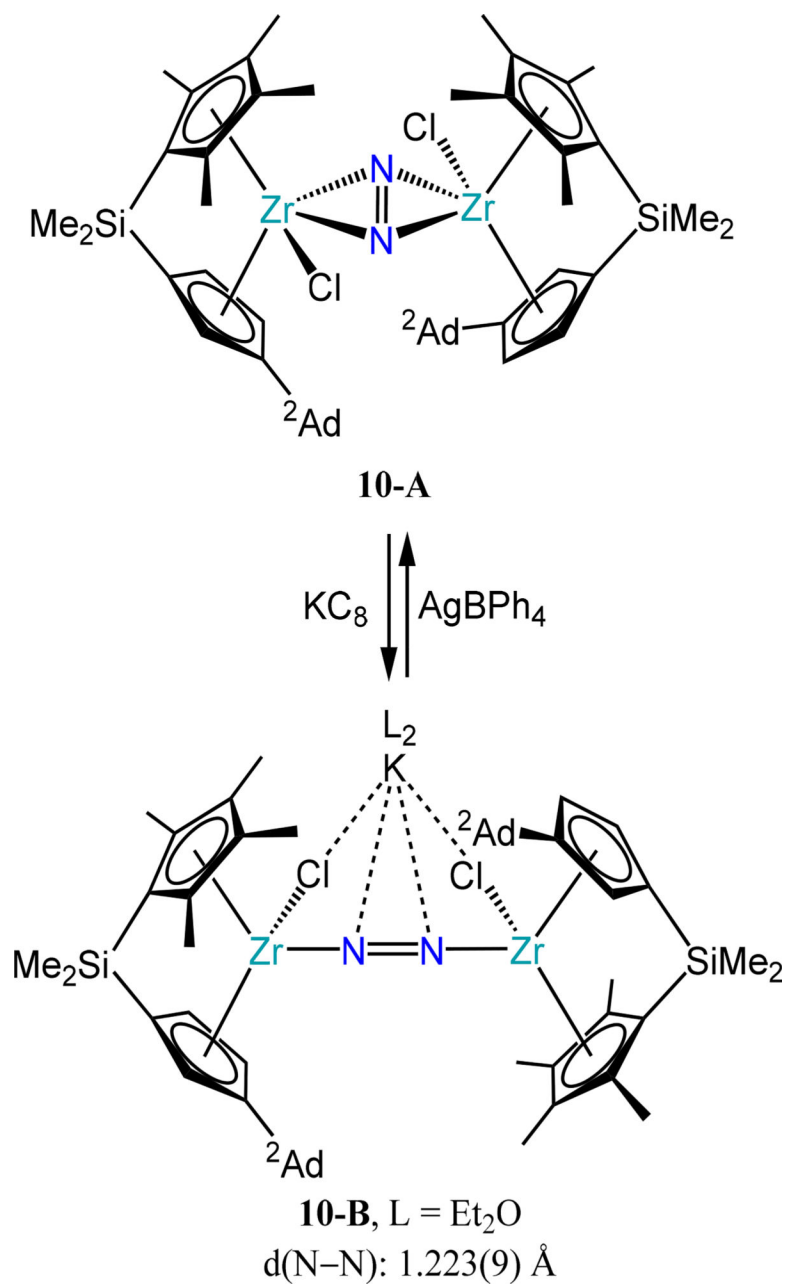
Scheme 4.
Conversion of 10-A to 10-B
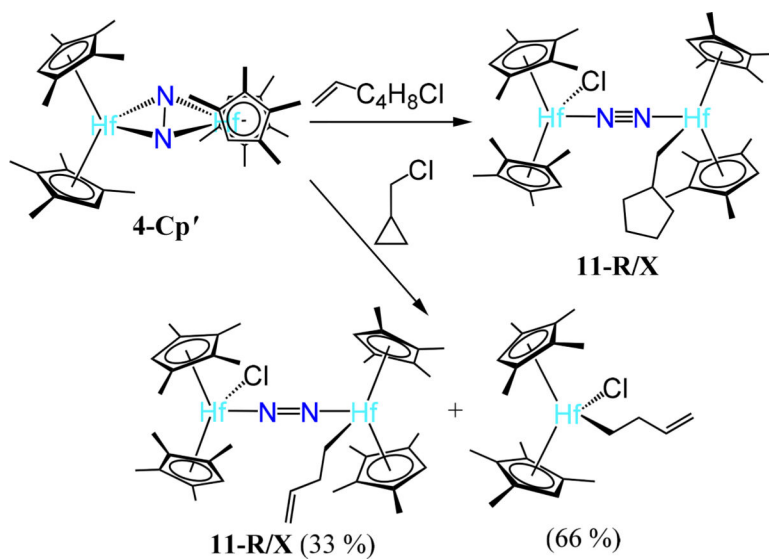
Scheme 5.
Reaction of 4-Cp′ With Radical Clock Substrates
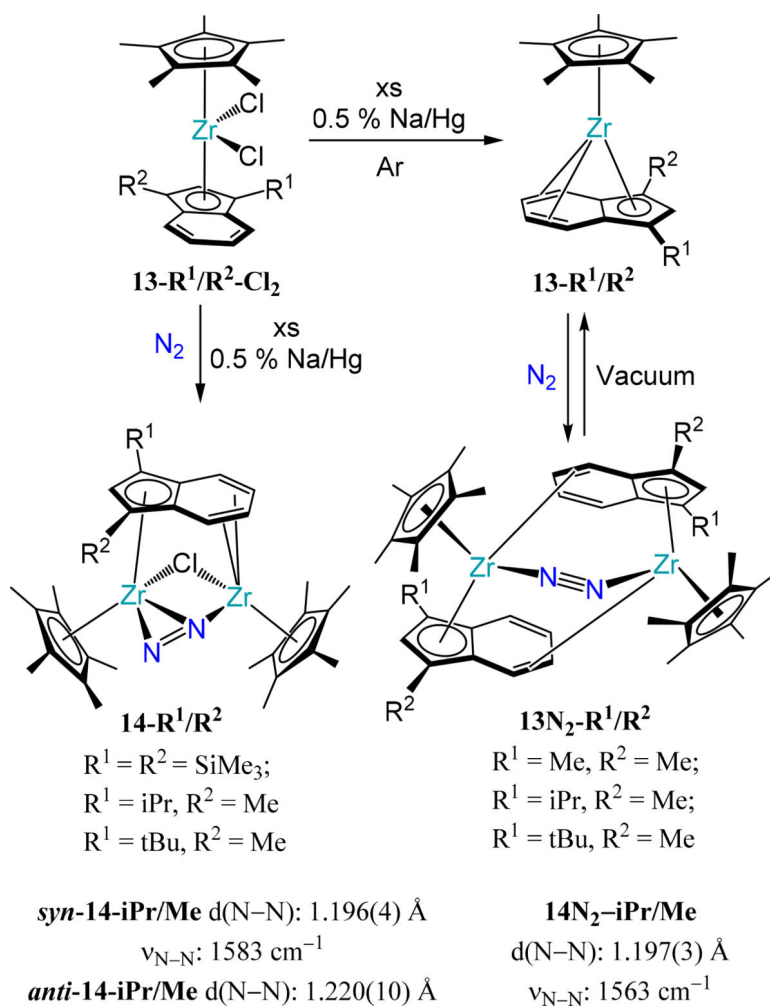
Scheme 6.
Reduction of 13-R^1/R^2-Cl$_2$
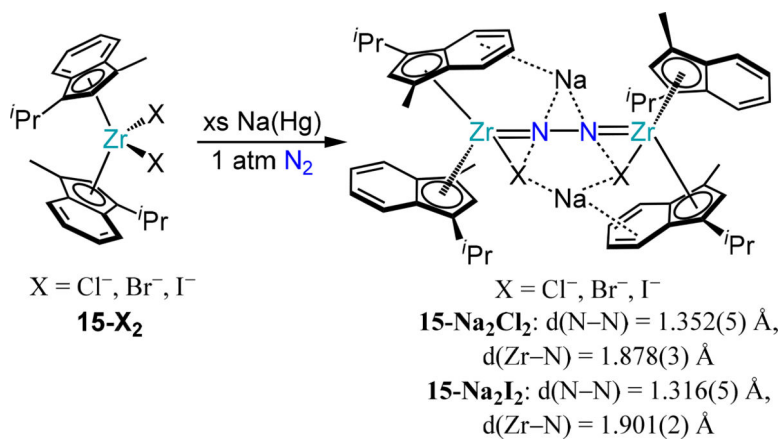
Scheme 7.
Reduction of 15-X$_2$ Under N$_2$ to Yield 15-Na$_2$X$_2$
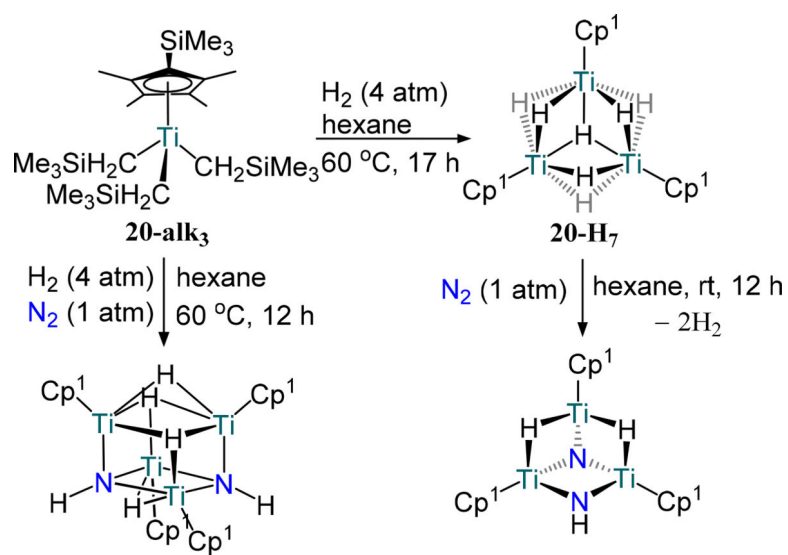
Scheme 8.
N_2 and H_2 activation by 20-alk$_3$

22-N$_2$
d(N−N): 1.43(1) Å

H$_2$
hexanes

22-N$_2$H/H
d(N−N): 1.389 Å
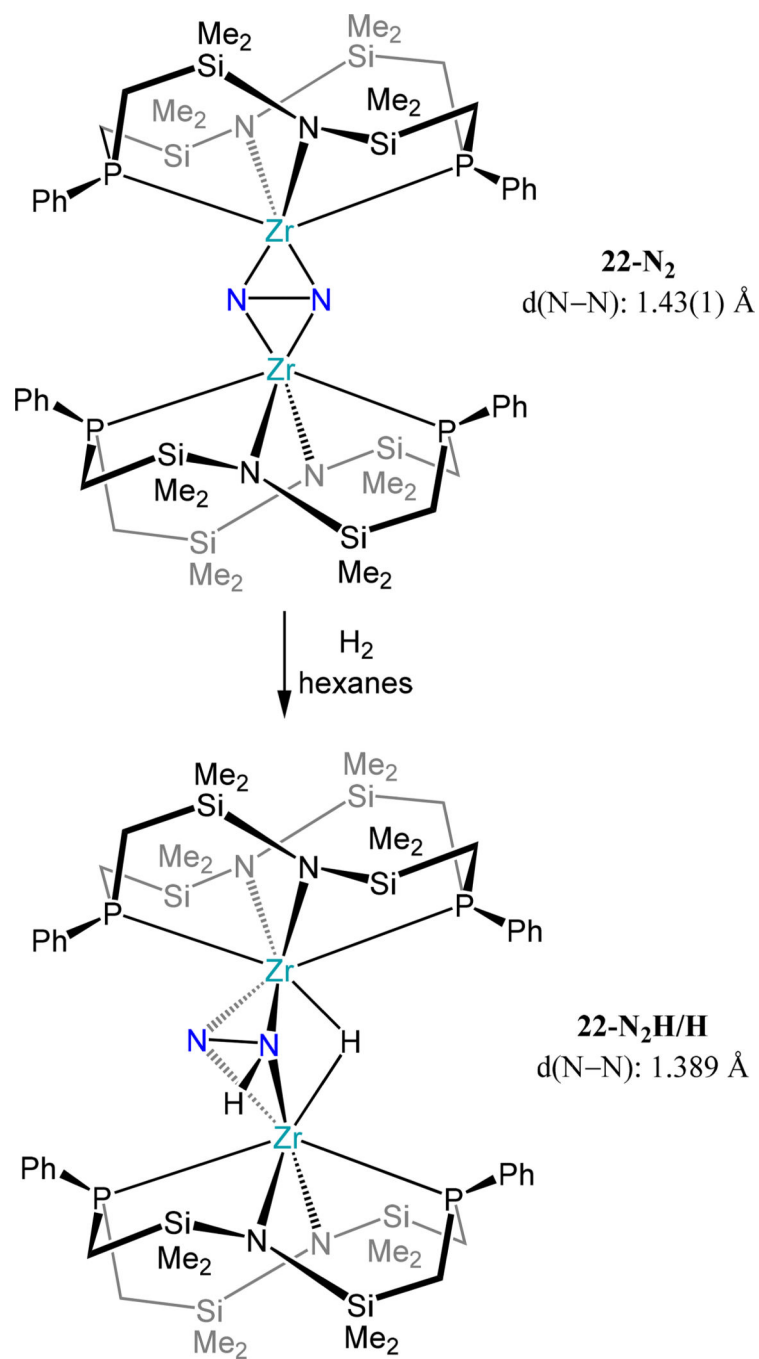
Scheme 9.
Reaction of 22-N$_2$ With H$_2$
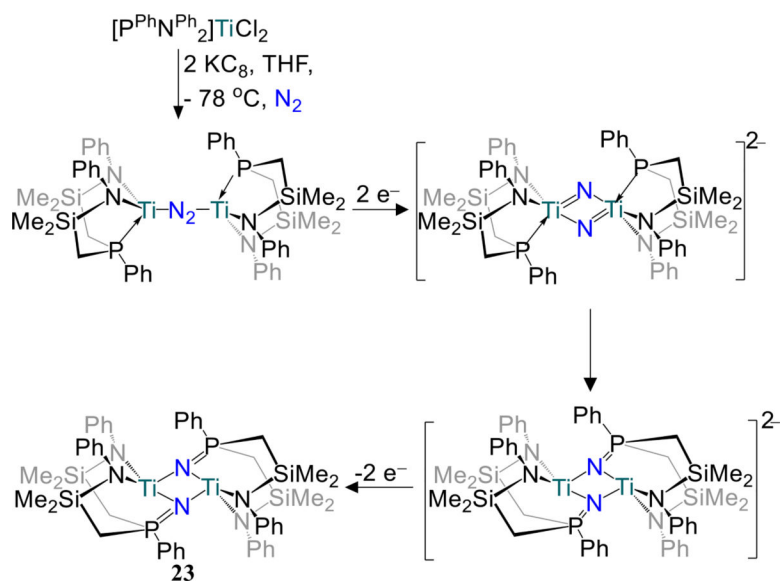
Scheme 10.
Proposed Mechanism for Formation of 23
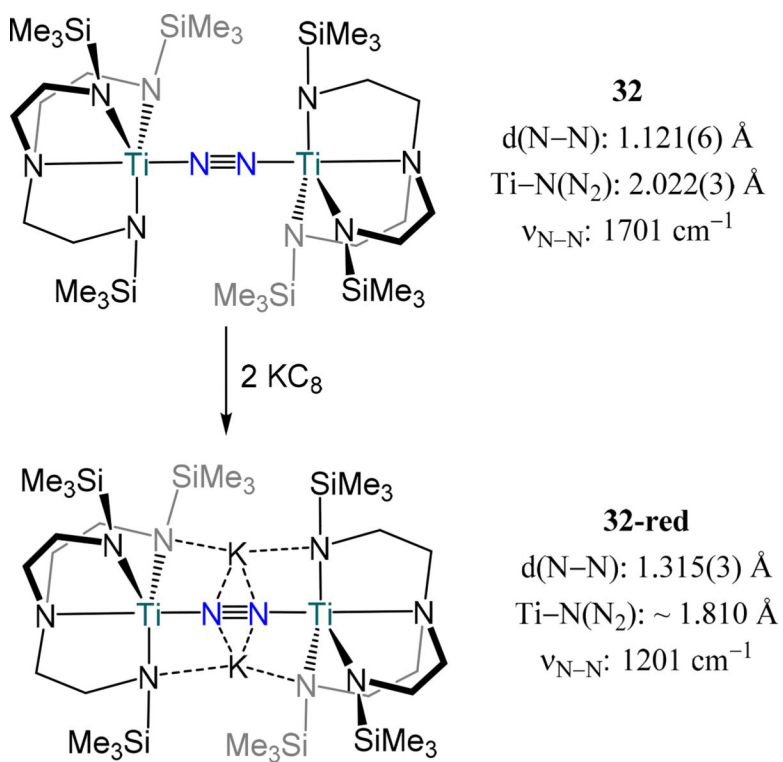
Scheme 11.
Two-electron reduction of 32
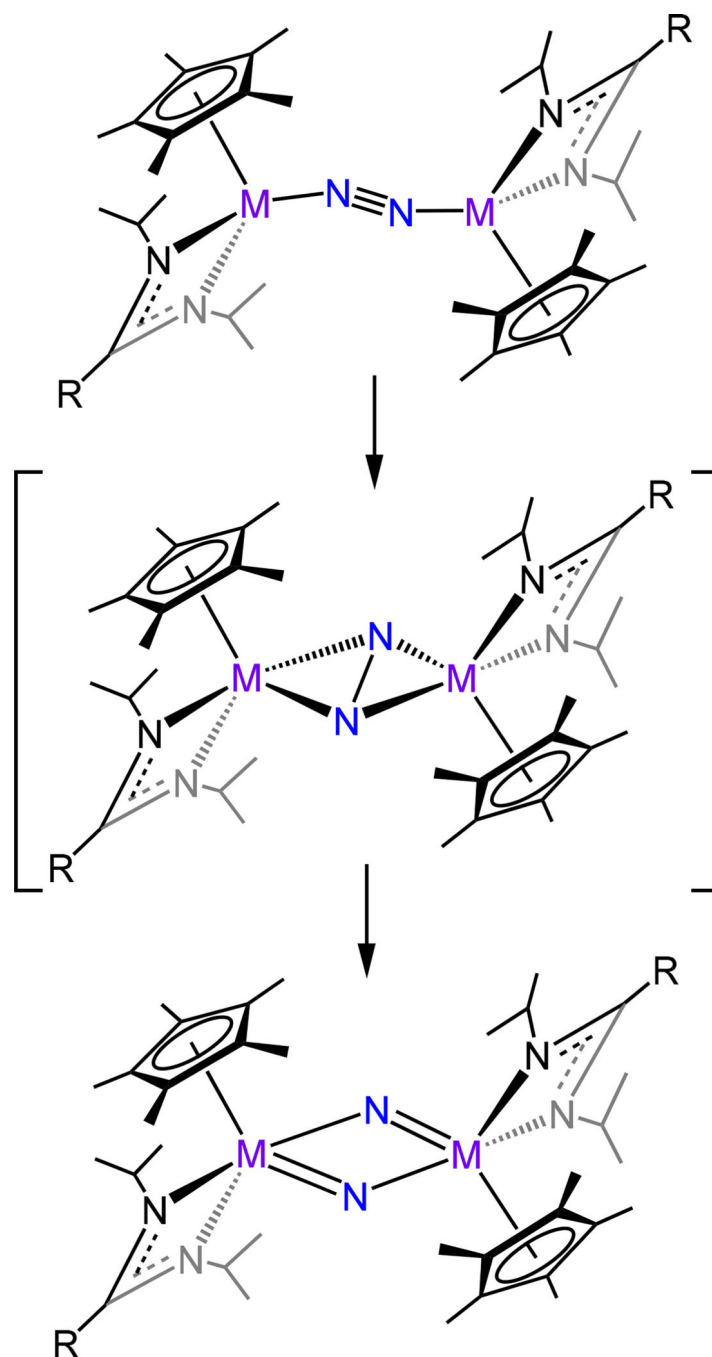
Scheme 12.
Proposed N_2 scission Via μ–1,2 to μ-η^2:η^2 Isomerization

39-Ta/R (R = Me, Ph, NMe₂)

N_2O (10 psi) | PhMe, –30°C
– N_2

40-Me: d(N–N) = 1.507(13) Å
40-Ph: d(N–N) = 1.504(4) Å
40-NMe₂: d(N–N) = 1.499(4) Å
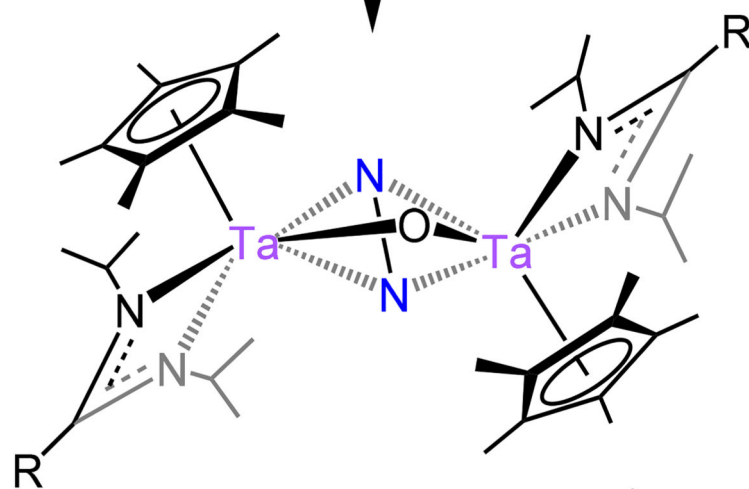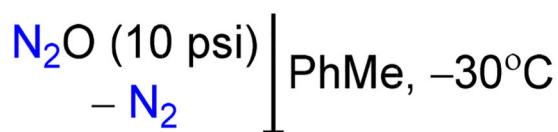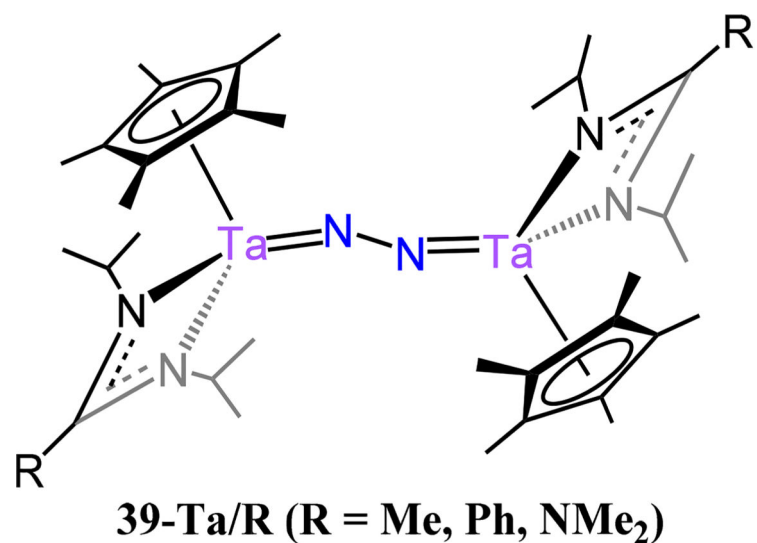
Scheme 13.
Reaction of 39-Ta/R With N_2O
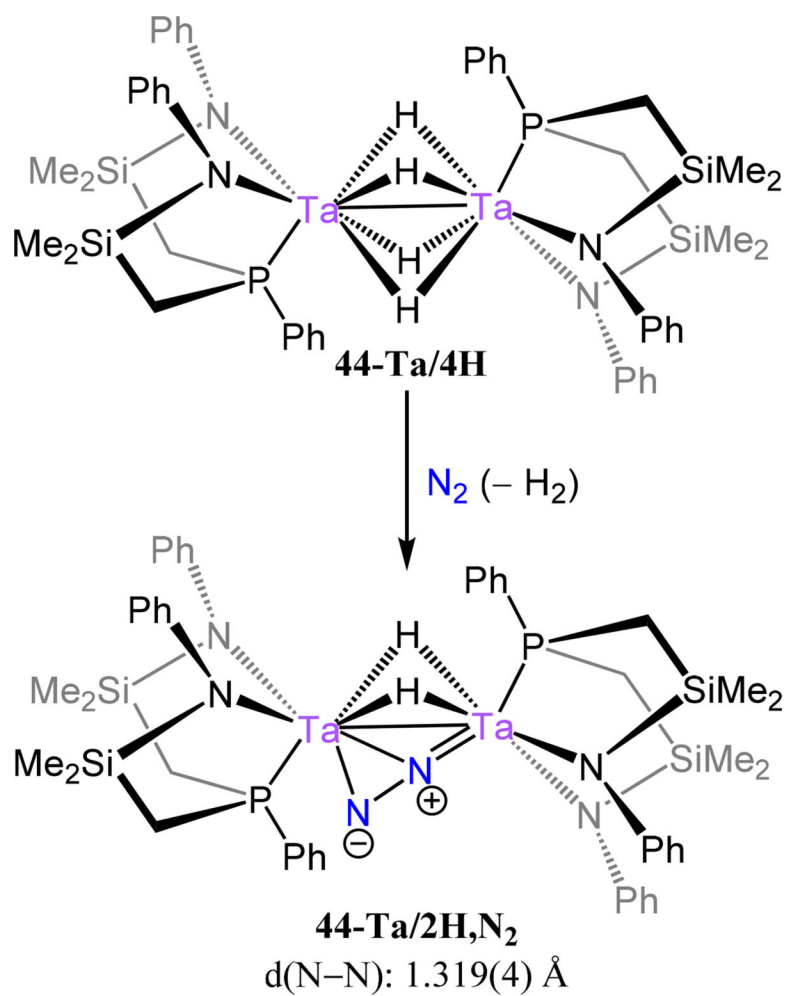
Scheme 14.
Synthesis of 44-Ta/2H$_2$N$_2$
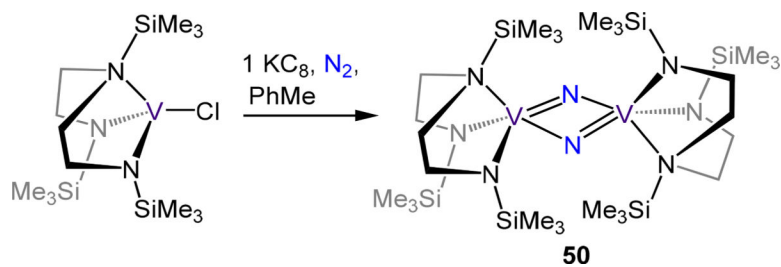
Scheme 15.
Synthesis of di(μ-nitride) 50
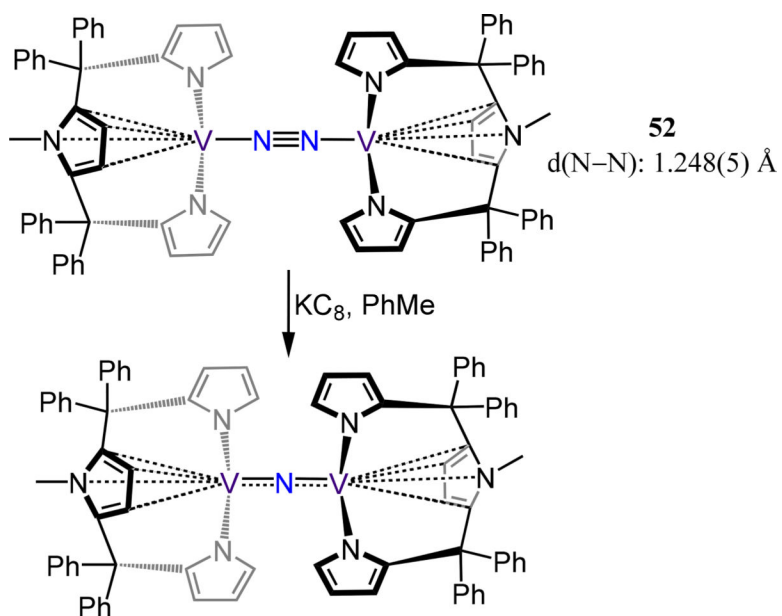
Scheme 16.
One-Electron Reduction of 52
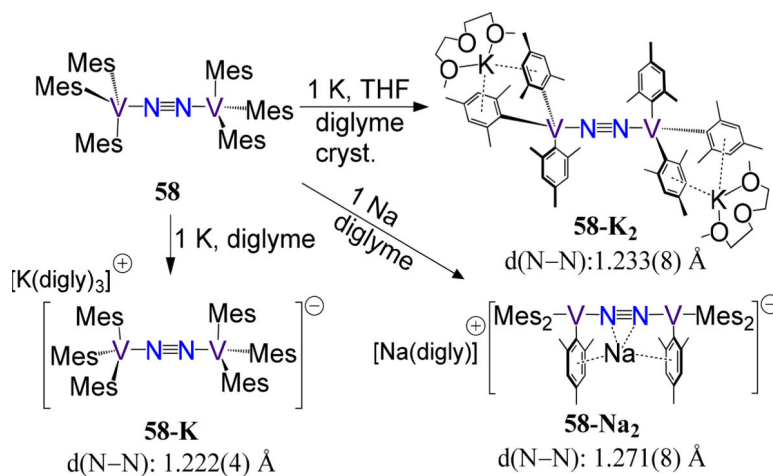
Scheme 17.
Reduction of 58
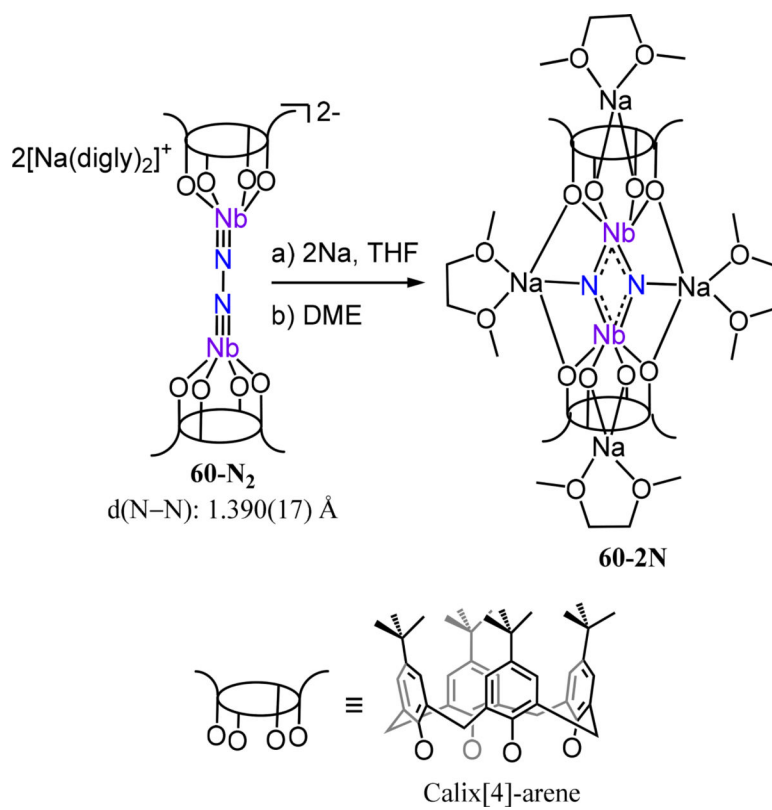
Scheme 18.
Reduction of 60-N$_2$
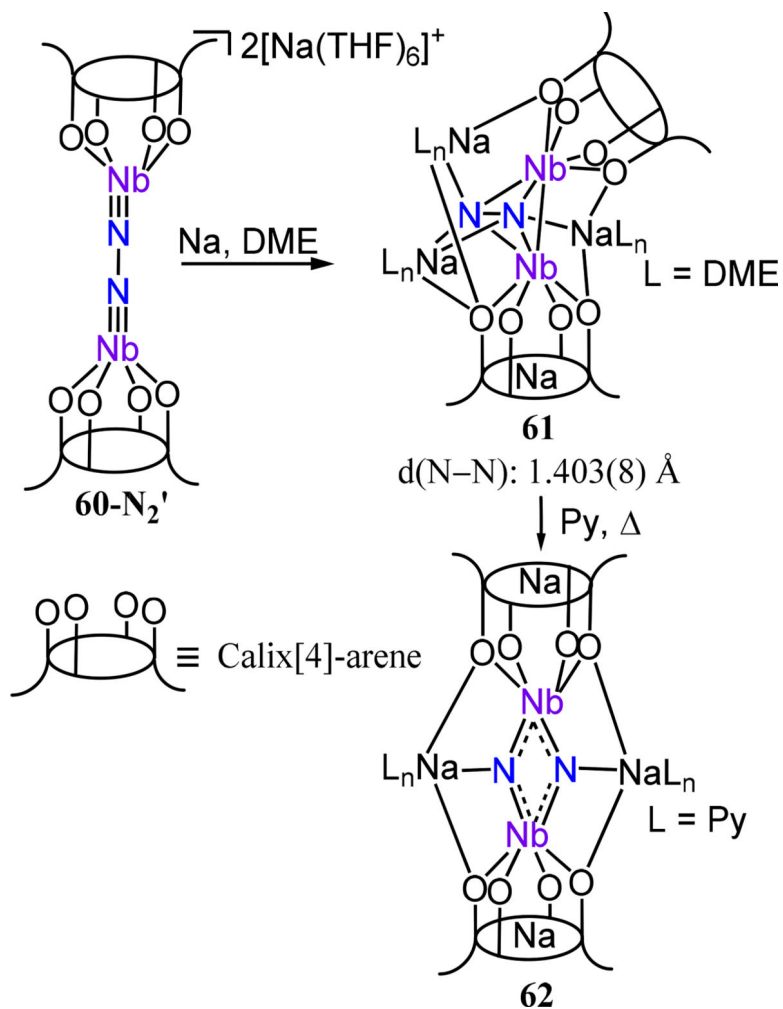
Scheme 19.
Reduction of the THF Solvate 60-N$_2$ $'$
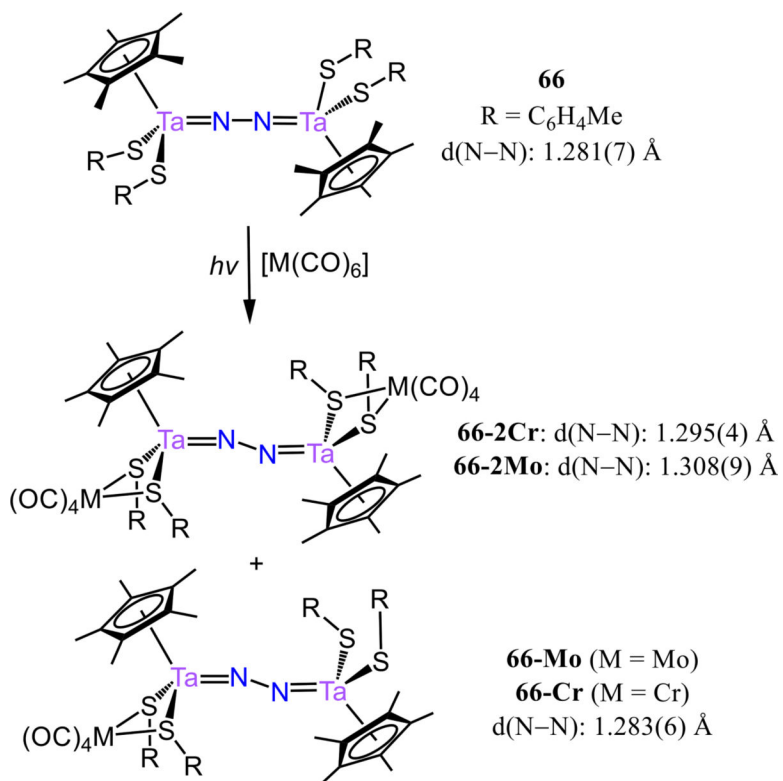
Scheme 20.
Synthesis of 66–2M (M = Cr, Mo) And 66-M (M = Cr, Mo)
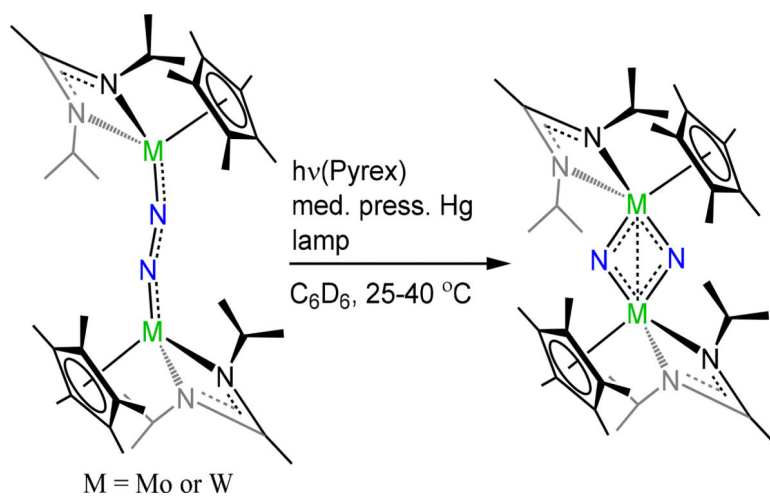
Scheme 21.
Photolysis of 73-M/N^{iPr},Me (M = Mo and W)
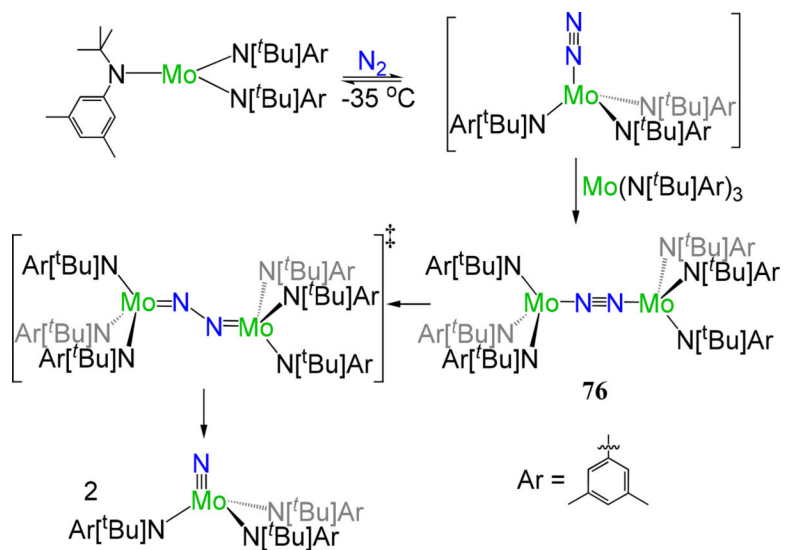
Scheme 22.
Proposed N_2 Cleavage Mechanism for Cummins' Tris(Anilido)Molybdenum(III) Complex
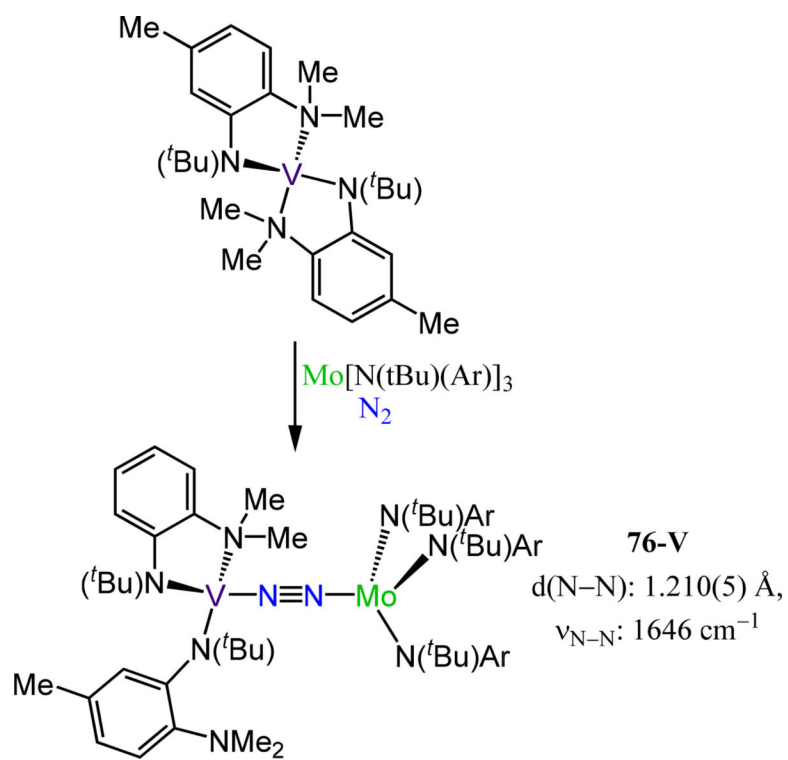
Scheme 23.
Synthesis of 76-V
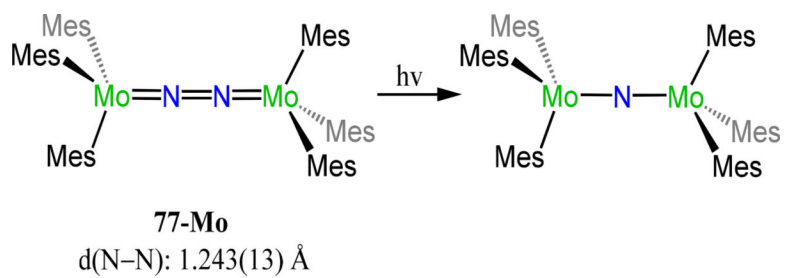
77-Mo
d(N−N): 1.243(13) Å

Scheme 24.
UV Irradiation of 77-Mo
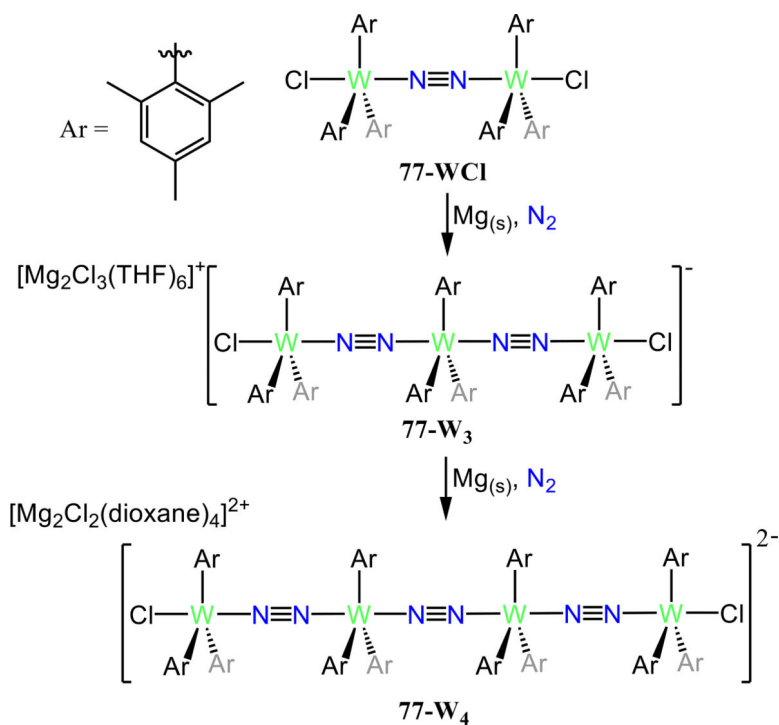
Scheme 25.
Synthesis of Multimetallic Tungsten Dinitrogen Complexes, 77-WCl, 77-W_3 And 77-W_4
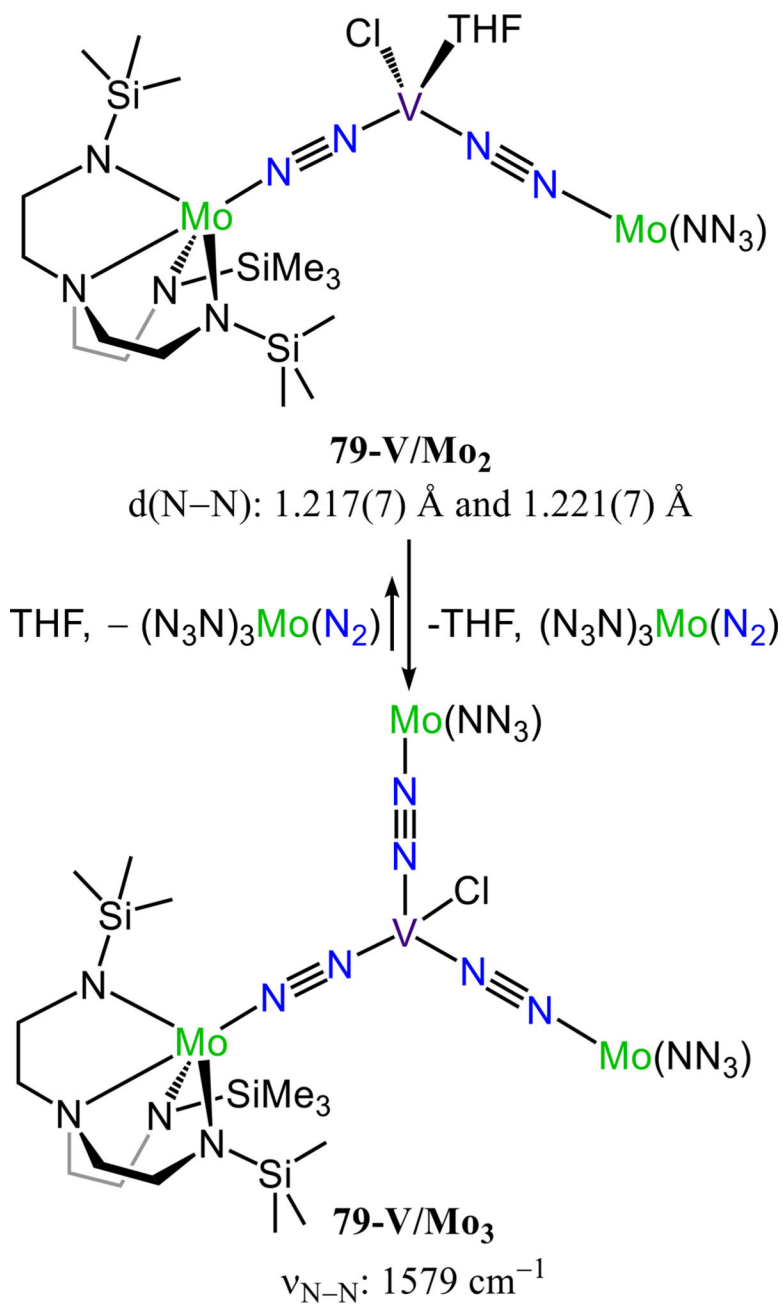
Scheme 26.
Interconversion of 79-V/Mo$_2$ and 79-V/Mo$_3$
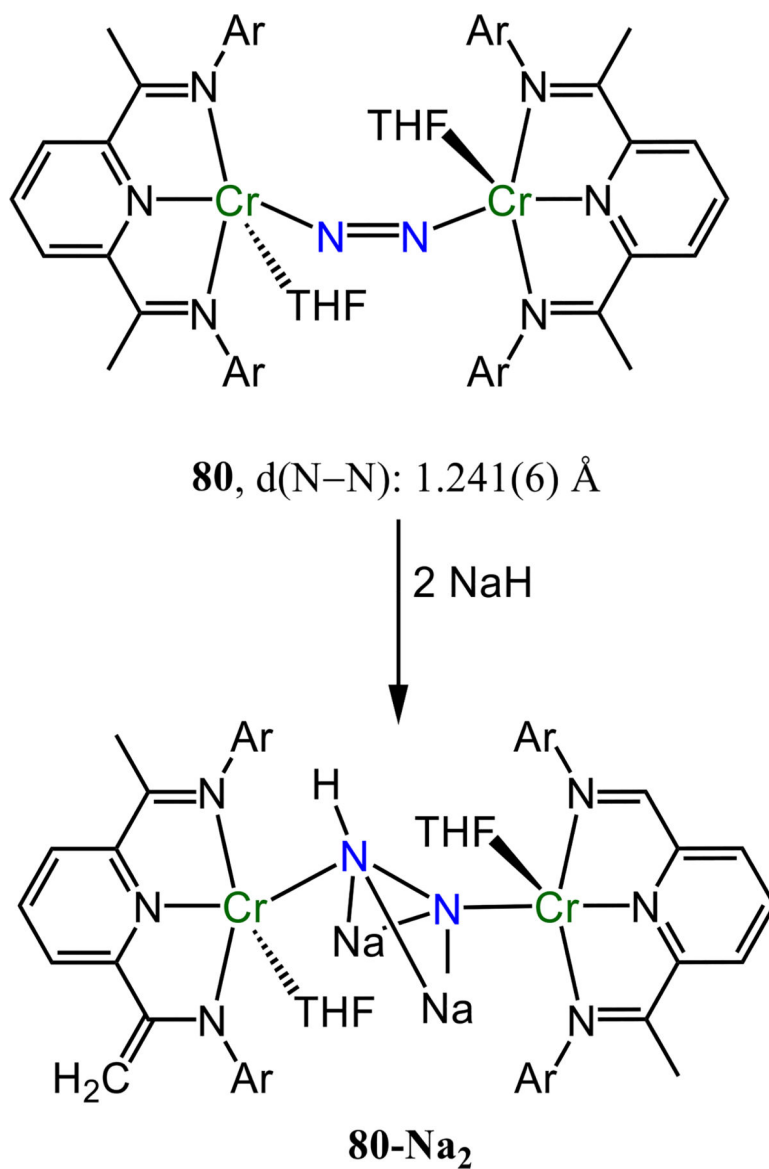
Scheme 27.
Reaction of 80 with NaH
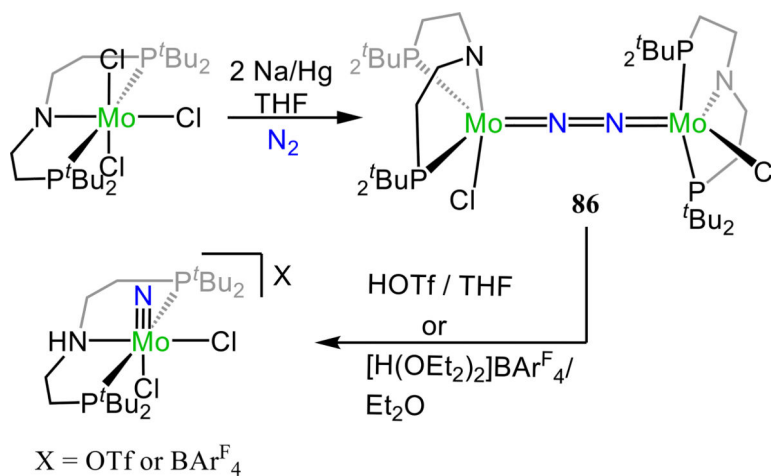
Scheme 28.
Synthesis of and H$^+$-triggered N$_2$ Scission by 86
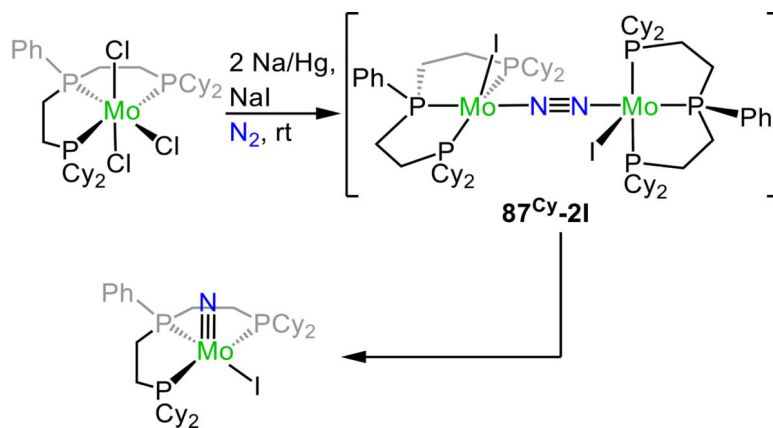
Scheme 29.

N$_2$ Cleavage Via Proposed Transient 87^{Cy}-2I
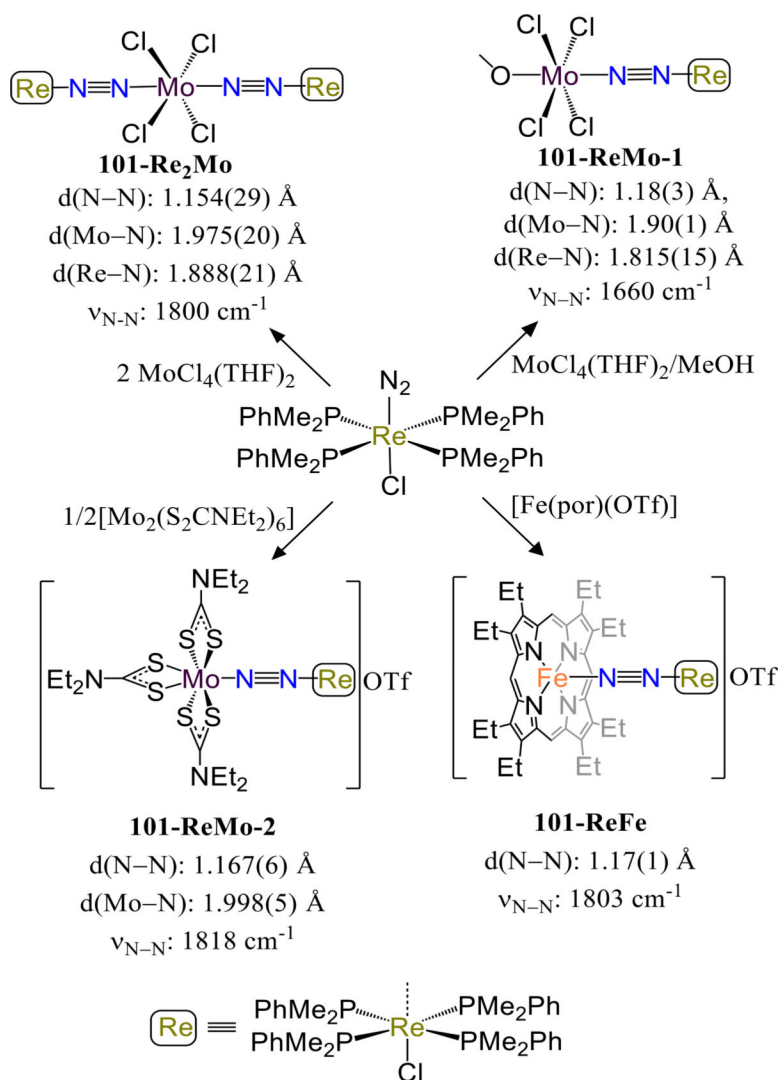
Scheme 30.
Heterometallic Complexes Containing Re(PMe$_2$Ph)$_4$(N$_2$)Cl
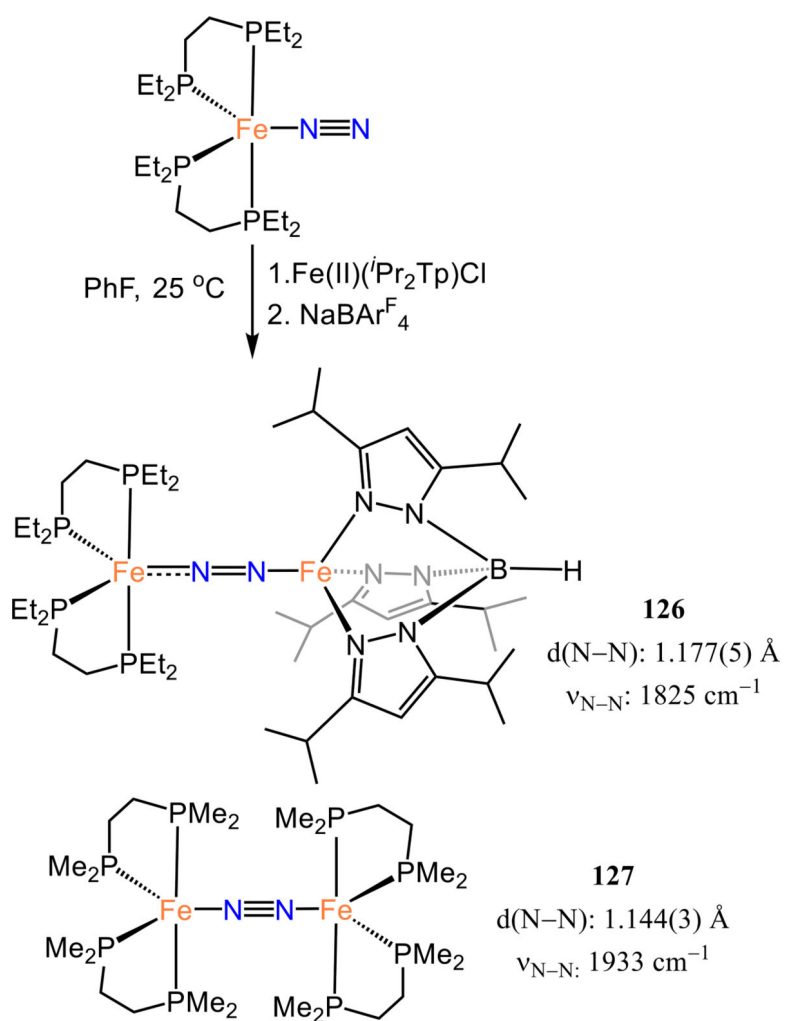
Scheme 31.
Complexes 126 and 127
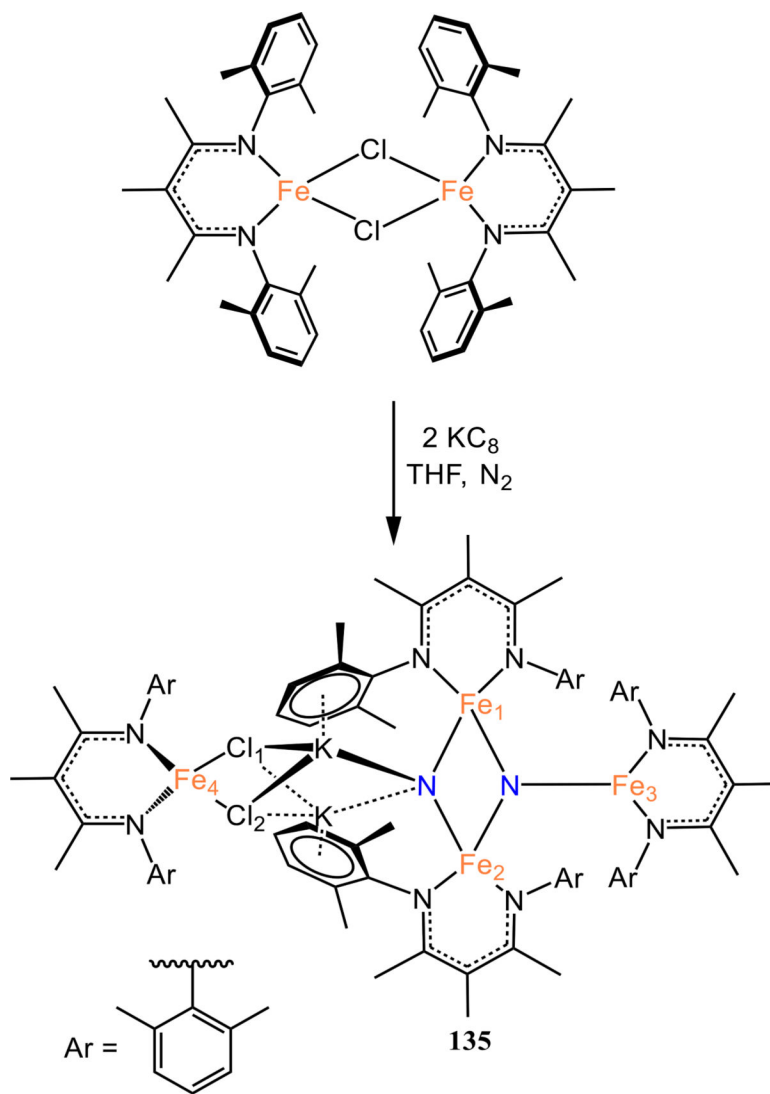
Scheme 32.
Synthesis of di(μ-nitride) 135

147
d(N–N): 1.065(4) Å
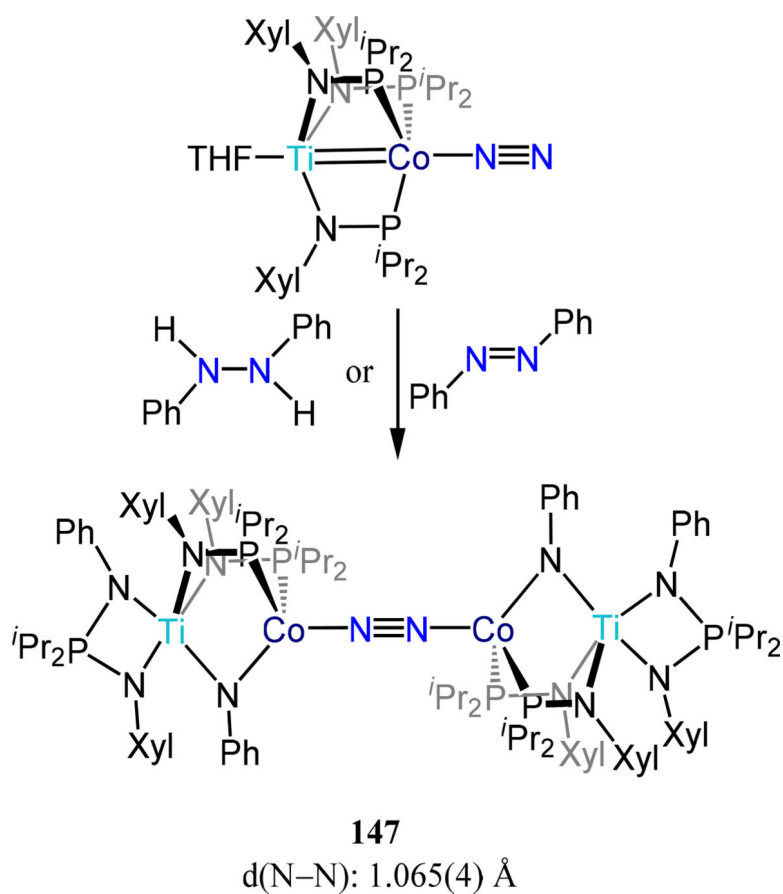
Scheme 33.
Synthesis of 147
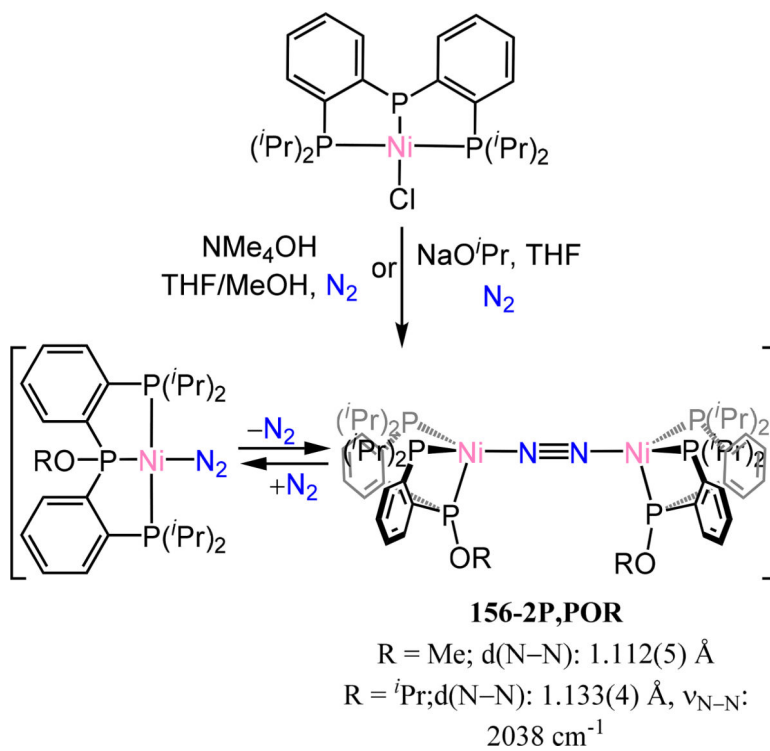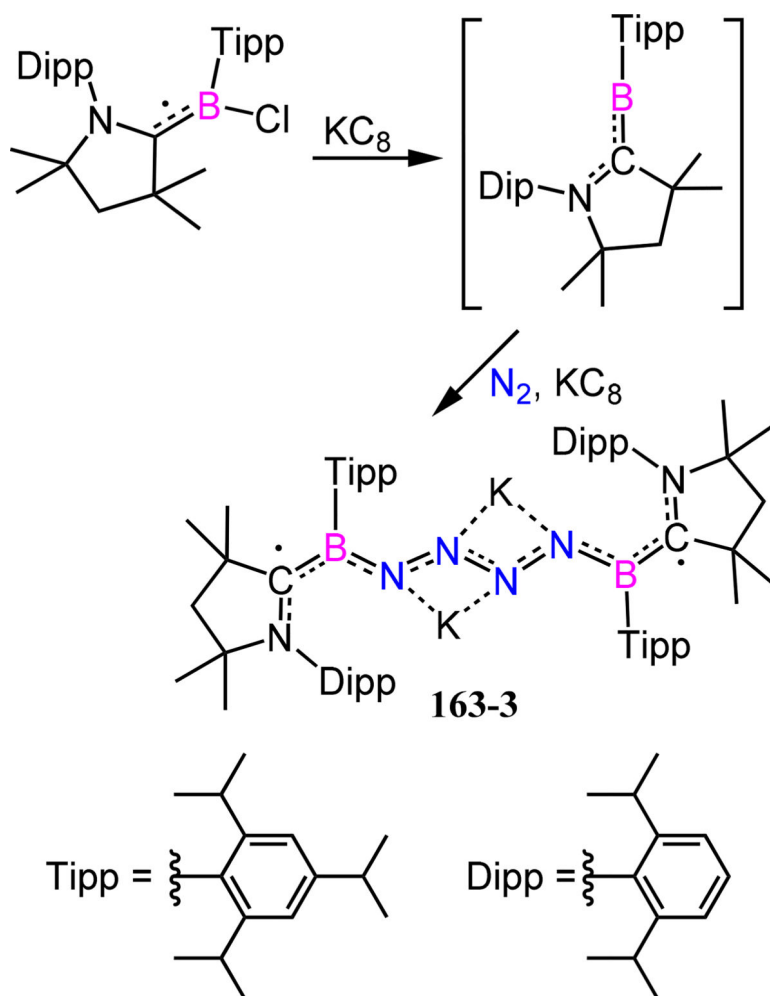
Scheme 34.
Synthesis of 156–2P,POR
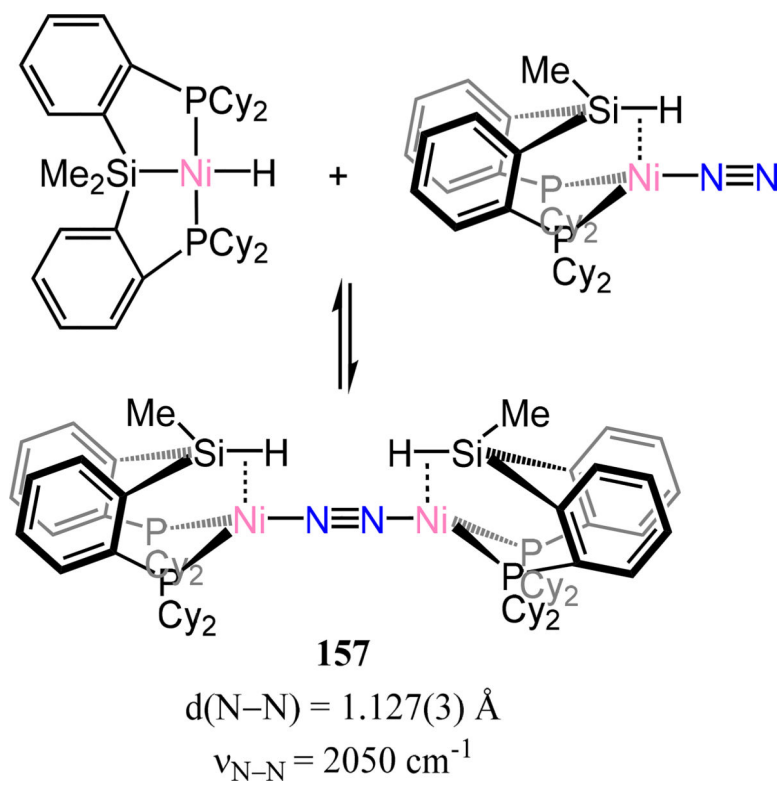
Scheme 35.
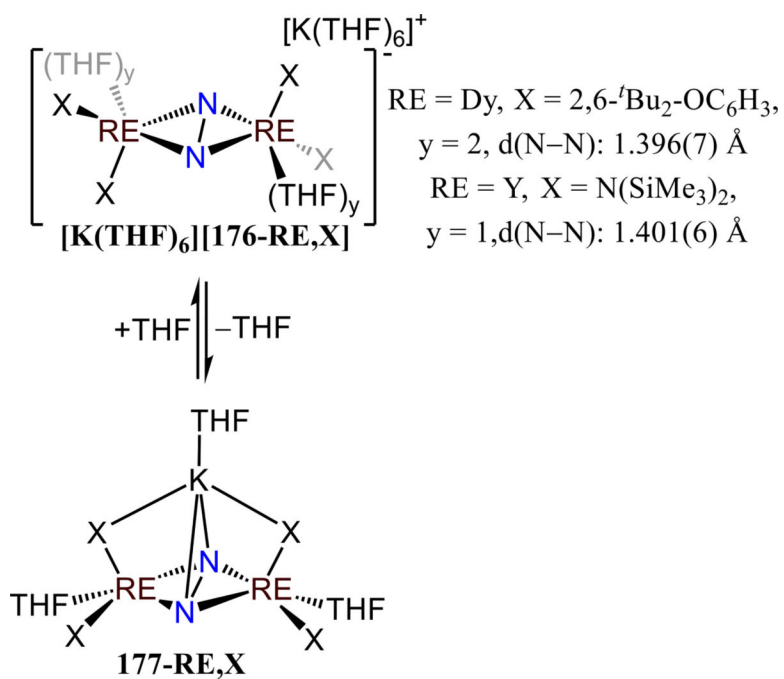Equilibrium of 157 with Mononuclear Species
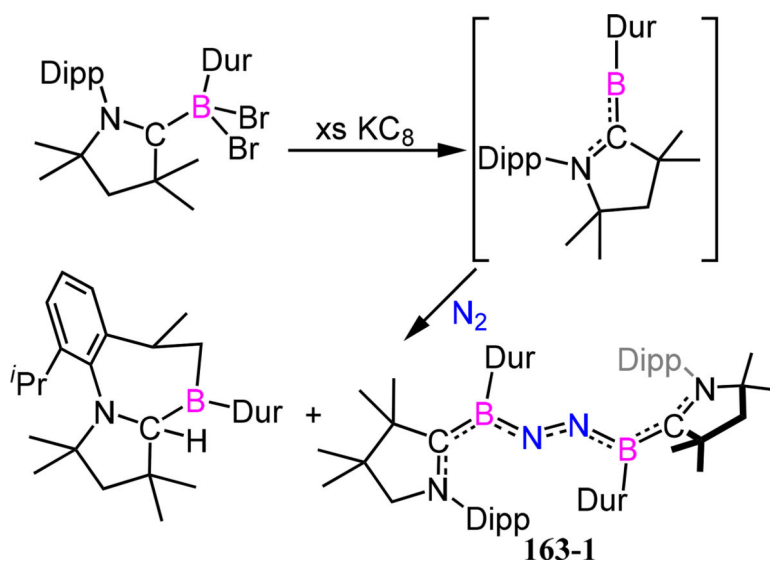
Scheme 36.
Synthesis of 163–1
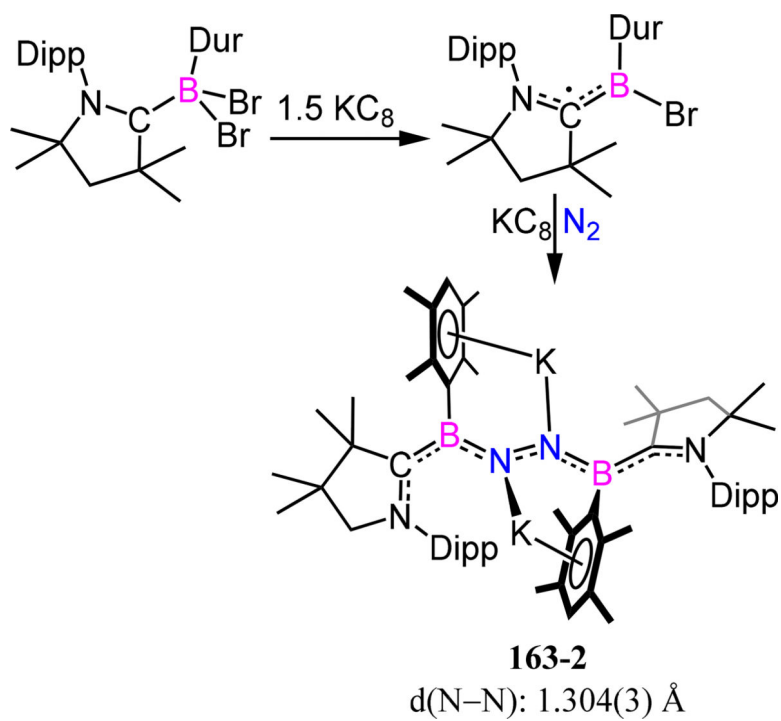
Scheme 37.
Synthesis of 163–2

Scheme 38.
Synthesis of 163–3

Scheme 39.
Interconversion Between [K(THF)₆][176-RE,X] and 177-RE,X